On the role of prelamin A in the heart

Brayson, Daniel James

Awarding institution:
King's College London

On the role of prelamin A in the heart

By Daniel Brayson

Submitted for the degree of Doctor of Philosophy from King's College London

June 2014

Supervisors: Professor Catherine M. Shanahan & Professor Ajay M. Shah

King's College London

BHF Centre of Research Excellence

Cardiovascular Division

James Black Centre

Abstract

Prelamin A is one of two protein products of the *LMNA* gene and undergoes proteolytic processing to become mature lamin A, a crucial protein for nuclear envelope structure and function. Evidence suggests that when this process is hindered, resulting in accumulation of prelamin A, premature ageing disorders and cardiovascular complications occur. Moreover, mutations to *LMNA* are known to lead to dilated cardiomyopathy (DCM), with some of these mutations possibly resulting in accumulation of prelamin A, thus potentially implicating prelamin A in DCM pathogenesis.

To explore whether prelamin A has a role in DCM and heart disease, I used targeted transgenesis to the Rosa26 locus of the mouse genome of an uncleavable prelamin A construct (L647R-*LMNA).* Cardiac selective expression was achieved via MLC2v promoter linked cre-recombinase mediated cassette exchange to yield mice which expressed prelamin A exclusively in cardiomyocytes—PLA Tg mice. They were compared to mice harbouring but not expressing the transgene, referred to as Wildtype (Wt).

Compared to Wt, PLA Tg mice failed to thrive and succumbed at 5-6 weeks of age from a phenotype indicative of DCM and heart failure as defined by echocardiographic analysis of cardiac function, i.e. ejection fractions were dramatically reduced in PLA Tg (19.56%) compared to Wt (60.6%). Additional characterisation identified myocardial disarray and inflammation, and cardiomyocyte death as occurring in PLA Tg heart tissue.

Molecular characterisation suggested accumulation of DNA damage leading to ATM mediated NF-κB signalling may initiate inflammation of the myocardium and may also contribute to 'myocardial senescence'. Disruption of gap junction formation via Cx43 mislocalisation occurred and later structural proteins of the nuclear envelope were misexpressed and disorganised, indicating that cardiomyocytes were susceptible to mechanical stress in the face of prelamin A accumulation.

Immunofluorescence staining of human heart showed that prelamin A accumulated in the nuclei of a number of DCM heart biopsies, strongly implicating a role for prelamin A accumulation in clinical DCM pathogenesis. Moreover, it was observed that prelamin A was expressed, in low levels, endogenously in Wt myocardium and may be a novel component of the sarcomere.

In conclusion, this thesis provides evidence that nuclear prelamin A accumulation occurs in certain settings of DCM pathogenesis which may be a direct consequence of *LMNA* mutations or which may occur downstream of other pathogenic events. In this setting, prelamin A may mediate pathology via mechanisms identified in PLA Tg mice.

Declaration

I declare that, except where acknowledgement has been made, the work undertaken in this thesis is all my own.

Acknowledgements

Firstly, I would like to give my utmost thanks to my primary supervisor Prof Cathy Shanahan for actually allowing me to set foot in the lab (I'm not sure I would have been so trusting of me), and also for her wisdom regarding the science of prelamin A, who is now my best friend. Because Cathy doesn't know what or where a heart is, I had to look elsewhere for expert advice on my project, therefore, I would also like to thank my second supervisor Prof Ajay Shah for guidance in matters of the heart although, I would like to iterate NOT the sentimental kind, that would just be weird.

I would like to thank my fellow 4-year BHFers Lozza Pozza and Iain Soil for embarking on such a treacherous adventure with me, if only you'd known what you were letting yourself in for. A special thanks to Drs Alison Brewer and Elisabeth Ehler, Gema Vizcay, Andrea Protti, Qiuping Zhang, and Derek Warren for lab guidance, expertise and support. Of course I would like to 'thank' everyone in my lab (for generally being in my way, (ironic LOL)).

To Arsene Wenger, thank you for keeping me on my toes for the duration of my PhD (and 13 years prior), please stay!

Naturally, I have to thank all of my real world friends for still (I think) being my friends despite my disappearing off the face of the planet to write a thesis. Just so you know (you know who you are), I probably wouldn't have done it had I known, and I am ready to reintegrate, if you'll have me. Beers are on you though because I'm effing skint.

To my family, The Braysons and the Brayson-Browns, Thank you, because you are all (mostly) awesome! This is despite my sometimes infantile and often adolescent behaviour in your presence. I promise to be less of a tool in the (PhD free) future.

Finally to DeeDee, only Darwin knows why, but you have, and you do. I'd probably have had to resort to Smack without you. Eternal thanks, Love xxx

For the Big Man

XXX

Table of Contents

List of Figures

Chapter 4

Chapter 5

List of Tables

List of Abbreviations

ACE	Angiotensin Converting Enzyme
Akt	Protein Kinase B
AMPK	AMP activated Protein Kinase
ANP	Atrial Natriuretic Peptide
ARVC	Arrhythmogenic right ventricular cardiomyopathy
ATM	Ataxia-telangiectasia mutated
ATP	Adenosine Triphosphate
ATR	ATM- and RAD3-related
BNP	Brain Natriuretic Peptide
C2C12	myogenic mouse myoblast cell line isolated from dystrophic mouse muscle
Ca^{2+}	Calcium
CCS	Cardiac Conduction system
ChK1/2	Checkpoint Kinase 1/2
CM	Cardiomyocyte
cMyBP-C	cardiac Myosin Binding Protein C
Cx43	Connexin 43
CXCL1	Chemokine C-X-C motif Ligand 1
DCM	Dilated Cardiomyopathy
DDR	DNA Damage Response
DSB	Double Strand Break
Dusp	Dual specificity phosphatase
EC	Endothelial Cells
ECM	Extracellular Matrix
EDMD	Emery dreifuss muscular dystrophy
EGR1	Early Growth Response Protein 1
ERK	Extracellular Regulated Kinase
FACE1	Farnesylated proteins converting enzyme
FHL1	Four and a Half LIM domain protein 1
FPLD	Familial Partial Lipidodystrophy

FTI	Farnesyl Transferase Inhibitor
HCM	Hypertrophic cardiomyopathy
HF	Heart Failure
HFpEF	Heart Failure preserved Ejection Fraction
HFrEF	Heart Failure reduced Ejection Fraction
HGPS	Hutchinson Gilford Progeria Syndrome
IF	Intermediate Filament
IL-	Interleukin
INM	Inner nuclear membrane
JNK	Jun N-terminal Kinase
K^+	Potassium
KASH	Klarsich, ANC-1 and Syne homology
LAP2 α	Lamina associated polypeptide 2 alpha
LGMD1B	Limb girdle muscular dystrophy type 1B
LINC	Linkers of nucleoskeleton to cytoskeleton
LV	Left ventricle
LVH	Left Ventricular Hypertrophy
MAD	Mandibuloacral dysplasia
MAN1	LEM Domain Containing Protein 3
MAPK	Mitogen Activated Protein Kinase
MCP-1	Monocyte chemotactic protein -1
MI	Myocardial Infarction
MLC2v	Myosin Light Chain 2 ventricular
MLP	Muscle LIM protein
MMP	Matrix metalloproteinase
MRI	Magnetic Resonance Imaging
mTOR	mammalian Target Of Rapamycin
NADPH	Nicotinamide adenine dinucleotide phosphate
NE	Nuclear Envelope
Nesprin	Nuclear Envelope Spectrin Repeat Protein
NF-κB	Nuclear factor kappa light chain enhancer of activated B cells

NFAT	Nuclear Factor of Activated T-cells
NOX	NADPH oxidase
OH•	Hydroxl radical
ONM	Outer nuclear membrane
PBS	Phosphate Buffered Saline
PLA Tg	Prelamin A Transgenic
PP	Pulse Pressure
PPAR	Peroxisome Proliferator Activated Receptor
PWV	Pulse wave velocity
RCM	Restrictive cardiomyopathy
RD	Restrictive Dermopathy
RNS	Reactive Nitrogen Species
ROS	Reactive Oxygen Species
RT	Reverse Transcription
RyR	Ryanodine Receptor
SASP	Senescence Associated Secretory Phenotype
SERCA	Sarcoplasmic Endoplasmic Reticulum Calcium ATPase
Situin	silent mating type information regulation 2 homolog
SREBP1	Sterol Response Binding Element Protein-1
SSB	Single Strand Break
SUN	Sad1p-UNC84
TNFα	Tumour necrosis factor alpha
UPS	Ubiquitin Proteasome System
VSMC	Vascular smooth muscle cell
Wnt	Wingless-related integration site
Wt	Wildtype
ZMPSTE24	human homolog Zinc metalloproteinase STE24
α-MHC	Alpha-Myosin Heavy Chain
β-MHC	Beta-Myosin Heavy Chain

Chapter 1: Introduction

In the preceeding 15 years, the nuclear envelope (NE), which primarily consists of intermediate filament (IF) proteins and other membrane associated proteins that form the LInker of Nucleoskeleton to Cytoskeleton (LINC) complex[1], has been subject to intense scrutiny, in particular the nuclear A-type lamins, lamin A & lamin C. These two proteins are the product of the same gene, *LMNA*, occurring by alternate splicing. Whilst lamin C is translated in fully mature form, lamin A is translated as a precursor, prelamin A, and undergoes unique enzymatic processing by farnesylated proteins converting enzyme1 (FACE1) to yield mature lamin A. This event appears to play a key role in the manifestation of disease. The discovery that mutations to the *LMNA* gene result in a variety of 'premature ageing disorders' such as Hutchinson Gilford progeria syndrome (HGPS), has sparked scrutiny not only from researchers interested in rare genetic diseases but also those looking for answers within the field of ageing and age-related disease. The introduction for this thesis aims to inform the reader of the existing dogma of age associated cardiac decline and argue a case for prelamin A within this paradigm.

1.1 The Heart: structure and function

Myocardial structure is diverse. The dominant cell type is the cardiomyocyte (CM), which constitutes approximately 30% of cells in the heart. Additionally, there are endothelial cells, fibroblasts, pericytes, smooth muscle cells and arguably, cardiac stem

cells. Moreover, there are a number of extracellular matrix (ECM) components that are vital for the structural organisation of the heart and for dealing with load and tension. These are primarily glycoproteins and include collagen, laminin and fibronectin[2]. CMs are terminally differentiated cells that are defined structurally by repeating units of contractile proteins known as sarcomeres (Fig 1.1) and are connected to neighbouring CMs via the sarcolemma (muscle cell membrane) by intercalated discs which comprise many junctional proteins and whose role it is to propagate electrical signals and facilitate efficient contraction of CMs in a temporally regulated manner, meaning heart tissue contraction as a whole is synchronous.

The sarcomere is made up of thick myosin filaments and thin actin filaments that cross-bridge via myosin heavy chain (MHC) heads via the troponin tropomyosin complex to initiate contraction. When the cross-bridges are formed, the myosin heads act as levers to slide the filaments together, thereby shortening the cytoskeletal components of the sarcomere, such as the z-discs, and creating contraction. Relaxation occurs when the myosin heads dissociate and the sarcomere returns to normal length[3]. The key regulator of this process is calcium (Ca^{2+}). Increases in intracellular [Ca^{2+}] lead to the assembly of the troponin tropomyosin complex whereas dissociation is initiated by low $[Ca^{2+}]_i$[4]. Intracellular calcium concentration is in turn regulated by many intricate signalling mechanisms. Membrane depolarisation in CMs usually occurs via potassium (K^+) ion channels associated with junction proteins known as connexins from a neighbouring CM. This initial depolarisation leads to activation of voltage gated Na^+ channels leading to a rapid depolarisation. Na^+ channels subsequently close and K^+ and L-type Ca^{2+} channels open. Influx of Ca^{2+} leads to a phenomenon known as calcium

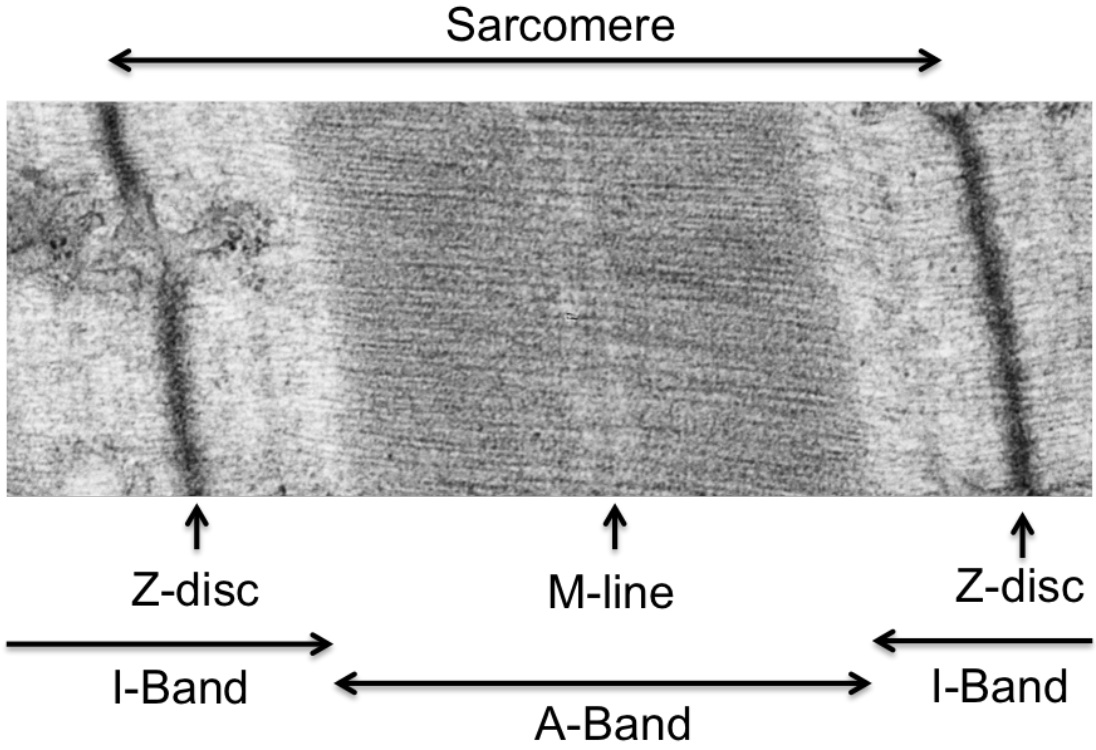

Figure 1.1. The sarcomere. An electron micrograph showing the sarcomere: The I-Band contains only thin actin filaments. The A-Band denotes the region where the thin actin filaments and thick myosin filaments overlap, whilst the M-line and Z-discs contain cytoskeletal proteins that provide structural compliance for efficient contraction-relaxation of actin and myosin.

induced calcium release (CICR). Within the cytoplasm a structure termed the sarcoplasmic reticulum (SR) acts as an internal reservoir for Ca^{2+} that is segregated from the cytoplasm. The SR is safeguarded by the ryanodine receptor (RyR), which is a calcium release channel incorporated into the SR membrane. The RyR is activated by a transient increase in Ca^{2+}, leading to channel opening and SR Ca^{2+} release into the cytoplasm, which initiates formation of the troponin tropomyosin complex that leads to contraction[5]. Relaxation is governed by Ca^{2+} reuptake by the SR via the sarcoplasmic endoplasmic reticulum calcium ATPase (SERCA)[6]. The process of electrical signalling leading to contraction is known as excitation-contraction coupling and is the focus for much research regarding arrhythmia and contractility[7].

Additionally, the role of cytoskeletal components has been studied[8]. The cytoskeleton provides the platform upon which the contractile machinery can exert force. As a result these components are critical for the transmission of force across a CM or myofiber. Cytoskeletal components include proteins such as titin, desmin, muscle lim protein (MLP), myosin and α-actinin. Mutations to all of these can lead to dilated cardiomyopathy (DCM)[9-13]. The NE may also be important to the structural integrity and mechanical efficiency of CMs. The NE contains many structural proteins, which may provide the structural stability required for transmission of force across the nucleus of a CM and contribute to overall mechanical stability in CMs. The importance of the NE in CMs is highlighted by the fact that mutations to the genes of NE components lamin A/C[14, 15], emerin[16, 17] and nesprin 1α[18] cause DCM phenotypes.

1.2 Cardiovascular ageing and heart disease

In the cardiovascular system a number of age related changes to physiology are observed. Possibly the first notable change is the increase in arterial impedance or 'stiffening of the arteries'. This results in an increased pulse wave velocity (PWV) widening of pulse pressure (PP) and an overall increase in blood pressure (BP). Subsequently a hypertensive phenotype is observed. This leads to increases in mechanical work done by the heart as a result of pressure overload, which is known to induce pathological remodelling of the heart such as left ventricular hypertrophy (LVH)[19-21]. Another key age associated change is increasing instability of atherosclerotic plaques leading to ischaemic attack and subsequently, myocardial infarction (MI) or stroke. Both LVH and non-fatal MI are capable of progressing towards cardiac dilatation and heart failure with terminal prognosis. The age-associated decline of the heart is summarised in Figure 1.2.

1.2.1 Heart failure

Heart Failure (HF) arises when the heart is no longer able to pump sufficient blood through the body to meet the metabolic demands of the respiring tissues. This occurs as a result of pathological changes to cardiac structure and function, which can accumulate over time, as in the case of LVH and pressure overload or as the result of injury caused by ischaemic attack. HF can also arise as an end-point to cardiomyopathies; in which case, the disease is the result of CM dysfunction and thought of as primary disease rather than secondary. HF is highly prevalent amongst the western population. The

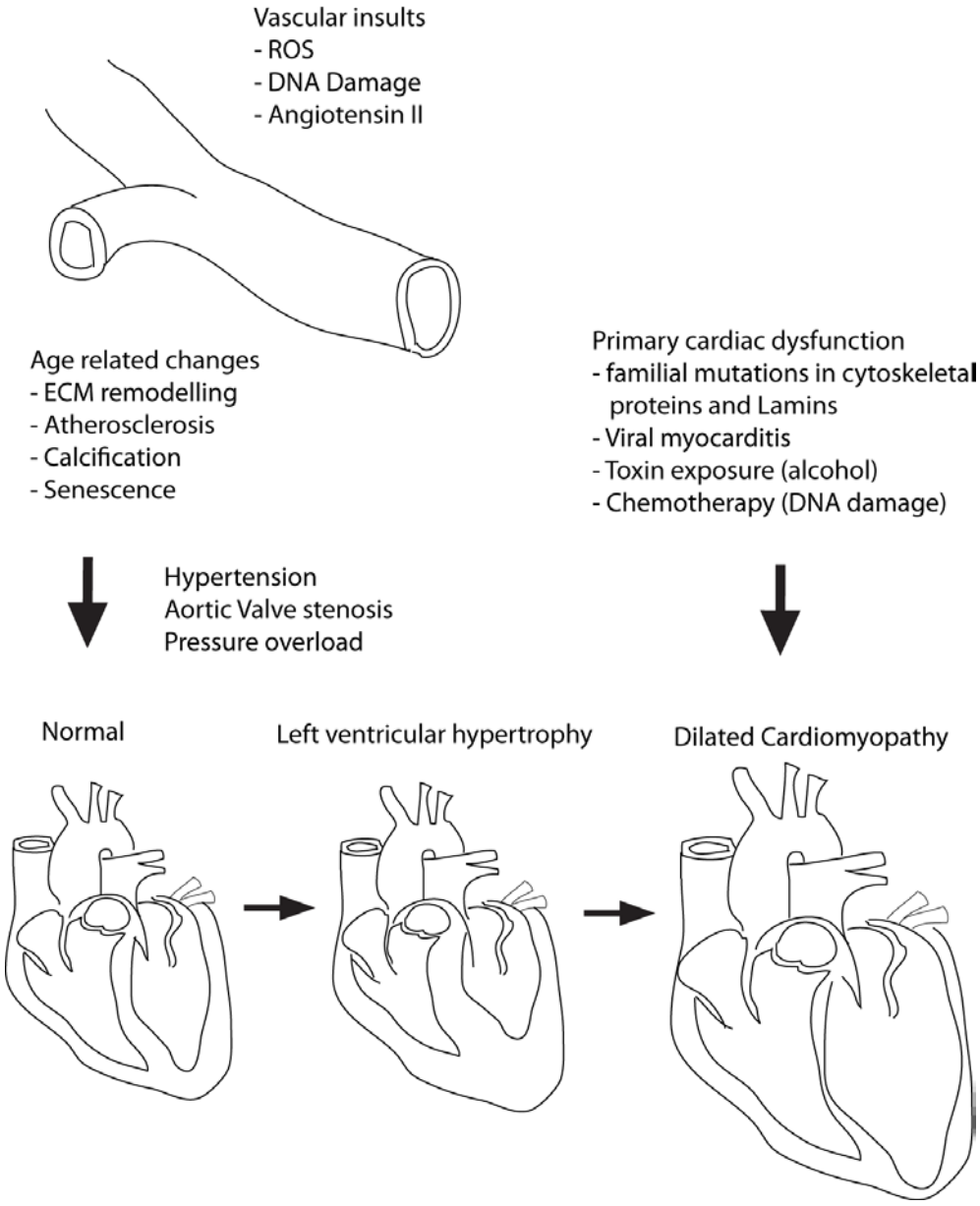

Figure 1.2. Cardiovascular ageing. In advancing age cardiovascular dysfunction is characterised by a variety of age-associated changes to the signalling pathways regulating vascular tone and cell cycle leading to pathogenesis and senescence, ultimately resulting in stiffened arteries and hypertension. Sustained pressure overload (PO) then stimulates hypertrophic remodelling of the heart, characterised by eccentric myocyte hypertrophy, interstitial fibrosis and contractile dysfunction. Persistent PO causes advanced remodelling and HF. Moreover, mutations to structural proteins in CMs lead to DCM. Toxins from dietary intake such as alcohol and from treatment regimes such as chemotherapy may also cause DCM associated with ageing.

Framingham heart study found that at 40 years of age, lifetime risk for HF for males and females is 21% and 20.3% respectively[22]. Such incidence presents a great strain to the health industry and has significant societal implications. Currently there is inadequate provision for the treatment of HF; β-blockers, aldosterone antagonists, angiotensin converting enzyme (ACE) inhibitors and angiotensin receptor blockers show significant efficacy in controlling the mortality and morbidity of some HF patients but only in those with reduced systolic function, and furthermore not in all cases[23]. HF is subdivided into two main categories: those who have reduced systolic function (HFrEF) and those with preserved systolic function (HFpEF). It is often assumed that patients with HFpEF have diastolic dysfunction, which is described as impaired filling of the left ventricle as a result of varying factors[24] such as impaired relaxation, affecting the ability of the LV to fill passively with blood, or from increased filling pressures[25, 26].

1.2.2 Left Ventricular Hypertrophy

Age induced dysfunction of the vasculature invariably leads to pathologic cardiac events, which characterise the critical disease phenotypes that provide great risk to life, crucial to which, is the progressive remodelling of the cardiac tissue known as left ventricular hypertrophy (LVH). Pathological LVH is characterised by a chronic decline in cardiac output resulting from a gradual decline in contractility as well as an increase in impedance of the cardiac tissue, leading to a decrease in diastolic filling and decrease in ejection fraction, stroke volume and cardiac output. These changes are mediated by interstitial fibrosis, hypertrophy of CMs and decrease in contractile function[27]. Relative to this increase in size, the number of capillaries supplying blood to the CMs has been

shown to decrease leading towards a deficit in oxygen supply[28]. The consequences of these pathological changes are severe and lead to a steady decline in cardiac health resulting in cardiac dilation and HF (Fig 1.2). There is evidence to suggest that A-type lamins play a role in hypertrophic signalling. It has been reported that haploinsuffiency of *Lmna* ameliorates the effects of pressure overload induced hypertrophy in mice[29]. The mechanism identified implies that impaired activation of the mechanosensitive gene *Egr1*, which encodes transcriptional regulator early growth response protein 1, is crucial to this phenotype. Additionally, mutation of the lamin binding partner and transcriptional regulator, Four and a Half LIM domain protein 1 (FHL1), has been implicated in development of a hypertrophy phenotype[30]. Overall, the cellular signalling mechanisms involved in LVH are complex, and therefore beyond the scope of this review, and covered in more detail elsewhere[20, 21, 31].

1.2.3 Cardiomyopathy

Cardiomyopathies arise as a product of intrinsic and age related dysfunction of the CMs. The causes of such events are varied and range from familial mutations of structural proteins such as actin, myosin, and A-type lamins, to environmental causes such as toxic exposure, e.g. alcohol and chemotherapeutic agents such as doxorubicin. Further to this, it has been suggested that DCM occurs late in viral myocarditis, and autoimmunity may also lead to DCM[32, 33]. In most cases, pathological cardiac manifestations of these types result in HF. The processes involved are discussed further below.

Cardiomyopathies have long been classified according to their functional and morphological features. It is thought that each classification accurately describes the phenotype of disease, and is useful in terms of prognosis and therapeutics[34]. The foremost classifications are dilated, hypertrophic, arrythmogenic right ventricular and restrictive, under which several subtypes emerge according to molecular characterisation of the disease phenotype[35]. Often the molecular characterisation in question is the presence of a gene mutation, and at the very least, identification of such mutations allows us to speculate and investigate the mechanisms for the apparent cardiac dysfunction. It is worth noting, however, that there appears to be a great deal of heterogeneity with respect to this point, which is highlighted by two known mutations to *MYH7*, the gene encoding sarcomeric β-myosin heavy chain affecting adjacent amino acids and leading separately to hypertrophic and dilated cardiomyopathy[36].

1.2.3.1 Hypertrophic Cardiomyopathy

An autosomal dominant disease of the heart, hypertrophic cardiomyopathy (HCM) is characterised by hypertrophy of the left (and sometimes right) ventricular myocardium that is not explained by haemodynamic overload. Unlike the uniform concentric hypertrophy seen as a result of pressure overload, hypertrophy is asymmetric and often there is involvement of the inter-ventricular septum[35]. In many cases there is associated fibrosis and myocyte disarray underpinning the phenotype. It is associated with high prevalence of arrhythmia and is the one of the most common causes of sudden cardiac death in young athletes[37].

Mechanistically it has been deemed a disease of the sarcomere although it may also be associated with AMP kinase (see later). Of 10 genes identified to have causal mutations, 9 of them encode sarcomeric proteins[38, 39]. Of these, the two most important encode cardiac myosin-binding protein C (*MYBPC3*) and β-MHC (*MYH7*) and account for the overwhelming majority of cases[40]. The remaining 7 genes account for approximately 1-5% of cases[40]. The mutations involved mostly lead to substitution of single amino acids, although half of mutations to *MYBPC3* are known to cause truncations to the protein product and lead to haploinsufficiency, which also underlies the phenotypic presentation of HCM[41, 42]. At the cellular level, increases in contractility occur. Analysis of these indicates that altered myosin kinetics and increased calcium sensitivity of thin-filaments are key factors[43-45]. These changes are known to activate hypertrophic signalling pathways and also may contribute to the characteristic diastolic dysfunction evident in HCM. Furthermore, evidence from a troponin T mutant transgenic model suggests that during diastole, SR calcium content is significantly elevated[46]. One hypothesis suggests that dysregulation of calcium handling can predispose patients to arrhythmia[47] and may also encourage aberrant signalling via multiple pathways such as calcineurin nuclear factor of activated T-cells (NFAT) and calcium-calmodulin-dependent protein kinase II signalling[48].

Sarcomeric mutations have been shown to perturb calcium handling via two main mechanisms. Firstly, the presence of mutations to troponin T, troponin I and tropomyosin increases the affinity of troponin C for calcium[49], and mutations to cMyBP-C lead to the formation of additional cross-bridges between thick and thin filaments which also increase sensitivity to calcium. Troponin is the principal calcium buffer in the SR; therefore, increased affinity should increase calcium levels in

diastole[50, 51]. The second mechanism identified suggests that contractile inefficiency compromises the energetics of the CM: the formation of cross-bridges between thick and thin filaments of the sarcomere requires approximately 70% of the ATP consumption of any given CM. HCM mutations in sarcomeric proteins that alter this process are hypothesised to confer a deficit in ATP availability and this is postulated to have ramifications for other ATP requiring processes within the cell, such as Ca^{2+} uptake via SERCA during diastole, thus potentially contributing to the manifestation of diastolic dysfunction that is characteristic in HCM[52]. The formation of a myocardial energetics hypothesis for HCM is supported by work suggesting that mutations to the γ2 subunit of AMP-activated protein kinase (AMPK) involved in energy sensing leads to HCM[53].

There are a couple of studies showing the involvement of lamins in HCM. In the first, HCM appears to be secondary to Familial Partial Lipidodystrophy (FPLD2) caused by a missense mutation to *LMNA* that confers an amino acid substitution at residue 591[54]. Interestingly, this patient was also insulin resistant indicating a potentially wider role for lamins in heart disease, as perturbations to lamins may also be involved in metabolic syndrome[55, 56]. Additionally there was a case reported whereby a patient with the R644C mutation displayed pathogenicity consistent with HCM[57].

1.2.3.2 Arrhythmogenic Right Ventricular Cardiomyopathy (ARVC)

ARVC is characterised by pathological remodelling, primarily of the right ventricle, in which myocyte death, inflammation and fibrofatty replacement of the myocardium are the main histological features[58]. *In vivo*, cardiac imaging shows ventricular wall

thinning, dilatation of cardiac chambers and systolic dysfunction. Using magnetic resonance it is possible to identify the fibrofatty lesions that pervade the myocardium as fat deposits appear as white spots amongst the grey myocardium in T1-weighted fast spin echo images. Additionally, injection of gadolinium contrast agent can identify fibrotic regions, which present late signal enhancement in recovery sequence images[59]. Alongside the morphological changes to the myocardium, patients are also prone to arrhythmia; indeed ARVC is known to be another lead cause of sudden cardiac death worldwide[60, 61]. Furthermore, arrhythmia and sudden cardiac death can occur with limited to no pre-existing morphological disturbances, making diagnosis difficult.

Due to the nature of mutations identified in ARVC, it has been termed a disease of the desmosome[62]. The desmosome anchors the IFs of one cell to the cytoplasmic membrane of another in order to create a lattice structure that provides mechanical strength to tissue. Mutations to a number of desmosomal genes have been identified in ARVC, including desmoplakin, plakoglobin, plakophilin-2, and desmoglein-2[63-66]. Other key mutations have been identified in transmembrane protein 43[67] and transforming growth factor β3[68]. The molecular mechanisms that regulate the progression to ARVC are somewhat unclear, but two main hypotheses have been postulated. Firstly, mutations to the desmosome may compromise the integrity of cell-cell interactions and as such make the tissue structure, in this case the heart, susceptible to mechanical stress leading to cell detachment and necrosis, which may then instigate an inflammatory response. In this setting it is thought that fibroadipose deposition is a reparative response to injury. Second is the transdifferentiation model, which proposes that desmosomal perturbations can dysregulate the Wnt/β-catenin signalling pathway

leading to activation of adipogenic and fibrogenic genes and a switch of cell fate from CM to adipocyte[69, 70].

Recently, a number of patients presenting with ARVC who did not have mutations to desmosomal genes were found to have *LMNA* mutations. Interestingly, the R644C mutation was again responsible in two of five mutations identified[71, 72].

1.2.3.3 Dilated Cardiomyopathy

DCM is characterised by dilation of one, if not both, ventricular chambers. Functionally, it is accompanied by a reduction of systolic function and structurally by fibrosis of the myocardium and CM death. It can arise as a result of sustained ventricular remodelling from pressure overload or as a result of primary causes[73]. Most commonly these come in the form of a mutation to a protein playing a key role in the cytoarchitechture of the CM. Indeed, inherited mutations (familial DCM, FDCM) are thought to account for up to half of cases, whilst the remaining cases (idiopathic DCM, IDCM) are thought to be a result of somatic de novo mutations or external causes such as myocarditis[74, 75], toxin exposure[76], chemotherapy[77] and potentially also autoimmunity[78].

Where gene involvement is concerned, initial findings suggested that sarcomeric mutations were the most important in determining a DCM phenotype, but now many mutations affecting cell compartments that are peripheral, or perhaps more pertinently, 'accessory', to the sarcomere have been identified as being equally if not more important, such as mutations in genes encoding proteins interacting with the sarcolemma and the desmosome (dystrophin), IFs (desmin) and importantly for this

thesis, the NE (lamin A/C). Upwards of 40 disease genes have been identified, most of which exist as autosomal dominant mutations[79]. The consequence of having such a diverse pool of genes that are causative for DCM is that, mechanistically, there is unlikely to be a common cellular process provoking disease, presenting a great challenge in terms of therapeutic intervention.

To a degree, some cellular mechanisms have been elucidated. Mutations to β-MHC are shown to reduce contractility in DCM, whereas mutations to thin filament proteins cause a reduction in Ca^{2+} sensitivity by attenuating the affinity of troponin to calcium. These mutations act to reduce the generation of force in the myocyte. Other proteins that are responsible for DCM include cytoskeletal components of the z-disc such as cypher[80], the costamere (δ-sarcoglycan[81], dystrophin[82]), which links the contractile apparatus of the myocyte to the sarcolemma and ECM, and IFs such as desmin[83], which help link the contractile apparatus to the ECM and also to the nucleus via the LINC complex. These mutations are thought to cause a disruption in transmission of force throughout the myocyte or may disaffect sensing mechanisms possibly involving Titin. Mutations to the Titin gene, *TTN*, are also now a well-established cause of FDCM[11]. Phospholamban, essentially known as the gatekeeper of the SERCA and crucial in regulating the diastolic phase of excitation-contraction coupling in CMs, is subject to an unusually common mutation, p.Arg14del, that causes DCM with associated arrhythmia[84]. This mutation inhibits SERCA, resulting in a reduction of Ca^{2+} reuptake in diastole and is probably the means by which ECGs often show low voltage. This specific mutation to *PLN*, the gene that codes Phospholamban, is thought to be one of the most common causes of FDCM. Interestingly, the *LMNA* gene is also commonly mutated in DCM. Mutations of the *LMNA* gene in humans have

been shown to result in cardiomyopathies leading to conduction defects resulting in arrhythmias leading to sudden cardiac death[85]. However, the recurrence of common DCM causing mutations is much lower; the Universal Mutations Database states that there are currently 132 unique DCM causing mutations to *LMNA* that are known. This diversity makes mechanistic analysis challenging, although some DCM causing *LMNA* mutations have been investigated in order to provide some insight into the workings of *LMNA* associated DCM.

1.3 Mechanisms of ageing

1.3.1 Myocardial senescence

Ageing is now recognised as the most potent risk factor for cardiovascular disease (CVD). Additionally, levels of DNA damage in vascular smooth muscle cells (VSMC), CMs and endothelial cells (EC) increase linearly with age, as do levels of reactive oxygen species (ROS). This implies a strong link exists between DNA damage response (DDR) and the onset of cellular senescence, defined as the point at which diploid cells lose their ability to divide[86], and also their ability to respond to external stimuli. It has been argued that terminally differentiated cells, CMs for example, despite their lack of cell division, may also cease to respond to external stimuli and become 'senescent'. The evidence for myocardial senescence is under intense debate. Classically CMs have a very low lifetime turnover, and the regenerative capacity of the heart, particularly in adulthood, is poor. Therefore, loss of CM function as a result of senescence is not easily

compensated for, unlike that of say, a troublesome epithelial tissue that may be at risk of oncogenesis[87]. Known ageing mechanisms and their potential relevance to cardiac ageing will be discussed further.

1.3.2 DNA damage and DNA damage response (DDR)

Genome integrity is under constant threat from daily cellular insults leading to DNA damage. DNA repair mechanisms are constantly operating to counter the effect of these insults. This relationship of damage and subsequent repair is therefore viewed as a normal process in order to maintain cellular homeostasis. Thus, it is widely accepted that the stability of genes depends upon DNA repair. DNA damage can occur from exogenous sources that include UV and ionizing radiation, environmental chemical toxins (e.g. cigarette smoke) and dietary toxins (low density lipoproteins), and endogenous sources including ROS or reactive nitrogen species (RNS), which are derived from numerous intracellular sites: as products of mitochondrial metabolism; from ROS generating enzymes such as NADPH oxidase (NOX); or RNS generating enzymes such as uncoupled nitric oxide synthase (NOS)[88]. The modifications made include DNA adducts, and single (SSB) and double strand breaks (DSB). This has led to the notion that DNA damage itself plays little role in pathogenesis and that often the accumulation of DNA damage which drives senescence and disease is due primarily to defective DNA repair mechanisms.

At a molecular level DNA repair occurs by a DDR pathway driven by a collective of sensors, transducers and effectors[89]. When DNA becomes damaged it is detected by DNA damage binding proteins, or sensors, that can recognise the lesions or

the chromatin reorganisations occurring as a result of the damage. Such proteins include the Mre11-Rad50-Nbs1 complex, which detects DSBs[90], and the 9-1-1 complex that detects SSBs[91]. The principle transducers of DNA damage response are the Ataxia-telangiectasia mutated gene product known as ATM, and the ATR (ATM and Rad3-related). Both belong to the phosphatidylinositol 3-kinase-like family of serine/threonine kinases (PIKK)[92]. ATM/ATR are able to influence, via various phosphorylations, a number of 'effector' or cell-cycle regulating proteins such as checkpoint kinase 1 and 2 (ChK1/2) and the tumour suppressor proteins p53, p21 and p16 which induce cell-cycle arrest in G1 and G2/M phases when activated[93-95], which are associated with development of senescence[96, 97]. In DDR, inhibition of the cell cycle paves the way for enzymatic repair of DNA. For example, base excision repair utilises DNA glycosylase to remove the damaged base leaving an abasic site, which is cleaved by apurinic or apyrimidinic endonucleases before it is fully repaired by DNA polymerase and DNA ligase[98, 99]. Overall, the importance of DDR for ageing paradigms can be extracted from work showing that when key mediators of DSB repair are absent in mice, they experience a premature senescence phenotype. For example, when the genes encoding the DSB repair proteins, ECCR1 and Ku86, are deleted in mice, the resulting phenotype is one of growth retardation and senescence[100, 101]. In the myocardium, the importance of DDR in pathological settings is an emerging field, with DDR mechanisms recently shown to be part of the adaptive response to myocardial infarction[102]. Interestingly, recent findings also suggest that DDR is responsible for the post natal loss of proliferative capacity of CMs[103].

1.3.3 Reactive oxygen species

ROS can arise from exogenous sources such as ionizing radiation (IR) but the most important for disease are derived endogenously and arise as part of cellular processes. It is widely accepted that the primary source of endogenous ROS production in cells is the mitochondria. During xenobiotic metabolism, the electron transport chain produces ROS that are released into the cytosol, primarily as by-products of complex I (NADH dehydrogensase) and complex III (ubiquinone-cytochrome c reductase)[104]. However, it is thought that there are several other enzyme systems that make a significant contribution to redox potential by ROS generation. Amongst these is the NOX family of enzymes. NOXs were the first identified proteins whose primary function it was to generate ROS[105]. Since their identification, many studies have shown their importance in several 'redox signalling' paradigms, a significant portion of which have identified key roles for Nox1, 2 and 4 in the development of cardiovascular dysfunction in response to stress[106-108].

The effects of ROS on nuclear DNA are well established[109]. Oxidative modifications to DNA are almost exclusively achieved by hydroxyl radicals and do not occur directly by O_2^- or H_2O_2. However, O_2^- and H_2O_2 can be efficiently converted to OH• via the Fenton reaction[110]. Modifications induced by hydroxyl radical attack include SSBs and DSBs, base modifications such as thymine glycol and 8-oxo-2-deoxyguanosina (oxo-8-dG), which lead to GT transition mutations[111, 112].

The importance of ROS and DDR in cardiac pathology can be seen in the context of doxorubicin cardiotoxicity. Doxorubicin is the most commonly used member of the anthracycline group of cancer chemotherapeutic agents and is known to lead to

DCM up to 10 years after initial treatment[113, 114]. Doxorubicin is capable of directly intercalating with DNA to induce irreparable DSBs but also produces large amounts of ROS. Furthermore, evidence suggests that doxorubicin cardiotoxicity is regulated by ROS dependent activation of DDR leading to ATM dependent phosphorylation of p53 and subsequent CM apoptosis[115].

1.3.4 Senescence associated secretory phenotype

The senescence associated secretory phenotype (SASP) is the term ascribed to a paradigm in which cells that have undergone cellular senescence are able to contribute to the regulation of the surrounding tissue microenvironment by the production and secretion of soluble factors such as cytokines, chemokines, hormones and proteases and insoluble factors that comprise the ECM such as fibronectin, laminin and collagen[116]. The secretion of these factors creates a physiochemical gradient, which, depending on the tissue model, have the potential to affect cell differentiation[117], stimulate epithelial and endothelial cell motility[118] and induce leukocyte recruitment[119]. It is well established that cellular senescence is a safeguard against cancerous proliferation of damaged cells[120]. However, the discovery that senescent cells exhibit a secretome[121], and subsequently have an active role within tissue environments, has led to the establishment of the SASP paradigm, evidence for which suggests that the detriments outweigh the benefits. Therefore, it seems that senescence is a double-edged sword capable of arresting tumorigenesis and being procarcinogenic; this contradictory response is part of an evolutionary model known as antagonistic pleiotropy[122].

A key aspect of SASP is the specificity with which it operates. There is a specific subset of secreted factors, which create a molecular signature for SASP. The main players include the pro inflammatory IL-6, IL-8 (CXCL-8), MCP-1 and MMP-3 (plus many more), whilst some are noticeably absent from any senescence response, e.g. IL-2,-4,-10,-11,-12, which are interestingly, anti-inflammatory cytokines. As such, the SASP is deemed a pro inflammatory response[116].

The SASP has not been actively investigated in cardiac tissue, but the science is transferable. Persistent DNA damage, such as that seen in chemotherapy mediated DCM, is capable of activating ATM, which is crucial in senescence associated IL-6 secretion[119]. Moreover, pathogenic changes to the myocardial milieu are known to induce immune responses that are regulated by myocyte signalling and involve nuclear factor kappa light chain enhancer of activated B cells (NF-κB) mediated secretion of cytokines, such as IL-6, MCP-1 and TNF-α[123] which, as previously stated, are heavily implicated in the SASP.

Prelamin A accumulation has also been linked with activation of the SASP. Studies of VSMCs subject to ectopic prelamin A overexpression showed a SASP like profile that was associated with DNA damage and induction of vascular calcification[124]. Furthermore, studies in *Zmpste24*$^{-/-}$ mice, in which mice are null for the prelamin A processing enzyme Zmpste24/Face1 and subsequently accumulate prelamin A, indicate that prelamin A is capable of inducing activation and nuclear translocation of the transcriptional regulator NF-κB, which consequently leads to transcription and secretion of SASP mediators IL-6, TNF-α and CXCL-1[125]. Interestingly, the mechanism of NF-κB activation is non-canonical and mediated by ATM activation. Finally, modulation of NF-κB signalling caused by perturbations to the NE has also been reported[126].

1.3.5 Other ageing mechanisms

Telomere length, regulated by the enzyme telomerase, is a well known indicator of cellular age[127]. In the heart, age dependent modulation of telomerase activity has been reported[128], and low telomerase is thought to be a risk factor for CVD[129, 130]. Telomerase activation and telomere attrition have been reported in human hearts[131-133], whilst telomerase deficient mice (*Terc*$^{-/-}$) display significant telomere erosion and subsequently succumb to ventricular dilation and heart failure[134].

Several lines of investigation have identified the importance of the lamina in telomere dynamics[135] and arrangement[136]. Moreover, the mutated form of prelamin A expressed in children with HGPS, Progerin, has been shown to induce telomere dysfunction in fibroblasts[137].

Many other mechanisms have been associated with cardiac ageing and may contribute positively or negatively to a cardiac senescence phenotype. Sirtuins, for example, are thought to confer lifespan extension properties when upregulated and have been shown to be cardioprotective, as well as linked to prelamin A[138-145].

Caloric restriction famously confers lifespan extension benefits in a number of models[146]. Two primary targets by which caloric restriction elicits its effects are by inhibiting Insulin and Insulin like growth factor (IIS) signalling and Protein kinase B/mammalian Target of Rapamycin (Akt/mTOR) signalling. Activated mTOR signalling is thought to mediate downstream repression of the stress response pathway known as autophagy, which is crucial for the clearance of cell debris. Crucially, IIS, Akt/mTOR and autophagy are implicated in heart disease phenotypes[147] and

accumulation of prelamin A and progerin has been implicated in the dysregulation of these pathways[148-150].

1.3.6 Summary of ageing mechanisms

There are many mechanisms associated with ageing per se, and evidence suggests that despite the obvious caveat that the myocardium is terminally differentiated, many of these are likely to be involved in the phenotypic and pathological changes that occur in ageing myocardium.

1.4 The nuclear envelope in health and disease

1.4.1 The nuclear envelope

As noted above, aspects of the NE have become the focus of ageing research. The stimulus for this has come from the discovery that a number of clinically distinct diseases, many exhibiting features of premature ageing and DCM, arise as a result of mutations in proteins that comprise and/or maintain the NE[17, 151-155].

The NE (Fig 1.3) primarily consists of an outer nuclear membrane (ONM) and an inner nuclear membrane (INM) that are separated by a ~50 nm luminal gap known as perinuclear space (PNS). These two lipid membranes serve to provide a physical barrier between the nucleoplasm and cytoplasm, thus facilitating compartmentalisation of the nuclear environment. Additionally, the NE is punctured with nuclear pore complexes (NPCs), which facilitate the trafficking of macromolecules across the NE. Structurally, the ONM is continuous with the endoplasmic reticulum (ER) with which it shares many

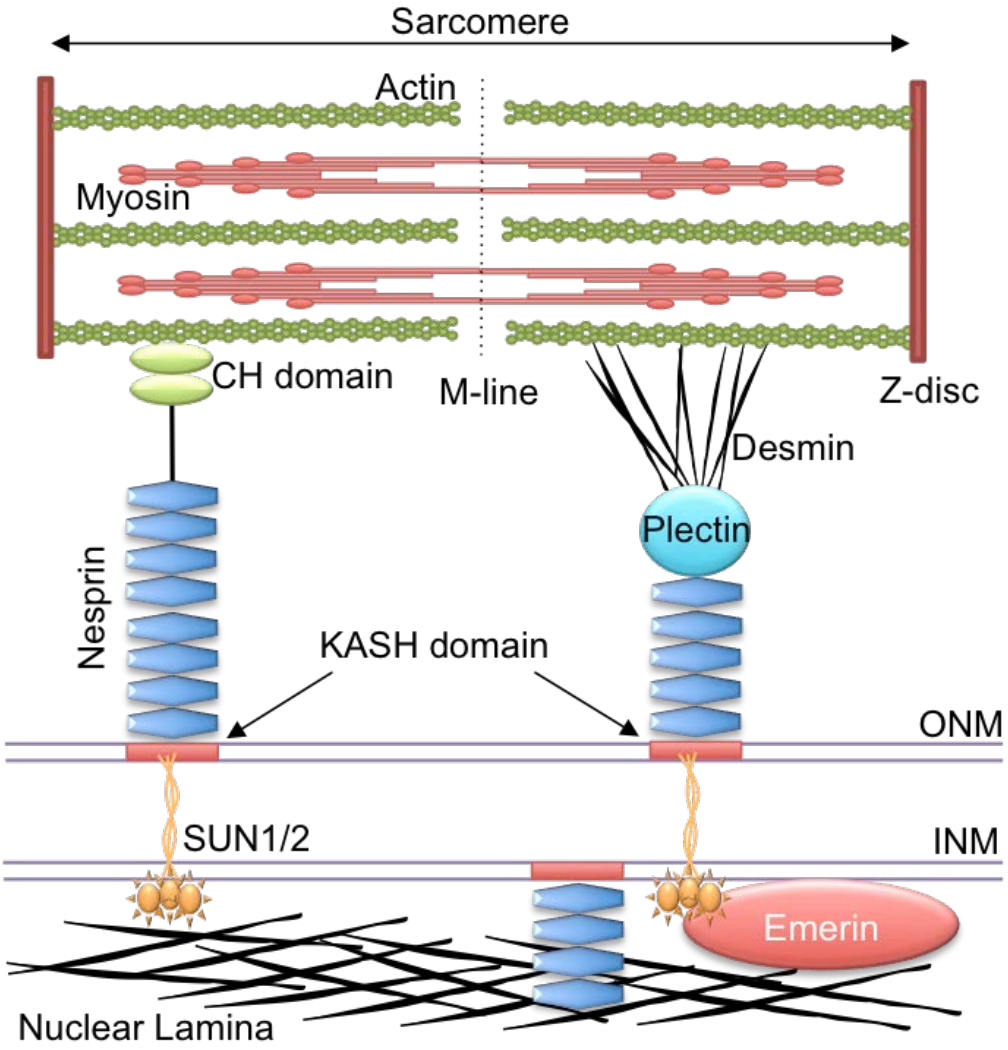

Figure 1.3 The nuclear envelope in CMs. The nuclear envelope provides a physical barrier for nuclear compartmentalisation and a platform for communication between the nucleus and cytoskeletal domains via a group of proteins termed the LINC complex. The outer nuclear membrane (ONM) contains the KASH domain proteins, nesprins, which bind to cytoplasmic filament proteins such as actin. The inner nuclear membrane (INM) contains SUN proteins and LEM domain proteins that connect the KASH domain to the nuclear lamina, consisting of lamins A, C and B. In CMs, it is thought that the NE is connected to the sarcomere by the LINC complex via CH domains in the N-termini of nesprins and also via plectin and desmin. The LINC complex plays a key role in nuclear integrity and is also thought to regulate transcription, DDR and mitosis. Mutations to LINC proteins are known to causes a plethora of disease phenotypes known as laminopathies, often characterised by premature ageing or cardiomyopathy.

of the same membrane proteins including FACE1 and KASH domain proteins such as nesprins, which also contain calponin homology domains and bind with cytoplasmic actin, thereby providing a link to the cytoplasmic domain[156-159]. In contrast, the INM has a set of distinct membrane associated proteins that include lamina associated polypeptide 2 (LAP 2), emerin and MAN1 (collectively termed the LEM domain proteins)[160] and SUN proteins, which bind the KASH domains and mediate physical communication between nesprins and the lamina[161]. The nuclear lamina is a meshwork of proteins lining the nuclear interface of the INM, and consists of type V IF proteins known as A- and B-type lamins, which form parallel coiled-coiled dimers and head to tail dimers to produce a large network that covers the entire INM[162]. The predominant A-type lamins are lamin A and lamin C and are alternative splice products of the same gene, *LMNA*[163]. Unlike lamin A, lamin C is translated as a mature protein, whereas lamin A is translated as a precursor, prelamin A, which must undergo a number of modifications before becoming mature lamin A[164]. B-type lamins are lamin B1, arising from the *LMNB2* gene, and lamins B2 and B3 from the *LMNB3* gene[165]. Whilst A-type lamins are thought to be specific to differentiated cell types, B-type lamins are thought to be present ubiquitously[166]. The sequential tethering of these NE spanning proteins is thought to be crucial for rapid physically mediated communication to the nucleus from the cytoplasmic and extracellular environment and is known as the linker of nucleoskeleton to cytoskeleton (LINC) complex[1].

The current dogma stipulates that the NE is crucial for mechanical stability, mechanical signalling, transcriptional regulation and DDR. The importance of the NE is highlighted by DCM causing mutations in genes of NE components emerin and lamin A/C that lead to uncoupling of the nucleoskeleton from the cytoskeleton under

mechanical stress[167]. Additionally, *Lmna*$^{-/-}$ and *Sta*$^{-/-}$ (*STA* encodes emerin) fibroblasts show impaired mechanotransduction in single cell models of mechanical stretch[168, 169]. It has also been shown that the NE may be able to detect perturbations in force and convert these perturbations into adaptive or pathological gene expression responses[126, 170, 171]. Finally, it is well documented that disrupting the nuclear lamina leads to large increases in DNA damage and inhibition of repair[172-174]. The consequences for disrupting these processes can be seen in cases of mutations to lamina-associated genes, which lead to pathological outcomes that have come to be known as laminopathies.

1.4.2 Laminopathies

It has been postulated that rare genetic conditions leading to premature ageing may give insights into normal ageing mechanisms[148]. There are to date at least 13 known disease phenotypes arising from mutations to the *LMNA* gene including Werner syndrome[175], Emery-Dreifuss muscular dystrophy[176] and the classical premature ageing disorder, HGPS[177] (Table 1.1). Furthermore, as previously mentioned, a search on the Universal Mutation Database brings up 132 unique mutations believed to be responsible for causing DCM (http://umd.be/LMNA/).

1.4.3 Mechanistic basis of laminopathies

1.4.3.1 Genotype phenotype correlations

Genotype phenotype correlations are often useful tools for aiding the elucidation of pathogenic mechanisms in the clinic. For example, mutations to *ZMPSTE24* have been

Table 1.1 Laminopathies

Disease	Gene	Reference
Atypical Werner syndrome	*LMNA*	Chen et al[178]
Charcot-Marie-Tooth disease	*LMNA*	De Sandre-Giovannoli et al[179]
Dilated Cardiomyopathy	*LMNA*	Charniot et al[180]
Emery-Dreifuss muscular dystrophy	*EMD* (X-linked), *LMNA* (autosomal dominant)	Bonne et al[152]
Familial partial lipidodystrohy of the Dunningan type FPLD	*LMNA*	Cao et al[153]
Hutchinson-Gilford progeria syndrome	*LMNA, ZMPSTE24*	Eriksson et al[155]
Limb-girdle muscular dystrophy	*LMNA*	Muchir et al[181]
Lipoatrophy with diabetes, hepatic steatosis, hypertrophic cardiomyopathy and leukomelanodermic papules (LDHCP)	*LMNA*	Caux et al[182]
Mandibuloacral dysplasia with type A lipodystrophy (MADA)	*LMNA*	Novelli et al[183]
Mandibuloacral dysplasia with type B liodystrophy (MADB)	*LMNA*	Agarwal[151]
Restrictive Dermopathy	*ZMPSTE24*	Navarro[184]

shown to correlate to disease severity. Mutations that caused a complete loss of function to FACE1 led to the neonatally fatal disease restrictive dermopathy (RD), whereas mutations in which there was residual FACE1 activity led to less severe disease types, such as atypical HGPS and mandibuloacral dyslasia (MAD)[185]. However, in the case of *LMNA*, the picture is not so clear. There are a subset of Laminopathies which are caused by a few 'hot spot' mutations which lead to specific phenotypes and are likely to share mechanistic traits[186]. These include classical HGPS, Werner syndrome, Charcot- Marie-Tooth disorder, and MAD. However, the more common laminopathies, which are primarily striated muscle disorders, e.g. autosomal EDMD, limb girdle muscular dystrophy (LGMD1B) and DCM, are caused by seemingly indiscriminate and promiscuous mutations which present fewer clues as to the mechanisms involved. For example, mutations that cause DCM have been found in all 12 exons of the *LMNA* gene (http://www.umd.be/LMNA/, search in "mutations" using terms "phenotypic group", "contains", "DCM"). Moreover, mutations that cause DCM can also cause EDMD, LGMD1B and FPLD in separate individuals or can lead to any of these diseases with associated DCM. The level of pleiotropy seen with some of these mutations is unusual. Indeed, one curious mutation to the *LMNA* gene, R644C, displays extreme phenotypic diversity in the clinic[187]. These findings suggest that epigenetic or other extrinsic factors may be important in disease pathogenesis and/or progression where lamins are concerned. Discussed herein are examples of the efforts made to solve the pathways of disease in the cases of HGPS, which has a consistent genotype phenotype link, and DCM, which does not.

1.4.3.2 Prelamin A processing and HGPS

HGPS patients are asymptomatic until around 2 years of age. From this point the disease progresses quickly. Phenotypically, patients display loss of subcutaneous fat, brittle skin, prominent scalp veins, micrognathia, convex nasal profile, hair loss and skeletal dysplasia[188-192]. These features compelled Hutchinson, in 1886, to report that his patient, a 3½ year old boy, 'presented a very peculiar withered, old-mannish look'[193]. Subsequently, HGPS patients die in the second decade of life primarily due to cardiovascular complications, usually in the form of an ischaemic event, a myocardial infarction or stroke. The disease is highly tissue specific, affecting mainly skin, bone and muscle. At a cellular level, the HGPS phenotype is typified by the presence of a protein termed progerin, the mutated form of the lamin A/C precursor, prelamin A[194]. Normally, prelamin A is processed by four post-translational steps to produce mature lamin A (Fig 1.4). This process begins with farnesylation (or isoprenylation) of a C-terminal cysteine thiol residue of a motif known as a *CaaX* box, which denotes the final four amino acids of the C-terminus[195]. This is followed by endoproteolytic cleavage of the remaining three amino acids of the C-terminus, known as AAXing, by a CaaX endoprotease, exposing the farnesylated cysteine residue[196]. Following AAXing the cysteine thiol is then further processed with the addition of a carboxyl methyl group by methyltransferases[197]. The final step is an upstream proteolytic cleavage of 18 amino acids between Tyrosine at position 646 and Leucine at position 647 in the amino acid sequence which releases mature lamin A[198], a step which is believed to be required for lamin A insertion into the nuclear lamina[197, 199, 200]. It has been discovered that this step

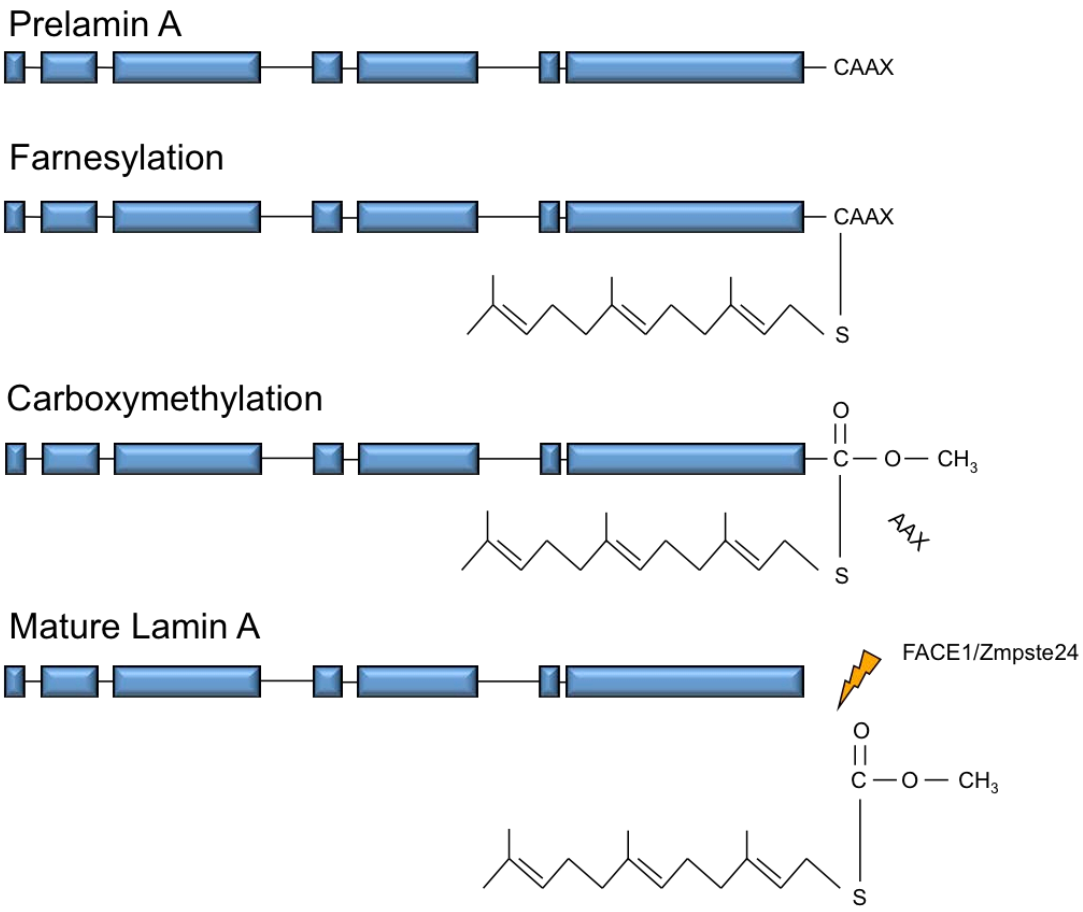

Figure 1.4. Prelamin A is processed by four post-translational modifications to produce mature lamin A. Firstly, farnesylation of the C-terminal cysteine from the CAAX motif occurs, which is followed by cleavage of the remaining three amino acids, then carboxymethylation of the cysteine, and finally cleavage of the entire farnesyl carboxymethylated tail. Mature lamin A is then inserted into the nuclear lamina to provide structure and mediate nuclear signalling.

is mediated and performed exclusively by the zinc metalloproteinase FACE1 transcribed from the *ZMPSTE24* gene[201]. Furthermore, FACE1 is also capable of performing the initial AAXing of the CaaX motif preceding carboxymethylation. In HGPS, the final enzymatic cleavage is abolished and the peptide remains permanently farnesylated, meaning it cannot be inserted efficiently or completely into the nuclear lamina[202]. In the most common form of HGPS, this occurs because of a single nucleotide C>T transition mutation in the *LMNA* gene, which confers no change to amino acid sequence (*LMNA* G608G), but that creates a donor splice site in exon 11 leading to a 50 amino acid deletion containing the FACE1 cleavage site[155, 203, 204]. The resulting truncated prelamin A mutant protein has been termed 'progerin'. It is also the case that loss of function mutations to *ZMPSTE24* lead to prelamin A accumulation and can also drive HGPS phenotypes in humans[205]. Consequently, cells expressing high levels of progerin or prelamin A display nuclear morphology defects, disorganised heterochromatin distribution and massive increases in DNA damage[172-174]. It is hypothesised that increases in DNA damage are caused by defective recruitment of DNA repair factors due to unstable heterochromatin caused by lamina disruption[206, 207]. Moreover, disruption to the lamina and subsequently the LINC complex is thought to have deleterious effects on mechanical coupling of cell compartments and subsequently lead to structural instability and susceptibility to mechanical load and stress[208]. Additionally, disruption to the lamina may impede mechanical signalling and regulation of mechano sensitive gene transcription[208]. Current understanding suggests that these may underlie most of the pathological processes of HGPS.

1.4.3.3 What attempts at therapeutic intervention have taught us about HGPS

A popular theory within the field of premature ageing suggests that accumulation of the farnesyl lipid anchor is central to accelerated ageing. This notion formed the basis for the development of treatments for progeroid syndromes with a group of compounds known as farnesyl-transferase inhibitors (FTIs). *In vitro,* FTIs lead to an almost complete rescue of the nuclear morphology defects associated with progerin/prelamin A accumulation and successfully delay the onset of senescence[209, 210]. Such findings prompted clinical trials for FTIs in progeria but have not led to a definitive cure[211]. It has been postulated that the low efficiency of FTI treatment is due to redundancy. In the event of farnesyl inhibition, the mutated progerin protein undergoes alternative gerangeranyltransferase mediated prenylation[212]. In this study, the authors show that combination treatment with aminobisphosphonates and statins ameliorate the progeria phenotype and increase longevity in a mouse model of human ageing. In light of these findings numerous models of progerin and prelamin A accumulation in various stages of processing have been developed. The Fong laboratory in California has performed much of the work to tease out the pathological significance of this. They have developed and tested an array of knockin/knockout mouse models in order to elucidate the role that prelamin A processing has in causing premature ageing diseases. In summary, *Zmpste24*$^{-/-}$ mice have no FACE1 expression, meaning the cleavage of prelamin A cannot occur. Consequently mice exhibit progeria like phenotypes[213, 214]. This has been phenocopied by a model of HGPS knock-in mice (*Lmna*$^{HG/+}$) and both these pathological presentations have been partially ameliorated by FTI treatment *in vivo*[215-217]. This indicated that the farnesyl tail of prelamin A was key to progeroid

phenotypes. Therefore, to further assess the role of the farnesyl lipid in progeroid syndromes, further knock-in models were developed. Non-farnesylated progerin (*Lmna*$^{nHG/+}$) unexpectedly led to progeria, suggesting that the farnesyl lipid was not as important to the development of premature ageing as initially thought[218]. However, a later model of non-farnesylated prelamin A (*Lmna*^{nPLAO}) failed to validate this observation as the mice were normal with regard to premature ageing but instead developed cardiomyopathy[219]. In light of this, another non-farnesylated progerin model (*Lmna*$^{csmHG/+}$) was developed[220] in which the mutation was a deletion of isoleucine from the *CaaX* motif (CSM) rather than the switching of the cysteine for serine (SSIM) as was the case for *Lmna*$^{nHG/+}$mice. This model led to complete amelioration of progeroid symptoms that once again supported the argument for FTI treatments but at the same time further increased the complexity of the pathological paradigm. Along with these, Fong *et al* have also made a lamin A only[221] model which bypasses normal prelamin A processing, and a lamin C only[222] model in which mice appear completely normal. These are interesting developments for the field of HGPS and premature ageing disorders because there appears to be some redundancy with regard to the A-type lamins, which brings into question the evolutionary purpose of prelamin A processing[223]. Additionally, this perhaps strengthens an argument for the toxic effects of mutant lamins and unprocessed prelamin A in a dominant negative manner. Indeed a cross of *Zmpste24*$^{-/-}$ and *Lmna*$^{+/-}$ mice leads to a reduction in prelamin A accumulation and amelioration of the progeroid phenotype and highlights the toxic nature of prelamin A[224]. These models are summarised in Table 1.2.

The current questions regarding the use of FTIs to treat HGPS are aimed at establishing why they do not completely abolish the symptoms. For example, whilst

Table 1.2. Overview of phenotypes associated with mouse models designed to elucidate the role of lamin processing in disease

Lmna deficiency	
Lmna$^{-/-}$	Normal at birth, develop Muscular Dystrophy and severe systolic dysfunction, live to 5-6 weeks[225, 226]
Lmna$^{+/-}$	Early onset cardiac conduction system (CCS) disease, DCM in advancing age[227]
Lamin C-only	
Lmna$^{LCO/LCO}$	Apparently normal[222]
Prelamin A-only	
Lmna$^{PLAO/PLAO}$	Only prelamin A made, which is subsequently processed by ZMPSTE24 to lamin A; apparently normal[219]
Mature Lamin A-only	
Lmna$^{LAO/LAO}$	Directly made lamin A which has bypassed prelamin A processing; apparently normal[221]
Non-farnesylated Prelamin A-only	
Lmna$^{nPLAO/nPLAO}$	Non-farnesylated prelamin A and unprocessed by ZMPSTE24; cardiomyopathy - males live to 40 weeks, whilst females live up to 80 weeks[219]
ZMPSTE24 deficiency	
Zmpste24$^{-/-}$	Progeroid phenotype—some reported cardiac manifestations at 16 weeks[214]
Zmpste24 $^{-/-}$ *& Lmna*$^{+/-}$	Apparently normal (rescue of Zmpste24$^{-/-}$ phenotype)[224]
Progerin	
Lmna$^{HG/+}$	Progeroid phenotype– subsequently die at 16 weeks[218]
Non-farnesylated Progerin	
Lmna$^{nHG/+}$	CSIM motif changed to SSIM; progeroid phenotype – subsequently die at 16 weeks[218]
Lmna$^{csmHG/+}$	CSIM motif changed to CSM; apparently normal[220]

FTIs rescue nuclear morphology defects, they do not prevent accumulation of DNA damage[172] and with increasing evidence pointing towards DDR in the onset of cellular senescence, the use of FTIs as a stand alone therapeutic is becoming increasingly questionable. Further elucidation of the pathways that result in pathogenesis is required to build a theoretical basis for successful treatment regimes, which would likely be combination therapies.

1.4.3.4 Mechanistic insight into *LMNA* associated DCM

As mentioned above, the importance of A-type lamins for cardiac health has been highlighted by the frequency of *LMNA* mutations that lead to cardiomyopathic presentation in the clinic. Moreover, HGPS patients were observed to suffer cardiomegaly and cardiac dilatation towards the end of life[228], and in a separate study HGPS patients who survived to older ages were observed to display cardiac remodeling and atrial enlargement[229]. Additionally, a number of animal models with modified *Lmna* genes have given detailed insight into the possible pathological mechanisms that arise from *LMNA* mutations. These are discussed below.

1.4.3.4.1 Lmna$^{H222P/H222P}$ mice

In the heart, many *LMNA* mutations have been shown to cause a variety of cardiomyopathies in humans[230, 231]. Of these, the *LMNA* mutation H222P has been extensively assessed *in vivo* using *Lmna$^{H222P/H222P}$* knock in mice[232]. Whilst these mice are born seemingly normal, at 16 weeks they display a classical DCM progression

leading to heart failure and death in males at 5-9 months and in females at 7-13 months. These mice experience a reduction in cardiac function (EF and FS) as well as cardiac fibrosis, which is thought to be triggered by increased nuclear translocation of Smad proteins and activation of TGFβ signalling[232]. Furthermore, elevation of ANP mRNA expression and dysregulation of myosin light chain 2 (MLC-2) and β-MHC mRNA expression indicates heart failure[233].

Biochemical analysis of the heart tissue suggests that mitogen activated protein kinase (MAPK) signalling is activated in these hearts, specifically the extracellular signal regulated kinase (ERK1/2) and c jun N-terminal kinase (JNK) branches of MAPK signalling. Pharmacological regulation of these pathways showed that a number of pathological mechanisms associated with DCM could be retrieved. Inhibition of JNK and ERK1/2 in mice significantly improved LV functional parameters, led to a reduction in fibrosis and collagen mRNA expression, normalised Myosin light chain (MLC) mRNA expression, and improved survival[234-236]. Moreover, the clinical relevance of activated ERK1/2 signalling in DCM has been confirmed in post mortem analysis of *LMNA* associated DCM cardiac tissue expressing alternative mutations, *LMNA* ΔK261 and *LMNA* IVS9 + 1g>a[237], and provides a potential therapeutic lead as Selumetinib, an ERK1/2 inhibitor, which is currently undergoing trials for treatment of cancer, currently reports improved survival rates and minimal adverse effects[238]. Additional analysis suggests a role for dual specificity phosphatase 4 (Dusp4), which is elevated in $Lmna^{H222P/H222P}$ mice. Conditional overexpression of Dusp4 leads to DCM similar to that of *LMNA* associated DCM and mechanistically results in activation of the Akt/mTOR signalling pathway and subsequently, negatively regulates autophagy[239]. Treatment of the $Lmna^{H222P/H222P}$ mice with an inhibitor of mTOR, temsirolimus,

subsequently led to activation of autophagy, coupled with amelioration of cardiac decline[240]

1.4.3.4.2 Lmna$^{-/-}$ mice

The observation that autophagic activity is impaired is mimicked in global *Lmna*$^{-/-}$ mice[241], which die between 6-8 weeks of age because of DCM and heart failure[225]. Moreover, intervention with the mTOR inhibitor rapamycin significantly improves cardiac function and survival in *Lmna*$^{-/-}$ mice, further strengthening the argument for mTOR signalling in *LMNA* associated DCM. Currently, modulation of Akt/mTOR signalling provides the most promising way forward for the treatment of *LMNA* associated DCM[242, 243].

Hearts of *Lmna*$^{-/-}$ mice also manifest a variety of other mechanistic traits that are important to consider. Phenotypically, *Lmna*$^{-/-}$ mice have irregular patterns of heart tissue histology and skeletal muscle dystrophy[226] and succumb to severe systolic dysfunction[225]. Detailed cardiac characterisation has shown *Lmna*$^{-/-}$ CMs to be mechanically unsound. They have nuclear morphology defects and appear to undergo disruption of the LINC complex via nesprin1α leading to uncoupling of the nucleus from the cytoskeleton resulting in mechanical instability and defective force transmission in CMs[244]. Additionally, the IF protein desmin, which serves to link sarcolemma to the sarcomere and also the sarcomere to the nucleus, is also heavily mislocalised in these mice and further supports this hypothesis[225]. Moreover, nuclear import of the lamin binding partner, sterol response element binding protein 1 (SREBP1) appears to be decreased along with peroxisome proliferator activated

receptor γ (PPARγ) expression. Activation of hypertrophic genes appears to be attenuated, and the suggestion is that *Lmna*$^{-/-}$ mice are unable to adapt to DCM progression with compensatory hypertrophy, which accounts for the speed of disease progression and short lifespan. Another key observation in *Lmna*$^{-/-}$ mice is that they also exhibit disorganisation and loss of connexins in the myocardium which would cause inhibition of cardiac conduction and may contribute to reduced force of contraction[245, 246]

1.4.3.4.3 Lmna$^{N195K/N195K}$ mice

The lamin A N195K mutation is known to cause DCM with conduction defects in humans[247]. *Lmna*$^{N195K/N195K}$ mice developed DCM with associated conduction defects and died at 2-3 months old as a result of arrhythmia[248]. This was associated with increases in ANP and BNP as well as increased interstitial fibrosis and abnormal desmin localisation. Moreover, *Lmna*$^{N195K/N195K}$ mice experience loss of Connexins 40 and 43, which accounts for reduced contractility and arrhythmia. Conduction defects could also be explained by an observed reduction in mRNA of *HF1b/Sp4*, a transcription factor that is important in the development of the cardiac conduction system[249].

1.4.2.3.4 Lmna$^{\Delta K32/+}$ mice

A crucial problem with many of the model systems of *LMNA* associated DCM is that most only show phenotypic changes when the mutation is homozygous, whereas in the

clinic, *LMNA* disease mutations are almost always heterozygous, leading to autosomal dominant phenotypes. Recently however, *Lmna*$^{\Delta K32/+}$ mice were investigated and found to be pathogenic[250]. Deletion of lysine at position 32 in the lamin A amino acid sequence is known to cause severe congenital muscular dystrophy phenotypes in humans[251]. Interestingly, these mice presented with a DCM manifestation that occurred in a stepwise fashion with two distinct pathomechanisms resulting in death between 35 and 70 weeks. The first mechanism observed that 'toxic' accumulation of ΔK32-lamin was avoided by degradation but led to a resultant decrease in lamin A/C expression, which, it was believed, began the process of cardiac remodelling and DCM. Secondly, the authors observed that after DCM was established, lamin A/C levels normalised. This was coupled with dysfunction of the ubiquitin proteasome system (UPS) and an increase in ΔK32-lamin, thereby worsening the dominant negative effect of ΔK32-lamin.

1.4.2.3.5 Lmna$^{MHC\text{-}M371K}$ mice

Another study that has circumvented the autosomal dominant problem looked at *Lmna*$^{MHC\text{-}M371K}$ mice. M371K substitution in the amino acid sequence of lamin A was shown to cause EDMD in humans[252]. In the mouse model, mutant DNA was incorporated onto the MHC promoter, creating a cardiac specific overexpression model in which wildtype lamins were unaffected. These mice had a very low survival ratio of 0.07 and those that did survive succumbed between 2-7 weeks from cardiac defects[253]. The implications of this study are that accumulation of the mutant M371K-lamin is toxic even in the presence of endogenous wildtype lamins.

1.4.2.3.6 Other lamin associated models with cardiac defects

Other lamina associated models with cardiac presentation include *Lmna*$^{+/-}$ mice, which have early onset cardiac conduction system (CCS) disease and late onset DCM[227], which could be alleviated by exercise and β-blockers[254]. *Lmna*$^{L530P/L530P}$ mice were progeric and also showed a cardiac phenotype[255]. *Zmpste24*$^{-/-}$ mice showed fibrosis and lymphocytic infiltration of the myocardium and observed thinning of the ventricular wall, suggestive of cardiomyopathy[214]. Another study of interest showed that accumulation of non-farnesylated prelamin A led to DCM in mice expressing a homozygous 'non-farnesylated prelamin A only' allele[219]. This is interesting because the data imply that different stages of prelamin A processing may lead to diverse cellular responses.

1.5 The special case of prelamin A

1.5.1 The role of prelamin A in normal ageing

The most compelling evidence for the role of prelamin A in normal ageing comes from recent work done by Ragnauth *et al* who postulated that prelamin A acccumulation may have real implications for the biology of normal ageing[256]. Indeed they showed that prelamin A accumulation is a signature of senescence in VSMCs. Furthermore, this accumulation is initiated not by changes in prelamin A but by a downregulation of FACE1 activity, which is mediated by oxidative stress. Additionally, by inhibiting FACE1 using siRNAs in early passage (young) VSMCs, prelamin A accumulation can accelerate senescence phenotypes and disrupt mitosis. Finally, analysis of aged VSMCs

displaying increased levels of prelamin A showed increases in DNA damage signalling suggesting that prelamin A induced DNA damage, which was confirmed by comet assays. Importantly, it is thought that oxidative stress may play a role in regulating FACE1 activity although the precise mechanism is unknown. Evidence from a study which looked at fibroblasts isolated from young, old and centenarian patients supports this notion[257]. Cells assessed from old and young patients that were subject to replicative stress were found to accumulate prelamin A and became senescent, whilst centenarian cells accumulated prelamin A but did not become senescent. Furthermore, young and old cells subject to oxidative stress experienced decreased FACE1 expression and increased prelamin A expression, a response that was attenuated in centenarian cells. Additionally, in young and old cells that were allowed to recover from stress, expression levels returned to pre-treatment levels. These observations, coupled with the fact that prelamin A accumulation in centenarians is not associated with senescence, suggests that prelamin A accumulation is an adaptive response. The hypothesis that senescence is an adaptive response in order to combat the oncogenic hegemony associated with advancing age is not a new idea, but these data suggest that prelamin A accumulation is part of the mechanism. Another study investigated Zmpste24 mosaic mice, which were null for *Zmpste24* on the autosomal *Zmpste24* locus (Chromosome 4) but had an extra copy of *Zmpste24* placed on the X chromosome at the *Hprt* locus. Consequently, animals accumulated prelamin A in half of cells whilst the other half produced wildtype lamin A. The results were intriguing. Contrary to the original *Zmpste24*$^{-/-}$ model, mice were long lived, despite expressing prelamin A. The mechanism put forward by the authors was that non-progeric cells rescued the phenotype of progeric cells and that, as such, cell-extrinsic mechanisms were crucial in

the development of progeroid syndromes. Additionally, the authors discovered that prelamin A expression in these mice was anti-oncogenic, as they found that prelamin A was capable of preventing metastasis and therefore identified ZMPSTE24/FACE1 as a target for cancer treatment[258].

In summary, the paradigm that emerges suggests that the accumulation of prelamin A may be intended to be an adaptive response to confer resistance against cancer phenotypes. However, the acute implications for prelamin A accumulation are deleterious as they cause cellular senescence.

1.5.2 Is there a role for prelamin A in heart disease?

Evidence for a prelamin A centric role in cardiac disease is beginning to emerge. Clinically, HGPS patients have been shown to display a cardiac phenotype[228, 229]. Furthermore, in a mouse model of HGPS, *Lmna*$^{G609G/G609G}$ mice[259] showed compelling evidence for cardiac dysfunction as the mice developed bradycardia between 9-15 weeks coupled with a prolonged QRS complex, suggesting an inhibition of ventricular depolarisation. However, these mice did not appear to develop DCM. As mentioned above, *Zmpste24*$^{-/-}$ mice, which accumulated prelamin A, although not yet subjected to a detailed cardiac characterisation, showed evidence of myocardial disruption[214]. Furthermore, *Lmna*^{nPLOA} mice, which accumulated non-farnesylated prelamin A, led to DCM *in vivo*[219]. Moreover, DCM causing mutations have been shown to accumulate prelamin A in a variety of systems. *In vivo, Lmna*$^{MHC\text{-}M371K}$ mouse heart tissue expressed unprocessed prelamin A intermediates[253], whereas in isolated cell cultures, viral

transduction and expression of the R89L lamin mutant prevented prelamin A processing[260].

It is well established that global accumulation of prelamin A leads to premature ageing but, considering the current dogma that laminopathies are essentially a subset of premature ageing disorders, it is curious that researchers have never explored the notion of myocardial senescence in models of *LMNA* associated DCM. The observation that mTOR signalling plays a key role in *LMNA* associated DCM (mTOR is a famous ageing pathway) supports a myocardial senescence paradigm and, incredibly, there have been no published observations regarding DNA damage accumulation in *LMNA* models of DCM. Many of the DCM models show nuclear morphology defects and some show heterochromatin disorganisation. These phenotypic features are also observed in HGPS and are associated with the accumulation of DNA damage, and it is thought these processes underlie the premature senescence paradigm.

The pleiotropic effects of single *LMNA* mutations, such as the R644C mutation for example[187], suggested that external factors may be important in the establishment of disease, a hypothesis which is now backed by evidence which implies that cells with prelamin A variants are susceptible to environmental stresses[258]. The nature of these stresses may influence pathogenesis. Finally, if one considers this evidence and the notion that dilatation of the cardiac chambers is an end stage process of progressive heart disease, often occurring as a product of age, it could be postulated that *LMNA* associated DCM is a form of premature cardiac ageing.

In summary, current evidence displays a variety of nuanced cardiac manifestations arising from defective prelamin A processing. Moreover, DCM observed in the setting of *LMNA* mutations may be a pathologic end point of a senescence-like

phenotype. Focussed investigation is needed to confirm the importance of prelamin A accumulation in cardiac pathogenesis.

1.6 Aims of thesis

To study the significance of prelamin A accumulation, we decided to utilise a system of targeted transgenesis to assess the impact of prelamin A in cardiac tissue of mice. The human L647R-prelamin A variant, which has a mutation at the FACE1 cleavage site and cannot be processed to yield mature lamin A, has been studied extensively by viral transduction *in vitro*[124, 256]. In our study it was placed into the ROSA26 locus and driven by the ventricular myosin light chain (MLC2v) promoter for CM specific expression. In doing so, the autosomal *Lmna* locus remained unaffected and lamin A/C expression was maintained. Using this model I aimed to: 1) Characterise the functional significance of prelamin A accumulation in the heart *in vivo*; 2) Use *in situ/ex vivo* techniques to identify morphological and histological traits in order to elucidate a cellular phenotype; 3) Utilise fluorescence microscopy and biochemical assays to elucidate potential pathogenic mechanisms for prelamin A induced DCM.

Chapter 2: Materials and Methods

2.1 Materials

All reagents and solutions are detailed in table or list format below; materials and machines are incorporated within the Methods text.

Table 2.1 Reagents

Laboratory reagents	Source	Catalogue number
30% Bis-Acrylamide solution	BioRad	161-0158
5x buffer & RNase inhibitor kit	Promega	M1705
Ammonium Persulfate (APS)	Bio-Rad	161-0700
BDM (2,3-Butanedione monoxomine)	Sigma-Aldrich	B0753
Biotin-16-dUTP	Roche	11388908910
Bovine Serum Albumin (BSA)	Sigma-Aldrich	A4503
Bromophenol Blue	Sigma-Aldrich	11,439-1
Chloroform	Sigma-Aldrich	C2432
Citrate Buffer	Vector Laboratories	H-3300
Cobalt Chloride, Hexahydrate	Sigma-Aldrich	255599
Collagenase, Type II	Worthington	4167
Coomassie G-250 stain	Bio-Rad	161-0786
3,3'- Diaminobenzidine (DAB)	Vector Laboratories	SK-4100
DAPI (4',6'-Diamidino-2-Pheylindoledihydrochloride)	Sigma-Aldrich	D9542
DC Protein Assay	Bio-Rad	500-0113, 500-0114
DEPC-treated water	Invitrogen	750023
Di-methyl formamide	Sigma-Aldrich	D4551
Disodium Phosphate ($NaHPO_4$)	Sigma-Aldrich	S5136
DMSO (dimethyl sulfoxide)	Sigma-Aldrich	D8418
DNase I	Sigma-Aldrich	AMPD1
dNTPs master mix	Promega	NU-0010-10
DPX mountant	VWR International	360292F
Dulbecco's Modified Eagle's Medium	Sigma-Aldrich	D5671
Earl's Balanced Salt solution (EBSS)	Sigma-Aldrich	E6267
Enhanced Chemiluminescent (ECL) kit	Pierce	32106
Eosin	Raymond A Lamb Ltd	Lamb/100d
Ethanol (CH_3CH_2OH, EtOH)	Sigma-Aldrich	E7023
Ethidium Bromide	Sigma-Aldrich	E1510
Ethylenediaminetetra-acetic Acid (EDTA)	Sigma-Aldrich	E5134
Foetal Bovine Serum (FBS)	Sigma-Aldrich	F7524

Gelatin	Sigma-Aldrich	G1393
Glucose	VWR	101174Y
Glutaraldehyde (EM grade)	Agar Scientific	R1314
Glycine	Fisher Scientific	BP381-500
Harris' Haematoxylin	Raymond A Lamb Ltd	Lamb/230d
Heparin	Leo Laboratories	PL 0043/0041R
HEPES	Sigma-Aldrich	H4034
HEPES	Sigma-Aldrich	H3375
Hiperfect transfection reagent	Qiagen	301707
Hydrogen Chloride (HCl)	Sigma-Aldrich	320331
Isofluorane	Abbott	B506
Isopentane	Sigma-Aldrich	M32631
Isopropanol (C_3H_8O)	Sigma-Aldrich	I9516
L647R-*LMNA* Adenovirus	In-House	-
M-MLV Reverse Transcriptase	Promega	M1701
M199 media	Sigma-Aldrich	M4530
Magnesium Sulphate ($MgSO_4$)	Sigma-Aldrich	M-2643
Manganese chloride (MnCl2)	Sigma-Aldrich	244589
Methanol (CH_3OH,MeOH)	Sigma-Aldrich	322415
Milk (dried skimmed)	Marvel	Any good corner shop
Monopotassium Phosphate (KH_2P0_4)	Sigma-Aldrich	P5655
Mowiol	Calbiochem	475904
NP-40 alternative	Calbiochem	492016
Oligo (dT) primers	Promega	C1101
Optimal cutting tempaerature (OCT) compound	Sakura finetek	4583
Pancreatin	Sigma-Aldrich	P3292
Paraformaldehyde (EM grade)	Electron Microscopy Sciences	15715-5
Paraformaldehyde powder	Sigma-Aldrich	P6148
PBS tissue culture grade	Sigma-Aldrich	D1408
Penicillin-Streptomycin-Glutamine solution liquid	Invitrogen	10378-016
Pentobarbital	Animalcare	1409CE102
Phosphate buffered saline (PBS) tablets	Oxoid	BR0014G
phosphomolydbic acid	Sigma-Aldrich	HT153
Picric acid	Sigma-Aldrich	P6744
Potassium Chloride (KCl)	Sigma-Aldrich	P5405
Potassium hexacyano-ferrate (II) Trihydrate	MP Biomedicals	152560
Potassium hexacyano-ferrate (III)	MP Biomedicals	152559
Potassium Hydrogen Carbonate	Sigma-Aldrich	P9144
primers (ZMPSTE24)	Qiagen	QT00024627

Protease Inhibitor Cocktail	Sigma-Aldrich	P8340
Protein standards (Precision Plus Protein™ Dual Colour Standards	Bio-rad	161-0374
PVDF membrane (Immobilon-P™)	Millipore	IPVH00010
Random Primers	Promega	C1181
RNA STAT-60™	AMS Biotechnology Ltd	CS-110
RNase away	Molecular Bioproducts	7003
SDS	Fluka Analytical	05030
Sirius red (Direct Red 80)	Sigma-Aldrich	365548
Sodium Cacodylate, Trihydrate	Sigma-Aldrich	C0250
Sodium Chloride (NaCl)	Sigma-Aldrich	S7653
Sodium Chloride (NaCl)	Sigma-Aldrich	S5886
Sodium Citrate, Trihydrate	Sigma-Aldrich	A4034
Sodium fluoride (NaF)	Sigma-Aldrich	201154
Sodium Hydrogen Carbonate	Sigma-Aldrich	S5761
Sodium orthovanadate (Na_3VO_4)	Sigma-Aldrich	S6508
SYBR green qPCR master mix	Eurogentec	RT-SY2X-03+NRWOUB
Taurine	Sigma-Aldrich	T-8691
TEMED	Bio-Rad	161-0801
Terminal transferase (TdT)	Roche	03333566001
Triton-X 100	Sigma-Aldrich	X100
Trizma™ base	Sigma-Aldrich	T6066
Trypsin (phenol red free) 10x	Invitrogen	15400-054
Trypsin 1x-EDTA solution	Sigma-Aldrich	T3924
Tween 20	Sigma-Aldrich	P2287
Urea	Sigma-Aldrich	U6504
VECTASTAIN ABC kit, Anti-Goat	Vetor Laboratories	PK-4005
X-gal (5-Bromo-4-chloro-3-indolyl β-D-galactopyranoside)	Sigma-Aldrich	B4252
Xylene	Sigma-Aldrich	534056
β-Mercaptoethanol (C_2H_6OS, βME)	Sigma-Aldrich	M6250

Table 2.2. Antibodies used for this investigation. WB = western blot, IF = immunofluorescence, IHC = immunohistochemistry

Primary Antibodies	Source	Dilution (WB)	Dilution (IF)	Dilution (IHC)
CD45	Abcam	1:1000	1:100	-
Cleaved Caspase3	Cell Signaling 9661	1:1000	-	-
Cleaved LC3 II	Abgent AP1805a	1:500	-	-
Connexin 43	Zymed 71007	1:100	1:100	-
Desmin	Dako M0760	1:100	1:100	-
Emerin	Leica Biosystems NCL-Emerin	1:500	-	-
GAPDH	Sigma-Aldrich G8795	1:1000	-	-
KDEL	Enzo life sciences ADI-SPA-827	1:2500	-	-
Lamin A/C (N-18)	Santa Cruz Biotechnology sc-6215	1:1000	-	-
Lamin B1	Abcam ab16048	1:1000	1:1000	-
Myomesin B4	E.Ehler (homemade)	1:1000	1:100-200	-
Nesprin 1α N3	Homemade	1:1000	-	-
Nesprin 2 N3	Homemade	1:1000	1:100	-
p-H2AX	Cell signalling 9718	1:1000	1:1000	-
p16	Cell signalling 4824	1:1000	-	-
p21	Cell signalling 2947	1:1000	-	-
p53	Cell signalling 9282	1:1000	-	-
p65	Santa cruz Biotechnology sc-372	1:500	1:200	-
Prelamin-A (C-20)	Santa Cruz Biotechnology sc-6214	1:200	1:1000	1:250
SUN 2	Abcam ab65447	1:100	1:100	-
Zmpste24/FACE1	Novus Biologicals NB100-2388	1:200	1:100	-
α-actinin	Sigma-Aldrich	1:1000	1:250	-

	A5044			
β-actin	Sigma-Aldrich A5316	1:10,000	-	-
Secondary Antibodies	**Source and cat number**	**Dilution (WB)**	**Dilution (IF)**	**Dilution (IHC)**
Anti-goat Alexa fluor 488.	Invitrogen A-11055	-	1:1000	-
Anti-goat Alexa fluor 568	Invitrogen A-11057	-	1:500	-
Anti-goat IgG HRP-conjugated	Sigma-Aldrich A5420	1:5000	-	-
Anti-mouse Alexa 488	Invitrogen A11004	-	1:1000	-
Anti-mouse Cy3	Jackson Laboratories 715-150-150	-	1:1000	-
Anti-mouse IgG, HRP-conjugated	GE healthcare NA931	1:5000	-	-
Anti-rabbit Alexa fluor 488	Invitrogen A-11011	-	1:1000	-
Anti-rabbit IgG, HRP conjugated	GE healthcare NA9340	1:5000	-	-
Biotinylated anti-goat	VECTASTAIN ABC kit (see reagents)	-	-	1:500
IRdye 800 Anti-goat	LICOR 926-32214	1:15000	-	-
IRdye 800 Anti-mouse	LICOR 926-32210	1:15000	-	-
IRdye 800 Anti-rabbit	LICOR 926-32211	1:15000	-	-
IRdye680 Anti-rabbit	LICOR 926-68073	1:15000	-	-

2.1.1 Solutions

(final concentrations dissolved in ddH_2O, unless otherwise stated)

1x Phosphate buffered Saline (PBS)

1 PBS pellet/100ml ddH_2O

1x Phosphate Buffered Saline with Tween (PBS-T)

1xPBS, 0.001% Tween-20

1x Tris Buffered Saline (TBS)

50 mM Tris-HCl pH 7.5, 150 mM NaCl

1x Tris Buffered Saline with Tween (TBS-T)

1x TBS, 0.001% Tween-20

1x Transfer Buffer

25 mM Tris, 192 mM glycine, 10% methanol

1x Running Buffer

25 mM Tris, 192 mM glycine, 0.1% SDS

1x Tris-Acetate-EDTA (TAE) Buffer

40 mM Tris-acetate, 1 mM EDTA

5x SDS-PAGE sample loading buffer (10 ml)

60 mM Tris-Cl pH 6.8, 2% SDS, 10% glycerol, 5% β-mercaptoethanol, 0.01% bromophenol blue

ADS Buffer

116 mM NaCl, 20 mM HEPES, 1 mM NaH_2PO_4, 5 mM Glucose, 5.4 mM KCl, 0.8 mM $MgSO_4$ -> pH=7.35 (NaOH). Filter sterilized.

Agarose gel

1.5% molecular grade agarose, 1x TAE

Blue Wonder Sample loading buffer

3.7 M urea, 134.6 mM Tris pH 6.8; 5.4% SDS; 2.3% NP-40; 4.45% beta-mercaptoethanol; 4% glycerol and 6 mg/100 ml bromophenolblue

Enzyme reagent

4 % Terminal transferase (TdT) in TdT storage buffer

Enzyme Solution (75 ml)

61.5 mg Collagenase (300 U/mg), 45.0 mg Pancreatin in 75 ml ADS buffer >Filter sterilized.

Formalin solution

4% Paraformaldehyde (w/v) in 1x PBS

Label reagent

0.4% Biotin-16-dUTP in TdT reaction buffer

Maintenance Media (500 ml)

400 mL DMEM #D5671, 100 ml Medium 199 #M2154, 5 ml Pen/Strp/Glutamine 100x

Membrane blocking buffer

5% milk, 1x TBS-T

Mowiol Mounting Media (25 ml)

32 µM Mowiol, 2.67 M Glycerol 6ml ddH_2O. Mix and leave ON. Add 13 ml 0.2 M TRIS pH 8.5, Stir at 50°C until dissolved.

Physiological saline solution (PSS)

113 mM NaCl, 4.7 mM KCl, 1.2 mM $MgSO_4$, 0.6 mM Na_2HPO_4, 0.6 mM KH_2PO_4, 12 mM $NaHCO_3$, 10 mM $KHCO_3$, 30 mM Taurine, 10 mM HEPES.

Plating medium

340 ml DMEM #D6546, 85 ml Medium 199 #M2154, 50 ml Horse serum, 25 ml Non-Heat inactivated FBS, 5 ml Pen/Strp/Glutamine 100x.

Radioimmunoprecipitation (RIPA) buffer (100 ml)

100 µl NP-40, 0.5% Sodium deoxycholate, 100 µl 10% SDS, 98.4 ml 1x PBS

SDS-PAGE Stacking Gel (5%)

331 mM Bis-acrylamide, 62.5 mM Tris pH 6.8, 0.1% APS, 0.1% SDS, 0.01 % TEMED

SDS-PAGE Resolving Gel (8%)

525 mM Bis-acrylamide, 375 mM Tris pH 8.8, 0.1% APS, 0.1% SDS, 3.4 mM TEMED

SDS-PAGE Resolving Gel (10%)

641 mM Bis-acrylamide, 375 mM Tris pH 8.8, 0.1% APS, 0.1% SDS, 3.4 mM TEMED

SDS-PAGE Resolving Gel (12%)

778 mM Bis-acrylamide, 375 mM Tris pH 8.8, 0.1% APS, 0.1% SDS, 3.4 mM TEMED

SDS-PAGE Resolving Gel (12%)

973 mM Bis-acrylamide, 375 mM Tris pH 8.8, 0.1% APS, 0.1% SDS, 3.4 mM TEMED

Senescence associated β-Galactosidase solution

40 mM Citric acid/NaP, 5 mM KFeCN II, 5 mM KFeCN III, 150 mM NaCl, 2 mM MgCl, 0.1% X-Gal.

Stop wash buffer

300 mM NaCl, 30 mM $Na_3C_6H_5O_7$.

TdT reaction buffer

25 mM Tris-HCl, 200 mM $C_2H_7AsO_2$, 0.25 mg/ml BSA, 1 mM $CoCl_2$.

TdT reaction mixture

10% Enzyme reagent in label reagent

TdT storage buffer

60 mM K_2HPO_4, 150 mM KCl, 1 mM 2-mercaptoethanol, 0.5% Triton X-100, 50% glycerol. >pH 7.2 HCl

X-Gal solution

2% X-Gal (anhydrous) in Dimethylformamide.

2.2 Methods

2.2.1 *In vivo* studies

2.2.1.1 Generation of cardiac specific prelamin A transgenic mice

All procedures were performed in accordance with the Guidance on the Operation of the Animals (Scientific Procedures) Act, 1986 (UK Home Office). Our laboratory has previously shown that transduction of a viral plasmid vector containing uncleavable prelamin A leads to premature senescence of VSMCs[35]. The construct contains a mutated *LMNA* sequence resulting in the translation of a protein containing an arginine at position 647 in place of leucine, (L647R-*LMNA*) which is normally present in the wild type amino acid sequence. This allows the first cleavage step and prenylation to take place but not the final cleavage step, therefore resulting in a permanently farnesylated prelamin A protein. The toxic nature of this protein *in vitro* led to the hypothesis that *in vivo* expression would lead to a phenotype representative of premature ageing. Therefore, in collaboration with Taconic artemis GmbH, a conditional transgenic system was devised to assess the *in vivo* effects of uncleavable prelamin A expression. The system involves recombinase mediated cassette exchange (RMCE) of the Rosa26 gene whereby L647R-*LMNA* cDNA is inserted into an exchange vector containing a neomycin resistance gene, a strong CAGGS promoter sequence and a STOP cassette flanked by loxP sites (Fig 2.1). Electroporation into the embryonic stem (ES) cells of C57BL/6 mice led to site-specific recombination by the recombinases F3 and FRT. Neomycin resistant clones that had undergone RMCE were selected. After administration of hormones, superovulated BALB/c females were mated with BALB/c

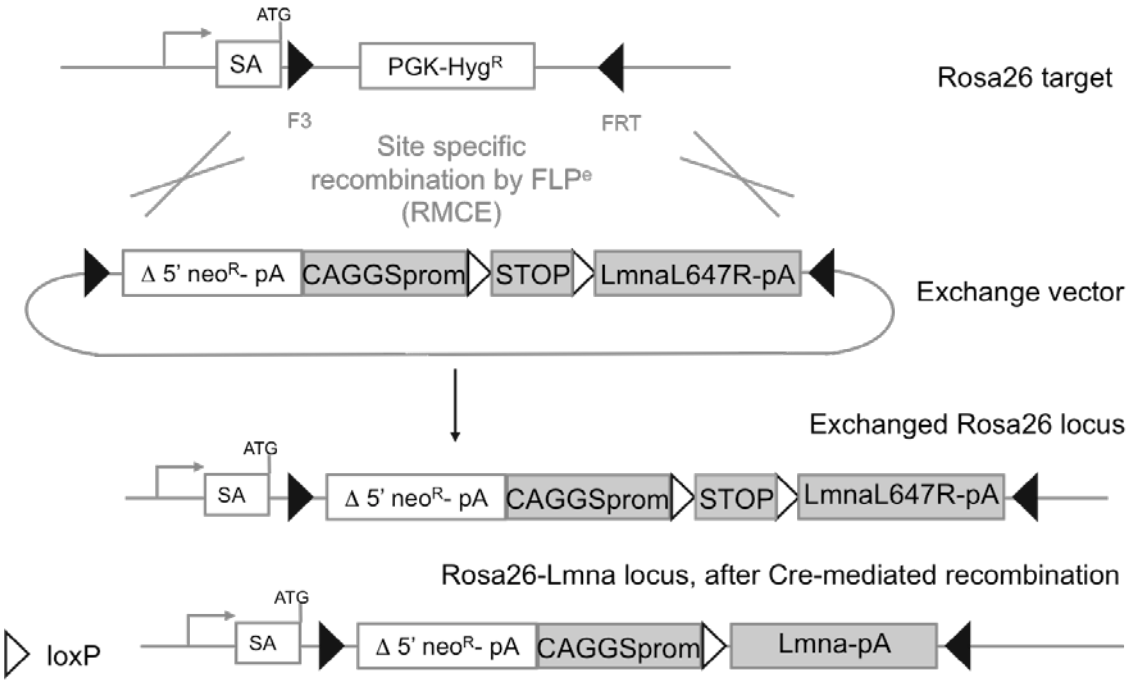

Figure 2.1. Generation of cardiac-specific L647R *LMNA* transgenic mouse line. Modified from: "Targeted Transgenic Mouse Models" (URL: http://www.taconic.com/CMGS/TransgeneExpression/TargetedTransgenesis). SA: Splice Acceptor site, pA: Polyadenylation signal, STOP: Transcription termination site, CAGGSprom: CAG promoter, neo^R/Hyg^R: Neomycin/Hygromycin B resistance gene.

males. Blastocysts were isolated from the uterus at 3.5 days post coitum (dpc) for microinjection. Blastocysts were placed in a drop of DMEM with 15% FCS under mineral oil. A flat tip, piezo actuated microinjection-pipette with an internal diameter of 12-15 µm was used to inject 10-15 targeted C57BL/6NTac ES cells into each blastocyst. After recovery, 8 injected blastocysts were transferred to each uterine horn of 2.5 dpc, pseudopregnant NMRI females. Chimerism was measured in chimeras (G0) by coat colour contribution of ES cells to the BALB/c host (black/white). Highly chimeric mice were bred to strain C57BL/6 females.

2.2.1.2 Genotyping

For genotyping, DNA was isolated from ear biopsies by incubation in 300 µl 50 mM NaOH at 95°C for ~5 min followed by vortexing and addition of 25 µl Tris-HCL pH 8. Genotyping for transgene identification was achieved with primers (Table 2.3) designed to identify the wildtype Rosa26 and L647R-*LMNA* modified Rosa26 alleles simultaneously. PCR was achieved with 5 µmol primers (1 µl 100 µmol stock solution), 2 µl DNA, 10 µl of 2x PCR master mix containing dNTPs, MgCl, 2x buffer concentration and loading dye, made up to 20 µl with ddH_2O. The contents of the reaction were mixed by pipetting up and down in a 0.2 ml thin-walled PCR tube and subjected to the following thermal cycling parameters: initial denaturation 95°C 1 min, denaturation 95°C 30 seconds*, annealing 60°C 30 seconds*, extension 72° 1 min*, final extension 72°C 10 min, cooled to 4°C indefinitely (*repeated for 35 cycles). PCR products were separated by agarose gel (containing $5x10^{-5}$ % ethidium bromide) electrophoresis and PCR products were visualised using UV detection. Mice positive

Table 2.3 List of PCR primers used in this investigation for genotyping

Primers	Sequence (5'-3')	Amplicon size (bp)
PLA Tg	F – GTGGATGCTGAGAACAGGC R –TCCACCTGGTCCTCATGC	Wt Rosa26 – 377 Modified Rosa26 – 200
Cre	F – TGCCAGGATCAGGGTTAA R – CCCGGCAAAACAGGTAGTTA	200
GAPDH	F – CGTAGACAAAATGGTGAAGG R – GACTCCACGACATACTCAGC	300

for the transgene were selected for breeding with mice expressing Cre recombinase. Identification of offspring was achieved by performing two separate PCRs: one to identify carriage of the transgene and one to identify Cre recombinase (Table 2.3). Mice positive for both the transgene and Cre were selected as experimental (PLA Tg) animals. Littermates positive for only the transgene were selected as wildtype (Wt) controls.

2.2.1.3 Echocardiography

Echocardiography was performed using a Vevo® 2100 imaging system with a 30 MHz linear transducer specially designed for small animal studies (VisualSonics, USA). Echocardiography was performed with 5% isofluorane fast induction of anaesthesia followed by maintenance of 1-1.5% isoflurane anaesthesia for 4 week old mice and 2.5% isofluorane for 2 week old mice, which was vaporized in 100% oxygen delivered at 1.5-2 liters/min. Heart rate was kept at ~400-450 beats per minute while respiratory rate was ~100 breaths per minute. Body temperature was ~36.5±1°C.

2.2.1.4 Magnetic Resonance Imaging (MRI) of hearts

Cardiovascular MRI was performed by Dr Andrea Protti on a 7 Tesla (T) horizontal MR scanner (Varian Inc., Palo Alto, CA) with mice in the prone position. The gradient coil had an inner diameter of 12 cm, the gradient strength was 1000 mT/m (100 G/cm), and rise-time was 120 ms. A quadrature transmit/receive coil (RAPID Biomedical GmbH, Germany) with an internal diameter of 39 mm was used. Anesthesia was maintained

with 1.5% isoflurane/98.5% oxygen and body temperature was maintained at 37°C using a warm air fan (SA Instruments, Stony Brook, NY). The ECG was monitored by means of two metallic needles placed subcutaneously in the front paws. A pressure-transducer for respiratory gating was placed on the animal abdomen. To synchronize data acquisition with the ECG and to compensate for respiratory motion, simultaneous ECG triggering and respiration gating (SA Instruments) were applied.

2.2.1.5 Harvesting of mouse heart

Mice were anaesthestised with 2% isofluorane. When unconscious, mice were removed from the anaesthesia chamber and subject to cervical dislocation. Mice were then laid on their back and secured to a dissection surface (cork or polystyrene). The chest cavity was then opened and held back with a hemostat. Prior to harvesting, a syringe was clamped approximately 1 metre above the dissection surface. It was fitted with plastic tubing capable of servicing the dissection area, which was in turn fitted with a needle at the end. The syringe was filled with a salt solution containing 5% KCl and 0.9% NaCl capable of arresting the heart in diastole. The reasoning for having a raised reservoir was to, in some way, mimic the perfusion pressure of blood flow into the heart and to maintain a consistent pressure and therefore preserve cardiac anatomy. The hearts were injected with the needle and the stop-cock turned to on. The hearts were perfused until they had ceased beating and were pale, indicating efficient removal of blood from the hearts. The hearts were excised and washed in cold PBS. They were blotted with tissue to remove excess fluid and then weighed (wet weight). The lungs were also excised, washed and weighed; the right hind limbs of the mice were removed; and the

gastrocnemius was trimmed from the tibia and the tibia was measured using calipers for morphometric analysis.

2.2.1.6 Morphometry

Mice were subject to observation and weighed regularly. When it became apparent that the phenotype of the PLA Tg mice was failure to thrive and premature death, it was decided that when the weight of a mouse fell below 75% of its Wt littermates, it was deemed to be suffering the maximal threshold of pain permitted on the project license and was culled. The age was recorded and used for Kaplan-Meier survival analysis. Post-mortem morphometry analysis was performed using heart and lung weight as well as tibia length.

2.2.1.7 Tissue fixation and processing

Post-PBS washing, tissue was placed in 1% Formalin solution at 4°C. Tissue was washed once in PBS and then placed into processing cages in 75% Ethanol. Tissues were subject to dehydration protocol and mounted in wax blocks. They were stored at room temperature for future use.

2.2.1.8 Tissue cryopreservation

Upon dissection and excision from the chest cavity, hearts were cryopreserved by immersion in isopentane whilst simultaneously immersing the container in liquid

nitrogen. Upon cessation of the gaseous plume emitted from the container of isopentane, the hearts were presumed frozen and transferred to a cryotube. The tubes were stored at -80°C.

2.2.2 *Ex vivo* studies

2.2.2.1 Human heart specimens

Human specimens were obtained by Dr Elisabeth Ehler from The University of Sydney, Australia via St Vincent's Hospital (Hospital Research Ethical Committee approval #H03/118; University of Sydney ethical approval #12146). Human materials were used in accordance with the ethical guidelines of King's College London (College Research Ethical Committee 04/05-74; REC reference 12/EM/0106) and the current UK law.

2.2.2.2 Sectioning of tissue mounted in wax blocks

Wax blocks were kept at -20°C for 1 hour prior to sectioning. A water reservoir was pre heated to 45-50°C. Upon removal from the freezer, the blocks were mounted onto a microtome rotary sectioner and slices were cut 7-10 μm thick. Slices were transferred to the water reservoir to allow any creases or folds to smooth out. The slices were then mounted onto high quality polylysine or superfrost slides and allowed to air dry on a surface heated to 45°C.

2.2.2.3 Sectioning of cryopreserved tissue

Tissue was removed from storage at -80°C and warmed to -20°C for approximately 1 hour. Tissue was then mounted onto the stage of a cryostat with OCT compound and allowed to equilibrate to the ambient temperature of the cryostat for 5 min; for cutting heart tissue or skeletal muscle, the stage temperature was set to -22°C and the knife was set to -20°C. The sections were then cut to 10 μm thick and mounted onto high quality polylysine or superfrost slides. The sections were allowed to air dry for approximately 1 hour and then stored at -80°C.

2.2.2.4 Indirect immunofluorescence of cryosectioned tissue

Sections were allowed to dry completely and fixed by immersion, in a coplin jar, in pre cold 100% methanol at -20°C for 5 min or 4% formalin for 10 min RT. Sections were washed 2x5 min in PBS. Sections were permeabilised in 0.5% NP-40 for 3 min RT and washed 3x5 min in PBS. Sections were blocked in 3% serum originating from a species to which the antibody was not raised against for 1 hour RT. Primary antibody was diluted appropriately in blocking solution applied to the sections and incubated in a humidified chamber overnight at 4°C. Sections were washed 3x5 min in PBS and secondary antibody conjugated to a fluorophore was diluted as appropriate, applied to the sections and incubated in the dark in a humidified chamber for 1 hour RT. DAPI was added 1:10,000 for 5 min at the end of the incubation for visualisation of nucleic structures. Sections were washed 3x5 min in PBS in the dark and then mounted in

mowiol mounting media and allowed to dry in the dark overnight. Antibody dilutions can be found in Table 2.2.

2.2.2.5 Homogenisation of Tissue

Cryopreserved heart tissue was homogenised by placement into a pre-liquid nitrogen cooled steel chamber (Independent metal worker) followed by crushing administered by a pre-liquid nitrogen cooled stainless steel rod (Independent metal worker) and rubber mallet (any good hardware store) and is henceforth referred to as the 'rod-in-chamber' technique.

2.2.2.6 Immunoblotting

Whole cell lysates were made by scraping cells into 100-150 µl RIPA lysis buffer and transferring to clean sterile tubes. Lysates were incubated for 5 min on ice. A protein assay was then performed to determine protein concentration and lysis buffer and/or 4x sample buffer was added to give a concentration of 1.5-2 mg/µl accordingly. Alternatively, tissue samples were homogenised using the 'rod-in-chamber' technique and 200 µl blue wonder sample buffer was added. The tubes were heated to 85°C for 5 minutes. A chamber was prepared with an SDS gel of 10% acrylamide concentration. 20µl was then loaded into each well of the gel. The proteins were separated at 150 mV. Transfer was achieved in wet conditions. The proteins were subject to electrophoretic transfer onto PVDF membranes that had been incubated in methanol for 20 seconds and then washed in distilled water. The transfer conditions were 65 Amps at 4°C ON. The

membrane was blocked for 1 hour with 5% Milk in TBS-T. Primary antibodies were added (Table 2.2) with TBS-T/5% milk and incubated overnight at 4°C. The membrane was washed 3x5 min with TBS-T. The blots were then incubated in secondary antibody coupled to horseradish peroxidise for 1 hour at room temperature or secondary antibody conjugated to a fluorophore for 1 hour. The blots were again washed with TBS-T and bound antibody was detected by ECL plus western blotting analysis system. Signals were detected by exposure to X-ray film. In the case of fluorophore conjugated secondary antibodies, an Odyssey® scanning detection system (LI-COR Biosciences, U.S.A) was used to detect signals. Western blots were quantified using ImageStudio™ software (LI-COR Biosciences, U.S.A).

2.2.2.7 Extraction of RNA from tissue samples

200 µl RNA stat-60™ was placed onto the homogenate and allowed to freeze. The pellet was removed, placed into a cryo-tube and allowed to thaw, and an additional 800 µl of RNA stat-60™ was added. The homogenate was kept at room temperature for 5-10 min to allow dissociation of nucleoprotein complexes. The samples were then frozen overnight at -80°C and thawed the following day. After thawing, 0.2 ml of chloroform was added, and then the tubes were closed tightly and shaken vigorously for 15+ seconds. The samples were left to incubate for 2-3 min RT. The homogenate was then centrifuged at 12,000 g for 10 min at 4°C. After centrifugation, two phases were discernable: a lower red phenol chloroform phase and a colourless upper aqueous phase. The upper aqueous phase containing uncontaminated RNA was carefully pipetted and transferred to a fresh tube and mixed with 500 µl of isopropanol. Samples were

incubated for 10 min RT and then centrifuged at 12,000 g for 5 min at 4°C. After centrifugation, a white pellet containing RNA remained. The supernatant was then carefully removed and the pellet washed once with 75% ethanol and vortexing. The pellets were centrifuged at 7,500 g for 5 min at 4°C and the supernatant discarded. The pellets were allowed to air-dry before solubilisation in 30 µl of DEPC treated water. RNA yield was determined by Nanodrop ND 1000 (Labtech International).

2.2.2.8 Making complementary DNA from RNA

2 µg RNA was diluted into 10 µl of double distilled (dd) H_2O. 0.3 µl Oligo dT primer, 0.3 µl random primer and 1µl dNTPs was added to this and heated to 65°C and then cooled to 4°C in a thermocycler. 4 µl 5x Buffer, 3.9 µl DEPC-treated H_2O and 0.5 µl reverse transcriptase (M-MLV) was added and samples were heated in a thermocycler to 25°C for 10 min, 37°C for 50 min and cooled to 4°C. After the reaction, the samples were diluted to 100 µl total volume for qPCR.

2.2.2.9 Quantitative (q)PCR

qPCR was carried out using the ΔCt and standard curve methods. When the ΔCt method was used the primers had been pre-validated and were part of a standard protocol for the lab.

9 µl cDNA was added to 10 µl 2x Sybr green PCR master mix and 5 µmol of forward and reverse primers (Table 2.4). Cycling parameters were 94°C for 15 seconds, followed by single-step annealing and extension at 60°C for 1 min (35 cycles).

Table 2.4 List of qPCR primers used in this investigation

Primers	Sequence (5'-3')
ANP	F – CGTGCCCCGACCCACGCCAGCATGGGCTCC R –GGCTCCGAGGGCCAGCGAGCAGAGCCCTCA
BNP	F –AAGGGAGAATACGGCATCATT R – ACAGCACCTTCAGGAGATCCA
α-MHC	F – CAGAGATTTCTCCAACCCAGCTGCG R – AGTCAGCCATCTGGGCGTCCG
β-MHC	F –AGCAGCAGTTGGATGAGCGACT R – CCAGCTCCTCGATGCGTGCC
GAPDH	F – CGTGCCGCCTGGAGAA R – CCCTCAGATGCCTGCTTCAC

Reactions were carried out in a Corbett RotorGene-3000. The cycle threshold (Ct) was determined manually as an arbitrary point during the linear phase of amplification and mRNA expression was quantified as a ratio of GAPDH expression. mRNA expression of PLA Tg groups was expressed as fold change compared to Wt groups.

2.2.2.10 Immunohistochemistry

Tissue samples were fixed in 4% PFA and dehydrated overnight. The samples were then embedded in wax blocks and cut to sections of 6 μM thickness and mounted on glass slides (superfrost plus, VWR International). Slides were baked at 60°C overnight. Tissue samples were rehydrated by incubation in xylene for 2x5 min and then sequential incubation in decreasing concentrations of ethanol (EtOH) 100%, 96% (3 min), 75%, 50% 25%, ddH_2O (1 min). Antigen unmasking was then achieved by heating the samples in a citrate buffer in a conventional vegetable steamer (Russell Hobbs) for 15 min. The lid was removed and samples allowed to cool for approximately 30 min. The samples were washed in TBS-T for 3x5 min followed by incubation in 3% H_2O_2 for 10 min. The samples were washed 2x5 min in TBS-T followed by 2x5 min in ddH_2O. Sections were then blocked 1 hour in normal goat or rabbit serum depending on the specifications of the primary antibody. Sections were washed 3x5 min in TBS-T and incubated overnight at 4°C. Primary antibodies were added as appropriate for 1 hour, RT. Sections were washed as before and secondary antibodies (Table 2.2) were added for 1 hour, RT. Sections were washed 3x5 min in TBS-T then incubated with ABC reagent (containing avidin DH and biotinylated horseradish peroxidase). The sections were washed 3x5 min in TBS-T then subject to incubation with the peroxidase substrate

solution DAB until the desired stain intensity had developed. Slides were lightly counterstained with eoisin's hematoxylin (1 min) washed briefly with acid alcohol and cleared with sequential ethanol incubations (50, 75, 96, 100%) and xylene, and then mounted with DPX.

2.2.2.11 Haemotoxylin and Eosin staining

Heart sections were subject to a haematoxylin and eosin staining procedure. After rehydration, sections were washed under running tap water for 5 min, and then placed in Harris' haematoxylin solution for 5 min. The sections were then washed under running tap water until the water ran clear followed by differentiation in acid alcohol. The sections were again placed under running tap water for 5 min and then stained with eosin solution for 3 min. The sections were dunked 5 times in tap water and then subject to dehydration in ethanol and clearance in xylene. Coverslips were mounted using DPX and allowed to dry overnight.

2.2.2.12 Picro-sirius red staining

Tissues were processed and rehydrated as previously described. After rehydration, slides were left under running tap water for 10 min. Slides were left in ddH_2O for 5 min followed by a 30 second incubation in 0.2% phosphomolybdic acid. Slides were rinsed in ddH_2O and then left in 1% Sirius red solution for 90 min. Slides were washed 2x2 min in acidified ddH_2O (0.05% acetic acid) followed by a 15 min incubatation in Picric acid. Slides were rinsed several times in ddH_2O followed by dehydration by sequential

ethanol treatment: 25%, 50%, 75%, 96% (1 min each) 100%, (2x3 min) xylene, (2x5 min) Glass coverslips were mounted with DPX and allowed to dry overnight.

2.2.2.13 Senescence associated β-Galactosidase assay

Hearts were cryosectioned into 5mm thick slices and mounted onto superfrost slides. Sections were allowed to dry for 30-60 min. Senescence associated β-Galactosidase (SA-β-Gal) staining solution was freshly made and applied to each heart section so that they were generously submerged (approx. 50 µl per heart section). The slides were incubated in a heavily humidified chamber overnight (approx. 16h) at 37°C. The slides were washed 2x5 min in PBS and once in 100% methanol for 2 min, the heart sections were then viewed and photographed under brightfield microscopy.

2.2.2.14 TUNEL staining

Deparaffinised sections were digested in 20 µg/ml proteinase K solution at 37°C for 10 min and washed 3x5 min in PBS. Sections were then incubated in 3% H_2O_2 for 10 min RT to block endogenous peroxidase activity and washed 3x5 min in PBS. Sections were then pre-incubated in TdT reaction buffer for 10 min RT and then incubated in TdT reaction mixture for 1 hour at 37°C in a humidified chamber. Sections were then washed in stop wash buffer for 10 min RT and rinsed in PBS-T 3x5 min. Sections were incubated with streptavidin-HRP for 20 min RT. Sections were incubated in DAB chromagen solution for 1-10 min (until brown staining appeared) and left under running

tap water for 5 min. Coverslips were mounted with DPX and allowed to dry for 2 hour or overnight (ON).

2.2.2.15 Transmission Electron Microscopy (TEM)

2 and 4 week old mice were injected intraperitoneally with heparin (5000 u/kg body weight). This was followed by intraperitoneal injection of 50mg/kg body weight of sodium pentobarbital to induce terminal anaesthesia. The chest cavity was opened and secured with a hemostat. The left ventricle was injected with a needle connected via a pump to a reservoir of pre-wash buffer. Flow rate of the pump was adjusted as to perfuse mouse heart at a pressure between 90-100 mmHg with pre-wash buffer. Pre-wash buffer was a standard physiological tyrode solution containing 10mM BDM to arrest the heart in diastole and 2.5% PVP to replace the protein content of blood, thereby maintaining colloidal pressure and preventing haemorrhage at vascular sites in the heart. By taking these measures, it was hoped that the cardiac ultrastructure would remain as intact as possible. Following prewash, the hearts were perfused with fixative solution containing 2% Glutaraldehyde and 2% Paraformaldehyde until 20ml of fix had been perfused. Hearts were dissected and the mid left ventricle was isolated and cut for further processing. Samples were dehydrated through a graded series of ethanol washes and embedded in epoxy resin. Semithin sections (0.2 μm) were stained with toluidine blue for light microscopy examinations and were used to guide sampling for TEM studies. Thin sections (0.09 μm) were collected on 150-mesh copper grids and double stained with uranyl acetate and lead citrate for examination under TEM (H7650, Hitachi, Tokyo, Japan). Dehydration, sectioning, and staining were kindly performed by

Dr Gema Vizcay at the Centre for Ultrastructural Imaging (CUI), King's College London.

2.2.3 *In vitro* studies

2.2.3.1 Isolation of neonatal rat CMs

Sprague dawley rat pups at 1-2 days old were individually subject to cervical dislocation, whereupon they were decapitated. Scissors were then used to open the chest cavity, the heart dissected out and placed in a 7ml bijous tube containing ADS buffer. After the hearts (approx. 11-12) were collected in the bijous tubes, they were finely diced using sharp scissors. Once the hearts were cut into small pieces, the ADS buffer was drained carefully in order not to discard any heart tissue and washed once in ADS buffer. The heart tissue pieces were then transferred to a 50 ml falcon tube using a sterile plastic pasteur pipette and subjected to an initial enzymatic digest in 5 ml of enzyme solution for 5 min at 37°C. The enzyme solution containing collagenase and pancreatin in ADS buffer was filter sterilized before use. After the initial digest, the heart tissue was resuspended 30 times using a sterile plastic pasteur pipette. The tissue was allowed to settle and the supernatant was removed carefully and discarded. The tissue was then subject to a second digest of the same parameters except that the supernatant was retained and placed into a 50 ml falcon tube containing 20 ml of plating medium. The digest was repeated and the supernatant collected in the same tube of plating medium as previously. The tube of plating medium was then passed through a cell strainer and spun at 1000 rpm RT for 5 min to pellet the cells. The cells were resuspended in 10 ml of plating medium and kept at 37°C. This process was repeated

twice more, at which point all tissue was adequately digested. After the final spin, the contents of the three falcon tubes containing plating medium and cells were combined in a T75 tissue culture flask and incubated for 1 h at 37°C, 5% CO_2 to allow fibroblasts to adhere to the plastic surface. After 1 h, NRCs which did not adhere to tissue culture plastic were removed and plated at approximately 400,000 per 10cm well of tissue culture dishes which had been pre coated with gelatin for at least 1 h 37°C. The cells were left overnight to adhere and the plating medium was replaced the following day with maintenance medium.

2.2.3.2 C2C12 Cell Culture

C2C12 mouse myoblasts are a cell line originally derived from dystrophic mouse skeletal muscle[261]. They were maintained in culture using DMEM with 20% FBS and antibiotics (PenStrepGlut) and kept at 37°C, 5% CO_2. They were grown to 80% confluence before passaging which occurred approximately every second day. To passage, cells were washed once in DPBS and then covered with 2.5 ml trypsin-EDTA for 5 min 37°C to lift cells from the tissue culture plastic. The cells were quenched with 7.5 ml DMEM 10% FBS and reseeded on fresh flasks at 1:10 dilution.

To induce the formation of myotubes, cells were grown to 60% confluency and then incubated with DMEM containing 2% Horse serum at 37°C 5% CO_2 for several days. Cells were observed daily for the formation of myotubes, the characteristics of which include a distinct change in morphology from rounded to spindle like cells and the presence of multi nuclei within the spindle like cells.

2.2.3.3 Viral transduction of L647R *LMNA* plasmid

NRCs were kept in serum free maintenance media in 35x10 mm dishes. Cells were counted and Adenoviral constructs containing mutated L647R-*LMNA* DNA were applied to the media with a multiplicity of infection of 5 viruses per cell for immunofluorescent staining readouts, and 10 viruses per cell for western blotting.

2.2.3.4 Indirect immunofluorescence of isolated cell cultures

Cells were grown on glass coverslips and fixed in 4% paraformaldedhyde (PFA) for 10 min or in methanoacetone for 2 min, and then washed three times in PBS. Cells fixed in formaldehyde were then permeabilised in 0.2% NP40 for 2 minutes and washed three times in PBS. Cells were then incubated for 1 h with 1% BSA in PBS at room temperature to prevent non-specific binding. The coverslips were incubated with primary antibodies (Table 2.2) overnight 4°C or for 1 h RT and then washed in PBS. They were then incubated with fluorescent secondary antibodies (Table 2.2) 1 hour RT and then DAPI diluted 1:10,000 5 min RT to visualise nucleic structures. The coverslips were then washed and mounted onto glass slides with mowiol fluorescent mounting media.

2.2.4 Microscopy

Immunohistochemical and general tissue staining was analysed by brightfield light microscopy using an Axioskop 2 microscope (Carl Zeiss MicroImaging, NY). Images

were acquired using Volocity Software (PerkinElmer Inc, USA). Immunofluorescence was analysed using widefield fluorescence microscopy whereas images were captured using a Leica SP5 confocal microscope (LeicaMicrosystems, UK). Confocal images were processed in Photoshop CS3 (Adobe) and minimal adjustments to brightness and contrast were made where necessary, e.g. when images were deemed too dark for comfortable viewing.

2.2.5 Statistics

All *in vivo* and *ex vivo* data of PLA Tg mice compared to Wt were analysed using the Student's unpaired T-test for normal distribution. Where assymetric distribution of data occurred the nonparametric Mann-Whitney test was applied. For the analyses of body weights at 4 weeks versus 5 weeks, a paired t-test was selected. Kaplan-Meier survival curves were assessed by the log-rank Cox-Mantel test. C2C12 studies were subject to One-Way ANOVA with Tukey's post-test. Values were expressed as means ± the standard error of the mean (SEM). Tests were performed in Excel (Microsoft) or Prism 5.0 (GraphPad).

Chapter 3: Characterisation of a model of CM specific expression of prelamin A in mice

3.1. Introduction

Currently, a role for prelamin A accumulation has neither been specifically identified nor rigorously investigated in the context of heart pathology. The rationale for doing so in this study is supported by several slightly disparate lines of investigation, which converge on a hypothesis of prelamin A associated heart dysfunction. Accumulation of prelamin A is known to cause nuclear abnormalities and disruption of the LINC complex. It is thought that this underlies the mechanism by which disease occurs. The broadest association is with models showing disruption of the LINC complex such as in *Lmna*$^{-/-}$ mice, which develop systolic dysfunction and heart failure at 8 weeks old[225]. Additionally, some *LMNA* mutations that cause DCM have been rigorously investigated in mouse models, which lead to cardiomyopathic phenotypes resulting in attenuated survival[232, 248, 250, 253]. Although these studies were not carried out in the context of prelamin A accumulation, evidence suggests that prelamin A accumulation can occur in the presence of some of these *LMNA* mutations[253, 260]. Furthermore, there is evidence that older HGPS patients exhibit cardiac abnormalities[228, 229], whilst a mouse model of HGPS, *Lmna*$^{G609G/G609G}$, indicates a cardiac conduction deficiency phenotype[259] and *Zmpste24*$^{-/-}$ mice display histological abnormalities of the myocardium[214].

To further investigate the role that prelamin A plays in heart disease, I utilised a mouse model of targeted transgenesis to the ROSA26 locus of human *LMNA* cDNA

containing a missense mutation leading to a change in the amino acid sequence that prevented cleavage by Zmpste24, which was designed to cause accumulation of farnesylated prelamin A.

3.2 Results

3.2.1 MLC2v-Cre mediated recombination of the floxxed *Rosa26*$^{L647R\text{-}LMNA}$ transgene results in prelamin A accumulation in CMs of mice

In order to obtain experimental mice, it was necessary to mate mice carrying the *Rosa26*$^{L647R\text{-}LMNA}$ transgene to mice expressing the MLC2v promoter linked cre recombinase. MLC2v is a part of the contractile machinery of myocytes and is postulated to be specifically expressed in CMs of the ventricle, making it ideal to drive cardiac specific expression of transgenes. After the mice were born, they were genotyped by PCR and agarose gel electrophoresis (Fig 3.1A & B). Mice carrying the transgene that also expressed cre recombinase were deemed to be prelamin A transgenic (PLA Tg) mice. Mice that contained only the transgene were selected as 'wildtype' (Wt) littermates. This 'Wt' control would ensure that any phenotypic changes could not be ascribed to merely possessing a transgene on the *Rosa26* locus. The remaining mice with neither a transgene nor cre expression, and mice with only cre expression were not used for the study and culled as surplus. Genotypic analysis of n= 242 pups showed that the presence or expression of the transgene did not affect Mendelian birth ratios (Fig 3.1C).

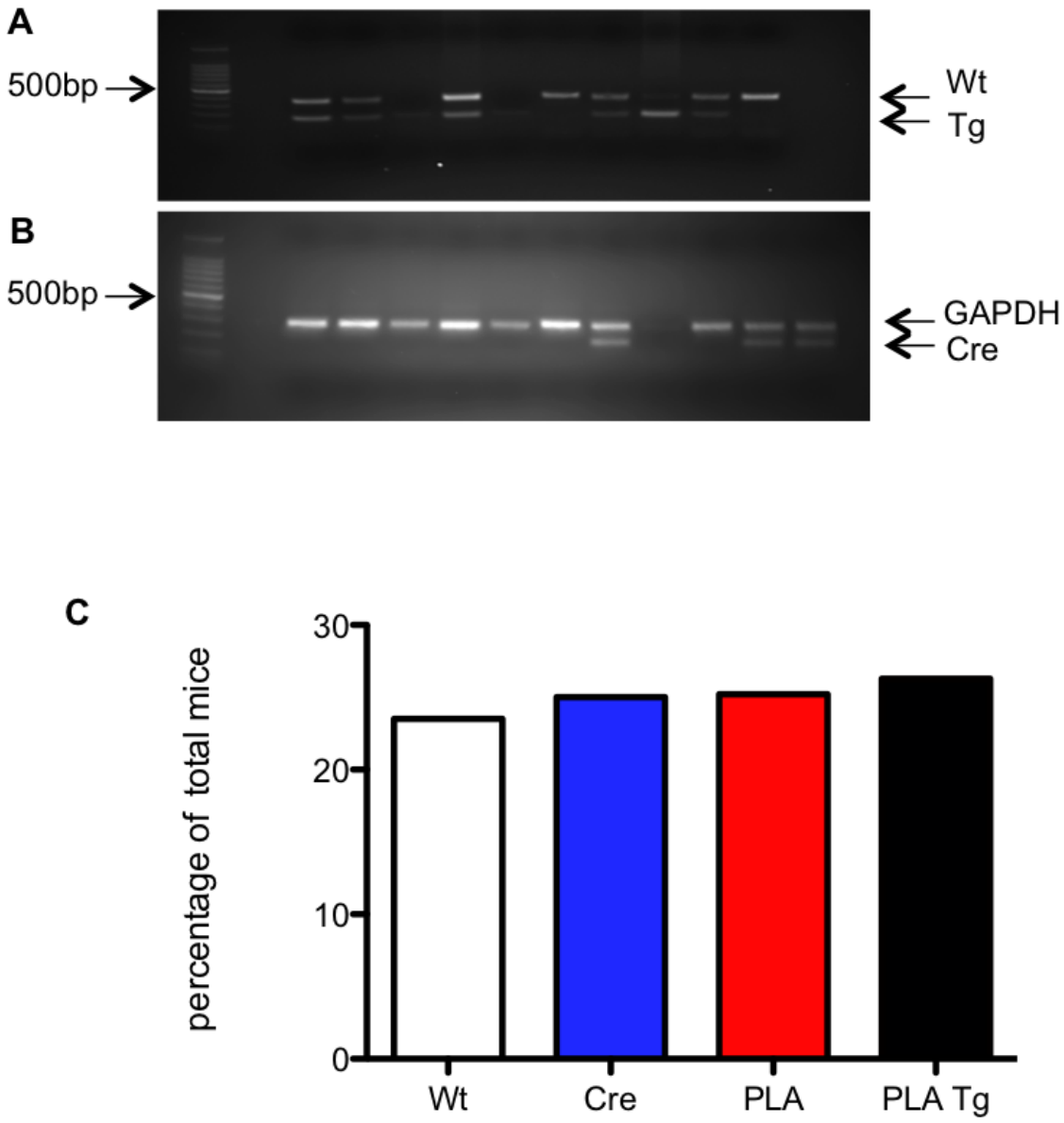

Figure 3.1. Transgenic mice were born in the expected Mendelian ratios. DNA was extracted from ear biopsies and then amplified by PCR using primers designed to ampify (A) the modified Rosa26 allele 200bp (Tg) and wildtype Rosa26 allele (Wt) 500bp and (B) cre recombinase 200bp and GAPDH 300bp. (C) Genotype ratios were expressed as a percentage of the total number of mice, which were born in the expected Mendelian pattern of 1:1:1:1. N=242

Cardiac specific expression of prelamin A protein in the heart was confirmed by western blotting of whole tissue lysates using lamin A/C C-20 antibody (detects prelamin A only) (Fig 3.2A). Immunohistochemistry showed nuclear rim localisation of accumulated prelamin A in PLA Tg mouse heart sections (Fig 3.2B).

3.2.2 Mice that accumulate cardiac specific prelamin A fail to thrive and succumb by 6 weeks of age with apparent cardiac phenotypic abnormalities

Due to the short life span of other *Lmna* mouse models, PLA Tg mice were initially observed; at birth and then also upon weaning, mice appeared normal. Shortly after weaning, PLA Tg mice appeared smaller (Fig 3.3A & B). From weaning, mice were weighed every second day to reveal that PLA Tg mice reached peak weight at 30 days old (12.2 g ± 0.6) and experienced weight loss thereafter. Comparatively, at 30 days old, Wt littermates were 13.8 g ± 0.6 and continued to experience steady growth after this timepoint (Fig 3.3C). At 35 days old, PLA Tg mice were 11.9 g ± 0.9 compared to Wt 17.1 g ± 0.8. Failure of PLA Tg mice to thrive was subsequently coupled with poor survival rates (Fig 3.3D). Kaplan-Meier analysis showed that the range of survival for PLA Tg mice was between 29 and 38 days, whilst the Wt littermates all survived to 80 days of age at which point the study was ended. Log-rank Mantel-Cox test for PLA Tg compared to Wt returned a P value of <0.0001 indicating statistical significance. Previous studies investigating *Lmna* mouse models have also reported phenotypic differences between genders[262]. Here, gender comparison showed median survival of 33 days for male compared to 32.5 for female mice. Log-rank Mantel-Cox test returned a

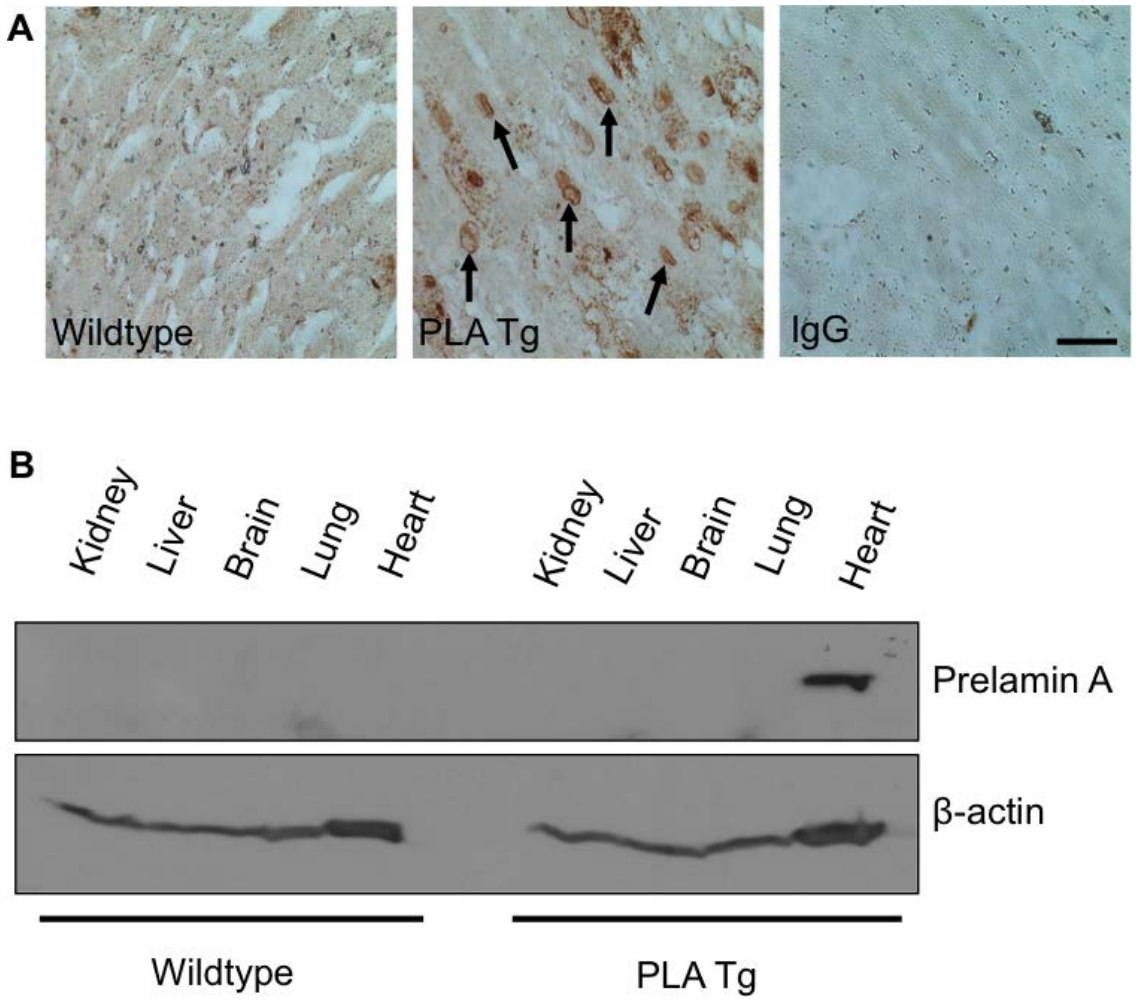

Figure 3.2. MLC2v Cre mediated recombination led to the expression of prelamin A exclusively in the myocardium. (A) Immunohistochemical staining with prelamin A antibody showed nuclear rim localisation of prelamin A in PLA Tg hearts only Scale bar = 30 μm. (B) Western blotting of whole tissue lysates showed cardiac specific expression of prelamin A in PLA Tg hearts. N=1/group.

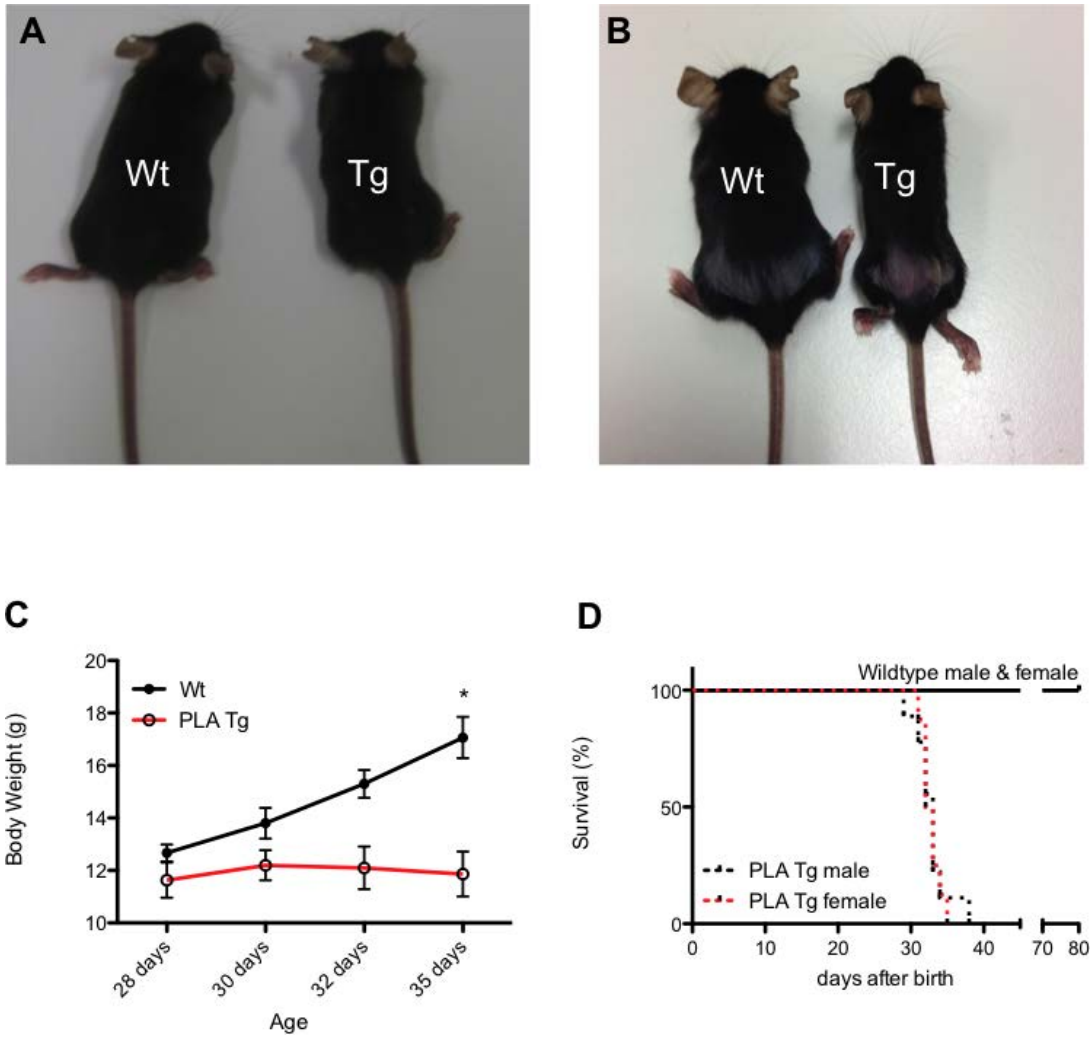

Figure 3.3. PLA Tg mice failed to thrive and died between 5-6 weeks of age. Representative photographs of Wt and PLA Tg mice at 4 weeks of age are shown in panels (A) and (B). (C) Longitudinal analysis of body weight shows that PLA Tg mice failed to grow past 4 weeks of age. *P>0.05 N=6/group (D) Kaplan-Meier survival analysis shows death of PLA Tg mice occurs between 5 and 6 weeks of age. Log-rank Mantel-Cox test was performed to show P<0.001 for PLA Tg mice compared to wildtype, N=6/group

P value of 0.85, indicating that there were no statistical differences between male and female survival of PLA Tg mice.

Because of the presentation of a phenotype and because mice were still viable, it was decided that characterisation of the phenotype should be carried out on 4 week old mice. Tissue was harvested and morphometric analysis carried out. Upon excision, hearts were photographed. PLA Tg hearts were noticeably larger in size compared to Wt and appeared to be dilated (Fig 3.4). 4 week body weights were recorded for male and female mice. Male PLA Tg mice were 11.96 g ± 0.46 which was significantly less than 15.23 g ± 0.59 for Wt controls (Fig 3.5A). Female PLA Tg mice were 10.71 g ± 0.38 compared to 12.8 g ± 0.38 for Wt controls (Fig 3.5A). Post mortem wet heart weight for male PLA Tg mice was 106.2 ± 10.5 compared to 96.7 ± 9.9 for Wt. Female PLA Tg were 93.1 ± 8.6 compared to 79.1 ± 5.6 for Wt (Fig 3.5B). There were no statistical differences between groups. Heart weight to body weight ratios were derived (mg, heart weight/g, body weight) to show values for male mice of 8.34 ± 0.66, which were significantly higher compared to 5.78 ± 0.23 for Wt. Female PLA Tg mice also had a significantly higher ratio of 9.34 ± 1.18 compared to 5.35 ± 0.23 for Wt (Fig 3.5C). Because of fluctuations in body weight between Wt and PLA Tg cohorts, it was decided that heart weights should be normalised to the potentially more reliable parameter, tibia length. Tibia lengths for male PLA Tg mice were 10.13 mm ± 0.23 compared to Wt 10.07 mm ± 0.19. Tibia length for female PLA Tg mice was 10.30 mm ± 0.15 compared to 10.00 ± 0.08 for Wt (Fig 3.5D). There were no statistical differences between Wt and PLA Tg cohorts. Heart weight to tibia length ratio was derived (mg, heart weight/mm, tibia length). In male PLA Tg mice (9.25 ± 0.40), the ratio was slightly elevated compared to Wt (8.29 ± 0.53) with no statistical significance.

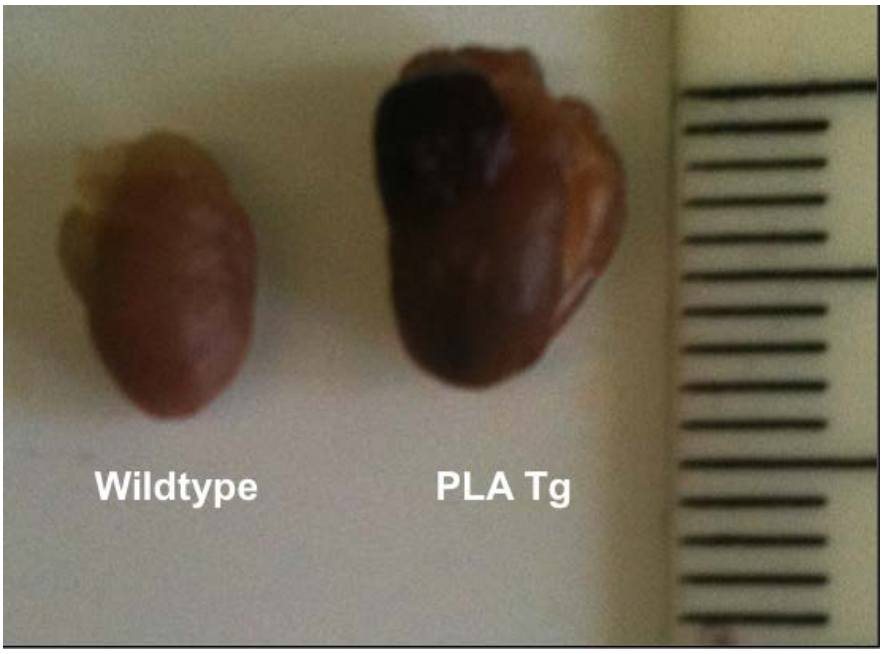

Figure 3.4. At 4 weeks of age, PLA Tg hearts were larger than Wt hearts. Hearts were excised and photographed and revealed that PLA Tg hearts (right) were much larger than Wt hearts (left).

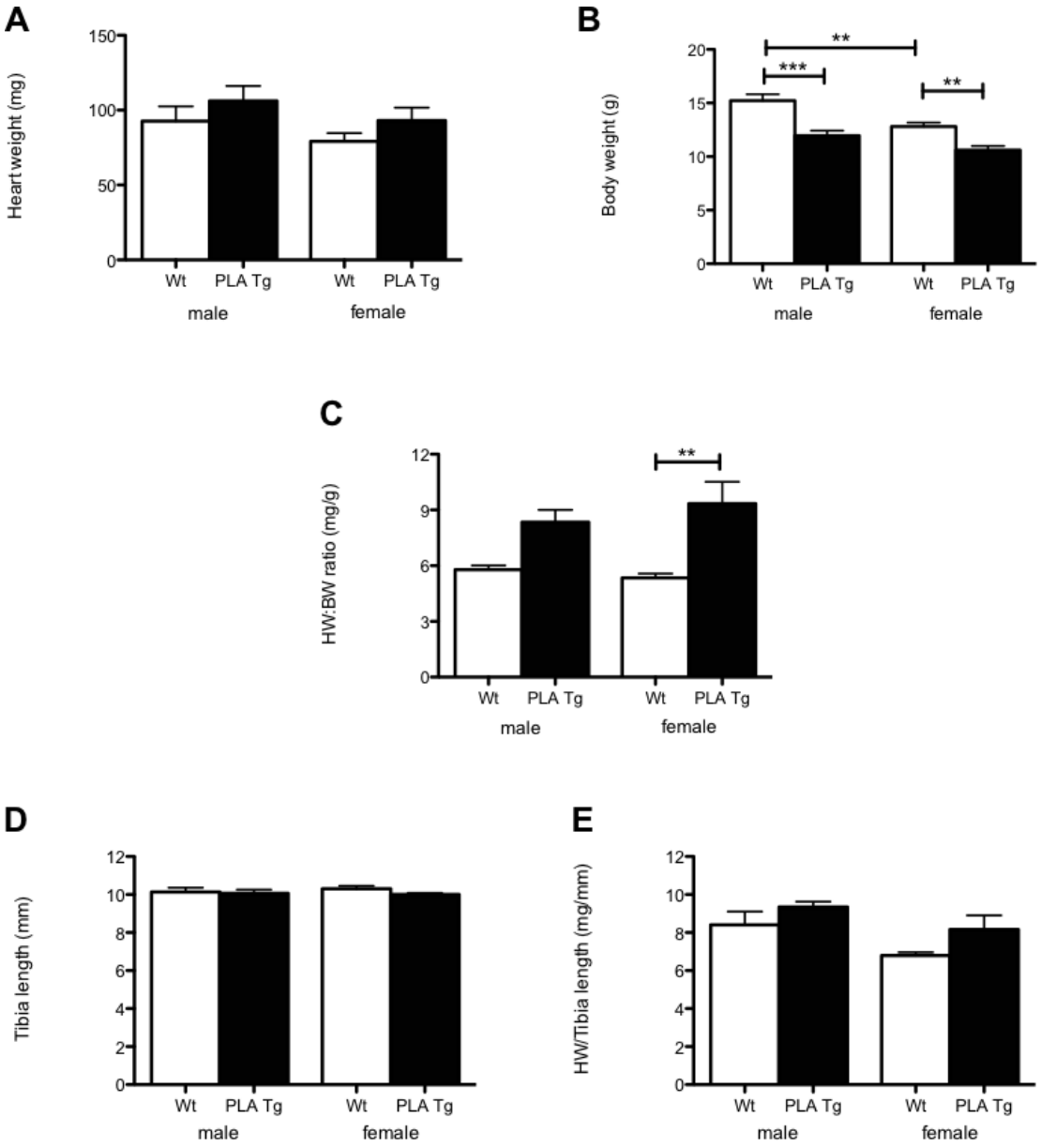

Figure 3.5. At 4 weeks, morphometric analysis showed that heart weight was not significantly different in PLA Tg hearts compared to Wt. Post mortem analysis of morphological parameters was performed by recording body weight, heart weight and tibia length. Graphs show: (A) Nominal increases in heart weight in male and female PLA Tg hearts compared to Wt; (B) Significantly decreased body weight in PLA Tg mice compared to Wt; (C) The ratio of body weight/heart weight was significantly increased in PLA Tg mice compared to Wt; (D) Tibia length was consistent between Wt and PLA Tg mice; (E) Ratio of heart weight/tibia length was nominally increased in PLA Tg mice but was not significant, **P<0.01, ***P<0.001, N= 6/group

This was also the case for female PLA Tg mice (8.16 ± 0.74) compared to Wt (6.80 ± 0.80) (Fig 3.5E).

3.2.3 Functional assessment of the cardiac phenotype shows a marked decline in contractility of the myocardium with evidence of myocardial remodelling in mice accumulating prelamin A in the heart

3.2.3.1 Echocardiography

Measurement of cardiac function by ultrasound (Echocardiography) is now a reliable and relatively inexpensive tool for preclinical analysis of rodent cardiac function[263]. Moreover, echocardiography has been used to assess cardiac function in several relevant studies. For example, *Lmna*$^{-/-}$ and Lmna$^{H222P/H222P}$ mice had depressed cardiac function, whereas *Lmna*$^{G609G/G609G}$ mice did not exhibit depressed systolic or diastolic function, but did show altered ventricular depolarisation when assessed by ECG.

In this study, 2 dimensional long-axis B-mode images of the left ventricle were analysed in favour of 1 dimensional longitudinal M-mode images because the increased spatial resolution seen with B-mode images was deemed to be more important in assessing LV parameters, particularly in the setting of isofluorane anaesthesia which has a depressive effect on heart rate, meaning the superior temporal resolution of M-mode analysis could be somewhat negated.

Again, males and females were separately assessed. Firstly, structural parameters were analysed. Interventricular septal thickness in systole (IVS;s) and diastole (IVS;d) was nominally, but not significantly, reduced in PLA Tg males and

females compared to their Wt counterparts. Left ventricular internal diameter in diastole (LVID;d) showed a trend towards an increase in male and female PLA Tg hearts compared to their Wt counterparts but was not statistically significant. Left ventricular internal diameter in systole (LVID;s) was significantly increased in PLA Tg males (3.37 mm ± 0.14) compared to Wt (2.30 mm ± 0.10) $P<0.001$ and PLA Tg females (3.36 mm ± 0.18) compared to Wt (2.26 mm ± 0.22) $P<0.01$. Moreover, in male mice, left ventricular posterior wall thickness in diastole (LVPW;d) was significantly decreased in PLA Tg mice (0.57 mm ± 0.03) compared to Wt (0.69 mm ± 0.04) $P<0.01$ and though a decrease was also seen in PLA Tg female mice compared to Wt, it was not statistically significant, $P=0.075$. Left posterior wall thickness in systole (LVPW;s) was significantly reduced in male PLA Tg mice (0.65 mm ± 0.04) compared to Wt (0.80 mm ± 0.02) $P<0.01$ and female PLA Tg mice (0.59 mm + 0.03) compared to Wt (0.70 mm ± 0.04) $P<0.05$. Area of the LV in systole (Area;s) was significantly increased in both PLA Tg males (16.83 mm^2 ± 1.16) compared to Wt (10.62 mm^2 ± 0.52) $P<0.001$ and PLA Tg females (17.00 mm^2 ± 1.24) compared to Wt (9.81 mm^2 ± 1.21) $P<0.01$. Area in diastole was not significantly different between Wt and PLA Tg for male and female mice. These findings are displayed in Table 3.1 and Figure 3.6.

Next functional parameters were analysed. Ejection fraction (EF), the proportion of the end diastolic volume ejected from the LV at the end of systole, was measured. In male PLA Tg mice, EF was found to be significantly reduced (19.56 % ± 5.44) compared to Wt (60.61 % ± 2.51) and also for female PLA Tg mice (14.92 % ± 1.70) compared to Wt (60.28 % ± 4.62). Fractional shortening (FS) was measured. FS is the degree of shortening of the left ventricle diameter between end-diastole (EDD) and end-systole (ESD) and is defined as (EDD-ESD)/EDD. FS was significantly decreased in

Table 3.1. B-mode Echocardiographic analysis of hearts in long axis orientation showed significant cardiac dysfunction in PLA Tg hearts at 4 weeks old

B-mode Parameter	Units	Male Wildtype	Male PLA Tg	Male P value	Male sig.	Female Wildtype	Female PLA Tg	Female P value	Female sig.
IVS;d	mm	0.54 ± 0.03	0.52 ± 0.02	0.689	N	0.57 ± 0.03	0.52 ± 0.03	0.306	N
IVS;s	mm	0.63 ± 0.04	0.53 ± 0.04	0.084	N	0.63 ± 0.05	0.53 ± 0.03	0.099	N
LVID;d	mm	3.37 ± 0.20	3.52 ± 0.14	0.543	N	3.18 ± 0.14	3.44 ± 0.17	0.254	N
LVID;s	mm	2.30 ± 0.10	3.37 ± 0.14	0.000	***	2.26 ± 0.22	3.36 ± 0.18	0.003	**
LVPW;d	mm	0.69 ± 0.04	0.57 ± 0.03	0.037	*	0.58 ± 0.02	0.52 ± 0.02	0.075	N
LVPW;s	mm	0.80 ± 0.02	0.65 ± 0.04	0.005	**	0.70 ± 0.04	0.59 ± 0.03	0.050	*
Area;d	mm2	18.39 ± 0.63	19.43 ± 0.75	0.315	N	17.07 ± 1.05	19.22 ± 1.52	0.271	N
Area;s	mm2	10.62 ± 0.56	16.83 ± 1.16	0.001	***	9.81 ± 1.21	17.00 ± 1.24	0.002	**
Cardiac Output	ml/min	12.00 ± 0.51	4.13 ± 1.07	0.000	***	8.96 ± 0.66	3.28 ± 0.53	0.000	***
Ejection Fraction	%	60.61 ± 2.51	19.56 ± 5.44	0.000	***	60.28 ± 4.62	14.92 ± 1.70	0.000	***
Fractional Shortening	%	15.77 ± 1.99	7.19 ± 2.26	0.017	*	18.11 ± 1.99	7.58 ± 0.73	0.001	**
Heart Rate	BPM	455.79 ± 12.37	453.71 ± 25.59	0.943	N	408.26 ± 27.83	465.86 ± 25.53	0.158	N
Stroke Volume	ul	26.40 ± 1.21	9.10 ± 2.53	0.000	***	22.12 ± 1.43	7.32 ± 1.44	0.000	***
LVEDV	ul	43.73 ± 1.93	47.99 ± 2.83	0.241	N	37.91 ± 3.85	47.16 ± 5.78	0.213	N
LVESV	ul	17.33 ± 1.49	38.90 ± 4.16	0.001	**	15.80 ± 2.96	39.84 ± 4.51	0.001	**

Values expressed as mean±SEM, N=6/group, *P<0.05, **P<0.01, ***P<0.001, ^{N}P=No significance

IVS = Interventricular septum

LVID = Left ventricular internal diameter

LVPW = Left ventricular posterior wall

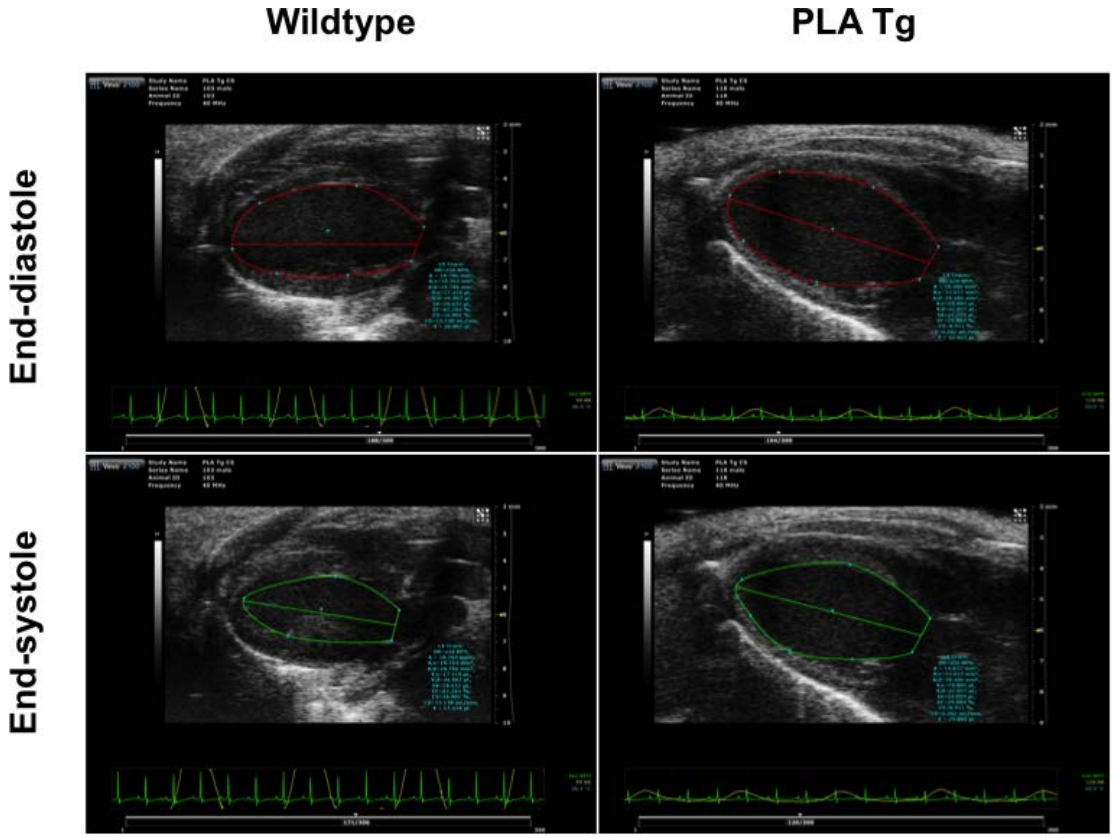

Figure 3.6. Heart chamber size appeared increased in 4 week old PLA Tg hearts. Representative B mode images of the LV long axis from echocardiography movies used to analyse cardiac function showing that chamber size was increased in transgenic hearts during the systolic phase of contraction, supporting the analysed data from Table 3.1.

male PLA Tg mice (7.19 % ± 2.26) compared to Wt (15.77 % ± 1.99) P<0.05 and also in female PLA Tg mice (7.58 % ± 0.73) compared to Wt (18.11 % ± 1.99) P<0.01. Volumetric parameters were analysed and showed that there was a minor but non significant increase in left ventricular end diastolic volume (LVEDV) in PLA Tg hearts of male and female mice compared to Wt. Left ventricular end systolic volume (LVESV) of male PLA Tg hearts (38.90 µl ± 4.16) was significantly increased compared to Wt (17.33 µl ± 1.49) P<0.01 and also in female PLA Tg hearts (39.84 µl ± 4.51) compared to Wt (15.80 µl ± 2.96) P<0.01. Accordingly, stroke volume (SV) was decreased in male PLA Tg hearts (9.10 µl ± 2.53) compared to Wt (26.40 µl ± 1.21) P<0.001 and also in female PLA Tg hearts (7.32 µl ±1.44) compared to Wt (22.12 µl ± 1.43) P<0.001. There was no difference in heart rate between Wt and PLA Tg groups in male and female mice. Cardiac output was measured and found to be significantly attenuated in male PLA Tg mice (4.13 ml/min ± 1.07) compared to Wt (12.00 ml/min ± 0.51) P<0.001 and also in female PLA Tg mice (3.28 ml/min ± 0.53) compared to Wt (8.96 ml/min ± 0.66) P<0.001. These findings are displayed in Table 3.1 and Figure 3.5.

3.2.3.2 MRI

MRI utilises strong magnetic fields to excite hydrogen atoms and then detects the frequency emitted in order to build images of organs of interest in human anatomy, including the heart. Cross sectional images of the ventricular chambers were acquired and analysed for some of the functional parameters that were assessed with echocardiography. MRI is thought to be more accurate than echocardiography because, unlike 2D echocardiography, it does not rely on geometric assumptions in order to make

quantified analyses. No gender comparison was made during MRI studies. Volumetric parameters were assessed and revealed that LVEDV was significantly elevated in PLA Tg mice (48.47 µl ± 2.54) compared to Wt (32.45 µl ± 2.03) P<0.001. LVESV was also significantly higher in PLA Tg mice (35.27 µl ± 3.34) compared to Wt (11.13 µl ± 1.15) P<0.001. Accordingly, SV was significantly attenuated in PLA Tg mice (13.20 µl ±1.13) compared to Wt (21.30 µl ± 1.38) P<0.01. Moreover, EF was significantly lower in PLA Tg mouse hearts (28.05 % ± 3.61) compared to Wt (65.87 % ± 2.59) P<0.001 (Fig 3.7). Representative images are shown in Figure 3.8.

3.2.4 Post mortem analysis of chest cavity and modulation of mRNA markers indicate heart failure was the cause of mortality in PLA Tg mice

Heart failure (HF) has been shown to exhibit a specific molecular signature. Modulation of α- (decrease) and β- (increase) isoforms of myosin heavy chain mRNA[264] coupled with increases in atrial natriuretic peptide and brain natriuretic peptide mRNA are reliable markers of HF. Moreover, transudative pleural/pericardial effusions, whereby excessive fluid penetrates into the pleural space, are caused by elevated filling pressures in the heart, and are a reliable indicator of HF[265].

To test this, mice were sacrificed and the chest cavity was carefully dissected, observed and photographed. It was clear to the eye that a colourless fluid had penetrated the pleural cavity in PLA Tg mice and not in Wt (Fig 3.9).

Next, quantitative PCR (qPCR) was performed to test for mRNA markers of HF. Primers for α-MHC, β-MHC, ANP, and BNP were used to amplify cDNA of Wt and PLA Tg heart tissue. Wt values were normalised to those of GAPDH for control

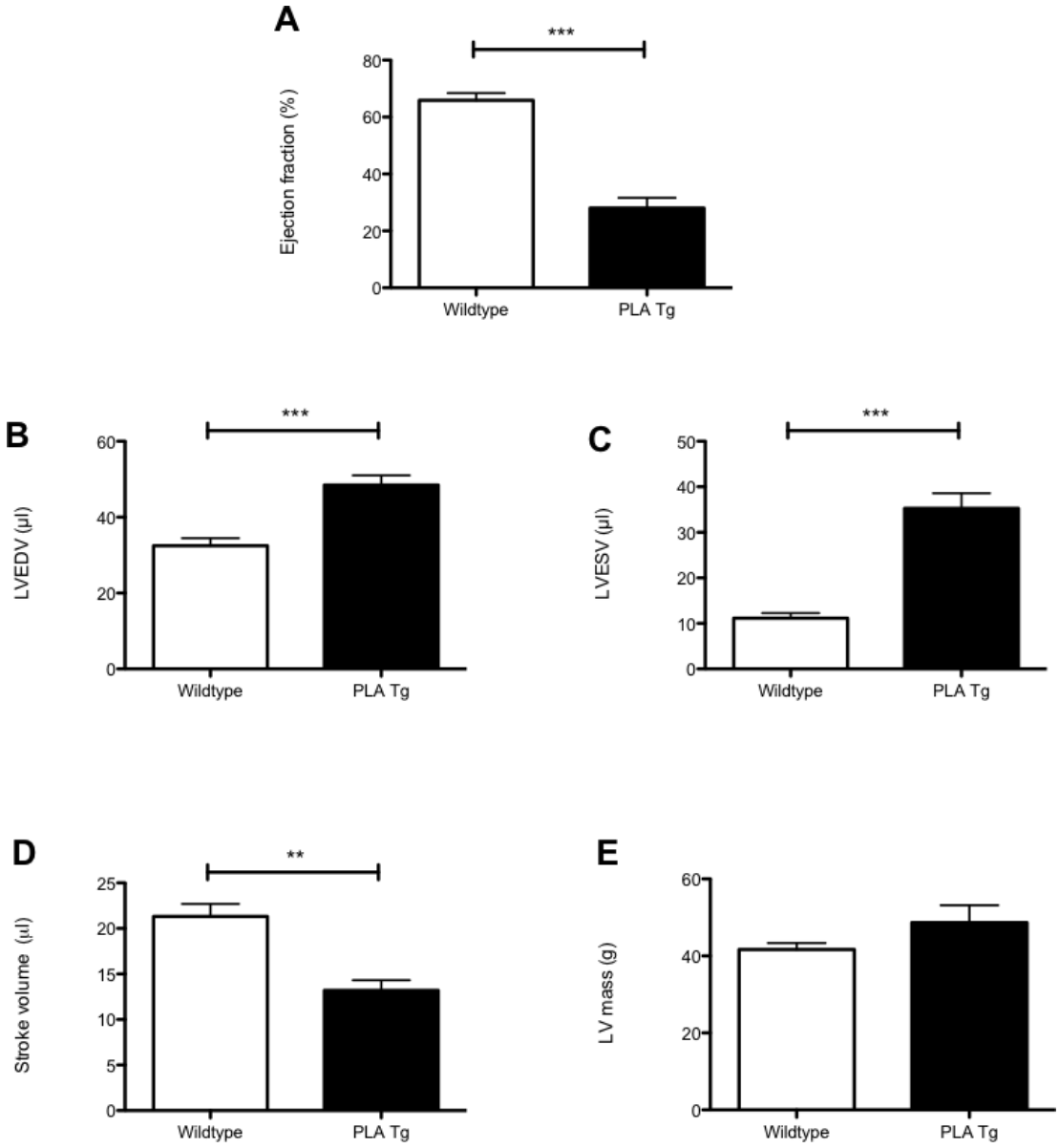

Figure 3.7. At 4 weeks of age, cardiac function was attenuated in PLA Tg hearts compared to Wt. MRI was used to assess cardiac function in Wt and PLA Tg hearts. Analysis of MRI images showed: (A) ejection fraction is attenuated in PLA Tg mice;(B) LV end-diastolic volume; and (C) LV end-systolic volume are increased in PLA Tg mice, whilst (D) Stroke volume is attenuated. (E) LV mass is not significantly different in PLA Tg hearts compared to Wt. Values expressed as mean±SEM, **P<0.01, ***P<0.001, N=5/group of mixed gender cohorts

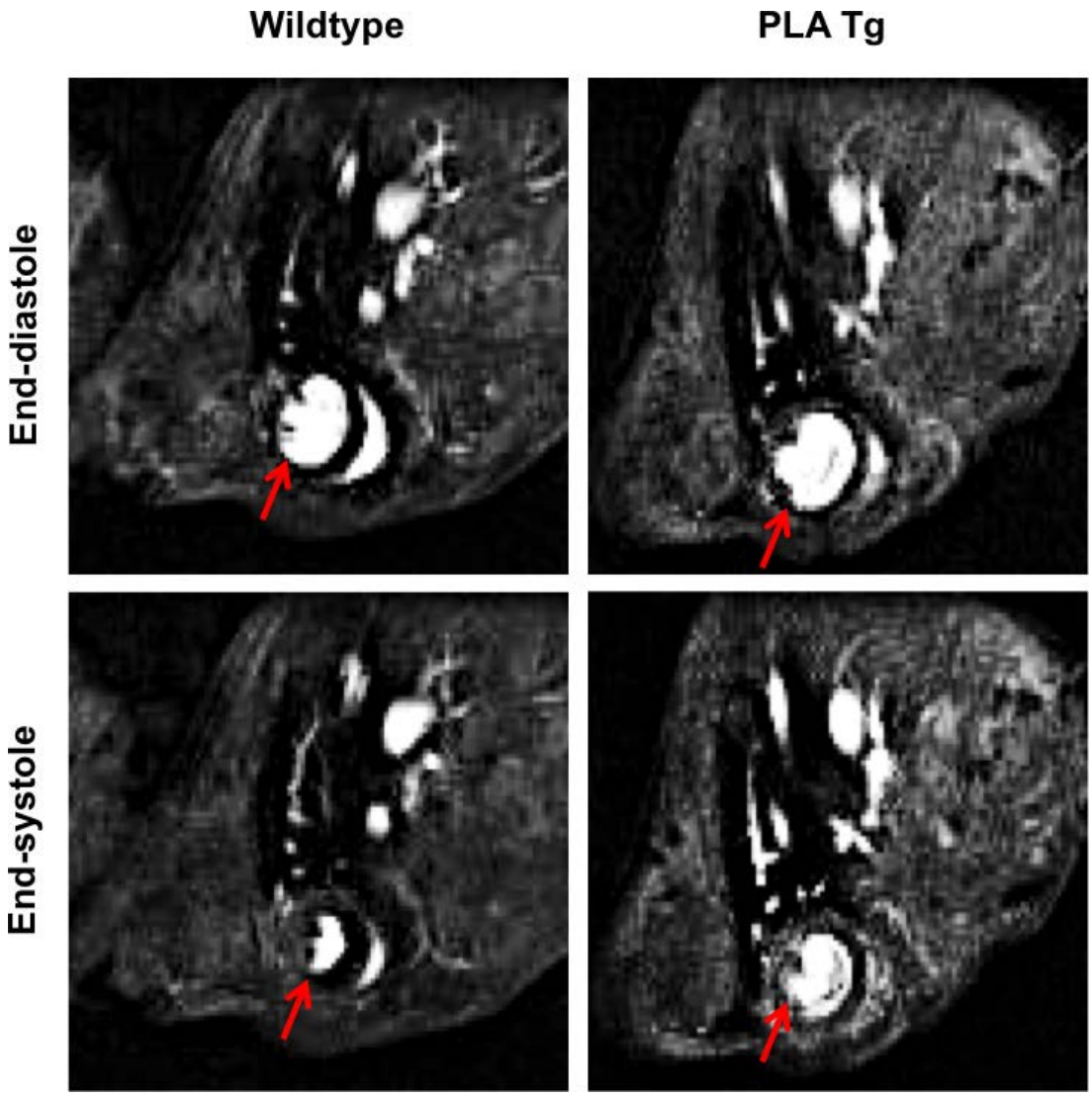

Figure 3.8. Cardiac MRI showed that heart chambers were larger in PLA Tg mice compared to Wt. Representative MR images of the short axis of the heart showing that cardiac chambers of PLA Tg hearts appear larger than Wt (arrows) and support the analysed graphical data from Figure 3.7.

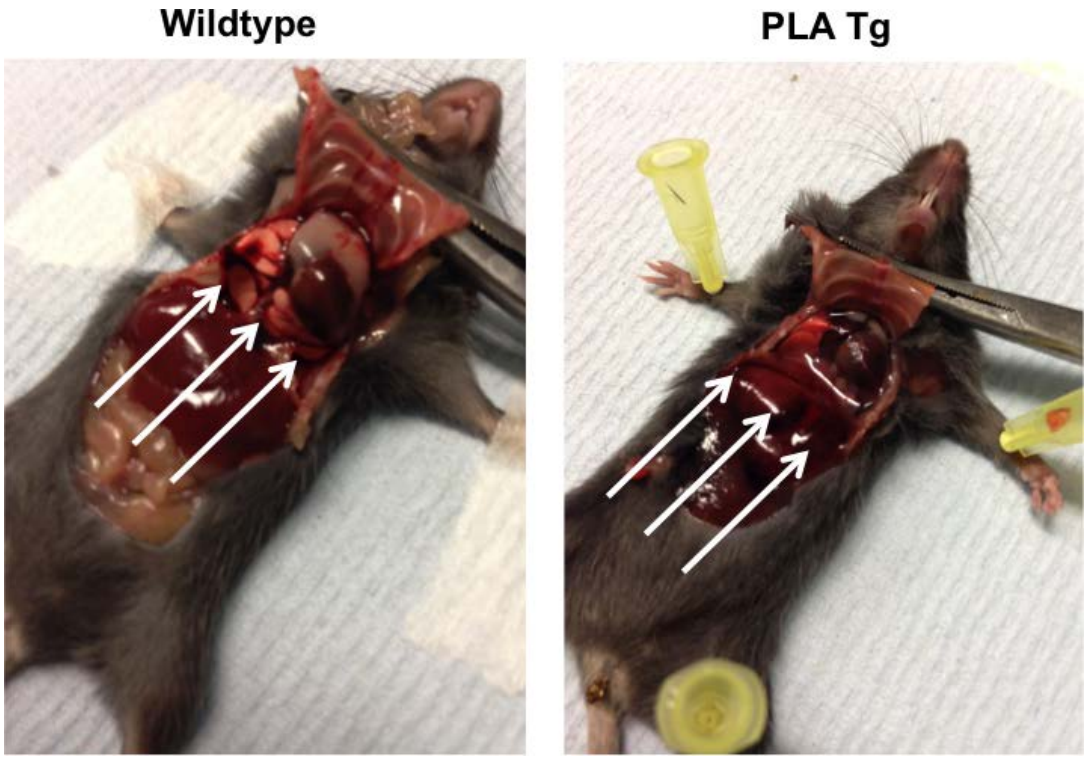

Figure 3.9. Transudative pleural effusion in PLA Tg mice indicated heart failure at 4 weeks of age. Mice were sacrificed and the chest cavity was carefully dissected open and photographed to show the accumulation of clear liquid in the pleural space of PLA Tg but not Wt hearts, indicating heart failure in PLA Tg mice**.**

purposes and adjusted to 1. PLA Tg values were expressed as fold change compared to Wt. α-MHC mRNA levels were significantly decreased in PLA Tg hearts (0.41 fold change ± 0.11) compared to Wt (1.0 ± 0.11) $P<0.05$. β-MHC mRNA in PLA Tg hearts was 38.07 ± 16.02 fold greater than Wt ($P<0.05$). ANP mRNA was 23.55 ± 11.09 fold greater in PLA Tg hearts compared to Wt ($P<0.05$). Finally, BNP mRNA levels were 19.01 ± 11.74 fold greater in PLA Tg hearts compared to Wt ($P<0.05$) (Fig 3.10).

3.2.5 Histological examination of hearts shows post mortem dilatation of cardiac chambers, myocardial disarray, and evidence of fibrotic remodelling of cardiac tissue in PLA Tg mice

Haemotoxylin and Eosin staining was performed on 4 week old ventricular long axis and short axis cross sections and viewed with low power light microscopy to reveal that dilatation of the ventricular chambers had occurred in PLA Tg hearts compared to Wt (Fig 3.11 & 3.12). High power light microscopy of the same H&E stained hearts showed myocardial disarray and nucleic infiltration, assumed to be of a lymphocytic lineage (Fig 3.13).

Sirius red staining was viewed using light microscopy. A large proportion of the myocardium had been replaced by fibrotic regions in PLA Tg hearts compared to Wt (Fig 3.14). These sections were also viewed under circular polarised light, which preferentially detects abnormally cross-linked collagen fibers, which occur in fibrotic remodelling and was quantified using colour threshold analysis to show that PLA Tg

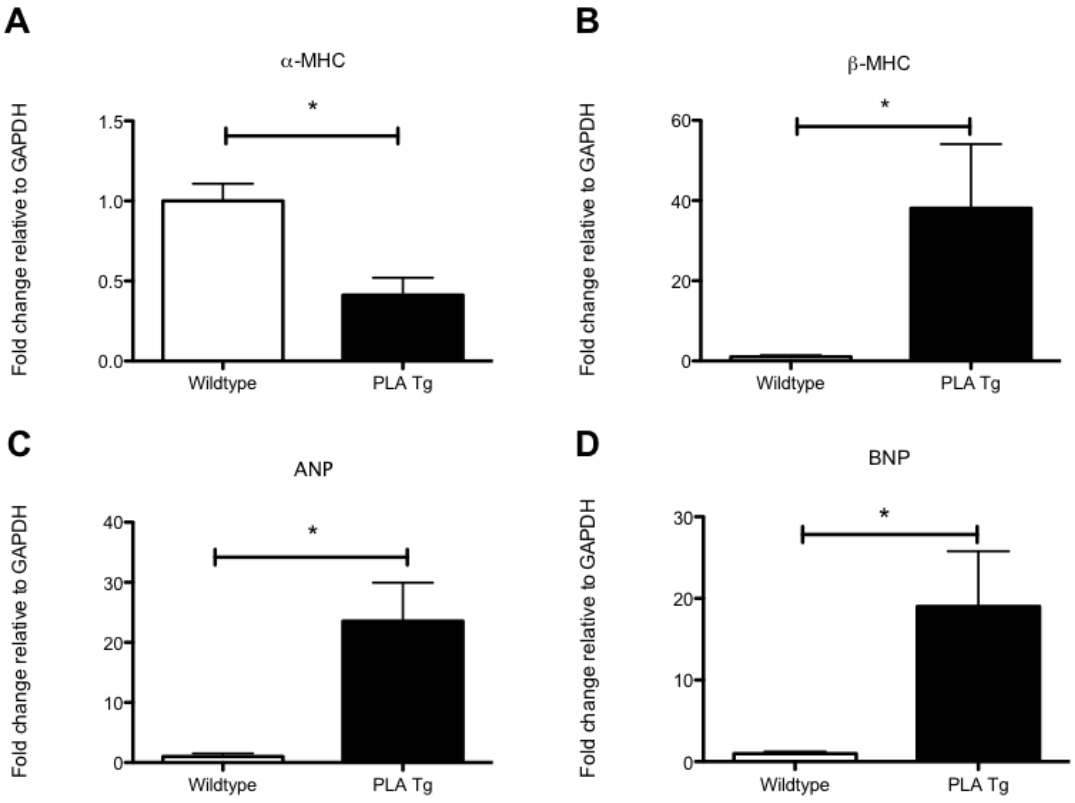

Figure 3.10. Analysis of mRNA markers indicated heart failure in 4 week old PLA Tg hearts compared to Wt. qPCR was performed to assess mRNA markers of heart failure and showed: (A) α-MHC mRNA is significantly decreased; (B) β-MHC is significantly increased; (C) ANP is significantly increased; and (D) BNP is significantly increased in PLA Tg hearts compared to Wt, indicating heart failure. Values expressed as mean±SEM, *P<0.05, N=3/group

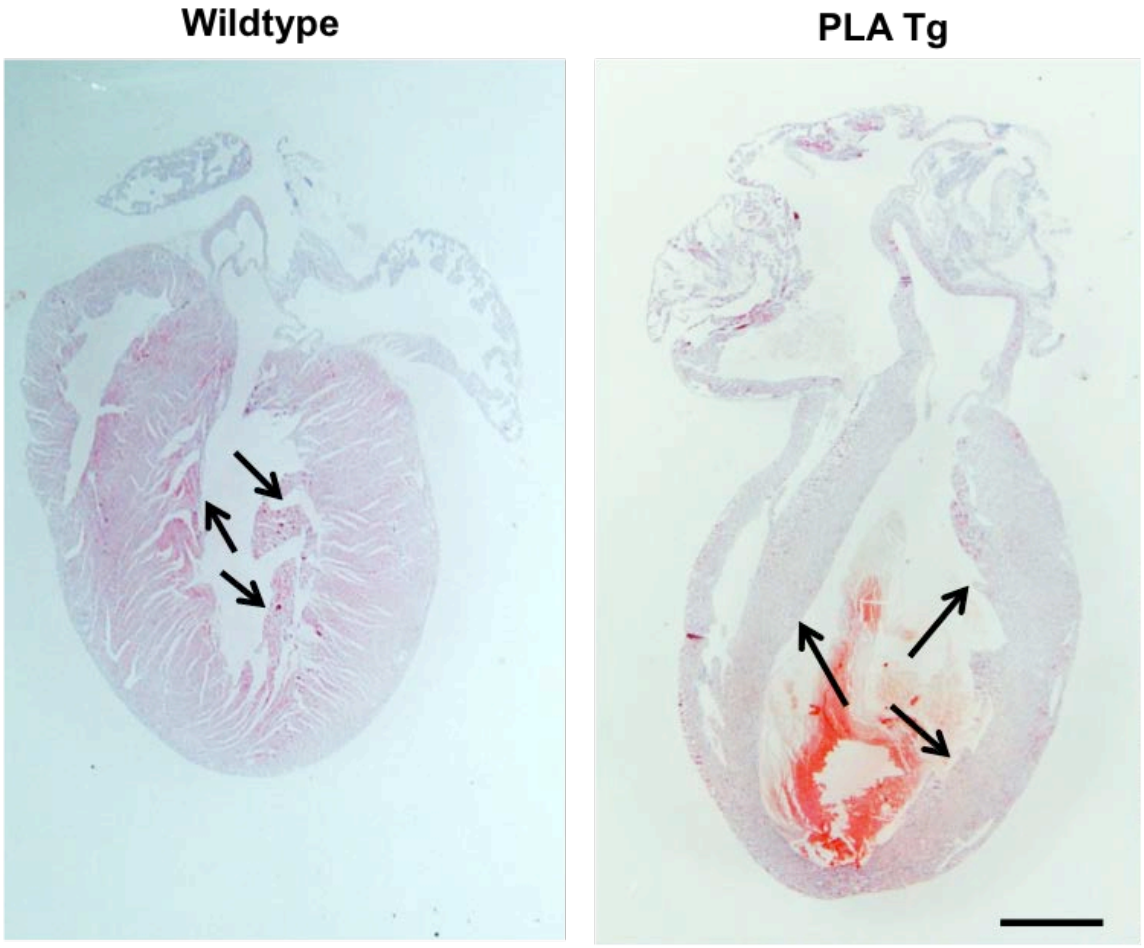

Figure 3.11. At 4 weeks, cardiac chambers were dilated and the myocardium appeared thinner in PLA Tg hearts compared to Wt in the long axis view. H&E staining was performed on long axis sections of paraffin embedded Wt (left) and PLA Tg (right) hearts and viewed under low power light microscopy to reveal that cardiac chambers were dilated in PLA Tg hearts compared to Wt. Moreover, substantial thinning of the myocardium appears to have occurred in PLA Tg hearts. Scale bar = 2mm

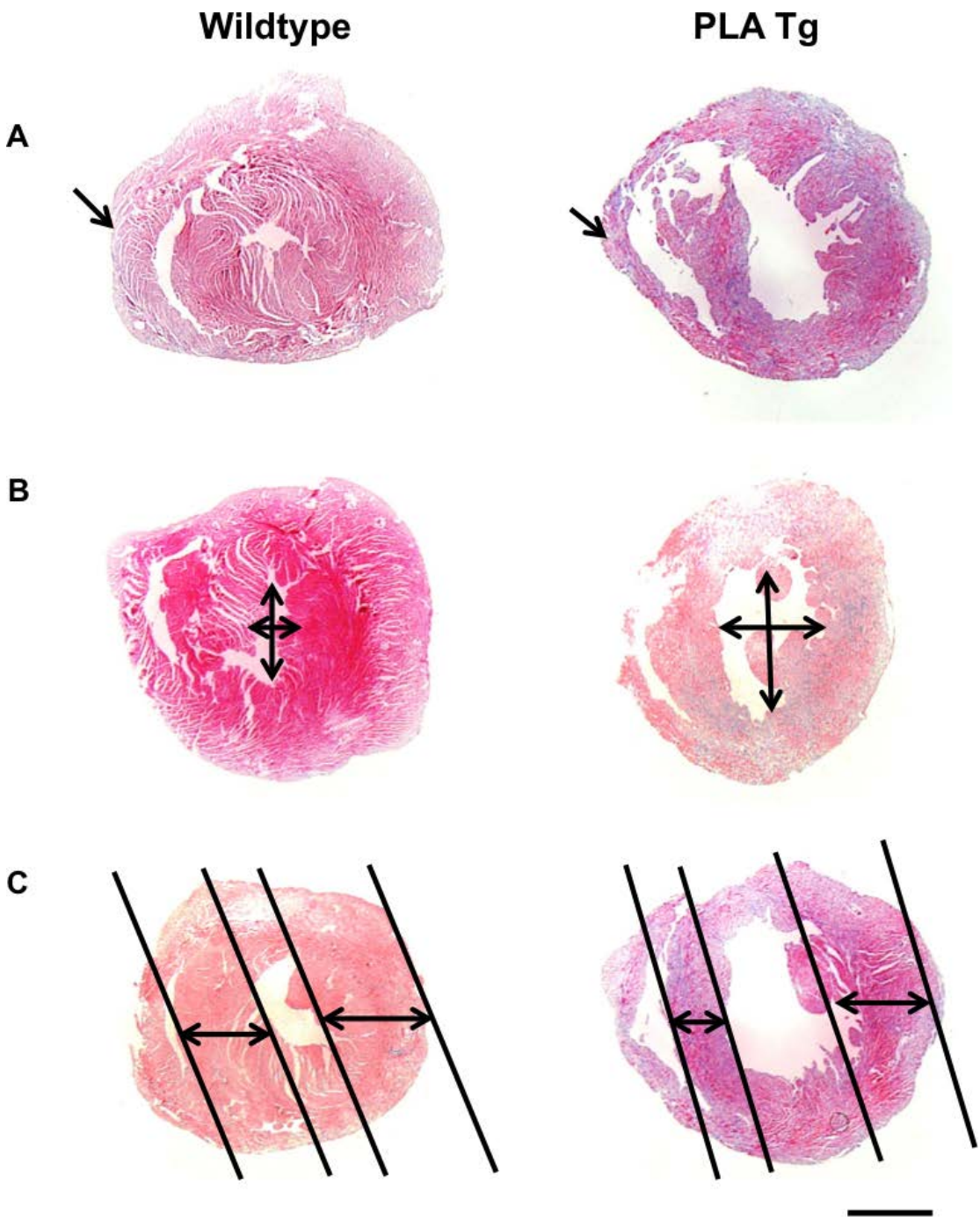

Figure 3.12. At 4 weeks, cardiac chambers were dilated and the myocardium appeared thinner in PLA Tg hearts compared to Wt in the short axis view. H&E staining of paraffin embedded cross sections of Wt (left panels) and PLA Tg (right panels) hearts was performed and viewed with low power light microscopy and showed dilatation of cardiac chambers and thinning of the myocardium in PLA Tg hearts compared to Wt. Scale bar = 2mm

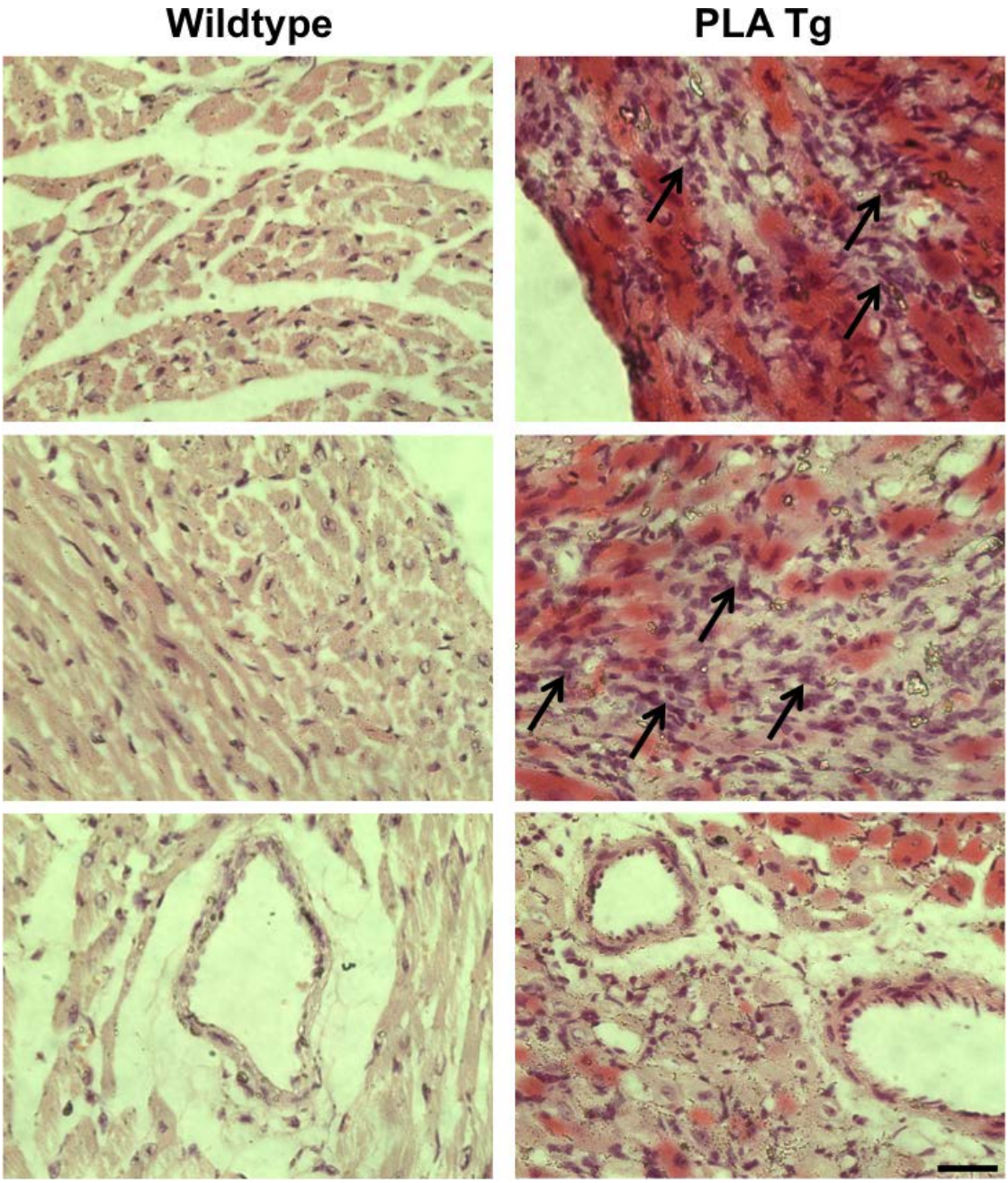

Figure 3.13. Myocardial structure was disrupted in hearts of 4 week old PLA Tg mice compared to Wt. H&E staining of paraffin embedded heart cross sections was viewed under high power light microscopy and showed that, whilst Wt heart sections present expected myocardial histology (left panelling), PLA Tg hearts have myocardial disarray and clustering of nuclei in the myocardium (right panelling), indicative of pathological leukocyte invasion. Scale bar = 30μm

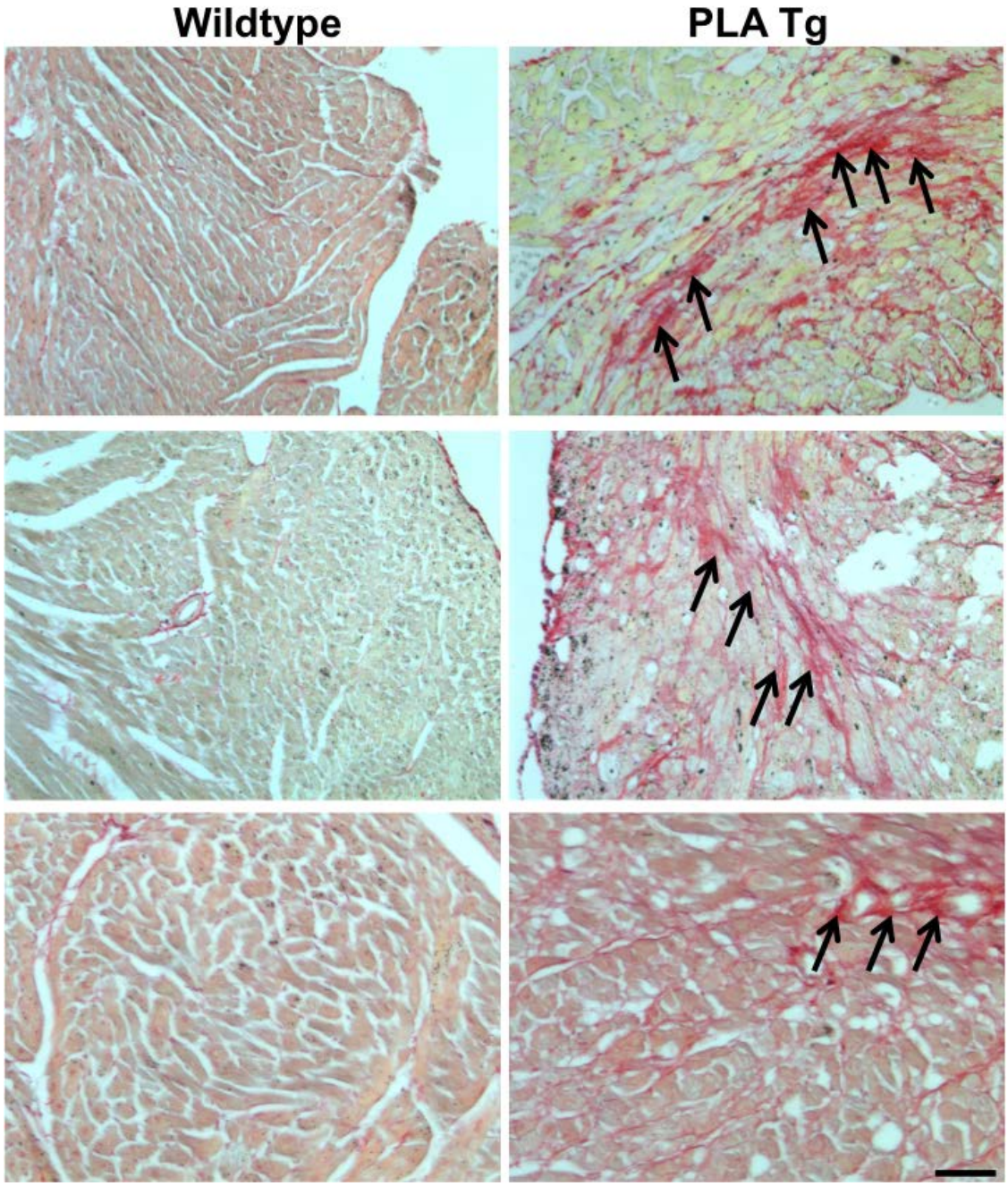

Figure 3.14. At 4 weeks, hearts accumulating prelamin A developed interstitial fibrosis whereas Wt hearts did not. Picrosirius red staining was performed on paraffin embedded heart cross-sections of Wt (left panelling) and PLA Tg (right panelling) mice. PLA Tg hearts appeared to have significantly more bright red staining than Wt indicating the presence of fibrosis. Scale bar = 60 μm

mice (2.324 % ± 0.135) have more abnormally linked fibres than Wt (0.568 % ± 0.218) P<0.001 (Fig 3.15). Images of the cardiac ultrastructure were obtained and confirmed this finding as PLA Tg hearts showed many regions punctuated with collagen-style filamentous structures indicative of fibrosis, whereas Wt hearts did not (Fig 3.16). Additionally, cardiac MRI of patients with DCM associated *LMNA* mutations has shown that the majority have myocardial fibrosis when late gadolinium enhancement is performed[266]. Indeed, myocardial inversion recovery sequences in late gadolinium enhancement showed a significant increase in R1 values in the myocardium of PLA Tg mice (1.960 1/sec ± 0.068) compared to Wt (1.620 1/sec ± 0.66) (Fig 3.17).

3.2.6 Immunofluorescence staining, western blotting and electron microscopy indicates infiltration of leukocytes into myocardial tissue of PLA Tg mice

Lymphocytic infiltration into cardiac tissue has been reported in *Zmpste24*$^{-/-}$ mice as defined by H&E staining and histological observation. In the current study, it was observed that a similar histopathological phenotype was presented. To confirm that inflammatory cells were present in the myocardium of PLA Tg mice, indirect immunofluorescence staining of cryopreserved heart sections using an antibody to CD45 was performed. CD45, also known as common leukocyte antigen (CLA), is present on the cell surface of all cells of lymphocytic lineage and is therefore a reliable marker for inflammation. It was observed that PLA Tg mice appeared to have larger populations of CD45+ cells accumulating in the myocardium compared to Wt (Fig 3.18). This was then quantified by cell counting to reveal that there were indeed

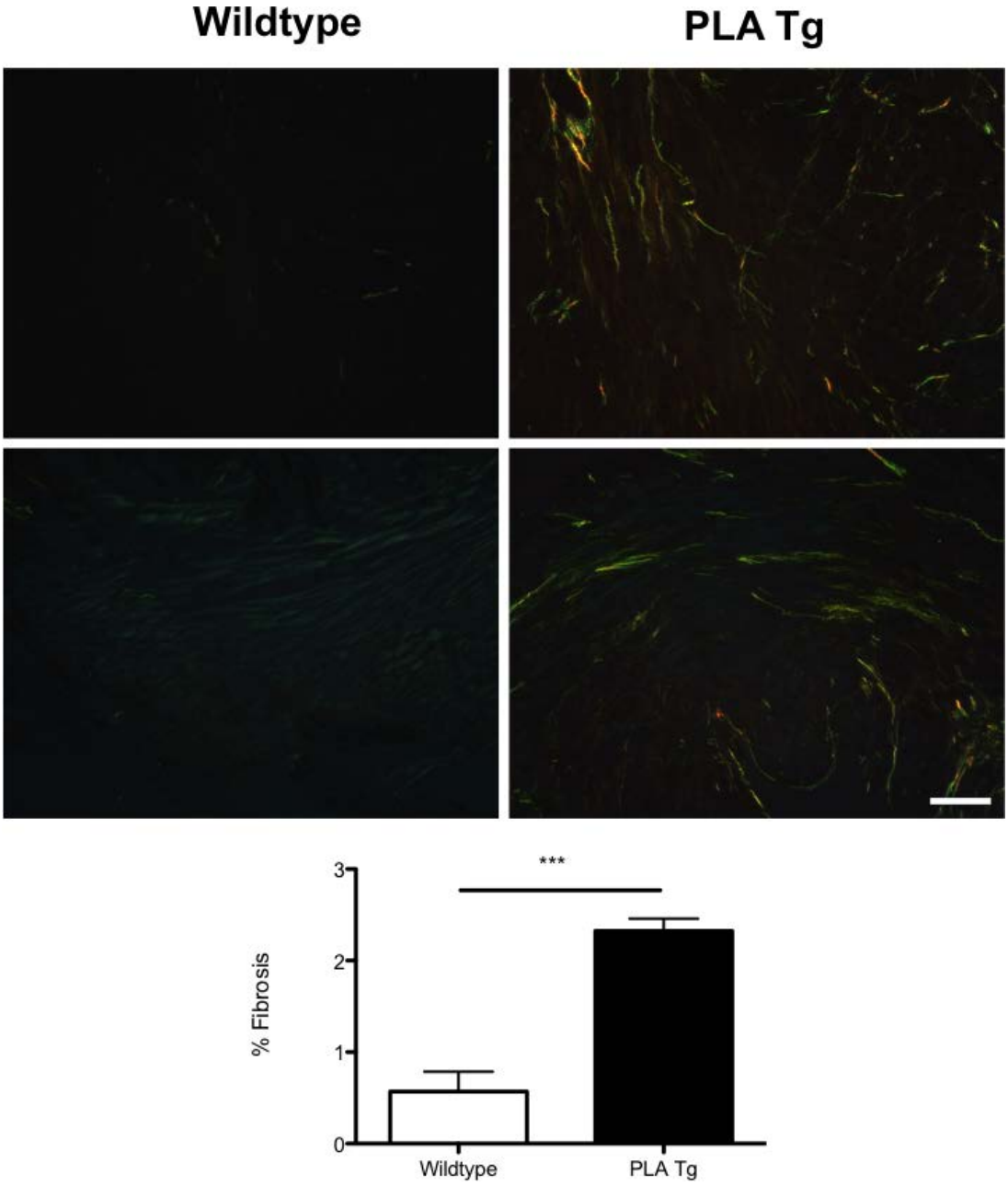

Figure 3.15. Polarised light microscopy showed evidence of fibrosis in the hearts of 4 week old PLA Tg mice. Picrosirius red stained heart sections were viewed under polarised light to reveal birefringence associated with fibrotic lesions was significantly increased in PLA Tg hearts compared to Wt as quantified by colour threshold analysis with volocity® software. Values expressed as mean±SEM, ***P<0.001, N=3/group, Scale bar = 60 μm

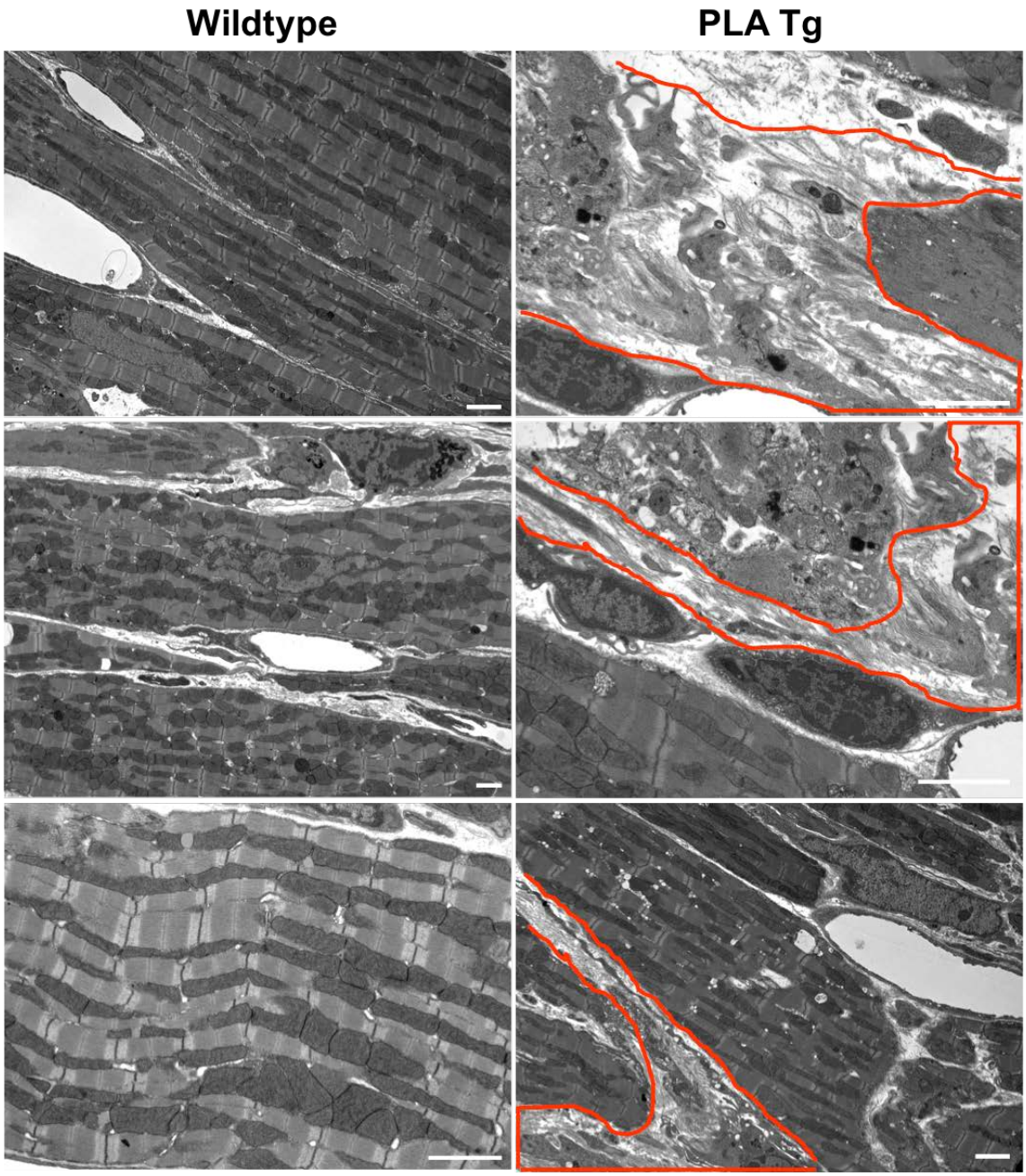

Figure 3.16. Interstitial Fibrosis of PLA Tg hearts was evident in the cardiac ultrastructure of 4 week old mice. Perfusion fixed hearts were processed and stained for TEM. Evidence for fibrosis was clear in PLA Tg hearts (right panelling), identifiable as filamentous thread like structures, shown here within the confines of the red borders. Wt hearts (left panelling) showed no evidence of this. Scale bar = 2 µm

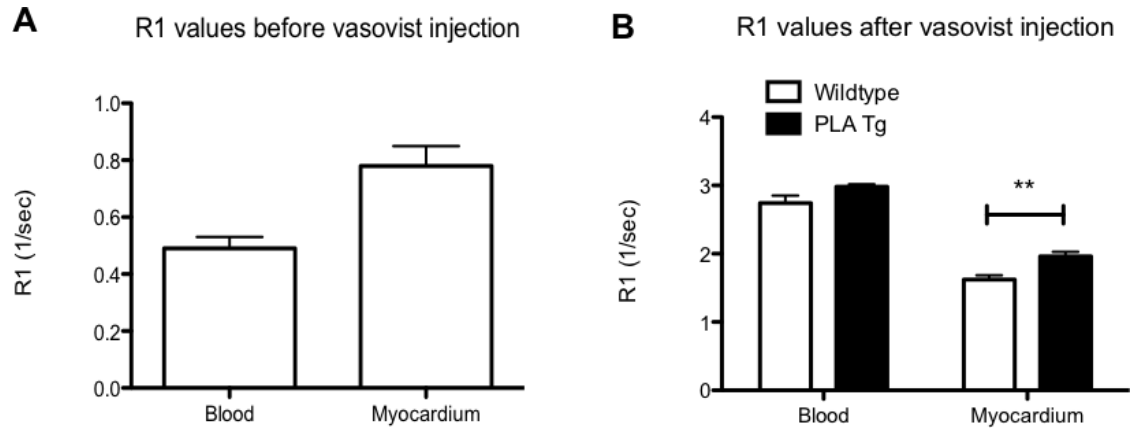

Figure 3.17 Increased myocardial tissue enhancement indicated the presence of fibrosis in PLA Tg mice hearts. Anaesthetised mice were subject to MRI before and after intraperitoneal (i.p.) injection of Vasovist (Vasovist, Bayer Schering Pharma AG, Berlin, Germany), a gadolinium-based contrast agent. T1-weighted sequences were analysed to assess the R1 values of blood and myocardium. (A) R_1 (relaxation) values for the blood and myocardium before injection of Vasovist. Similar values were achieved in Wt and PLA Tg mice. (B) R_1 values 30 minutes after injection of Vasovist. R_1 values were non-significantly increased in blood, while a significant difference was found in the myocardium. This is indicative of a higher accumulation of the contrast agent in the myocardium, and likely to be related to the presence of diffuse fibrosis. Values expressed as mean±SEM, *P<0.05, **P<0.01, N=6/group of mixed gender cohorts

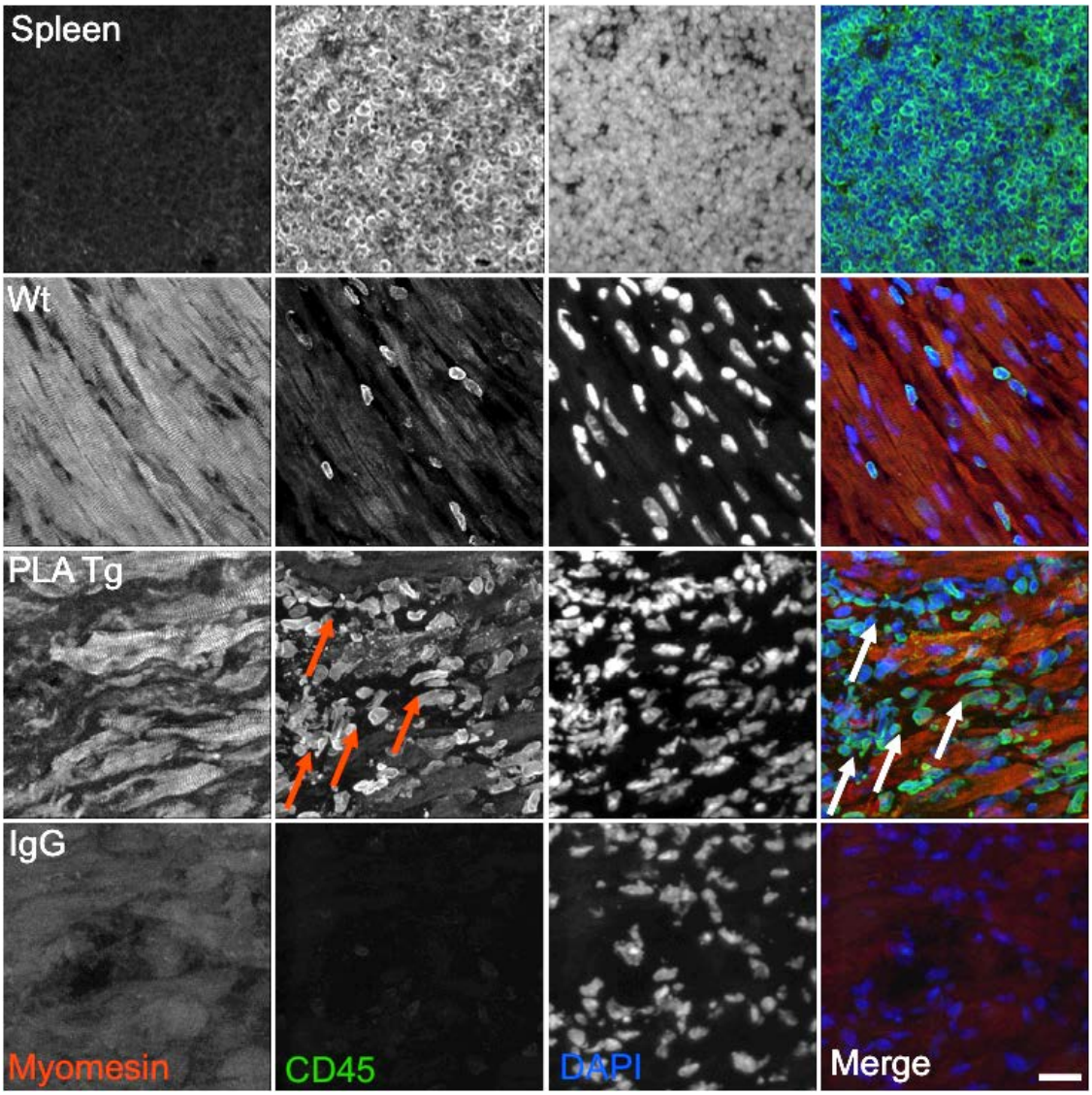

Figure 3.18. Prelamin A accumulation led to leukocytic invasion of the myocardium at 4 weeks of age. Cryopreserved heart cross-sections were co-stained with antibody to CD45 (green) and myomesin (red) and viewed with fluorescence microscopy to show that PLA Tg hearts (second bottom row) appeared to have many more CD45 positive cells within the myocardium than did Wt hearts (second top row). Cryopreserved spleen (top row) was used as positive control for the CD45 antibody whereas serum IgG was used as a negative control. Scale bar = 20 μm

significantly more cells in PLA Tg hearts (171.9 cells per field of view ± 19.73) compared to Wt (46.98 ± 6.54) $P<0.01$ (Fig 3.19A). Western blotting of whole tissue lysates confirmed that there was a general increase in CD45 protein expression in PLA Tg hearts compared to Wt (Fig 3.19B & C). Additionally, upon observation of the cardiac ultrastructure it was clear that there were activated leukocytes present in the interstitium of PLA Tg myocardium but not in Wt myocardium (Fig 3.20).

3.2.7 Cell death

The TUNEL assay labels unrepaired DNA breaks thereby enabling the detection of fragmented DNA, which is a classical response in apoptosis pathways. Here, TUNEL assay and cell counting was performed on wax-mounted heart sections to reveal that PLA Tg mice hearts (21.27 cells per field of view ± 3.30) had significantly more TUNEL positive nuclei than Wt hearts (2.7 ± 0.91) (Fig 3.21).

Caspase 3 is a key mediator in the apoptosis pathway, therefore western blotting of whole tissue lysates was performed to show that caspase 3 was not expressed in PLA Tg or Wt heart tissue (Fig 3.22), suggesting that apoptosis may not have been contributing to the observed increased TUNEL positivity.

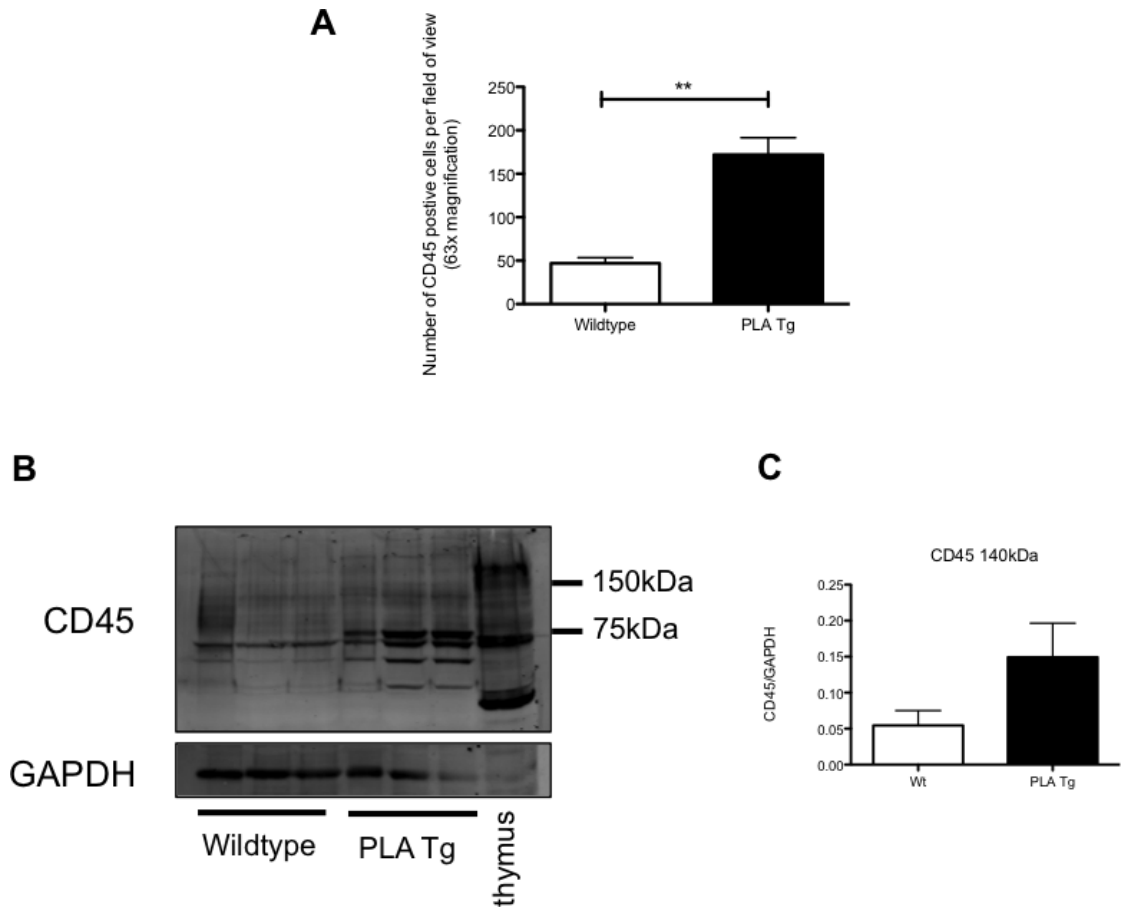

Figure 3.19. Quantification of CD45 microscopy confirmed an increase in CD45 positive cells and total CD45 protein expression in PLA Tg hearts compared to Wt. (A) CD45 positive cells per field of view on 63x magnification were counted by eye and revealed that there were significantly more CD45 positive cells in PLA Tg myocardium than Wt. Values expressed as mean±SEM, **P<0.01, N=3 /group, 20 randomly selected fields of view from each section were counted. (B) CD45 antibody was used to probe western blots of whole tissue lysates from hearts to show (C) increases in CD45 expression in PLA Tg hearts compared to Wt according to densitometric analysis. N=3/group

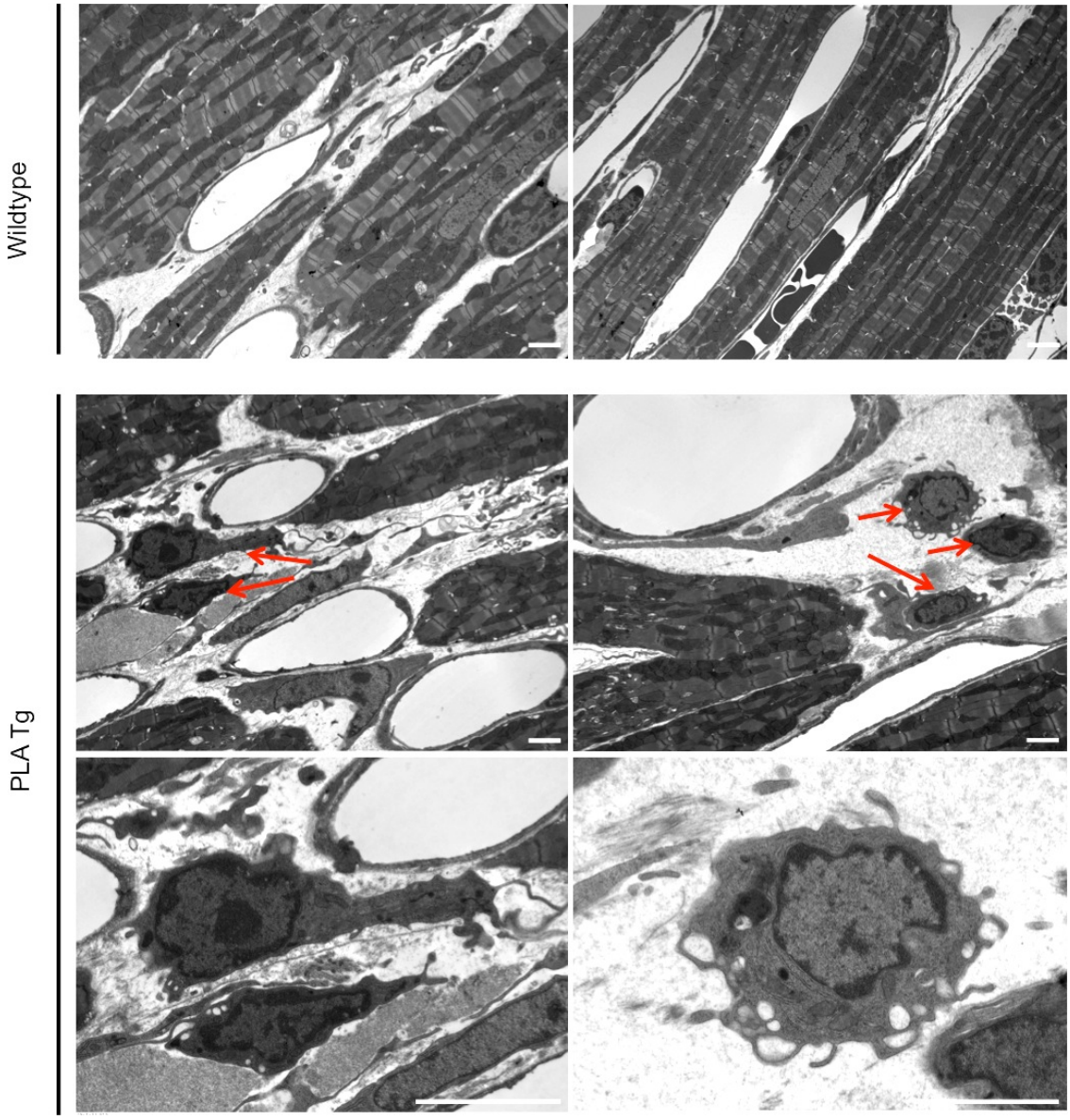

Figure 3.20. Leukocytes were present in hearts that accumulated prelamin A at the ultrastructural level. Perfusion fixed hearts were processed and stained for viewing with TEM. Presence of morphologically distinct dendritic leukocytes was observable in PLA Tg myocardium (bottom four panels) but not in Wt myocardium. Scale bar = 500 nm

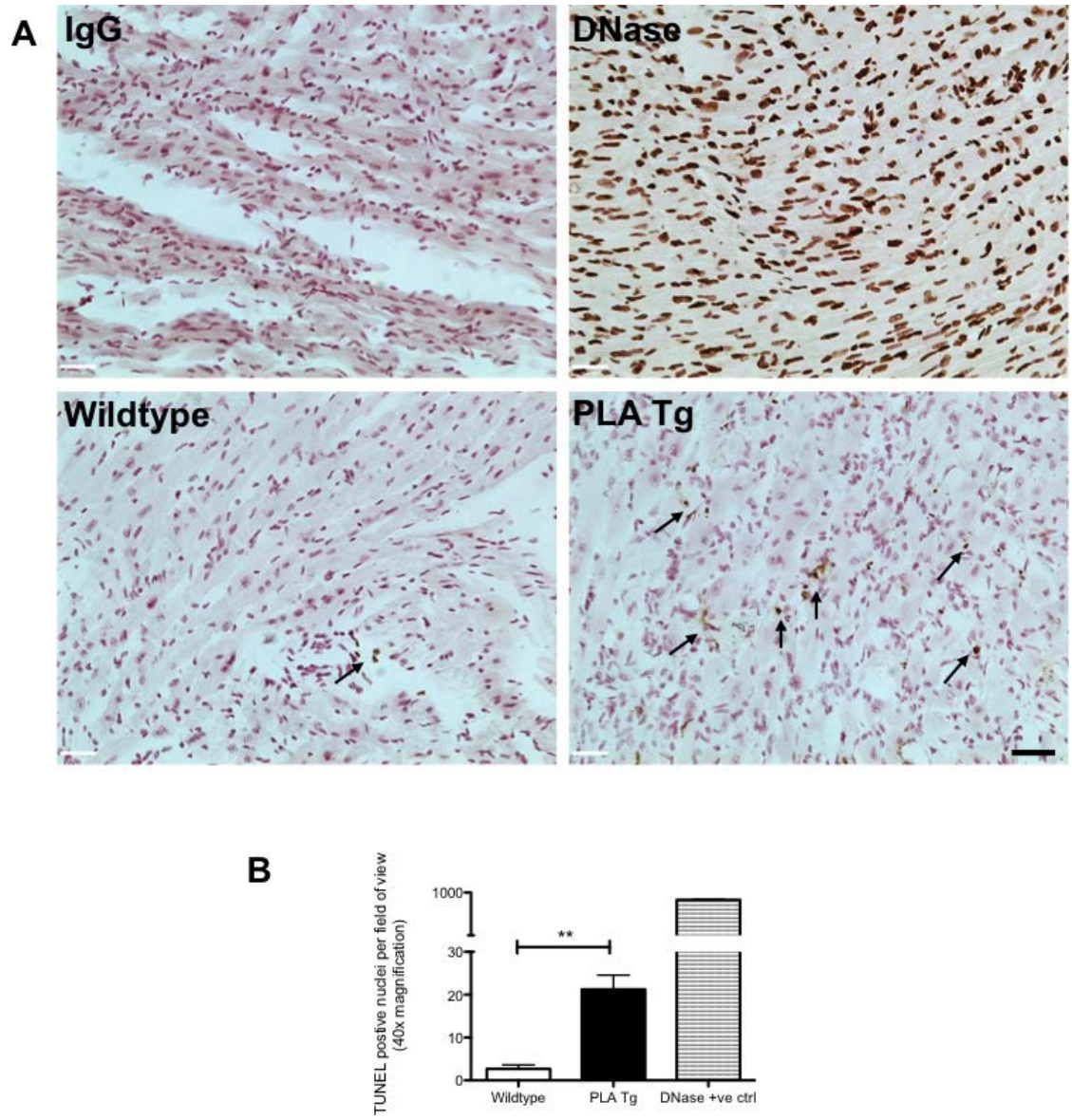

Figure 3.21. Prelamin A accumulation led to myocardial cell death. (A) Paraffin embedded cross sections were subject to TUNEL staining and viewed under light microscopy to show a perceived increase in TUNEL positive (brown staining) cells in PLA Tg (bottom right panel) compared to Wt (bottom left). Shown also are IgG negative control (top left panel) and DNAse treated positive control sections (top right). Scale bar = 30 μm (B) Number of TUNEL positive cells per field of view at 40x magnification were counted and showed a significant increase in the number of TUNEL positive cells in PLA Tg hearts compared to Wt. Values expressed as mean±SEM, **P<0.01, N=3/group; 10 randomly selected fields of view from each section were counted.

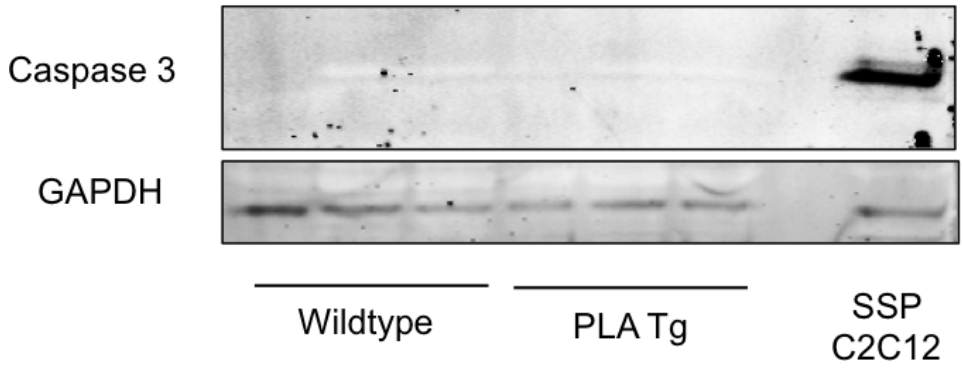

Figure 3.22. Cell death in hearts accumulating prelamin A was independent of Caspase 3 activation. Caspase 3 antibody was used to probe western blots of whole tissue lysates from Wt and PLA Tg hearts to show that caspase 3 was not expressed in Wt or PLA Tg hearts. C2C12 mouse myoblasts were treated with staurosporin (SSP C2C12) and run as a positive control for caspase 3 expression.

3.3 Discussion

3.3.1 Targeted transgenesis of L647R *LMNA* to the Rosa26 locus and Cre recombinase mediated stop cassette removal results in prelamin A accumulation in the nuclei of CMs

Initial characterisation of the targeted transgenesis model suggested that the system that was chosen to study prelamin A accumulation in the heart was efficient in achieving this aim. According to genotyping, mice were born in the expected Mendelian ratios and prelamin A was expressed exclusively in the hearts of PLA Tg animals. Moreover, it was shown that prelamin A accumulated in the nuclear rim of myocytes, as it does in premature ageing disorders, and laid the foundations to elucidate the biological significance of this potentially pathological process.

3.3.2 Cardiac specific prelamin A accumulation leads to a severe DCM and HF phenotype in PLA Tg mice

The *Lmna* mouse models present with a variety phenotypes. The most severe are the $Lmna^{-/-}$ mice, which succumb to HF at 8 weeks of age. Survival of $Lmna^{G609G/G609G}$ and $Zmpste24^{-/-}$ mice is approximately 3 months and the $Lmna^{H222P/H222P}$ mice survive to older ages still. At birth and up to weaning, PLA Tg mice appeared morphologically normal compared to Wt control mice. Soon after weaning, it became quickly apparent that mice accumulating prelamin A failed to thrive and died in a very short window of time. Although post-mortem assessment of PLA Tg mice heart weight to tibia length

ratios was not statistically significant compared to Wt, there was an incremental increase in both males and females indicating that remodelling of the heart may have occurred. This finding was supported by echocardiographic measurement of myocardial tissue walls, the dilated appearance of the heart upon excision and myocardial wall thinning evident in PLA Tg hearts compared to Wt as defined by histological staining. Echocardiographic analysis also showed that cardiac function was dramatically compromised in PLA Tg mice with enormously attenuated EF and FS values compared to their Wt counterparts. Interestingly, this DCM phenotype, which was ultimately fatal after 5 to 6 weeks of age, closely mimics the pathophysiological and survival phenotype observed in $Lmna^{-/-}$ mice, indicating that disruption of the lamina may be a key feature of pathogenesis. Data obtained from the MRI analysis of cardiac function reinforced the finding that cardiac function was severely attenuated. Indeed MRI analysis tended to agree with the echocardiographic analysis with regard to all but one parameter. LVEDV was much greater in PLA Tg hearts when measured by MRI compared to echocardiography indicating a more pronounced dilatation of the PLA Tg heart. It is difficult to attribute this difference to any specific aspect; however, in our study echo analysis was performed on a single 2D long-axis sections of the LV whereas MRI analysis was performed on a series of 2-D cross-sections. Therefore the echo analysis is based on much less spatial information, and may potentially underestimate the remodelling occurring in PLA Tg hearts in the cross-sectional plane. Another key feature of this model was progression to HF, which was shown by qPCR analysis of HF markers, and evidenced also by transudative pleural effusion.

Histological examination of hearts in related models of disease are phenotypically varied. $Lmna^{N195K/N195K}$ mice have mildly dilated hearts and $Lmna^{-/-}$

hearts are heavily dilated, whilst neither model shows any sign of disruption to the myocardial architecture on closer inspection. *Lmna*$^{H222P/H222P}$ and *Zmpste24*$^{-/-}$ mice present with myocardial disarray and fibrotic lesions, whilst hearts from *Zmpste24*$^{-/-}$ mice also appear to have lymphocytic infiltration into the myocardium. Histological examination of PLA Tg mice revealed myocardial disarray, and clustering of nuclei, which was confirmed by assessment of CD45 expression and TEM as leukocytic invasion of the myocardium. Sterile inflammation of the myocardium, a scenario in which the tissue becomes inflamed without any external source of pathogen, as in myocardial infarction, has been identified in the pathogenesis of heart failure[267]. Potentially, it can arise from damaged mitochondrial DNA, which escapes degradation and activates toll-like receptors in the heart, leading to an immune response and recruitment of leukocytes to the heart, and implicates metabolism and defective autophagic mechanisms[268].

Picrosirius red staining and TEM confirmed that severe fibrosis had occurred in the setting of prelamin A accumulation at 4 weeks of age. Cardiac MRI of contrast-injected mice also indicated the presence of diffuse fibrosis in the myocardium of PLA Tg mice further suggesting that significant cardiac remodelling was occurring in the setting of prelamin A accumulation. The importance of remodelling of the ECM cannot be overstated in heart failure paradigms. The elasticity of the myocardium is crucial to the heart's role as a pump and whilst remodelling is thought to occur as a reparative and adaptive response initially, the long-term effects are unequivocally detrimental and contribute greatly to congestive heart failure.

Another facet to be associated with DCM and heart failure is myocyte death. Cell death is thought to characterise end-stage DCM phenotypes presenting with

thinning of the myocardium[3]. Moreover, *Lmna*$^{+/-}$ mice experience DCM phenotypes and cardiac conduction disease as a result of apoptosis in the AV node tissue as defined by TUNEL assay and caspase-3 detection[227]. Additionally, *Lmna*$^{-/-}$ mice also show cell death on TUNEL staining[225]. To assess this, TUNEL staining was performed and gave a positive result that indicated that cell death occurred in PLA Tg hearts. However, Caspase 3, a commonly used marker for apoptosis, was negative. The implications of these somewhat contradictory results are that cell death is occurring, but not by apoptosis, meaning the CMs could be undergoing necrosis. Indeed the idea of apoptosis in DCM is a controversial one[269]. As previously stated, TUNEL labels unrepaired DNA 'nick ends' which are present as a result of the DNA fragmentation that often occurs during cell death. A potential pitfall of the TUNEL technique is that it is possible that unrepaired double strand breaks are also labelled and may in fact be an indicator of severe DNA damage as well as cell death. A previous study that focussed on this problem concluded that TUNEL is not a reliable indicator of cell death in DCM hearts and rather is an indicator of increased DNA repair activity[270], a point that is worth highlighting when considering that DNA damage accumulation is a hallmark of prelamin A/progerin accumulating diseases.

In summary, cardiac specific accumulation of prelamin A led to a multi-faceted pathological response involving remodelling of the myocardium via interstitial fibrosis, sterile inflammation and potentially cell death, which resulted in severe systolic dysfunction reminiscent of DCM, heart failure, growth retardation and ultimately led to death at 5-6 weeks of age. Comparisons to existing models are summarised in Table 3.2. As an aside, disease progression in PLA Tg mice mimics the progression of clinical HGPS, whereby infants appear normal and only begin to show symptoms after 2 years

of age, after which point children suffer retarded growth and rapid ageing of selective tissues and organs including the cardiovascular system. Moreover, rapid cardiac decline is seen in HGPS patients a matter of weeks before death[228], and suggests that intrinsic cardiac decline may occur in hearts of progeria patients independent of vascular changes.

Table 3.2. Phenotypic comparison of existing models of *LMNA* associated DCM.

Model	Survival	Heart pathology	Fibrosis	Inflammation	Cell death	Nuclear morphology defects
Lmna$^{-/-}$	6-8 weeks	DCM and heart failure	+	-	+	+
Lmna$^{+/-}$	Long-lived	Late onset DCM-CD	+	-	+	+
Lmna$^{N195K/N195K}$	12-14 weeks	DCM and heart failure	+	-		+
Lmna$^{H222P/H222P}$	Males: 4-9 months Females: 9-13 months	DCM and heart failure	+	-	-	+
Lmna$^{G609G/G609G}$	3-4 months	LQT and arrhythmia	?	-	?	?
Zmpste24$^{-/-}$	3-4 months	Non-specific	-	+	-	?
Lmna$^{MHC-M371K}$	2-7 weeks and prenatal lethal	Acute & subacute heart failure	-	-	-	+
MLC2v-PLA Tg (Current Study)	5-6 weeks	DCM and heart failure	+	+	+	+

Lmna$^{MHC-M371K}$ and MLC2v-PLA Tg models are specific for the heart whereas the remaining models are tissue non-specific and are expressed in all cells of the respective model.

+ = Yes, - = No, ? = unknown

Chapter 4: Molecular characterisation of mice accumulating CM specific prelamin A

4.1 Introduction

Models of *LMNA* associated disease have reported a variety of pathways to which pathogenesis may be attributed. These include mechanical, transcriptional, DNA damage, cell cycle, MAPK signalling, mTOR signalling and autophagy. For example, *Lmna*$^{-/-}$ mice have a distinct DCM-like phenotype involving reduction in contractility of the myocardium. *LMNA* deficiency has been associated with a number of cellular events including disruption of the LINC complex and the cytoskeleton which may impair mechanical coupling in the myocytes leading to reduction in force[225, 244]. Moreover, inhibition of mechanotransduction and altered signalling has been reported in *in vitro* models of *LMNA* deficiency[126, 168, 170]. In addition, AKT/mTOR signalling is thought to be elevated in *Lmna*$^{-/-}$ mice[241]. AKT/mTOR signalling has also been implicated in the pathogenesis of DCM in *Lmna*$^{H222P/H222P}$ mice[240]. Interestingly, defective autophagic responses were also reported in these mice, and may be linked to mTOR signalling. Another defect reported in *Lmna*$^{H222P/H222P}$ mice, *Lmna*$^{N195K/N195K}$ mice, which have DCM, as well as *Lmna*$^{-/-}$ mice, is mislocalisation and loss of connexins. In the heart, connexins are membrane bound ion channels that link the cytoplasmic domains of adjacent CMs, thus playing a vital role in propagating electrical signals from one CM to the next, enabling efficient and synchronous contraction of the myocardium. Loss of

connexins, particularly Cx43, has been associated with the cardiac conduction defects seen in *Lmna*$^{-/-}$ and *Lmna*$^{H222P/H222P}$ mice[245, 246, 248].

Zmpste24$^{-/-}$ mice have not been studied in detail in the context of heart disease. Although it is clear that there are histological abnormalities in the myocardium, it is not yet clear whether there is an overt cardiac phenotype. However, extensive systemic characterisation of the model shows an obvious progeroid-like phenotype and many molecular pathways have been identified in the pathogenesis of these mice. *Zmpste24*$^{-/-}$ mice are senescent and exhibit defective DNA repair mechanisms[271], altered p53 signalling[272], ageing like epigenetic patterns[273], deregulated miRNA repression[274], mitochondrial dysfunction[275], inhibition of somatotrophic signalling[149, 276] and systemic inflammation[125].

Genomic instability is a hallmark feature of progeroid disorders and can be shown as accumulation of DNA damage markers in the nuclei of cells. The current dogma suggests that this is due to faulty DNA damage repair mechanisms caused by destabilisation of the lamin scaffold. Lamins are thought to be crucial in chromatin arrangement and in facilitating optimal positioning for DNA damage repair. In the presence of prelamin A/progerin variants, the lamina is disorganised and heterochromatin cannot be positioned optimally leading to defective recruitment of DNA damage repair factors[207]. Moreover, cell cycle regulators are key mediators in the onset of senescence. Activation of p53 occurs in order to stall the cell cycle in G1/2 phase to allow DNA damage to repair before the cell continues through to DNA synthesis or mitosis. It is thought that persistent DNA damage can lead to constitutive p53 activation and permanent cell cycle arrest. Reports suggest that this occurs via ATM dependent phosphorylation of p53[94, 277, 278]. Expression and activation of p53 has

been linked to the ageing phenotype seen in *Zmpste24*$^{-/-}$ mice[272]. Moreover, whilst CMs are post mitotic, activation of p53 has been observed in CMs and is thought to regulate pathogenic pathways[279]. Additionally, activation of p16 and p21 has also been identified as potentially senescence inducing in many cell types[280-283]. These many pathways which regulate disease are not exclusive and may occur in tandem with each other and may even be co-dependent. In this chapter, the phenotype of the PLA Tg mice is characterised in more detail in order to define the mechanisms leading to cardiac dysfunction.

4.2 Results

4.2.1 Prelamin A accumulation causes expression changes in nuclear envelope proteins and mislocalisation of the intermediate filament protein, desmin

Prelamin A accumulation is known to disrupt the NE and cause changes to LINC complex proteins and our current model displays phenotypic similarities to *Lmna*$^{-/-}$ mice. Therefore, the LINC complex and cytoskeletal components of the myocyte were assessed in PLA Tg mice.

Western blotting of ventricular tissue lysates was performed and prelamin A was detectable only in PLA Tg heart lysates (Fig 4.1). The LINC complex proteins, lamins A, C and B1, appeared to be significantly increased in PLA Tg hearts compared to Wt. Emerin expression did not change between Wt and PLA Tg whilst SUN2 was decreased in PLA Tg hearts (Fig 4.1). Antibody to nesprin 1α (N3) showed that an isoform corresponding to ~95kDa was absent in PLA Tg hearts whilst nesprin 2 also appeared to

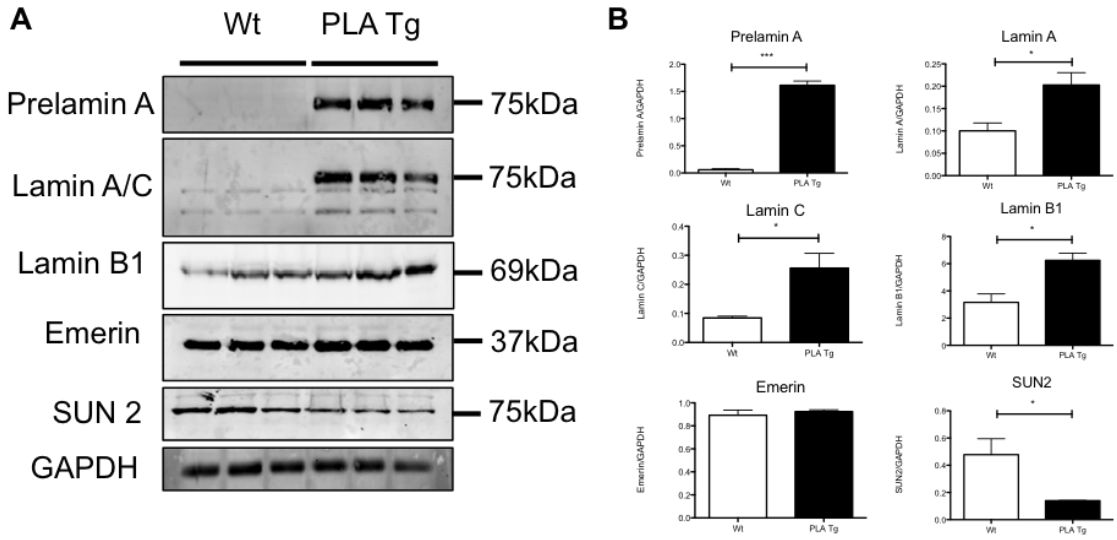

Figure 4.1. Expression of inner nuclear membrane associated proteins was dysregulated in 4 week old hearts of mice accumulating prelamin A. A) Ventricular tissue lysates were western blotted and membranes probed with antibodies for INM proteins prelamin A (C20), lamin A/C (N18), lamin B1, emerin and SUN2. GAPDH was used as loading control. B) Densitometric analysis showed that, as expected, prelamin A was increased in PLA Tg hearts. Significant increases were also apparent in lamin A and C and lamin B1. SUN2 significantly decreased in PLA Tg hearts tissue compared to Wt. Emerin remained unchanged. Values expressed as mean±SEM, *P<0.05 ***P<0.001, N=3/group

undergo an isoform switch as there was a significant increase in the 75kDa band in PLA Tg compared to Wt (Fig 4.2). Expression of desmin was significantly increased in PLA Tg hearts compared to Wt. Expression of sarcomeric myomesin was unchanged between Wt and PLA Tg mice, whilst α-actinin was significantly decreased in PLA Tg compared to Wt (Fig 4.2).

Next, cryopreserved heart sections were subject to immunofluorescence staining for LINC associated and cytoskeletal proteins. Prelamin A (C-20 antibody) staining confirmed that prelamin A was present in the nuclear rim of PLA Tg but not Wt CMs (Fig 4.3). Lamin A/C was localised to the nuclear rim of CMs in Wt and PLA Tg myocytes, whilst the number of lamin A/C positive nuclei appeared increased in PLA Tg hearts (Fig 4.4). Many of these nuclei were located within the interstitium of the myocardium, which also appeared more pronounced compared to Wt, indicating the presence of another cell type. Moreover the lamin A/C staining was more intense in interstitial cells compared to CMs. Lamin B1 was also distributed at the nuclear rim of CMs and interstitial cells in both Wt and PLA Tg hearts (Fig 4.5). Desmin distribution appeared more disparate in PLA Tg hearts compared to Wt. Whilst displaying the sarcomeric staining expected, the clear perinuclear localisation seen in Wt was largely absent in prelamin A positive nuclei and staining was also weaker at intercalated discs (Fig 4.1). Moreover, it appeared that desmin occasionally accumulated in a random, non-specific manner in the cytoplasmic domain of CMs. Staining for cytoskeletal components of the sarcomere showed that myomesin localisation was unchanged between PLA Tg and Wt heart sections (Fig 4.4 & 4.5), whilst α-actinin localisation was also unaffected – although there was some indication that staining was less intense

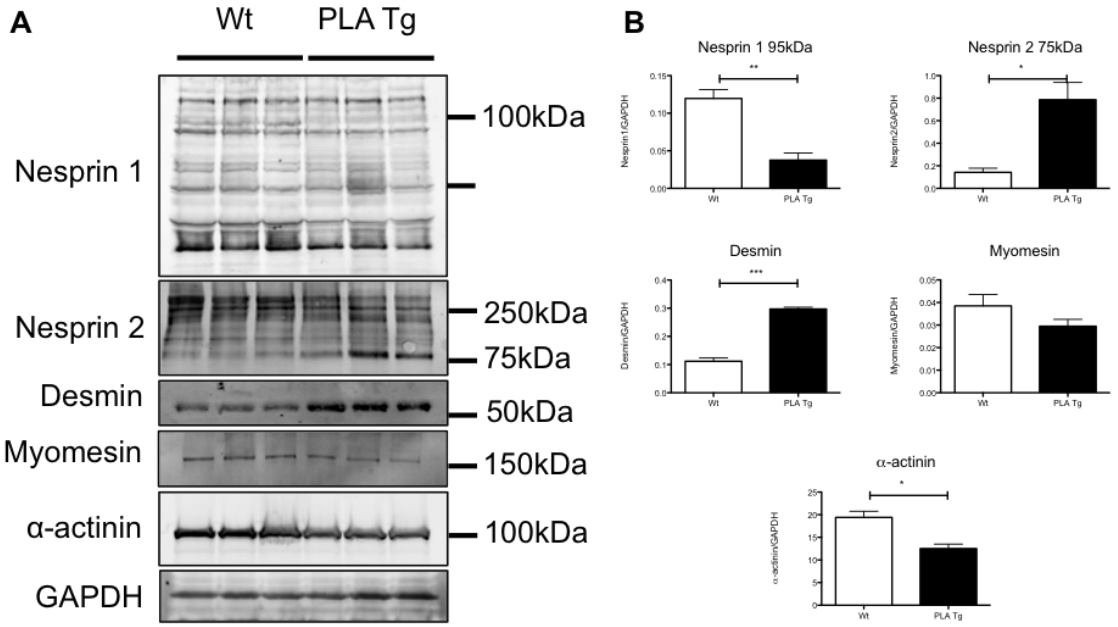

Figure 4.2. Expression of outer nuclear membrane proteins, intermediate filament proteins and cytoskeletal components of the sarcomere was dysregulated in 4 week old hearts that accumulate prelamin A. A) Ventricular tissue lysates were western blotted and the membranes were probed for antibodies to nesprin 1, nesprin 2, desmin, myomesin and α-actinin. B) Densitometric analysis showed that nesprin 1 expressed lower levels of the 95kDa isoform in PLA Tg heart compared to Wt. A nesprin 2 isoform of molecular weight 75kDa was significantly increased in PLA Tg hearts. Desmin significantly increased in PLA Tg hearts and α-actinin significantly decreased when compared to Wt. Myomesin showed a trend towards a decrease in expression in PLA Tg mice. Values expressed as mean±SEM, *P<0.05, **P<0.01, N=3/group

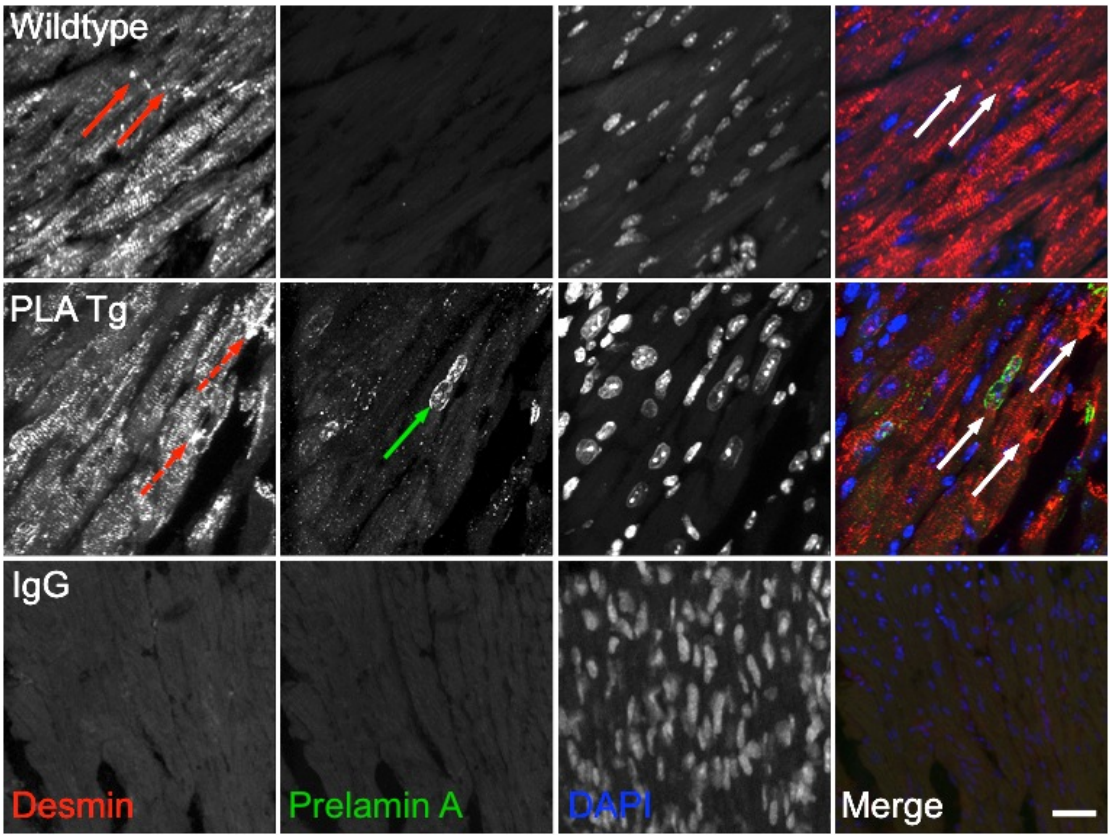

Figure 4.3. Prelamin A was localised to the nuclear rim and desmin appeared to show a more perinuclear localisation in PLA Tg hearts. Cryopreserved heart cross sections were subject to immunofluorescence staining with prelamin A (green) and desmin (red) antibodies, and viewed under fluorescent light. Prelamin A accumulated in the nuclear rim of PLA Tg mice mice and not Wt (green arrow). In PLA Tg hearts, desmin accumulated in aggregates at perinucler regions and sarcolemmal regions (dashed red arrows) compared to Wt, which showed localisation to the sarcomere and intercalated discs (red arrows). Sections stained with serum IgG were used as negative controls. Scale bar = 20 μm

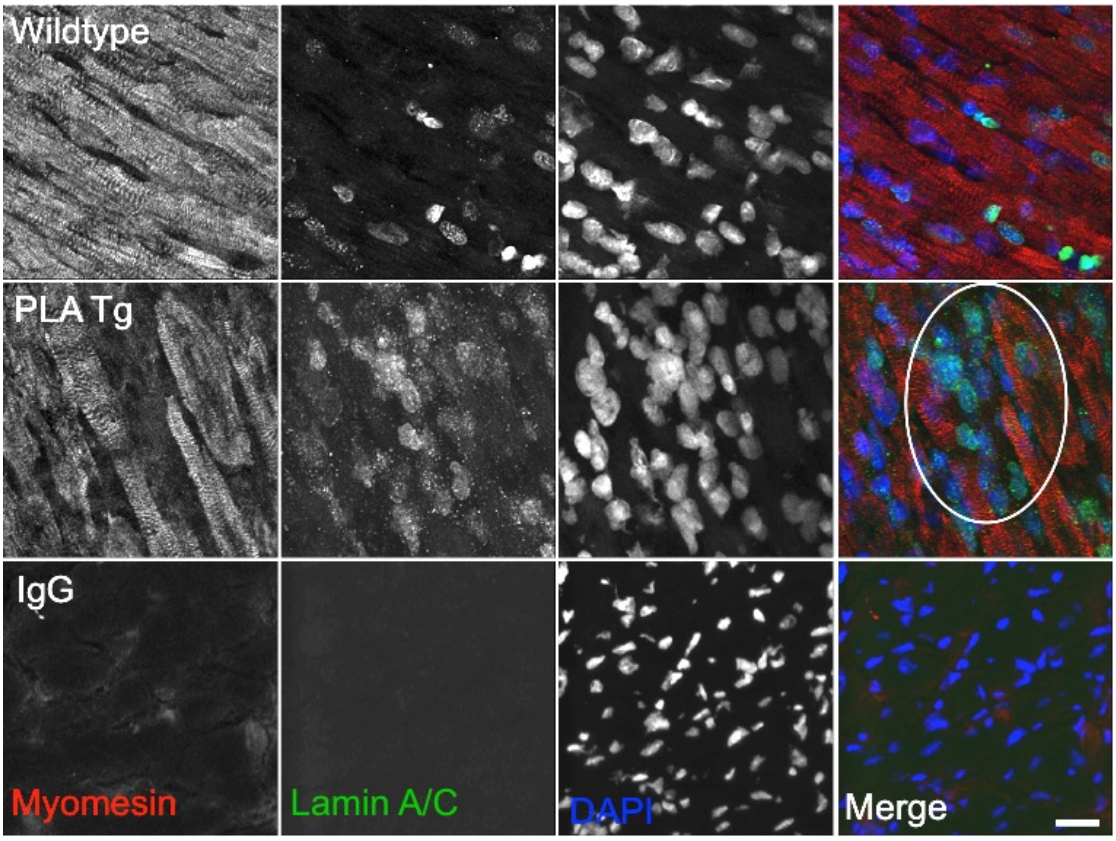

Figure 4.4. Lamin A/C was localised to the nuclear rim and nucleoplasm in all cells in the heart and myomesin was localised to the sarcomere in Wt and PLA Tg mice. Cryopreserved heart sections were subject to immunofluorescence staining with lamin A/C (green) and myomesin (red) antibodies and showed that myomesin was localised to the sarcomere in both Wt and PLA Tg mice with no observable differences. Lamin A/C was localised to the nuclear rim and nucleoplasm in CMs. Heart sections from PLA Tg mice appeared to have more lamin A/C positive nuclei than Wt within the myocardium which gathered in regions between the myomesin staining indicative of interstitial clusters of cells (within the ellipse). Sections stained with serum IgG were used as negative controls. Scale bar = 20 μm

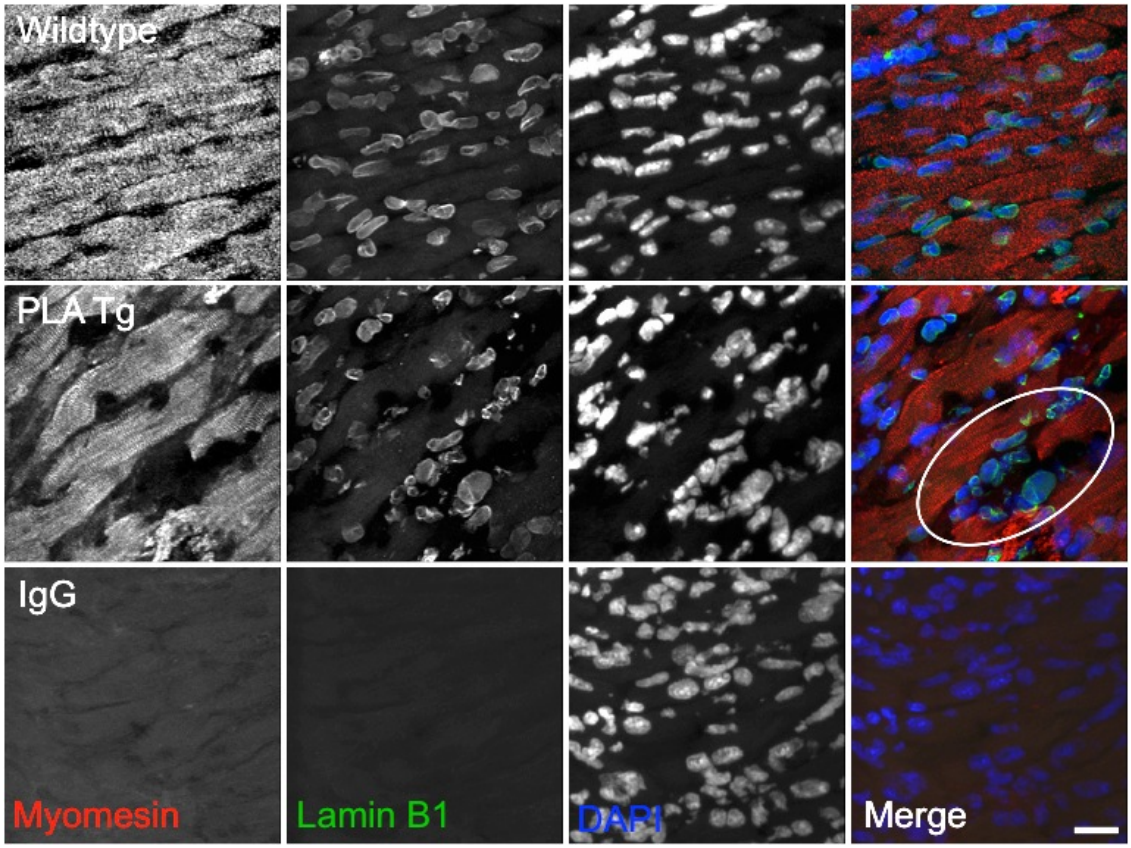

Figure 4.5. Lamin B1 localised to the nuclear rim in all cells of the myocardium in Wt and PLA Tg mice but appeared to be less intense in PLA Tg CMs. Cryopreserved heart sections were subject to immunofluorescence staining with lamin B1 antibody (green) and myomesin (red). Lamin B1 was localised to the nuclear rim in all cells but was was more intense in the nuclei of cells in the interstitium than the CMs. There appeared to be fewer CMs and more interstitial cells in PLA Tg mice compared to Wt (within the ellipse). Myomesin was used as a CM marker. Sections stained with serum IgG were used as negative controls. Scale bar = 20 μm

and less sharp (Fig 4.6). Interestingly, in Wt sections, prelamin A appeared to co-localise with α-actinin at the sarcomere, a feature which has not before been observed (Fig 4.6) and discussed in chapter 7.

4.2.2 Prelamin A accumulation causes misshapen nuclei and disruption to perinuclear organisation in CMs

It has been well reported that aberrant expression of lamins or lamin mutants has a deleterious effect on nuclear structure and results in nuclear morphology defects. Moreover, prelamin A accumulating diseases also report a loss of heterochromatin in affected nuclei, although this has not been shown in CMs.

To ascertain whether this occurs in prelamin A accumulating CMs, hearts were perfusion fixed and processed for electron microscopy. As expected, nuclei were often misshapen in PLA Tg hearts compared to Wt (Fig 4.7) and also underwent a loss of heterochromatin from the nuclear periphery. It was also possible to visualise an increased space between the nuclear membrane and the sarcomeres. This was also evident even in nuclei of PLA Tg hearts that were not misshapen. In contrast, the structure of the sarcomeres appeared unaffected in PLA Tg compared to Wt.

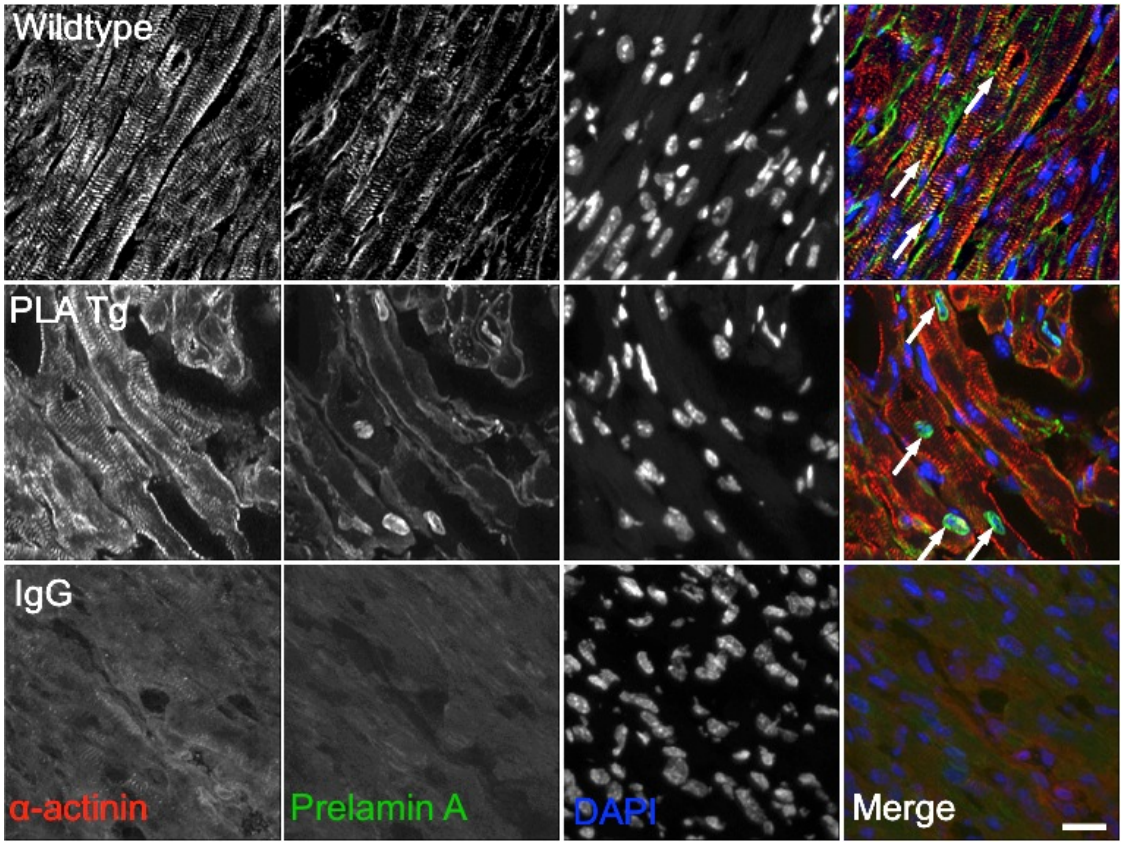

Figure 4.6. Prelamin A co-localised with α-actinin at the sarcomere in Wt hearts, whilst α-actinin staining intensity decreased in PLA Tg hearts. Cryopreserved heart cross sections were subject to immunofluorescence staining with prelamin A (green) and α-actinin (red) antibodies. Prelamin A appeared to colocalise with α-actinin at the sarcomere in Wt hearts to create a yellow colour in the merge (identified by arrows). In PLA Tg hearts, prelamin A localised to the nuclear rim as previously shown (arrows). Concomitantly, α-actinin staining was less intense and more diffuse in PLA Tg hearts compared to Wt. Sections stained with serum IgG were used as negative controls. Scale bar = 20 μm

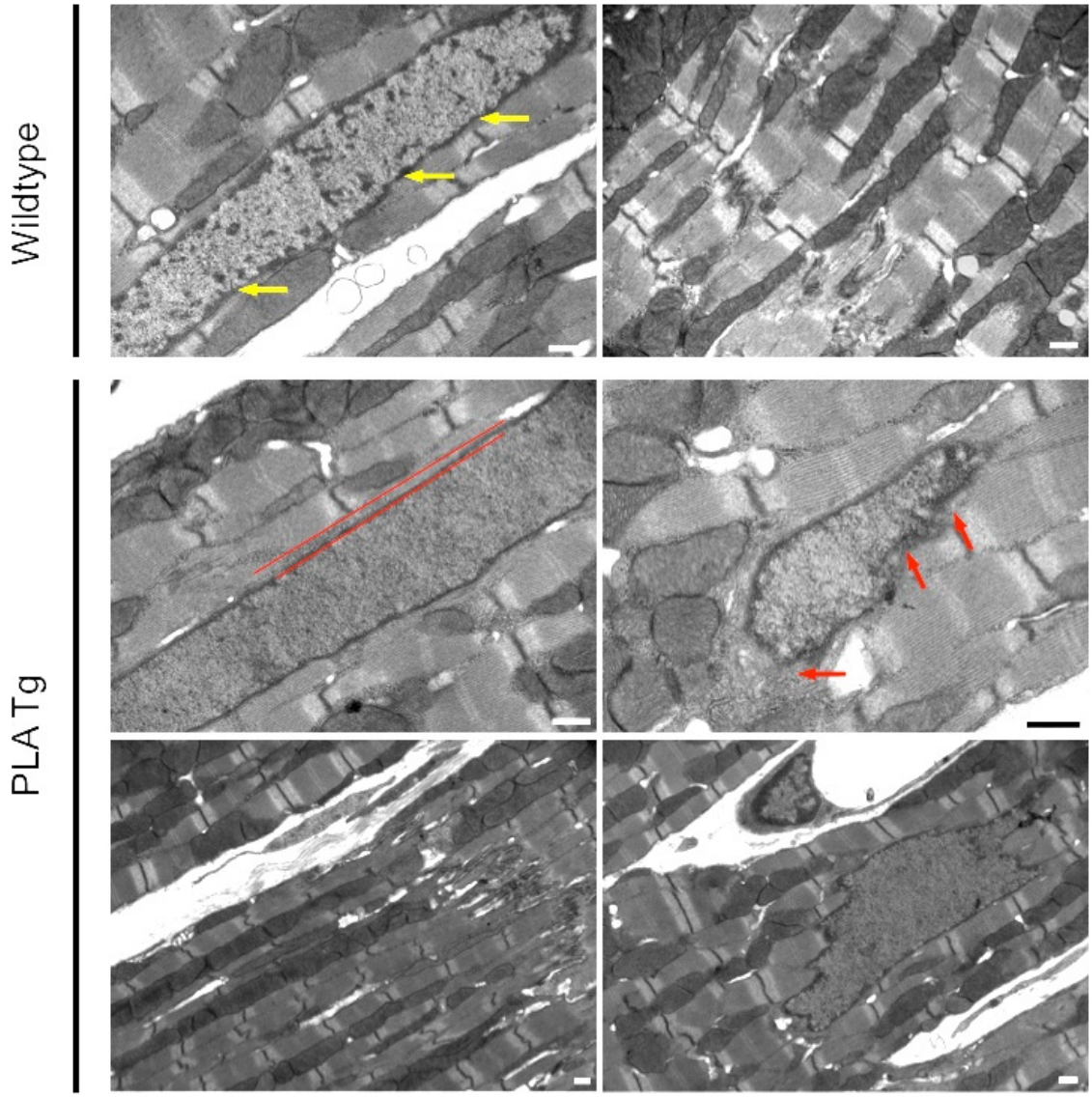

Figure 4.7. Prelamin A accumulation led to nuclear morphology defects, loss of heterochromatin and disruption of the nuclear membrane-sarcomere junction. Perfusion fixed hearts were processed and stained for TEM. The sarcomere organisation and nuclear morphology was normal in Wt hearts as was the appearance of heterochromatin (dark spots within the nucleus). Comparatively, PLA Tg nuclei were often dysmorphic with a loss of heterochromatin especially at the nuclear periphery. The distance between the sarcomere and nuclear membrane appeared to be increased in PLA Tg hearts (highlighted here with red border lines and red arrows) compared to Wt, which had no observable space between the nuclear membrane and sarcomere (yellow arrows). Scale bar = 500 nm

4.2.3 Prelamin A accumulation leads to mislocalisation and aberrant expression of Cx43

To ascertain whether Cx43 expression in the heart was affected in the setting of prelamin A accumulation, cryopreserved heart sections were subject to immunofluorescence staining using an antibody directed towards Cx43. Wt hearts showed intense staining that was clearly localised to intercalated discs, whilst Cx43 was disrupted in PLA Tg hearts, localising within cytoplasmic regions of CMs in a random manner (Fig 4.8A). Moreover, there appeared to be less Cx43 staining in PLA Tg hearts. Western blotting of whole tissue lysates confirmed that Cx43 showed a trend towards down regulated expression in PLA Tg hearts compared to Wt (Fig 4.8B & C).

4.2.4 Prelamin A accumulation leads to an increase in DNA damage marker γ-H2AX in CMs

In order to assess whether DNA damage was present in CMs that accumulated prelamin A, cryopreserved heart sections were subject to indirect immunofluorescence staining using an antibody directed towards phosphorylated-Histone 2AX (γ-H2AX). During DNA damage response, phosphorylation of H2AX is one of the earliest events in the DDR and acts as a sensor that initiates downstream effectors such as ATM. As such, it is an ideal marker for DNA damage accumulation in the current model. As expected, it was observed that γ-H2AX foci were increased in CMs of PLA Tg hearts compared to Wt. It was obvious that many more nuclei expressed γ-H2AX foci with many more γ-H2AX foci per nucleus (Fig 4.9A). Furthermore, western blotting of whole tissue

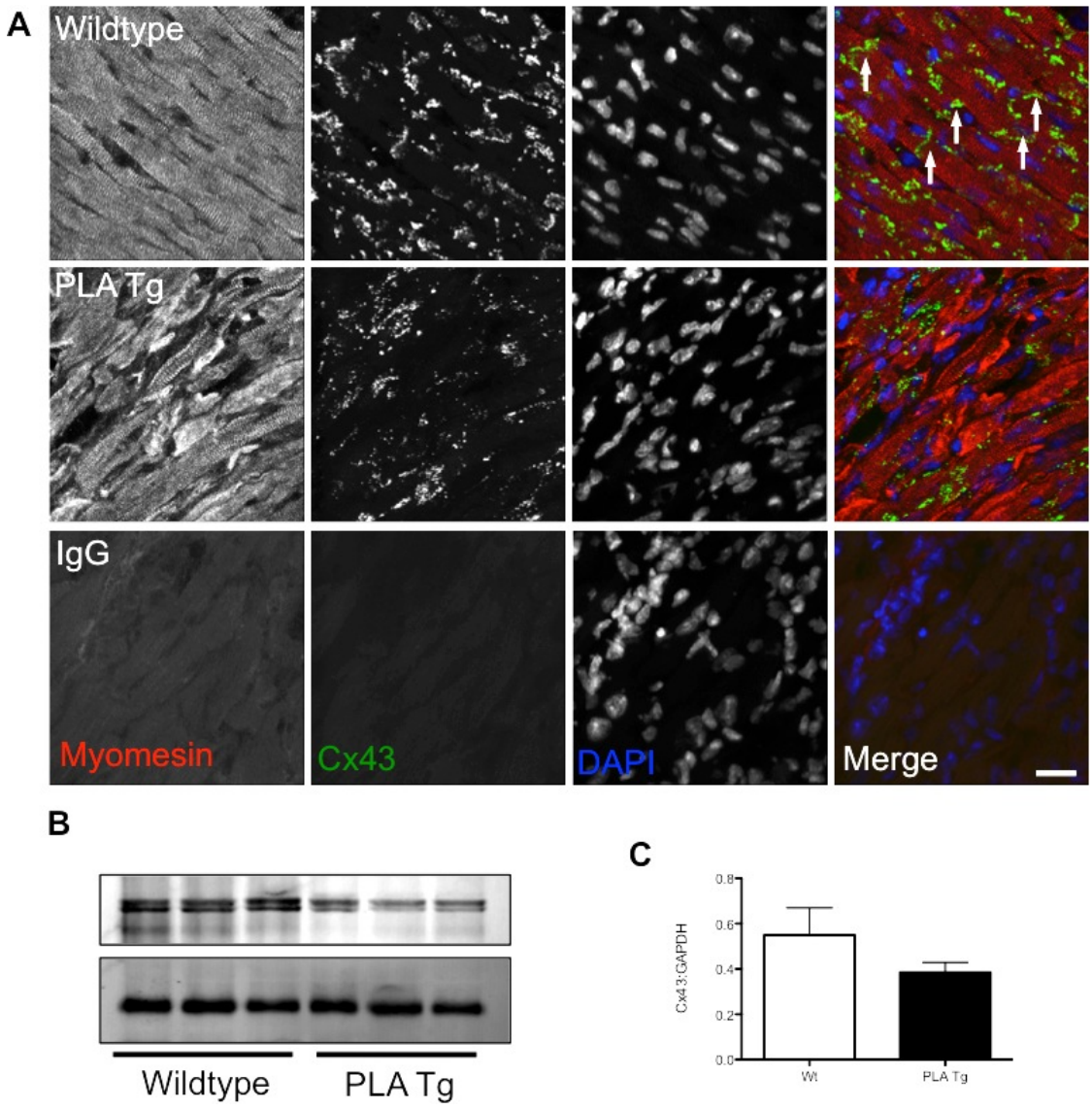

Figure 4.8. Prelamin A accumulation led to mislocalisation and loss of Cx43 in PLA Tg myocardium. (A) Cryopreserved heart cross sections were subject to immunofluorescence staining with Cx43 (green) and myomesin (red) antibodies. In Wt myocardium, Cx43 was localised to the intercalated discs with strong staining intensity (white arrows). Comparatively, Cx43 localisation was erratic and non specific within the cytoplasm of PLA Tg myocytes. Scale bar = 20 μm (B) Ventricular tissue lysates were western blotted and the membrane was probed with Cx43 antibody. There appeared to be a reduction in Cx43 expression in PLA Tg hearts compared to Wt. (C) Densitometry showed an incremental but non-significant decrease in Cx43 expression. Values expressed as mean±SEM, N=3/group

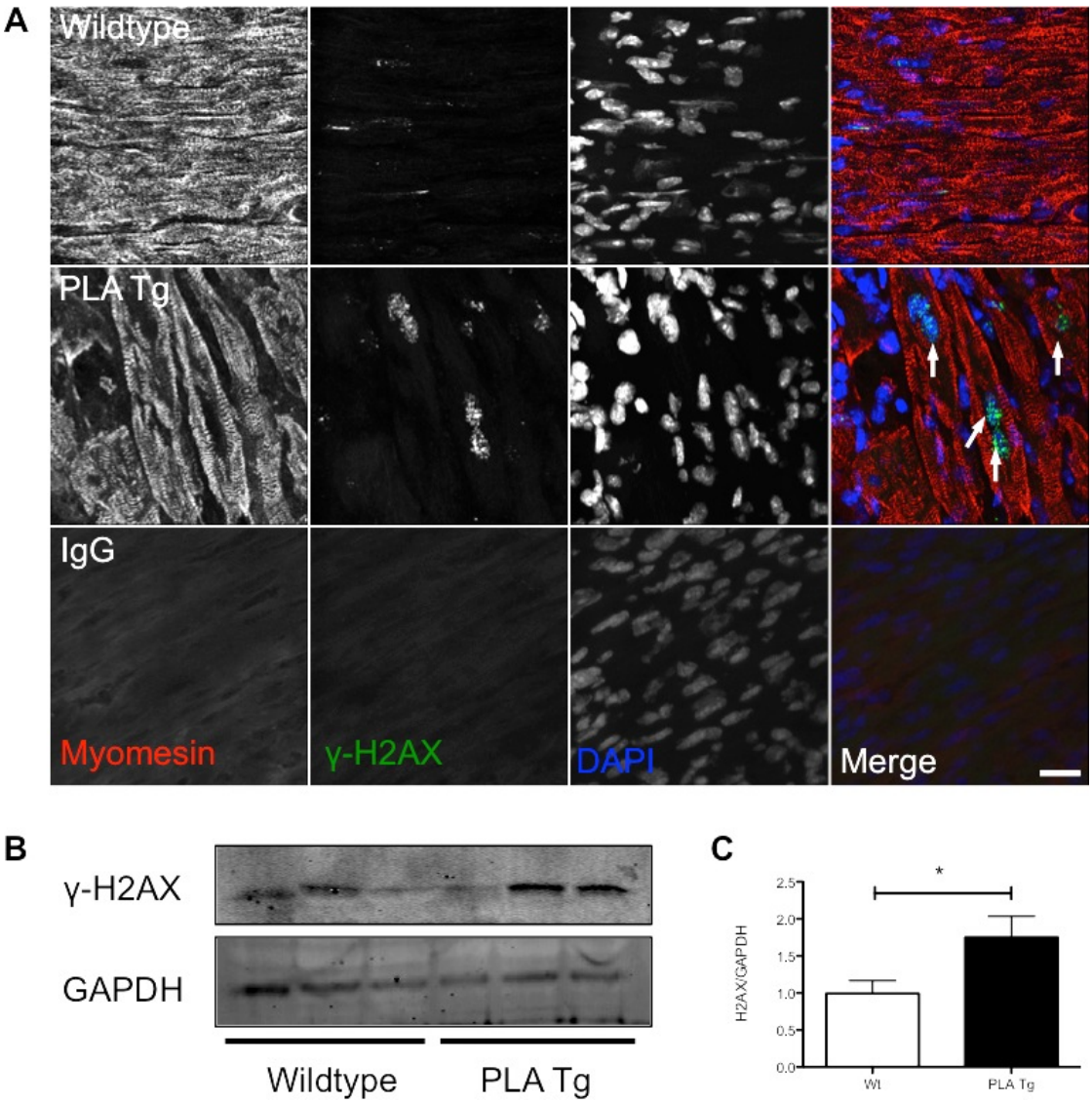

Figure 4.9. Prelamin A accumulation led to an increase in γ-H2AX foci and protein expression in PLA Tg hearts. (A) Cryopreserved heart cross sections were subject to immunofluorescence staining with γ-H2AX (green) and myomesin (red) antibodies. There were more γ-H2AX positive nuclei in PLA Tg myocardium compared to Wt and the number of γ-H2AX foci in the nuclei was also increased. Scale bar = 20 μm (B) Ventricular tissue lysates were western blotted and the membrane was probed with γ-H2AX antibody and showed that γ-H2AX expression was significantly increased in PLA Tg hearts compared to Wt. Values expressed as mean±SEM, *P<0.05, N=6/group

lysates showed a small, although significant, increase in γ-H2AX expression (Fig 4.9B & C).

4.2.5 Myocardium of hearts accumulating prelamin A express senescence associated β galactosidase

Accumulation of large amounts of DNA damage leading to permanent stalling of the cell cycle has been implicated in the onset of stress induced premature senescence (SIPS). Senescent cells are known to express elevated levels of lysosomal β-galactosidase that can be detected at pH 6.0 as opposed to pH 4.0[284]. The theory behind detection of β-gal at suboptimal pH is that enzyme expression is thought to be orders of magnitude greater in senescent cells compared to healthy cells, owing to the accumulation of damaged non degradable macromolecules in senescent cells[285]. Although SA-β-gal has never been shown in heart tissue sections, prelamin A accumulation in cell cultures of fibroblasts and VSMCs, both endogenous and ectopic, is known to result in expression of SA-β-gal[124, 256].

Thinly sliced (5 μm thick) cryopreserved heart sections were stained with β-galactosidase staining solution to reveal that PLA Tg hearts expressed large amounts of SA-β-gal whereas Wt hearts did not express SA- β-gal (Fig 4.10).

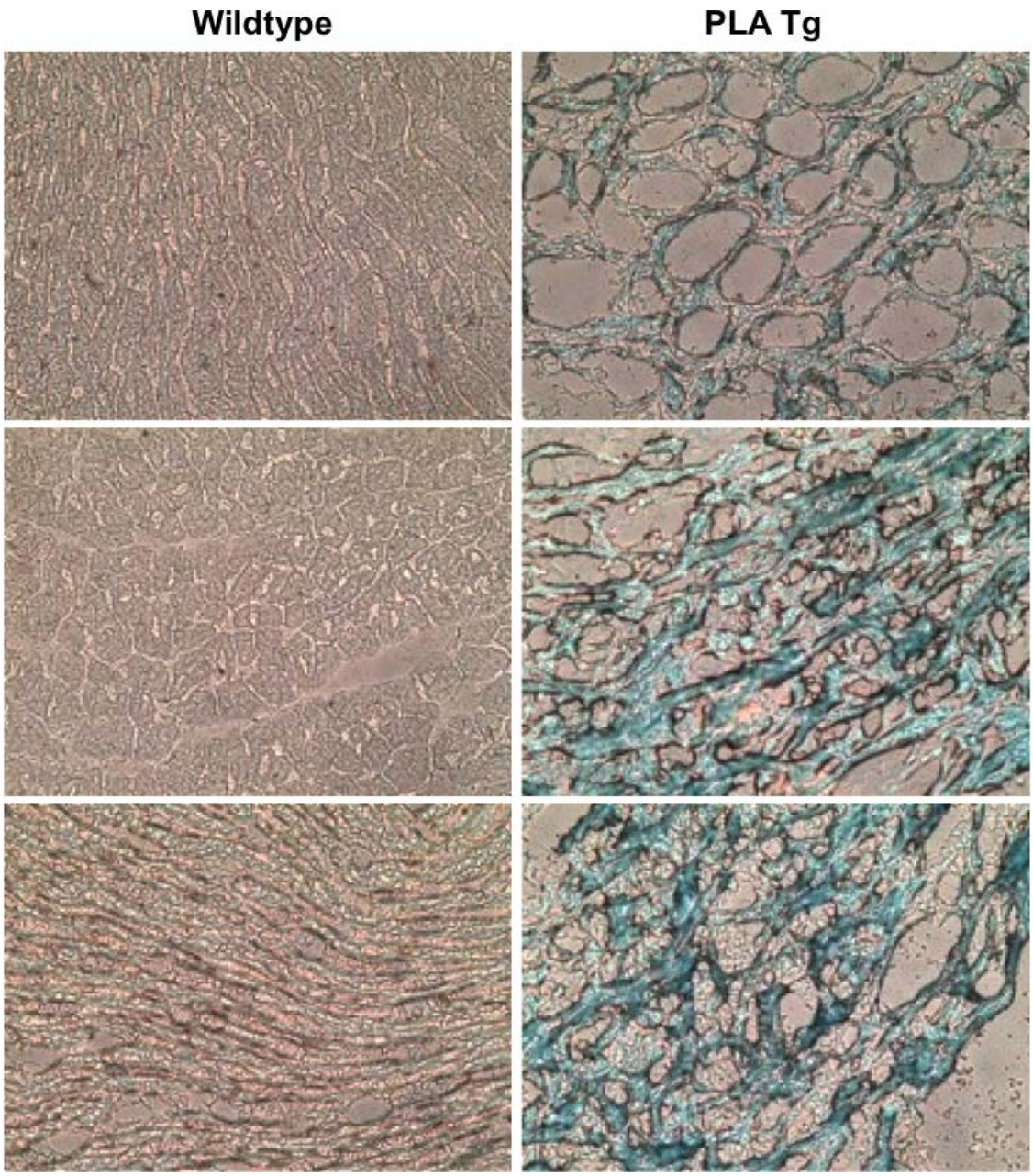

Figure 4.10. Prelamin A accumulation led to the expression of the senescence associated β-galactosidase in PLA Tg hearts. 5 µm thick cryopreserved heart cross sections were subject to staining with senescence associated β-galactosidase staining solution and viewed under light microscopy. SA-β-Gal positive staining (blue) was observed in PLA Tg but not Wt hearts. Disruption of the myocardium was also apparent in PLA Tg hearts as the tissue sections were punctured with holes. Scale bar = 60 µm

4.2.6 Expression of the cell cycle regulators appears unaffected by accumulation of prelamin A

In order to assess the role of cell cycle regulators, western blotting of whole tissue lysates was performed and showed that tumour suppressor protein p53 and the cyclin dependent kinase inhibitors p21 and p16 were barely detectable in all tissue lysates. C2C12 myoblasts treated with 1μM doxorubicin for 3 hours were used as a positive control and showed strong expression of p53, p21 and p16. There appeared to be no observable difference between Wt or PLA Tg hearts (Fig 4.11).

4.2.7 The unfolded protein response (UPR) and autophagy are not activated in the setting of prelamin A accumulation

Accumulation of toxic matter in cells is dealt with by stress response systems in which macromolecules are subject to proteosomal, lysosomal and autophagosomal degradation. The events preceding degradation involve stress sensing and labelling mechanisms including the unfolded protein response (UPR) and autophagy. During the UPR, chaperones such as Grp78 and Grp94 bind unfolded proteins and label them for degradation[286], whilst activation of autophagy is associated with the lipidation status and cleavage of LC3[287].

To assess whether the UPR was activated in the setting of prelamin A accumulation, western blotting of whole tissue lysates was performed using KDEL antibody, which detects Grp78 and 94. Neither Grp78 nor Grp94 were detectable in Wt or PLA Tg heart tissue (Fig 4.12A). Finally, to assess autophagy, western blotting of

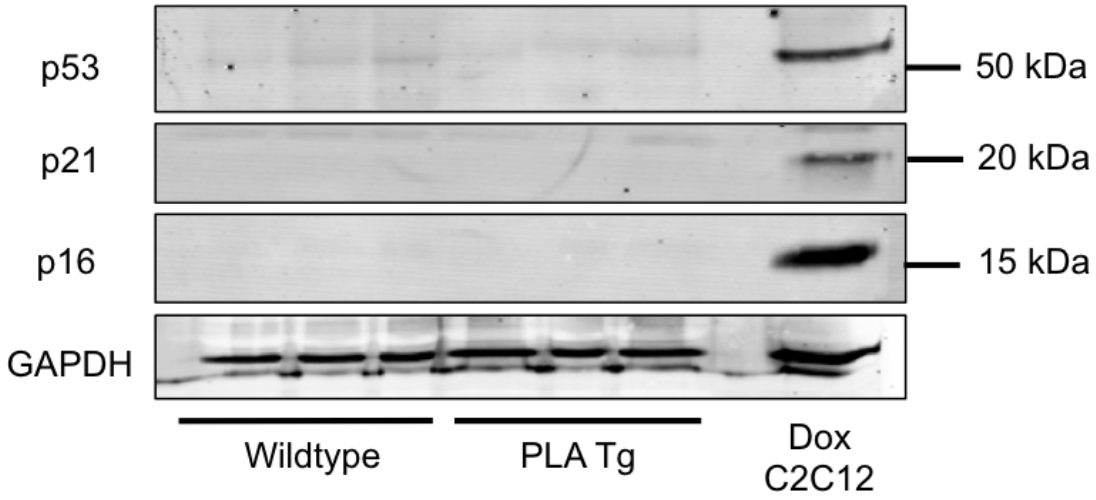

Figure 4.11. Expression of senescence associated cell cycle regulators was unaffected by accumulation of prelamin A in the heart. Ventricular tissue lysates were western blotted and membranes probed with p53, p21 and p16 antibodies. Expression levels were very low for p53, p21 and p16, with no observable differences between Wt and PLA Tg hearts. N=3/group

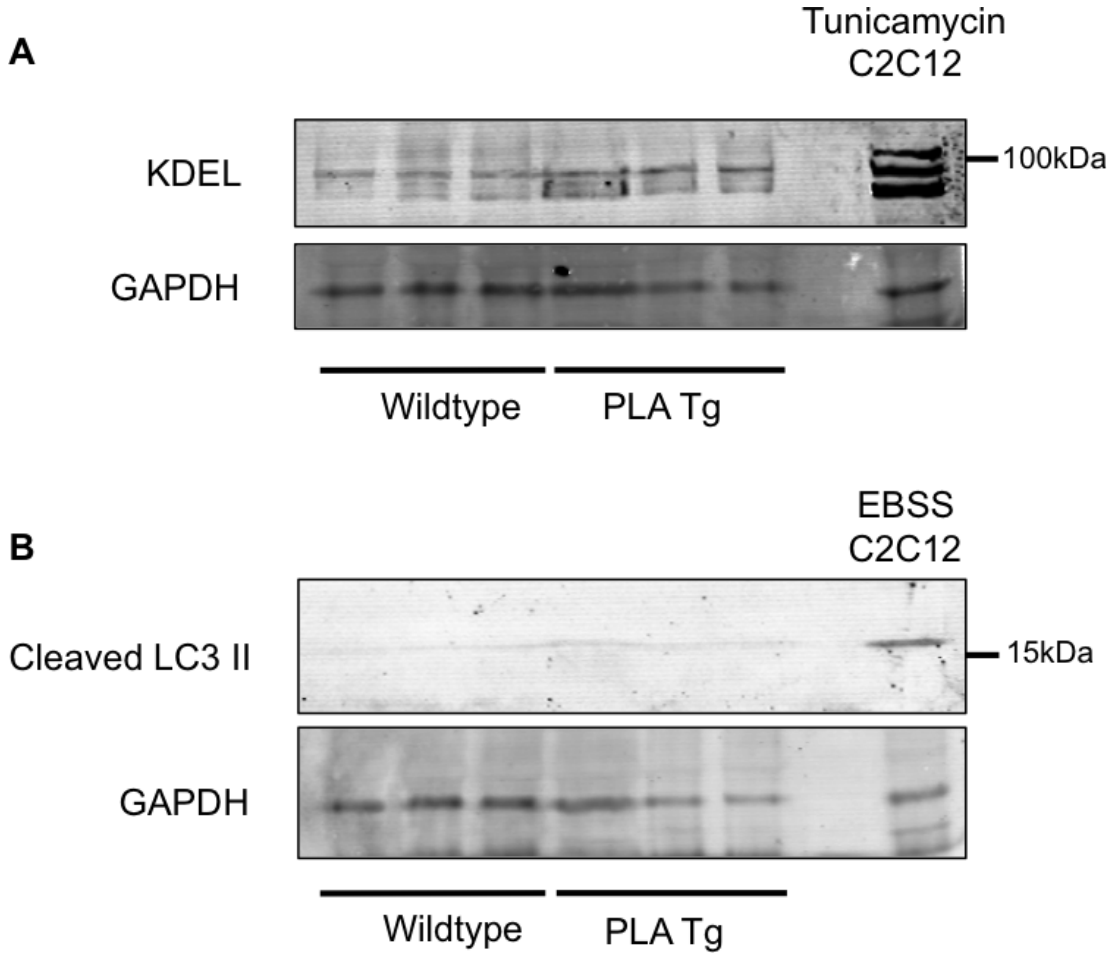

Figure 4.12. Accumulation of prelamin A in CMs did not activate ER stress or autophagic response pathways in PLA Tg mice hearts. Ventricular tissue lysates were western blotted and the membrane was probed with (A) KDEL antibody for detection of ER stress response chaperones Grp78 and Grp94. Expression of Grp78 and Grp94 remained unchanged between Wt and PLA Tg mice. Tunicamycin treated C2C12 myoblasts were used to positively control for this experiment. (B) The membrane was probed with antibody to cleaved LC3B II to assess activation of autophagy. Levels of LC3 II were barely detectable in Wt and PLA Tg mice, with no observable difference between groups. C2C12 myoblasts that were serum starved for 2 h in EBSS were used to positively control for this experiment. N=3/group

whole tissue lysates was performed with antibody to cleaved LC3II. Neither Wt nor PLA Tg heart tissue expressed cleaved LC3 II (Fig 4.12B). These results suggest that these stress pathways do not form part of the mechanism of pathogenesis associated with prelamin A accumulation in PLA Tg mice.

4.2.8 NF-κB signalling appears to be activated in hearts of mice that have accumulated prelamin A in a CM specific manner

Taking into account the strong inflammatory cell invasion seen in PLA Tg hearts, an emerging pathway associated with DNA damage and inflammation has been reported, which suggests that activation of the transcription factor NF-κB, a master regulator of inflammatory genes, can be driven, in a non-canonical pathway, by upstream activation of ATM[288]. NF-κB is a heterodimeric complex, potentially consisting of p65 (also termed Rel A) and p50. Subunits Rel B, cRel and p52 are also capable of forming NF-κB complexes[289]. NF-κB complexes are present in inactive forms in the cytoplasm bound to IκBα, which together form an inhibitory complex. Activation is initiated by phosphorylation of IκBα by upstream secondary messengers, which then dissociates from NF-κB, leaving NF-κB free to translocate to the nucleus and regulate gene transcription. ATM dependent activation begins with translocation of the NF-κB essential modulator (NEMO) to the nuclear domain from the cytoplasmic domain. Phosphorylation and activation of ATM leads to subsequent phosphorylation of NEMO and translocation out of the nucleus, where activation of the IKK complex occurs, leading to phosphorylation of IκBα, dissociation from NF-κB, and nuclear

translocation[290]. Importantly, prelamin A accumulation has already been identified in activating this pathway systemically[125].

To test whether NF-κB signalling was activated in an ATM dependent manner in hearts accumulating prelamin A, western blotting of whole tissue lysates from 4 week old hearts was performed using antibodies to phospho-ATM (pATM), IκBα, phospho-IκBα and p65. There was a clear and significant ($P<0.001$) increase in pATM expression in hearts of PLA Tg mice compared to Wt (Fig 4.13). IκBα showed two bands and indicated a trend in which there was a decrease in the smaller weight band (non-phosphorylated) and an increase in the higher weight band (phosphorylated) in PLA Tg mice compared to Wt (Fig 4.13). This finding was confirmed when phospho-IκBα also displayed a trend towards increased expression in PLA Tg hearts compared to Wt (Fig 4.13). Finally, a significant ($P<0.05$) increase in p65 was observed in PLA Tg hearts compared to Wt (Fig 4.13).

In order to assess whether NF-κB translocated to the nucleus in the setting of prelamin A accumulation, cryopreserved heart sections were subject to immunofluorescence staining using p65 antibody and viewed using fluorescence microscopy. Whilst expression levels were clearly increased in PLA Tg mice compared to Wt, p65 did not necessarily localise to the nucleus, as much of the p65 staining remained in the cytoplasmic domain of CMs (Fig 4.14).

In order to study this pathway further, CMs isolated from rat hearts were transduced with a virus containing a Flag-tagged *LMNA*-L647R construct. Immunofluorescence co-staining with Flag and p65 antibodies showed that many Flag positive cells expressed p65 in their nuclei or in peri nuclear regions, whereas non

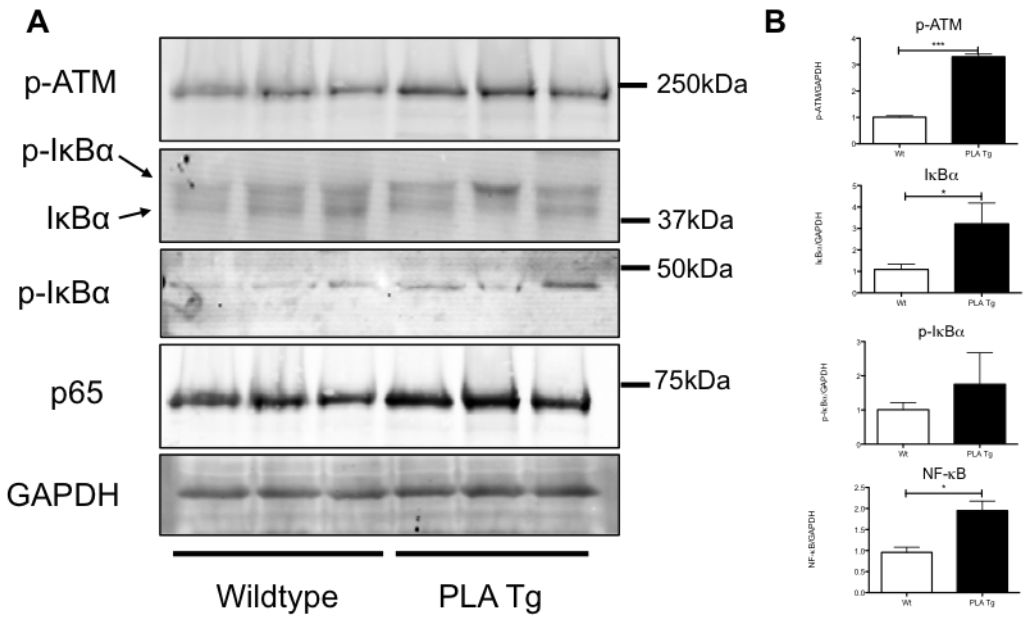

Figure 4.13. Accumulation of prelamin A led to activation of ATM dependent NF-κB signalling. (A) Ventricular tissue lysates were western blotted and probed with the antibodies: phosphorylated ATM/ATR substrate, IκBα, phosphorylated IκBα and p65 subunit of the NF-κB complex. (B) Densitometry showed that in PLA Tg hearts compared to Wt, p-ATM/ATR was significantly increased; IκBα appeared to be slightly but not significantly decreased; and p-IκBα also showed a trend for increased expresssion. p65 was significantly increased in PLA Tg myocardium compared to Wt. N=3/group

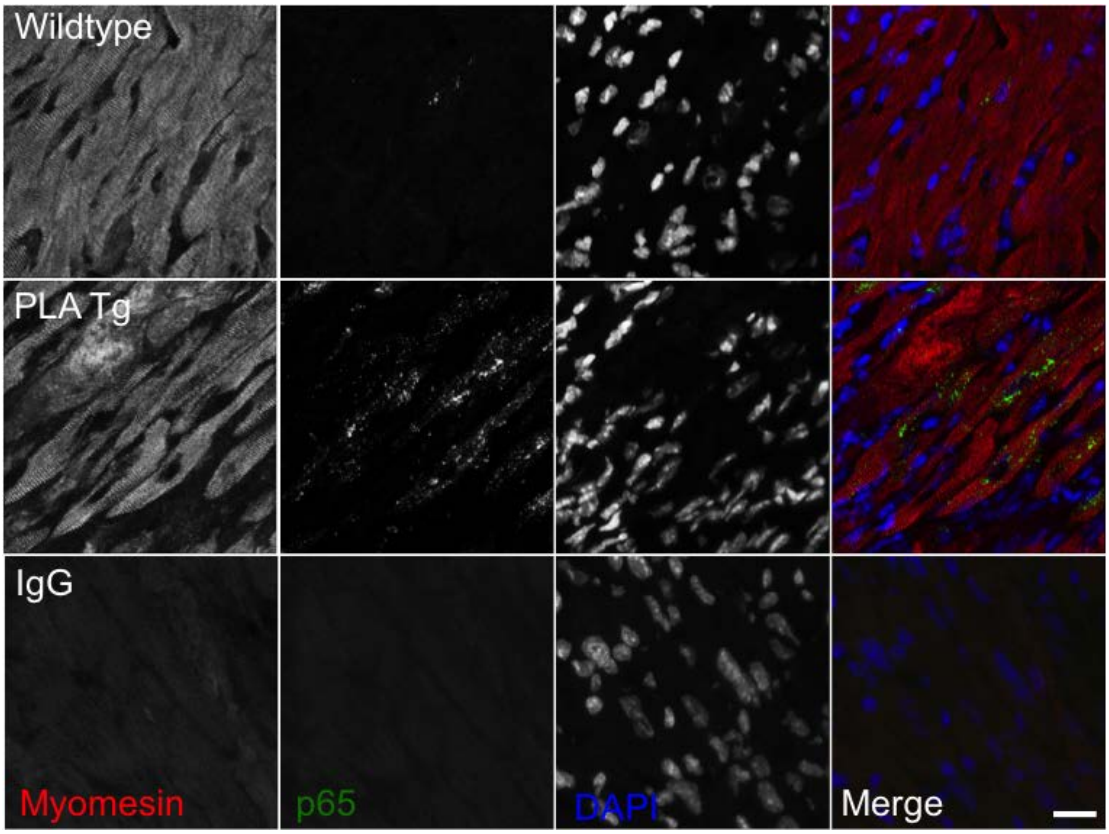

Figure 4.14. NF-κB subunit p65 was increased in hearts that accumulated prelamin A. Cryopreserved heart sections were subject to immunofluorescence staining using NF-κB subunit p65 (green) and myomesin (red) antibodies. P65 was present at very low levels in Wt tissue, whereas PLA Tg sections displayed abundant staining. Localisation appeared to be exclusive to CMs as defined by myomesin staining, although the patterning and localisation within the CMs appeared indiscriminate and difficult to define. Scale bar = 20 μm

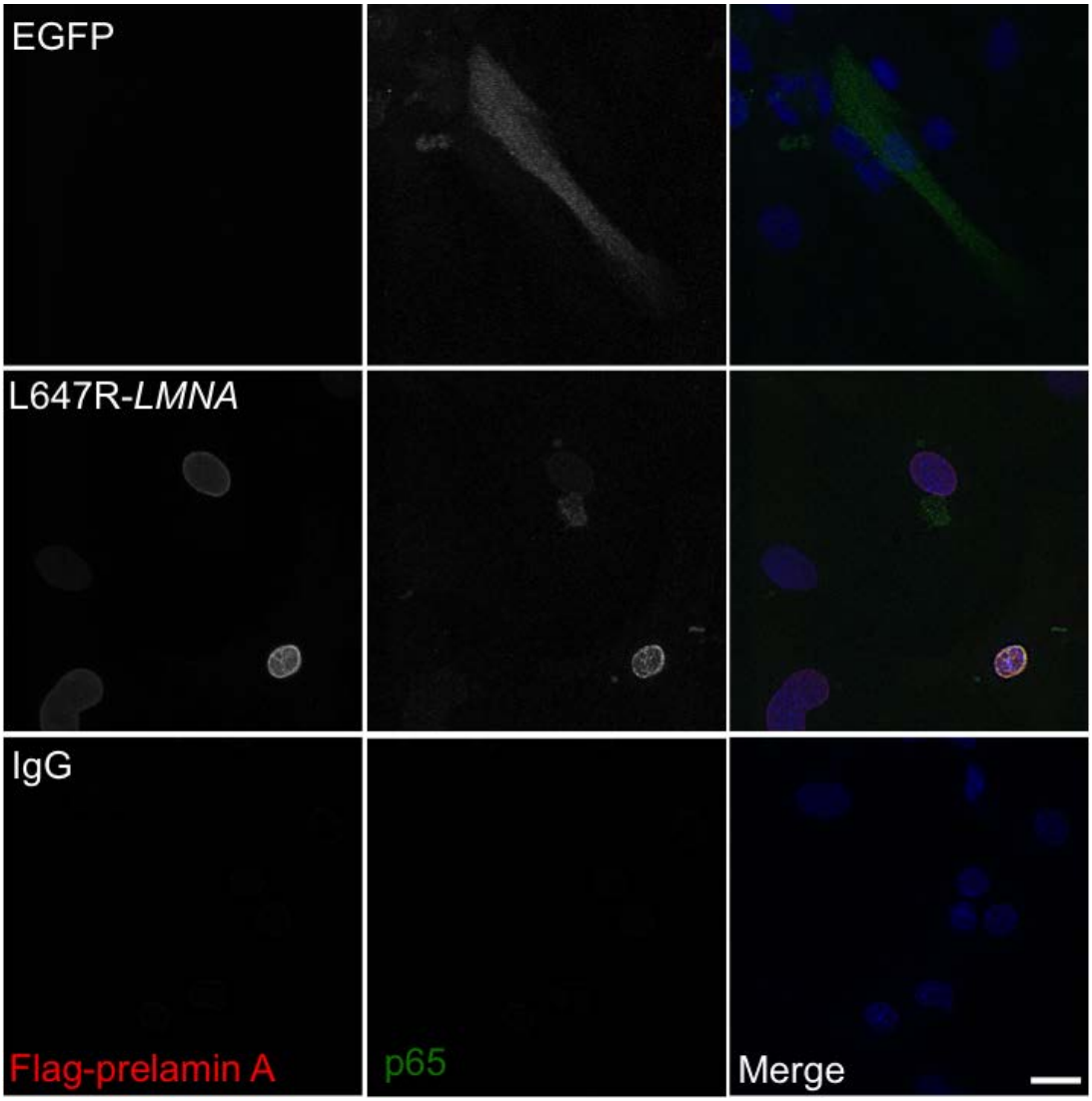

Figure 4.15. NF-κB subunit p65 localised to the nucleus in isolated CMs transduced with prelamin A. CMs isolated from rat hearts were subject to transduction with an adenovirus containing flag tagged uncleavable prelamin A DNA. Control cells were transduced with an empty EGFP vector adenovirus. Cells were subjected to immunofluorescence microscopy using NF-κB subunit p65 and flag antibodies. Flag-prelamin A localised to the nucleus in transduced cells. NF-κB subunit p65 was localised to the nucleus or in perinuclear regions in prelamin A transduced cells and were diffuse in the cytoplasm in EGFP transduced cells, suggesting prelamin A induces p65 translocation to the nucleus. Scale bar = 10 μm

transduced cells or cell transduced with an empty viral vector (EGFP control) had diffuse cytoplasmic localisation of p65 (Fig 4.15).

4.3 Discussion

4.3.1 Accumulation of prelamin A leads to disruption of the LINC complex, which may be a potential cause of contractile deficiency

The mechanical relationship between the cytoplasmic and nuclear domains via the LINC complex is thought to be crucial to cell homeostasis. It is postulated that certain cell types must be mechanically compliant in order to fulfil their function, meaning that the nucleus must be mechanically sound and coupled effectively to other cytoskeletal components of the cell. Disruption to these linkages and loss of coupling would therefore result in structural instability and reduction in force transmission, potentially having deleterious effects on a range of processes from cell motility to muscle contraction, depending on cell type[291]. Moreover, it has been established that these mechanical links can detect external signals such as sound or flow or mechanical stresses and perturbations such as stretch and activate transcriptional responses much more rapidly than soluble second messengers are able to and are actively involved in controlling cell responses[292, 293].

Data from this chapter indicate that in PLA Tg hearts that have accumulated prelamin A, LINC complex protein expression is dysregulated, as lamins A & C appeared to be increased as did lamin B1. Interestingly, cleavage of lamins was not apparent in PLA Tg mice. Cleavage of lamins is an established marker for apoptosis[294],

and this observation supports the assertion made in chapter 3 that despite positive TUNEL staining, apoptosis was not apparent. Localisation of lamin A/C and lamin B1 was in the nuclear rim as expected, although there were many more lamin A/C and lamin B1 positive nuclei in PLA Tg myocardium, presumably belonging to invasive leukocytes. Disruption of expression and localisation to SUN domain proteins is known to occur in the setting of HGPS[295] and MADA[296]. Decreased SUN2 in PLA Tg hearts compared to Wt is consistent with these observations. Neprins 1 and 2, for which the antibodies detect multiple isoforms, appeared to undergo a switch with regard to the dominant isoforms that were expressed in PLA Tg heart tissue compared to Wt. PLA Tg heart tissue appeared to undergo a loss of a 95 kDa band in the nesprin 1 immunoblot, which could correspond to the muscle specific isoform nesprin 1α, and corroborates with previous findings from *Lmna*$^{-/-}$ mice suggesting loss of this isoform occurs in the setting of lamina disruption[244]. Additionally, PLA Tg heart tissue underwent an increase in a 75 kDa nesprin-2 isoform, which is interesting because the opposite occurred in an *in vitro* mutational analysis of S143F-*LMNA* DNA, which is known to cause progeria phenotypes[297]. SUN2 and nesprins were inefficiently detected on cryosections and as such were inconclusive (not shown).

Desmin expression was greatly increased in PLA Tg hearts and appeared to become localised in cytoplasmic aggregates compared to Wt, which localised at intercalated discs, the sarcomere and the perinuclear domain. Indeed, desmin has been previously shown to aggregate in DCM and heart failure phenotypes and may be part of a common mechanism or response downstream of causative mutations in DCM pathogenesis[298-300].

The expression of sarcomeric proteins, myomesin and α-actinin, was decreased in PLA Tg hearts and, although the general localisation of myomesin and α-actinin appeared unaffected, α-actinin staining appeared less intense and more diffuse. As yet, more work is needed to see how these observations fit into the PLA Tg pathogenic model.

Interestingly, it was observed that prelamin A localised with α-actinin at the sarcomere in Wt heart sections, a novel finding, which was not apparent in PLA Tg heart tissue. If valid, one could speculate that prelamin A is a novel component of the sarcomere. Therefore, disruption to this complex by pathological expression of prelamin A may disrupt the finely tuned balance of protein expression and localisation required for normal sarcomere function and potentially complicate the analysis of this model. This phenomenon is explored in more detail in chapter 7. Furthermore, closer inspection of PLA Tg tissue sections by way of ultrastructural imaging suggested that PLA Tg nuclei were often dysmorphic and the nuclear membrane appeared to have become untethered from the sarcomere even in nuclei that were non-dysmorphic. It may be the case that accumulation of IF proteins in PLA Tg CMs reported above is an adaptive response in order to compensate for the disruption created by the expression of prelamin A. Further investigation is required.

To summarise, taken with the observations in chapter 3 showing that contractility of the myocardium in PLA Tg mice was deficient, these results provide compelling evidence for the view that disruption of the LINC complex leads to mechanical uncoupling of the nucleus from the cytoskeleton and a reduction in force transmission across the CMs leading to a global reduction in contractility of the myocardium.

4.3.2 Deregulation of Cx43

Another reason for the reduction in contractility of hearts that accumulated prelamin A was the reduction in expression and mislocalisation of Cx43 observed. Connexins, Cx43 in particular, are localised to gap junctions in the myocardium and vital in propagating electrical signals between CMs to facilitate synchronised excitation of related regions of the heart. Loss of Cx43, therefore, is likely to lead to attenuated electrical signalling and muted excitation-contraction coupling responses in the myocardium and therefore, reduced contractility.

4.3.3 Molecular responses to stress and senescence

Studies in isolated HGPS patient fibroblasts have shown that a hallmark of prelamin A/progerin accumulating diseases is the increase in DNA damage markers thought to be caused by defective DDR mechanisms. This chapter showed that DNA damage is also increased in the nuclei of CMs by detection of increased γ-H2AX foci and expression and supports the idea that accumulation of prelamin A at the nuclear rim also causes accumulation of DNA damage and may be a crucial part of disease pathogenesis in the heart. Sustained activation of DDR is thought to be the initial trigger in establishing a senescence phenotype, which, according to SA-β-gal staining, was also evident in PLA Tg myocardium.

Previously, the association between prelamin A, senescence and DNA damage led investigators to hypothesise that the accumulation of DNA damage could lead to activation of cell cycle regulators such as p53 and cause permanent arrest of cell cycle,

thus facilitating the senescence. This chapter showed that expression of cell cycle regulators p53, p21 and p16, which are known to inhibit cell cycle during the DDR, were unchanged in the myocardium of PLA Tg hearts compared to Wt, suggesting that the senescence-like phenotype occurs independently of cell cycle regulators. Expression levels of cell cycle regulators were barely detectable in PLA Tg or Wt heart tissue lysates, and this observation perhaps questions the role of cell cycle regulators in the heart, effectively a terminally differentiated organ (save for cardiac stem cells, cardiac fibroblasts and resident monocytes). Indeed, it has been shown that in fibroblasts, induction of SA-β-Gal, for example, is independent of cell cycle regulation and cell cycle arrest[281, 301, 302]. In addition, generation of the SASP response is thought to occur independently of cell cycle control via p53 and Rb[119], suggesting that senescence can be regulated by multiple mechanisms which are independent of cell cycle inhibition.

Due to the nature of the system of transgenesis, it was deemed important to establish whether other responses to stress were activated. It was suggested that the abundant accumulation of uncleavable prelamin A might alone activate stress pathways such as the unfolded protein response or autophagy and that these may interfere with, or even provide alternative mechanisms of, pathogenesis. However, it was found that these systems were not activated. This, coupled with the observation that the nuclear rim localisation of prelamin A in this model was very specific, suggests that the mechanism of disease is likely to be more complex than hyperactivation of cell degradation pathways. However, as highlighted by previous studies, it may also be the case that autophagic mechanisms are in fact defective in the setting of prelamin A accumulation/lamina disruption[240, 241], an interesting concept which provides a basis for future work on this model.

4.3.4 NF-κB signalling

The observation that accumulation of prelamin A in CMs led to inflammation of the myocardium was intriguing. As mentioned above and in chapter 1, inflammation of the myocardium is often observed in failing hearts, perhaps most commonly post MI in response to ischaemia-induced damage and as a result of CM necrosis. However, sterile inflammation, whereby the presence of an external inflammatory stimulus is absent also occurs, and was observed in the current model. Interestingly, Osorio *et al* have shown in a global model of premature ageing disease that *Zmpste24*$^{-/-}$ mice suffer from systemic inflammation arising from ATM dependent NF-κB signalling[125]. Expression analysis showed that the p65 subunit of NF-κB was upregulated in the myocardium of PLA Tg hearts. This was coupled with an increase in phosphorylated-ATM and phosphorylation of IκBα, which together provide evidence for activation of ATM dependent NF-κB signalling in hearts that had accumulated prelamin A. Moreover, p65 subunit expression was increased when assessed by immunofluorescence microscopy, although it was unclear whether translocation to the nucleus was occurring. To confirm this *in vitro*, immunofluorescence microscopy was used to show that, in prelamin A transduced cells, p65 localised to the nucleoplasm, whereas EGFP vector transduced cells appeared to display diffuse cytoplasmic localisation of p65. Not only do these findings support the idea that prelamin A is capable of eliciting an inflammatory response, per se, but that this can occur in sterile myocardium. Additionally, Osorio *et al* linked NF-κB activation to increases in transcripts of senescence associated secreted factors, Il-6, MCP-1 and TNF-α. Assessment of SASP associated factors in the current model would have been ideal for this line of investigation had time allowed. Indeed, the fibrosis phenotype

observed in chapter 3 could potentially be driven by SASP factors, of which MMPs and collagen are a part[116].

In summary, the mechanisms by which DCM and ultimately fatal heart failure occur in PLA Tg mice appear to be multitudinous but can be categorised into two distinct groups: 1) Loss of myocardial contractility involving disruption of the LINC complex and mechanical stability and loss of connexins; 2) Inflammation associated with DNA damage accumulation, NF-κB signalling and possibly the SASP, a process that appears to occur independently of cell cycle regulation. Whether these events are independent or occur in a stepwise process due to prelamin A accumulation is explored in the next chapter where animals at an earlier timepoint were investigated.

Chapter 5: Physiological and molecular characterisation of 2 week old mice that accumulate prelamin A in a CM specific manner

5.1 Introduction

In the current study, physiological characterisation of PLA Tg mice at 4 weeks old confirmed a DCM-like phenotype, which results in heart failure and death before 6 weeks of age. Moreover, molecular insights revealed a multifaceted response to prelamin A accumulation in CMs, including disruption of the NE and IF protein network, loss of connexins, DNA damage accumulation, and potentially, senescence. Moreover, the senescence phenotype appeared to be independent of control by p53, p21 and p16, whilst there is also evidence to suggest UPR and autophagic stress response/degradation pathways were not activated.

In order to further delineate the mechanistic pathways involved, the model was assessed at an earlier timepoint. It was hypothesised that this would give a clear indication as to which markers of disease arose first and enable the proposition of a temporally defined mechanism of pathogenesis.

5.2 Results

5.2.1 Part 1: Physiological characterisation

5.2.1.1 2 week old mice are unaffected by cardiac specific accumulation of prelamin A on morphometric analysis

2 week old mice were photographed and body weights were obtained. At 2 weeks, Wt and PLA Tg mice were morphologically similar (Fig 5.1): PLA Tg mice (7.13 g ± 0.27) weighed similarly to Wt mice (7.02 ± 0.24), P = 0.75 (Fig 5.2A); heart weights were comparable between PLA Tg (45.0 ± 1.44) and Wt (42.5 ± 1.23) cohorts, P = 0.22 (Fig 5.2B); heart weight to body weight ratios were also comparable (PLA Tg, 6.17 ± 0.16 and Wt, 6.10 ± 0.24, P = 0.83) (Fig 5.2C). Tibia length was unchanged between PLA Tg (7.05 ± 0.26) mice and Wt (6.86 ± 0.28), P = 0.63 (Fig 5.2D). Heart weight to tibia length ratio was also unchanged between PLA Tg (6.31 ± 0.11) mice and Wt (6.11 ± 0.26), P = 0.51 (Fig 5.2E).

5.2.1.2 Echocardiographic analysis shows that at 2 weeks, cardiac function is unaffected by prelamin A accumulation

Echocardiographic analysis was performed on images obtained from anaesthetised 2 week old mice. For all parameters measured—IVS;s, IVS;d, LVID;s,LVID;d, LVPW;s, LVPW;d, area;s, area;d, EF, FS, SV, LVESD, LVEDD—there were no major or statistically significant changes observed in PLA Tg hearts compared to Wt, indicating no difference in heart function between cohorts (Table 5.1 & Fig 5.3).

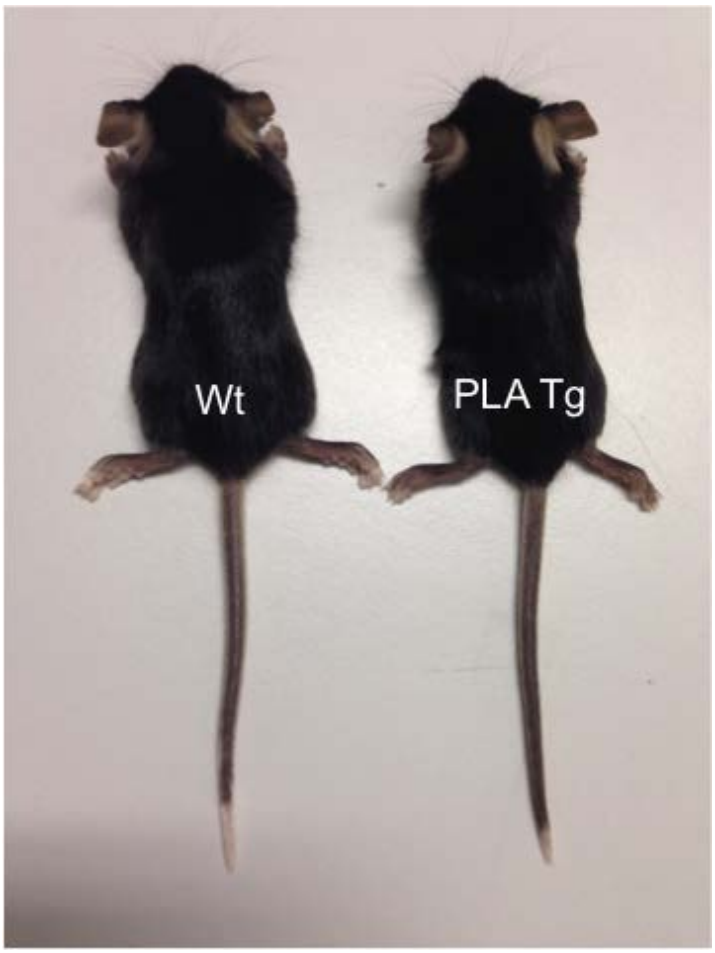

Figure 5.1. At 2 weeks of age, Wt and PLA Tg mice were comparable in size. Representative photograph of Wt and PLA Tg mice taken at two weeks of age.

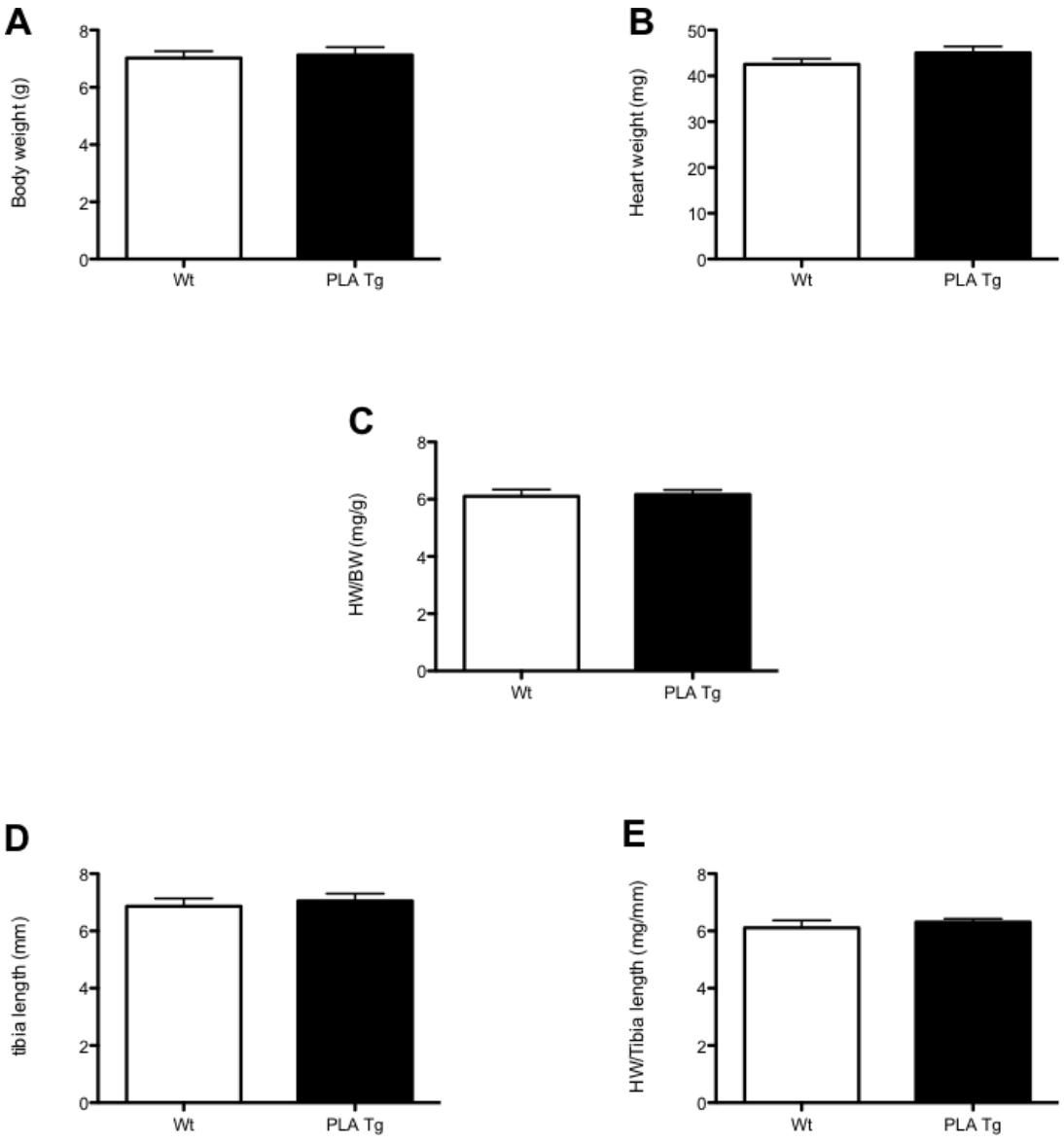

Figure 5.2. Morphometric analysis showed that at 2 weeks of age, Wt and PLA Tg mice were comparable. (A) Body weight, (B) heart weight, (C) heart weight/body weight ratio**,** (D) tibia length and (E) heart weight/tibia legth ratio were unchanged in PLA Tg mice compared to Wt. Values expressed as mean±SEM, N=6 females/group

Table 5.1. B-mode Echocardiographic analysis of PLA Tg hearts in long axis orientation showed no difference between cardiac dysfunction in PLA Tg hearts compared to Wt at 2 weeks old

Parameter	Units	Wildtype	PLA Tg	P value	sig.
IVS;d	mm	0.49 ± 0.03	0.46 ± 0.03	0.557	N
IVS;s	mm	0.56 ± 0.03	0.51 ± 0.04	0.336	N
LVID;d	mm	2.66 ± 0.07	2.57 ± 0.09	0.421	N
LVID;s	mm	1.84 ± 0.04	1.79 ± 0.08	0.612	N
LVPW;d	mm	0.54 ± 0.03	0.52 ± 0.03	0.622	N
LVPW;s	mm	0.63 ± 0.03	0.60 ± 0.05	0.534	N
Area;d	mm2	11.15 ± 0.21	11.56 ± 0.70	0.583	N
Area;s	mm2	6.95 ± 0.36	6.67 ± 0.40	0.624	N
Ejection Fraction	%	53.28 ± 4.19	59.32 ± 2.45	0.237	N
Fractional Shortening	%	15.42 ± 1.30	17.24 ± 1.61	0.399	N
Stroke Volume	ul	10.47 ± 0.91	12.33 ± 1.51	0.311	N
LVEDV	ul	19.61 ± 0.59	20.70 ± 2.07	0.621	N
LVESV	ul	9.14 ± 0.81	8.37 ± 0.79	0.508	N

Values expressed as mean±SEM, N=8 females/group

^{N}P=No significance

IVS = Interventricular septum

LVID = Left ventricular internal diameter

LVPW = Left ventricular posterior wall

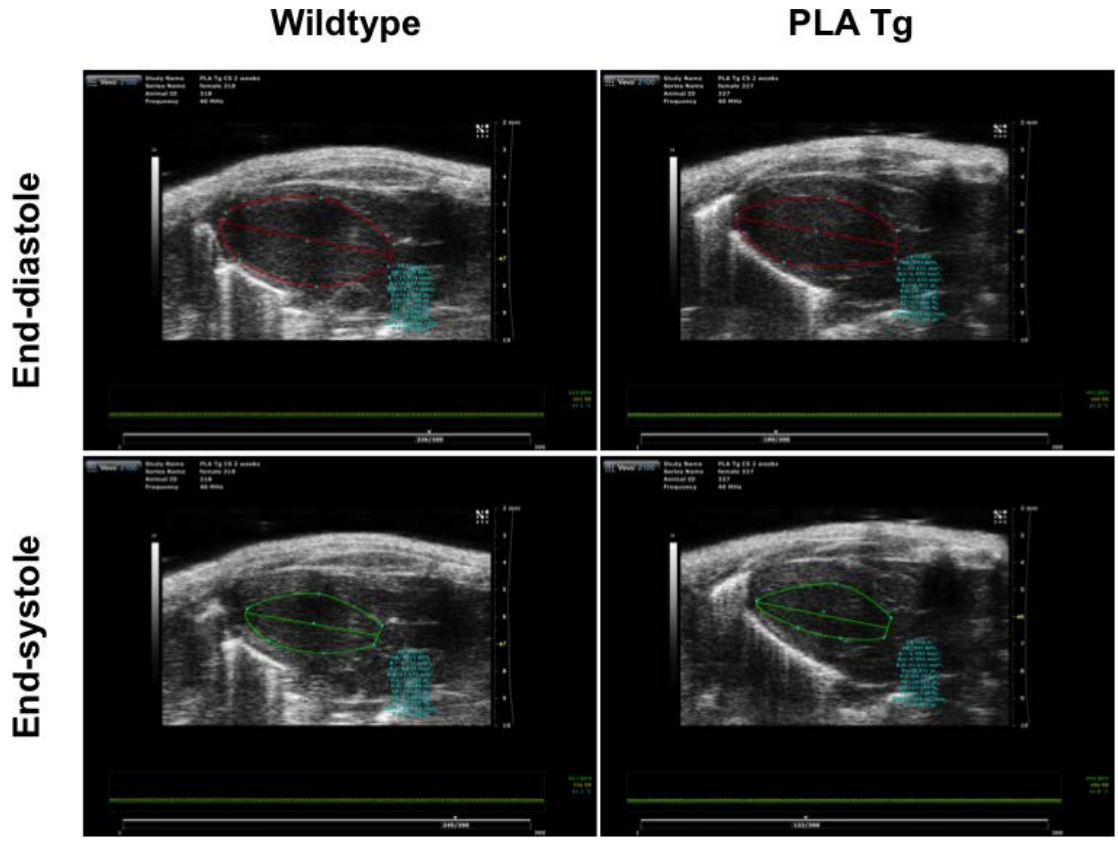

Figure 5.3. Heart chamber size was unchanged in PLA Tg hearts. Representative B mode images of the LV long axis from echocardiography movies were used to analyse cardiac function and showed that chamber size was comparable in PLA Tg hearts compared to Wt, supporting the analysed data from Table 5.1.

5.2.1.3 Histological analysis of 2 week old mice shows no evidence of myocardial disarray or fibrosis in the setting of prelamin A accumulation

H&E staining was performed. There appeared to be no major differences in the myocardial tissue arrangement of PLA Tg mice compared to Wt. One minor observation was the increased clustering of nuclei in the myocardial interstitium of PLA Tg mice (Fig 5.4). Additionally, picrosirius red staining showed no signs of pathologic fibrosis in PLA Tg hearts compared to Wt (Fig 5.5). Moreover, TEM of hearts showed that there were no observable differences in myofibril or sarcomeric structure in PLA Tg hearts compared to Wt and no sign of nuclear morphology defects or chromatin disorganisation (Fig 5.6).

5.2.1.4 At 2 weeks old, mRNA levels of β-MHC are significantly increased in hearts of mice that are accumulating prelamin A

qPCR was performed on 2 week old hearts to assess mRNA expression of markers commonly associated with heart failure. α-MHC, ANP and BNP were not significantly changed in PLA Tg hearts compared to Wt. However, β-MHC levels increased 3.55 fold in PLA Tg hearts compared to Wt, reaching significance ($P<0.05$) (Fig 5.7).

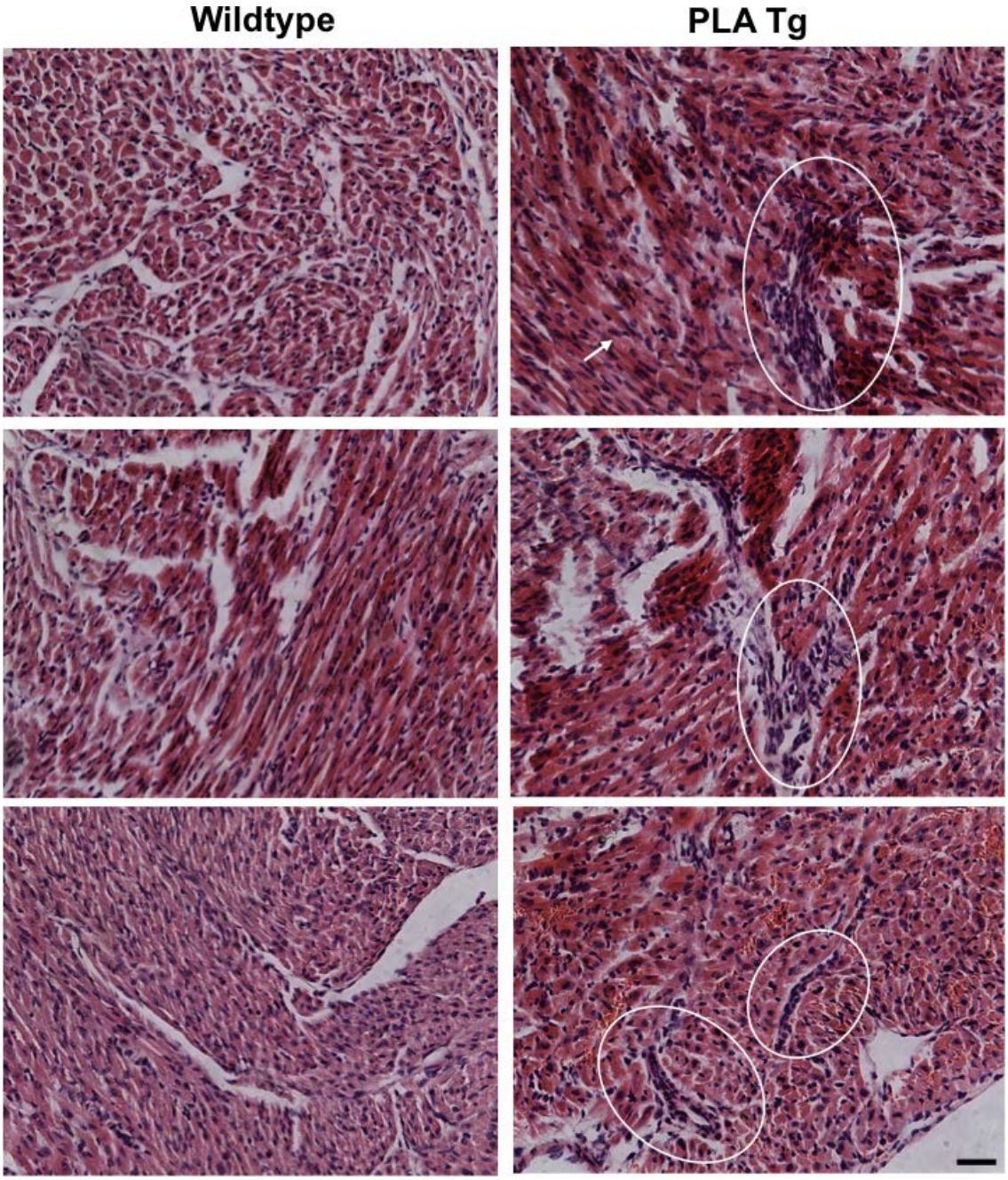

Figure 5.4. Histological examination of heart sections indicated leukocyte invasion of the myocardium had begun to occur in 2 week old PLA Tg mice. H & E staining of paraffin embedded heart sections were viewed under light microscopy to reveal that regions of PLA Tg hearts were characterised by clustering of nuclei within the myocardial interstitium (ellipses), thus indicating leukocyte invasion. Scale bar = 30 µm

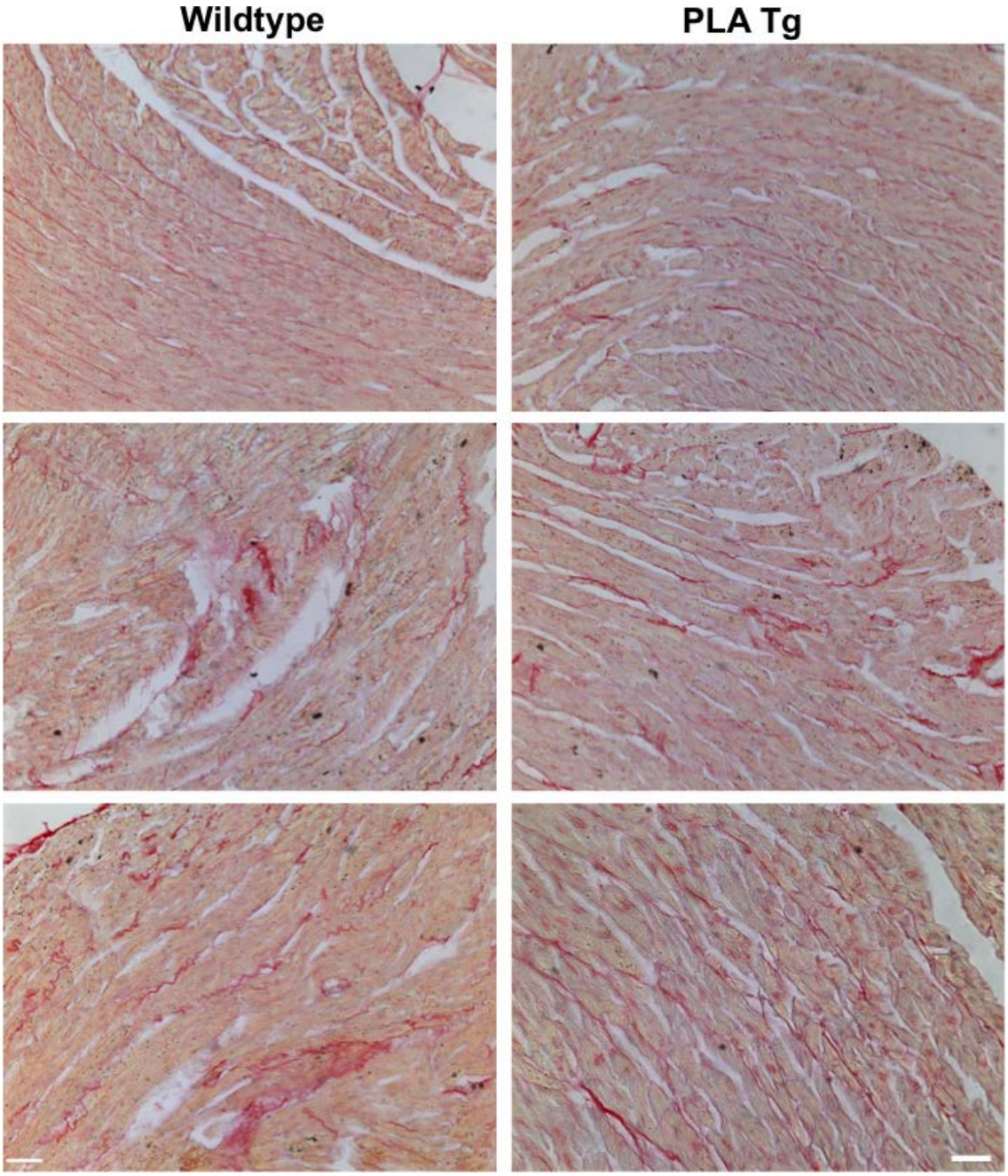

Figure 5.5. No fibrotic remodelling was detected in 2 week old hearts accumulating prelamin A. Picrosirius red staining was performed on paraffin embedded heart cross sections of Wt (left panelling) and PLA Tg (right panelling) mice. There were no observable differences between Wt and PLA Tg heart sections. Scale bar = 60 μm

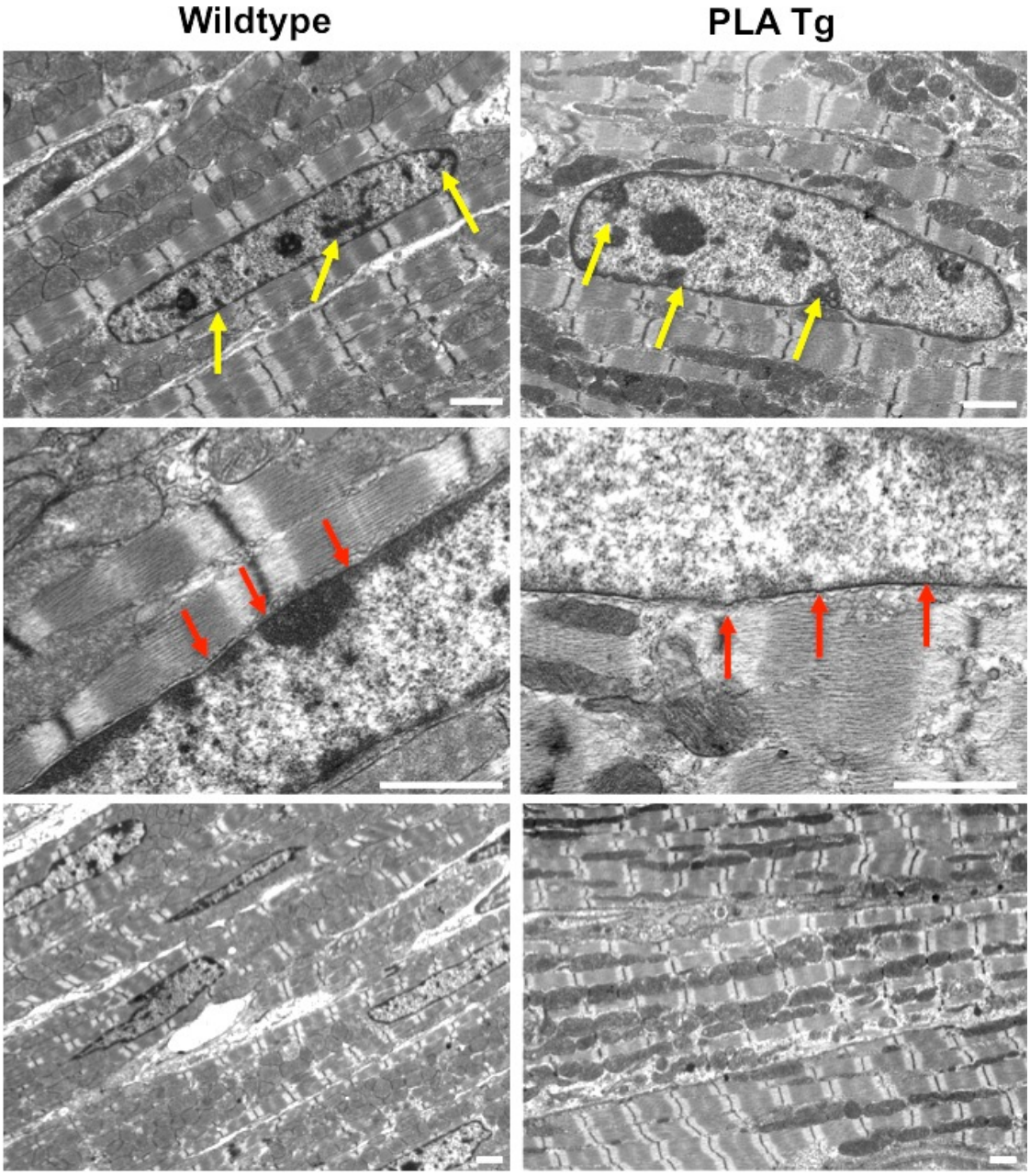

Figure 5.6. Nuclear morphology and cardiac ultrastructure was comparable between 2 week old Wt and PLA Tg myocardium. Perfusion fixed hearts were processed and stained for TEM. No differences were observed in nuclear morphology, heterochromatin organisation (yellow arrows), the nuclear membrane sarcomere junction complex (red arrows), or sarcomere organisation between Wt and PLA Tg hearts. Scale bar = 1 μm

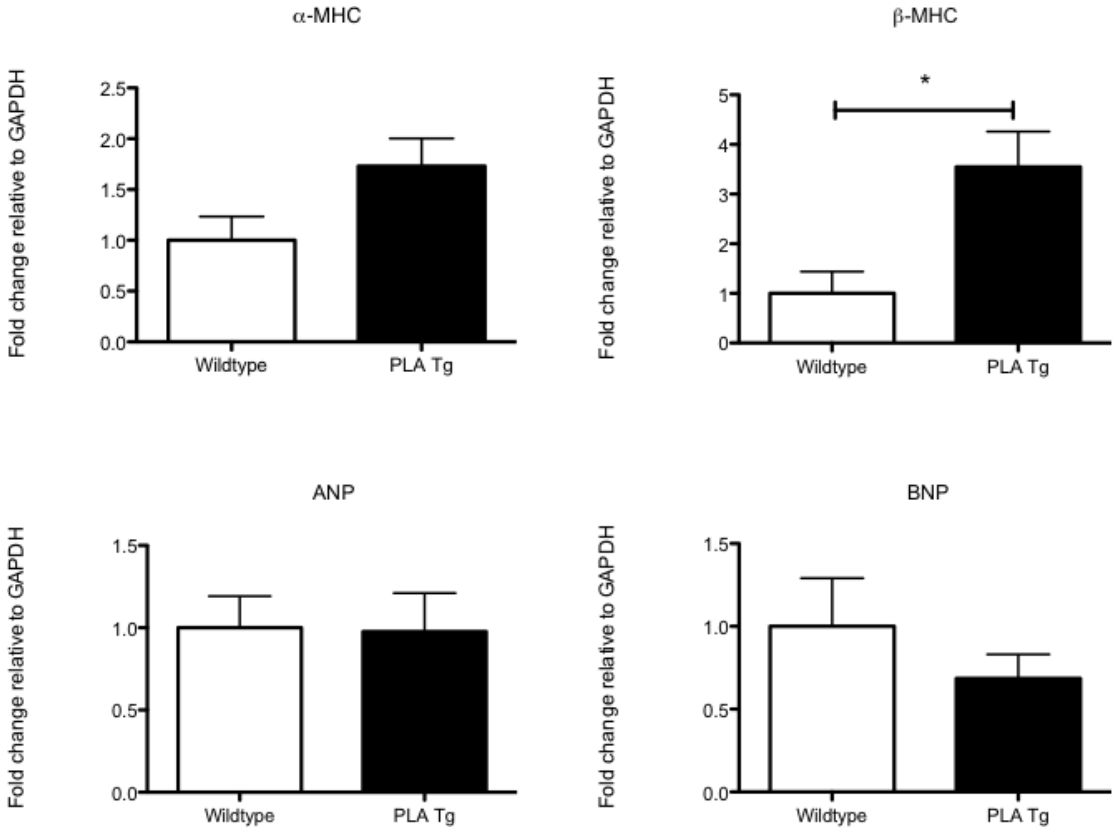

Figure 5.7. Analysis of mRNA markers suggested β-MHC was an early biomarker for DCM and heart failure in prelamin A accumulating hearts. qPCR was performed to assess mRNA markers of heart failure and showed that α-MHC mRNA was not significantly changed; β-MHC was significantly increased; ANP was unchanged; and BNP was not significantly changed in PLA Tg hearts compared to Wt. Values expressed as mean±SEM, *P<0.05, N=3/group

5.2.1.5 Leukocyte invasion occurs in 2 week old hearts that accumulate prelamin A

Leukocyte invasion was assessed by western blotting of whole tissue lysates and immunofluorescence staining on cryopreserved heart sections using a CD45 antibody. Microscopic analysis of cells and cell counting suggested there was a significant increase in the number of CD45 positive cells per field of view in PLA Tg hearts (100.5 cells per field of view ± 22.12) compared to Wt (35.44 ± 6.82) ($P<0.05$) (Fig 5.8B). Furthermore, Western blotting showed changes in CD45 expression between Wt and PLA Tg hearts (Fig 5.9A & B).

This was confirmed by TEM, which showed the presence of what, morphologically, appeared to be leukocytes present in the myocardial interstitium of PLA Tg hearts but not Wt (Fig 5.10).

5.2.2 Part 2: Molecular characterisation

5.2.2.1 At 2 weeks old, expression and distribution patterns of LINC complex and intermediate filament proteins in hearts accumulating prelamin A are unchanged

Western blotting of ventricular tissue lysates was performed on 2 week old hearts and probed with antibodies for prelamin A and the LINC complex proteins, Emerin, lamin A/C, lamin B1, SUN2, nesprin2 and the IF protein desmin. As expected, prelamin A was expressed in PLA Tg but not Wt hearts. However, expression levels were unchanged for lamin A/C, emerin, SUN2, nesprin2 and desmin (Fig 5.11).

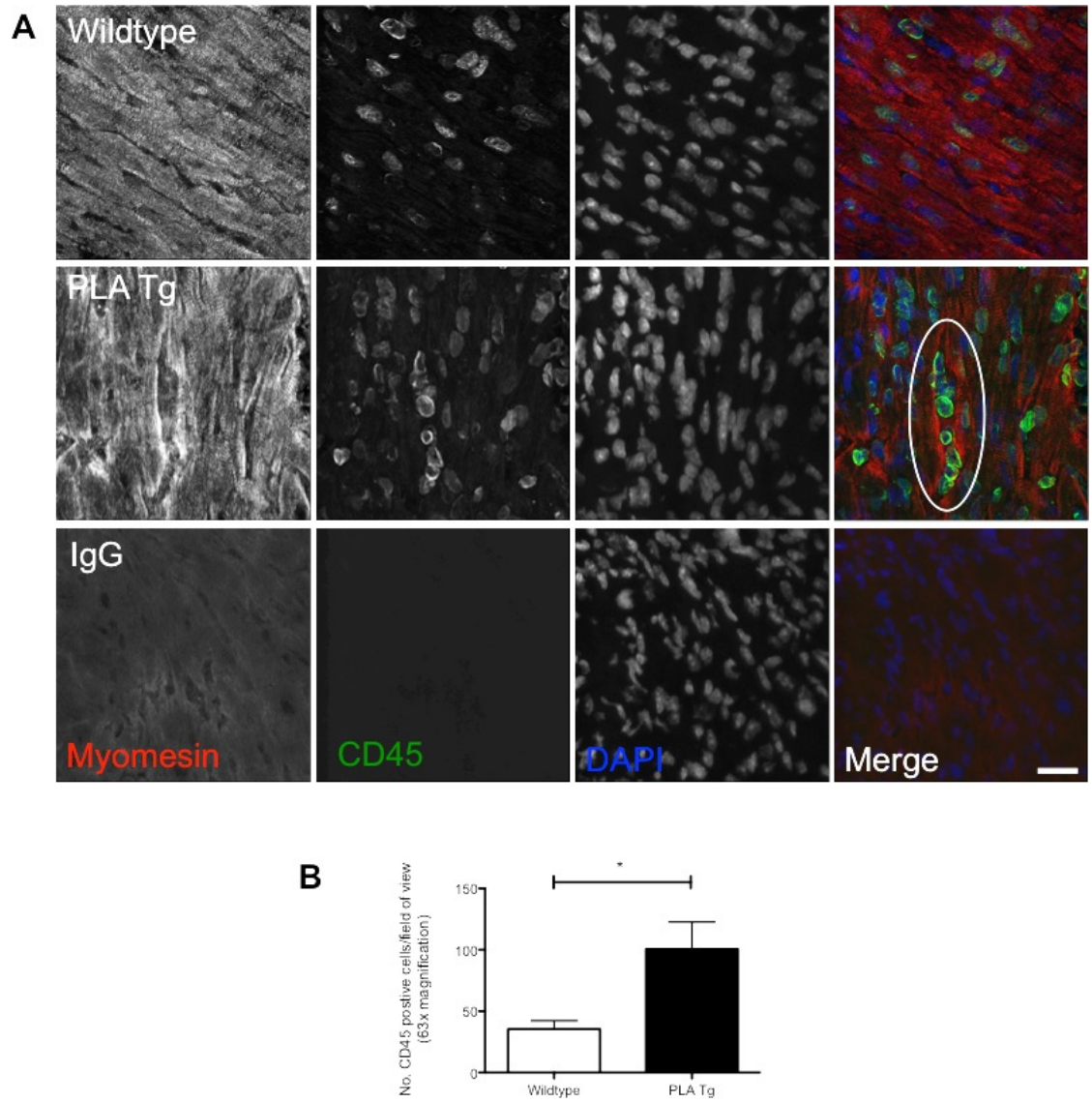

Figure 5.8. Prelamin A accumulation led to leukocytic invasion of the myocardium at 2 weeks of age. (A) Cryopreserved heart cross sections were co-stained with antibody to CD45 (green) and myomesin (red) and viewed with fluorescence microscopy to show that PLA Tg hearts appeared to have more CD45 positive cells within the myocardial interstitium than Wt hearts. Serum IgG was used as a negative control. Scale bar = 20 μm (B) CD45 positive cells per field of view on 63x magnification were counted by eye and revealed that there were significantly more CD45 positive cells in PLA Tg myocardium than Wt. Values expressed as mean±SEM, **P<0.01, N=3/group; 20 randomly selected fields of view from each section were counted.

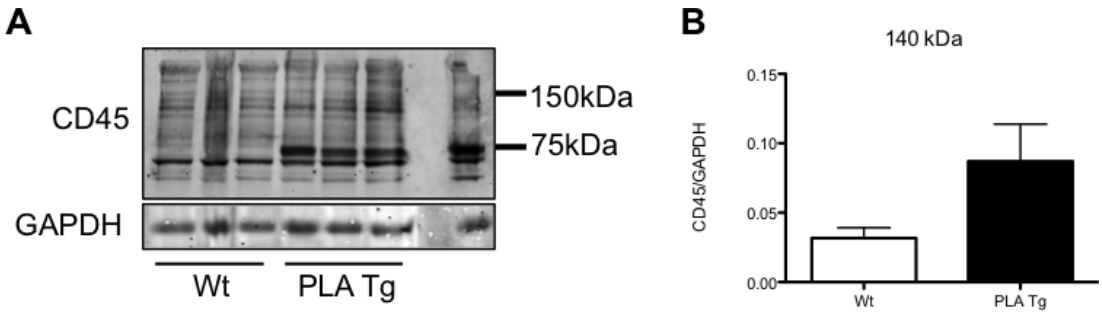

Figure 5.9. Prelamin A accumulation led to increased CD45 expression in the myocardium. (A) CD45 antibody was used to probe western blots of ventricular tissue lysates from hearts. (B) Densitometric analysis showed a trend towards increases in CD45 expression (140 kDa) in PLA Tg hearts compared to Wt. There was also an unknown band expressing in PLA Tg hearts that did not express in Wt. N=3/group

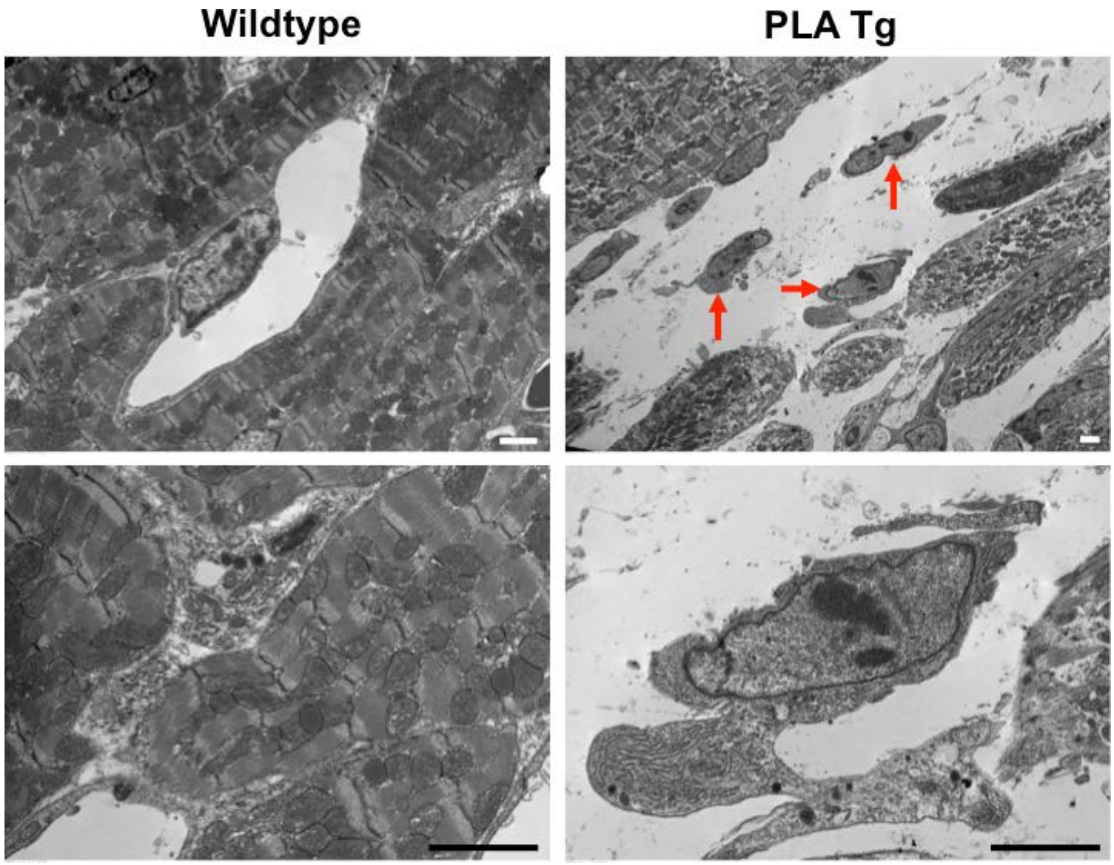

Figure 5.10. Presence of leukocytes in hearts that accumulate prelamin A was evident at the ultrastructural level at 2 weeks of age. Perfusion fixed hearts were processed and stained for viewing with TEM. Presence of morphologically distinct dendritic leukocytes was observable in spaces between CMs of PLA Tg myocardium but not in Wt myocardium. Scale bar = 500 nm

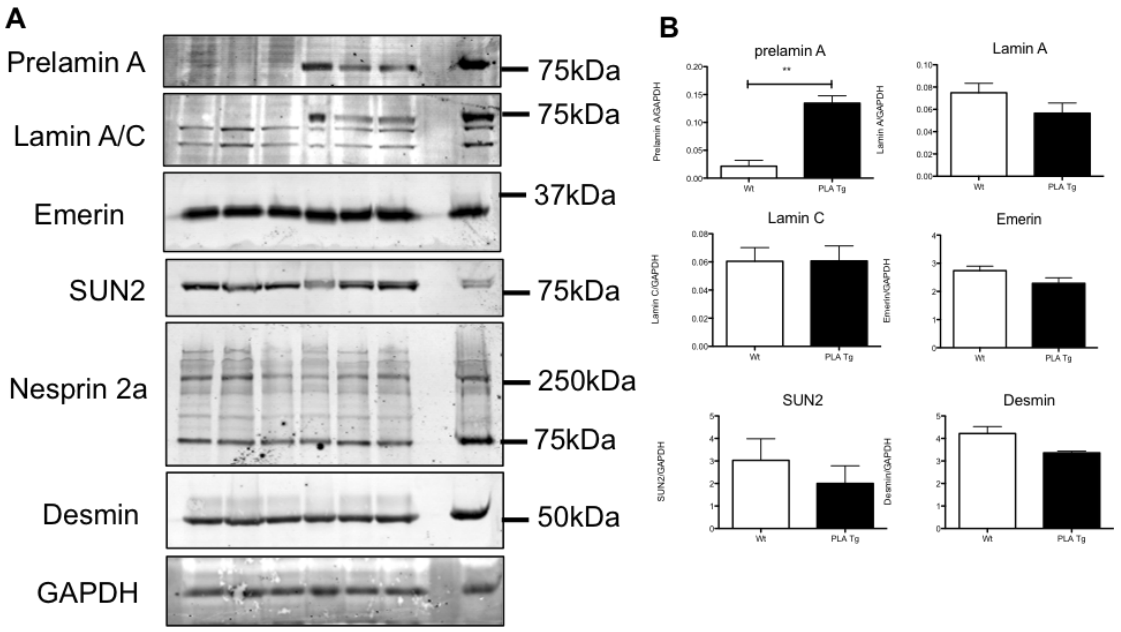

Figure 5.11. Expression of LINC complex proteins and IF protein desmin was unchanged in 2 week old hearts of mice accumulating prelamin A compared to Wt. (A) Ventricular tissue lysates were western blotted and membranes probed with antibodies for emerin, prelamin A (C20), lamin A/C (N18) and SUN2, nesprin 2 and desmin. GAPDH was used as loading control. (B) Densitometry confirmed that, as expected, prelamin A was present in PLA Tg hearts but not Wt. However, no changes were apparent in expression of emerin, lamin A/C, SUN2, nesprin2 and desmin in PLA Tg hearts compared to Wt. Values expressed as mean±SEM, **P<0.01, N=3/group

Cryopreserved 2 week old heart sections were subject to immunofluorescence staining, using antibodies for prelamin A, lamin A/C, lamin B1, desmin, α-actinin and myomesin. As expected, prelamin A was found to localise to the nuclear rim of CMs of PLA Tg mice (Fig 5.12). The distribution of lamin A/C (Fig 5.13), lamin B1 (Fig 5.14), desmin (Fig 5.15), α-actinin (Fig 5.12) and myomesin (Fig 5.13) appeared unchanged in PLA Tg hearts compared to Wt.

Moreover, TEM showed no observable differences between the heterochromatin organisation or NE structure of PLA Tg mice compared to Wt (Fig 5.7).

5.2.2.2 Expression of Cx43 appears to be altered in 2 week old hearts that have accumulated prelamin A compared to Wt

Western blotting of ventricular tissue lysates was performed using Cx43 antibody. Expression of Cx43 appeared marginally, but not significantly, increased in PLA Tg hearts compared to Wt (Fig 5.16B & C). In cryopreserved 2 week old hearts, Wt mice appeared to show a consistent staining pattern around the sarcolemma, and, whilst PLA Tg heart sections appeared to be similar, the pattern was intermittently interrupted suggesting loss of Cx43 at some sites. Additionally, in PLA Tg myocardium, Cx43 appeared to localise at intercalated discs, a feature missing from Wt myocardium (Fig 5.16A).

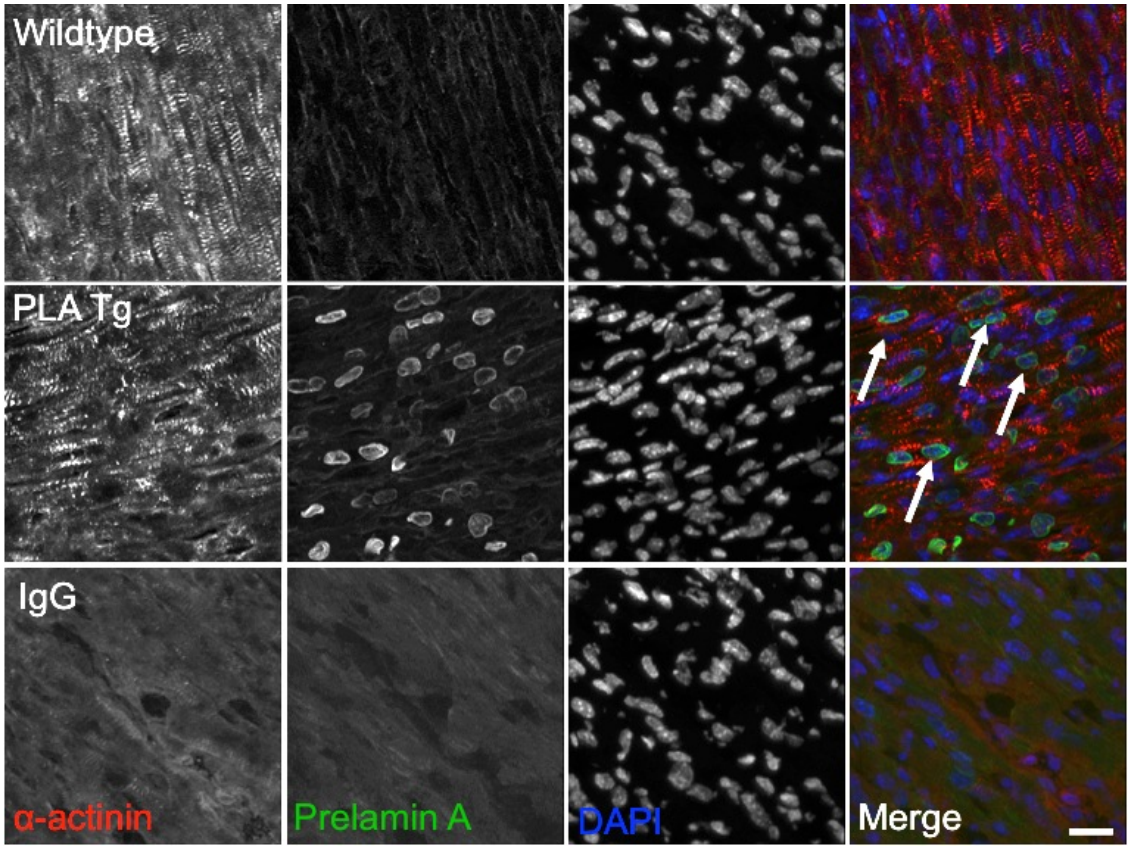

Figure 5.12. α-actinin appeared normal in PLA Tg hearts compared to Wt, but prelamin A did not appear to co-localise with α-actinin in Wt hearts. Cryopreserved heart cross sections were subject to immunofluorescence staining with prelamin A (green) and α-actinin (red) antibodies. In PLA Tg hearts, prelamin A localised to the nuclear rim as previously shown. In chapter 4, it was evident that prelamin A co-localised with α-actinin in Wt hearts. This was not apparent in 2 week old Wt hearts. Sections stained with serum IgG were used as negative controls. Scale bar = 20 μm

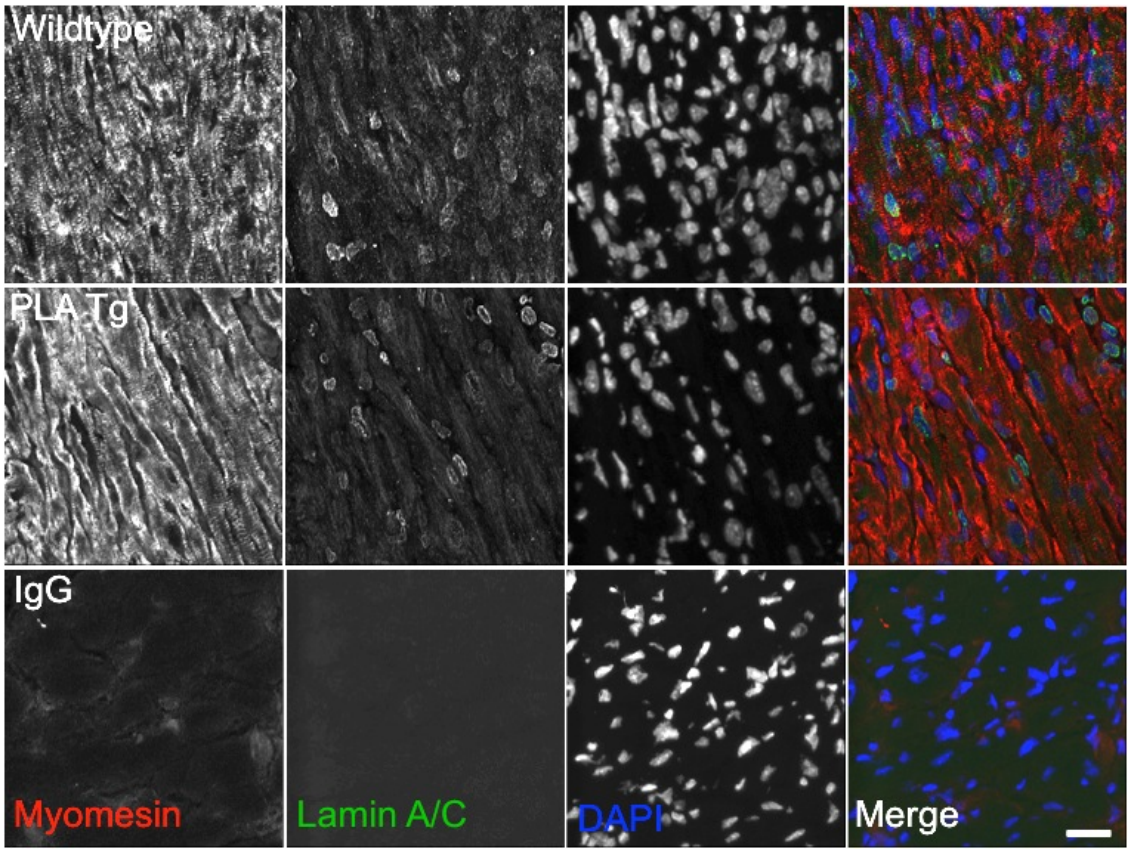

Figure 5.13. Lamin A/C was localised to the nuclear rim and nucleoplasm in all cells in the heart and myomesin was localised to the sarcomere in Wt and PLA Tg mice. Cryopreserved heart sections were subject to immunofluorescence staining with lamin A/C (green) and myomesin (red) antibodies and showed that lamin A/C was localised to the nuclear rim and nucleoplasm in CMs of Wt and PLA Tg mice. Myomesin was localised to the sarcomere in both Wt and PLA Tg mice with no observable differences. Sections stained with serum IgG were used as negative controls. Scale bar = 20 μm

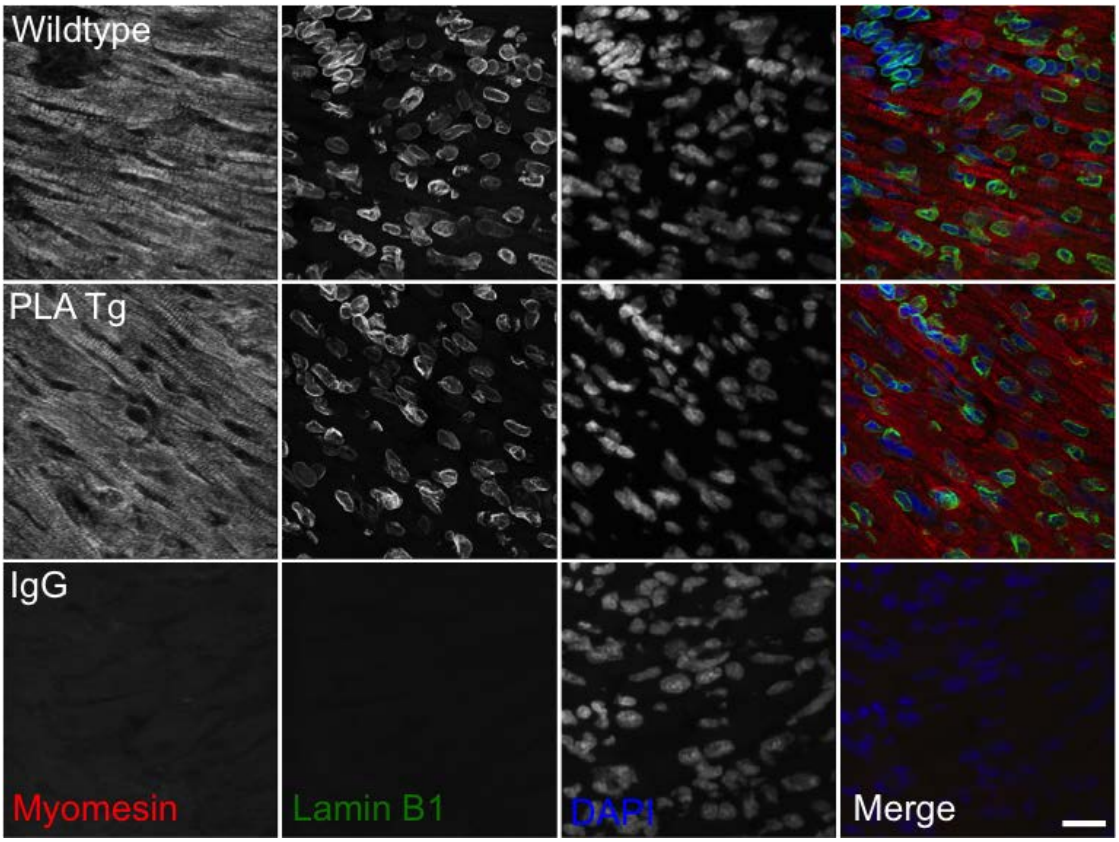

Figure 5.14. Lamin B1 localised to the nuclear rim in all cells of the myocardium with no observable differences between Wt and PLA Tg at 2 weeks of age. Cryopreserved heart sections were subject to immunofluorescence staining with lamin B1 antibody (green) and myomesin (red). Lamin B1 was localised to the nuclear rim in all cells, with no observable differences between Wt and PLA Tg mice. Myomesin was used as a CM marker. Sections stained with serum IgG were used as negative controls. Scale bar = 20 μm

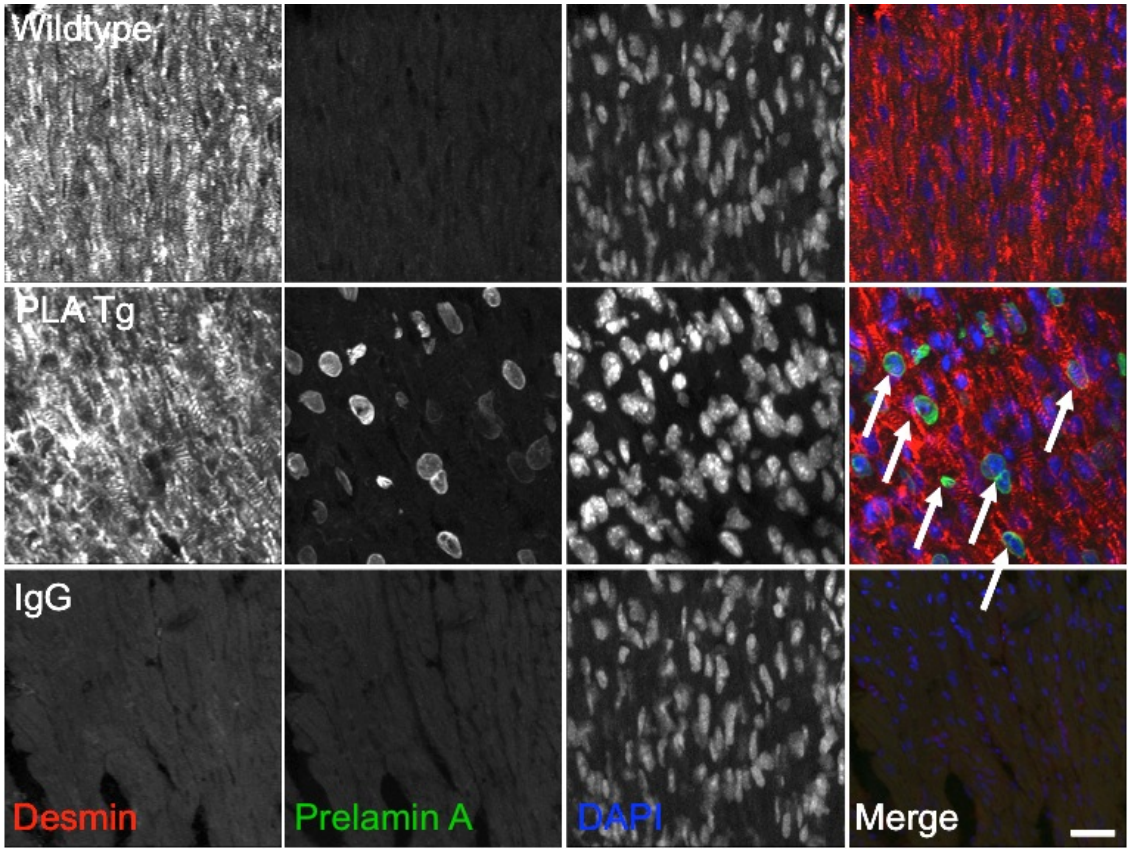

Figure 5.15. Prelamin A was localised to the nuclear rim and desmin appeared to localise normally in 2 week old PLA Tg mice. Cryopreserved heart cross sections were subject to immunofluorescence staining with prelamin A (green) and desmin (red) antibodies and viewed with fluorescence microscopy. Prelamin A accumulated in the nuclear rim of PLA Tg but not in Wt. Desmin expression appeared normal compared to Wt, with a predominantly sarcomeric localisation and some perinuclear staining. Sections stained with serum IgG were used as negative controls. Scale bar = 20 μm

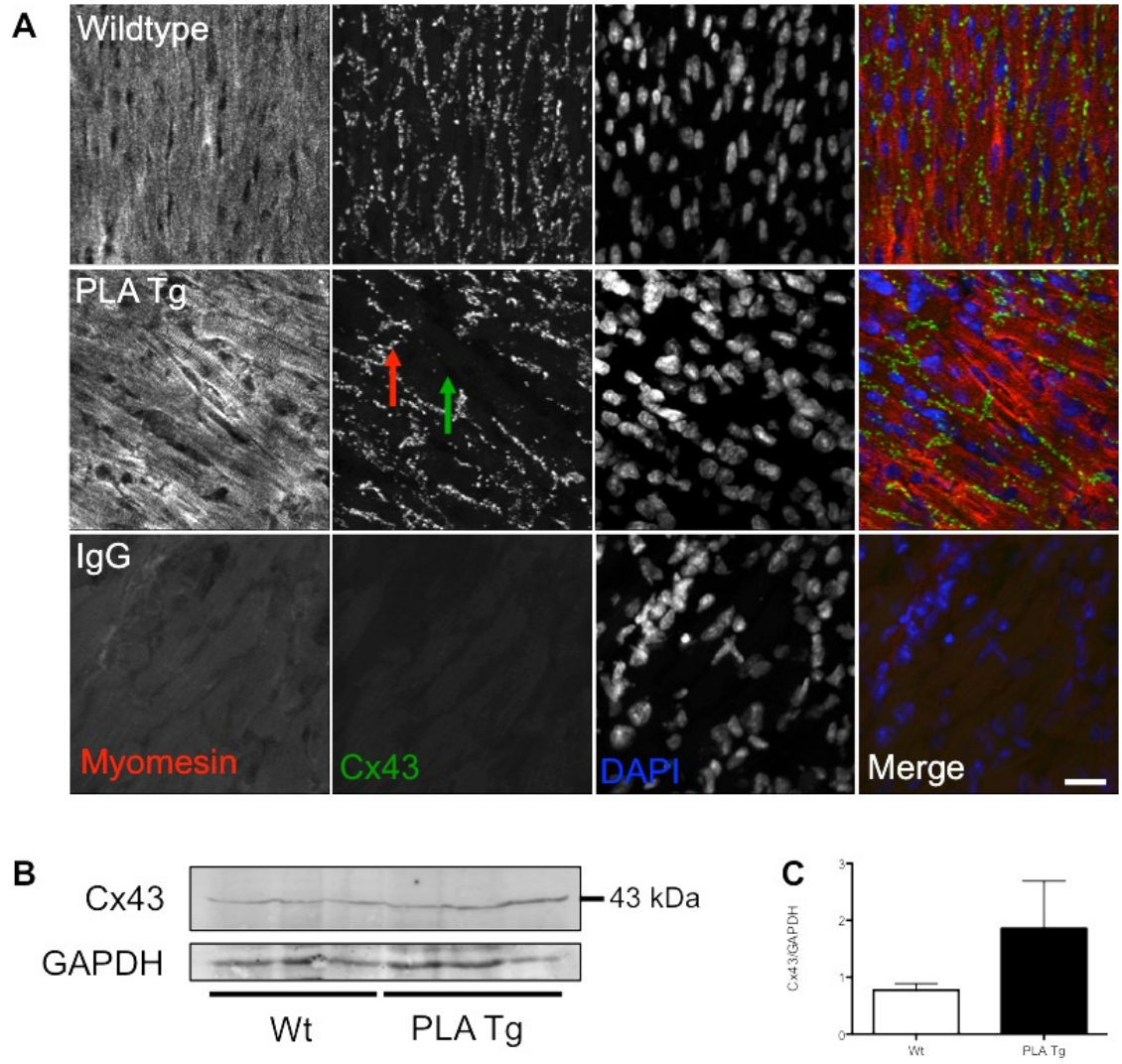

Figure 5.16. Prelamin A accumulation led to mislocalisation of Cx43 in 2 week old PLA Tg hearts. (A) Cryopreserved heart cross sections were subject to immunofluorescence staining with Cx43 (green) and myomesin (red) antibodies. In Wt myocardium, Cx43 was localised to the sarcolemma with even patterning and distribution. Comparatively, Cx43 localisation was a little uneven and punctuated with unstained areas. Scale bar = 20 μm (B) Ventricular tissue lysates were western blotted and the membrane was probed with Cx43 antibody. There appeared to be a trend towards increase in Cx43 expression in PLA Tg hearts compared to Wt, shown by (C) densitometric analysis of the western blot. Values expressed as mean±SEM, N=3/group.

5.2.2.3 Accumulation of prelamin A in 2 week old heart tissue leads to an increase in DNA damage

Increases in the number of γ-H2AX foci in nuclei are a reliable indicator of DNA damage accumulation. Cryopreserved 2 week old heart sections were stained with antibody raised to γ-H2AX and viewed under fluorescent light. It was observed that γ-H2AX foci appeared increased in PLA Tg heart sections compared to Wt (Fig 5.17A). Western blotting of ventricular tissue lysates was performed using γ-H2AX antibody and showed a trend for increased levels in PLA Tg mice compared to Wt (Fig 5.17B & C).

5.3 Discussion

5.3.1 At 2 weeks of age, mice that accumulate prelamin A in a cardiac specific manner are morphologically and physiologically normal, but histological changes have started to occur

Chapter 4 outlined a number of molecular events associated with the pathological onset of DCM. Many of these mechanisms have already been identified in other models of *LMNA* associated DCM or progeroid models of disease, but in many cases, they appear to have been studied only when a prominent phenotype was evident, meaning the initial trigger for disease remained unidentified. This chapter aimed to determine which of the molecular changes observed in the current study occurred earliest in order to establish a

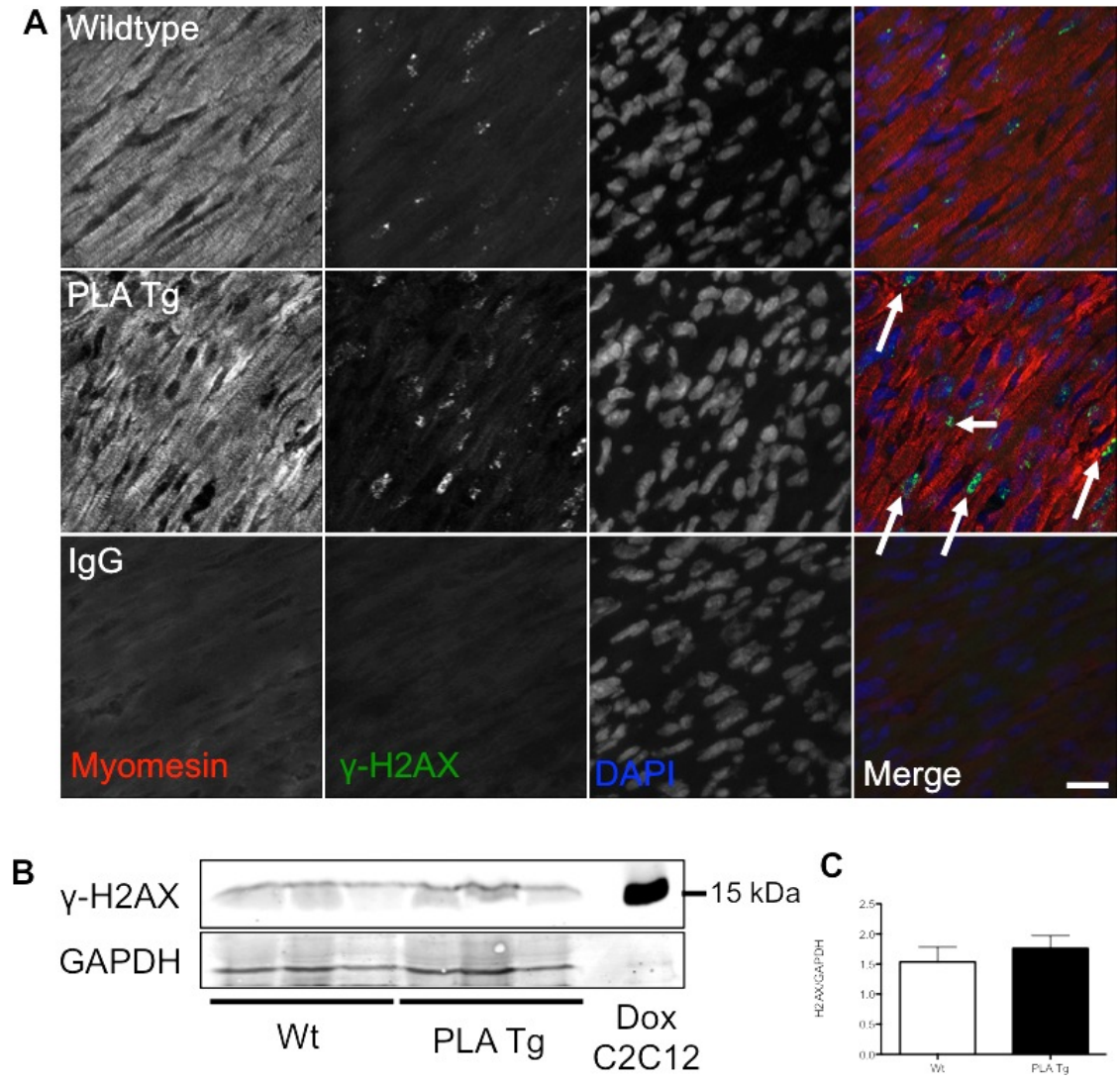

Figure 5.17. Prelamin A accumulation led to an increase in γ-H2AX foci in 2 week old PLA Tg hearts. (A) Cryopreserved heart cross sections were subject to immunofluorescence staining with p-H2AX (green) and myomesin (red) antibodies. There appeared to more H2AX positive nuclei in PLA Tg myocardium compared to Wt, and the number of H2AX foci in the nuclei also appeared increased. Scale bar = 20 μm (B) Ventricular tissue lysates were western blotted and the membrane was probed with p-H2AX antibody and (C) showed, using densitometric analyses, that p-H2AX expression in PLA Tg hearts was comparable to Wt. Values expressed as mean±SEM, N=3/group

temporally defined model of disease progression. To achieve this, mice were studied at 2 weeks of age, when they appeared to have no negative health effects caused by cardiac specific prelamin A accumulation.

At 2 weeks of age, PLA Tg mice appeared normal as evidenced by the photograph in Figure 5.1. Additionally, the mice displayed no unusual physical or behavioural traits compared to Wt littermates. Morphometry and analysis of cardiac function by echocardiography also suggested that, from a physiological perspective, the PLA Tg mice were free of pathology. The first indication otherwise came when analysing the histology of the myocardium, and although there appeared to be no overt disarray or fibrosis in PLA Tg mice, it was evident that there were more clusters of nuclei in the myocardial interstitium in PLA Tg hearts than there were in Wt hearts, indicating that leukocyte infiltration, as observed in 4 week old mice, had started to occur at 2 weeks of age. This was confirmed by analysis of CD45 expression and distribution within the myocardium and could also be observed in the cardiac ultrastructure. Additionally, mRNA expression of β-MHC had significantly increased in PLA Tg hearts at 2 weeks of age. Increases in β-MHC mRNA are commonly associated with heart failure, including in the case of lamin disruption, suggesting that detrimental changes were beginning to occur as early as 2 weeks of age[236, 262, 303].

5.3.2 The LINC complex appears to be normal at two weeks but subtle changes to Cx43 and γ-H2AX are detectable in 2 week old PLA Tg hearts

At 2 weeks of age, LINC complex protein expression was normal compared to Wt. Moreover, no differences were observable in the localisation of the lamins, desmin and

the sarcomeric proteins α-actinin and myomesin. However, Cx43 expression and localisation appeared to be dysregulated in PLA Tg hearts. In Wt hearts, Cx43 appears to stain around the sarcolemma in all myocytes in a consistent manner. In PLA Tg myocardium, there appeared to be a staining pattern more consistent with 4 week old Wt mice with staining at the intercalated discs being more prominent (although there were some observable gaps in the staining pattern suggesting incomplete formation and localisation of connexins). This observation led to the following speculations. Firstly, that during heart development, Cx43 localises evenly throughout the sarcolemma and then polarises to intercalated discs upon maturation; indeed, this is an established model of gap junction development and formation[304]. Secondly, that this process is disrupted in prelamin A accumulating hearts, pointing towards a model whereby gap junctions polarise to intercalated discs prematurely in comparison to Wt hearts. This means that prelamin A potentially hastens the development of gap junctions and may form part of the pathologic mechanism.

It was also observed that the occurrence of γ-H2AX foci appeared increased in PLA Tg hearts. Although not necessarily supported by expression levels on western blots, by immunofluorescence, increases in the number of foci in each nuclei, if not necessarily the number of nuclei affected, were observed. This indicates that DNA damage accumulation was occurring in 2 week old hearts and implicates responses to DNA damage either directly or indirectly in the progression of disease in this model. Taken with the observation that leukocytic invasion has already started to occur, these results potentially suggest an important role for ATM dependent NF-κB signalling in pathogenesis of PLA Tg mice. Very little is known about the timing of mechanistic activation in models of prelamin A mediated disease and, due to time constraints of the

current project, further insights were not achieved. Therefore, more work is required to establish whether this is the case, especially with regard to activation of NF-κB signalling.

To summarise, whilst PLA Tg mice were physiologically normal, there were cellular and molecular indicators that some of the pathological mechanisms observed in 4 week old mice were beginning to occur at 2 weeks of age. β-MHC may be an early biomarker for disease, whilst regulation of Cx43 and gap junction formation appears to be an important aspect of pathogenesis. Moreover, DNA damage accumulation and sterile inflammation of the myocardium are evident at 2 weeks and potentially linked by NF-κB signalling. The LINC complex appears to be unaffected at this time point, which suggests that changes to the structural protein network may occur as an adaptive response to mechanical stress. However, it cannot yet be ruled out that these events occur downstream as a direct action of prelamin A accumulation. For example, ATM dependent NF-kB activation of inflammation could lead to leukocyte invasion; leukocytes migrating through the interstitium could phagocytose components of the ECM and cause physical perturbations to the ECM and create tension changes[305]. The subsequent changes in ECM tension may be detected by the CMs via mechanosignalling, which may confer expression changes to structural proteins. Moreover, the ECM changes potentially caused by this mechanism may also initiate the fibrotic remodelling of the ECM as perturbations may also lead to secretion of profibrotic factors from surrounding cardiac fibroblasts. Additionally, cell death may contribute to this pathway, as matter from necrosed CMs may be capable of activating TLR signalling which could lead to leukocyte infiltration. Further investigation is required.

Further investigation is also required into the mechanical stability of CMs, both isolated and as intact tissue, to determine whether cells that accumulate prelamin A are susceptible to mechanical stress and whether this induces expression changes of important structural scaffold proteins. Therefore, although more work is required, a temporally defined model of pathogenesis is beginning to emerge and is highlighted by Figure 5.18.

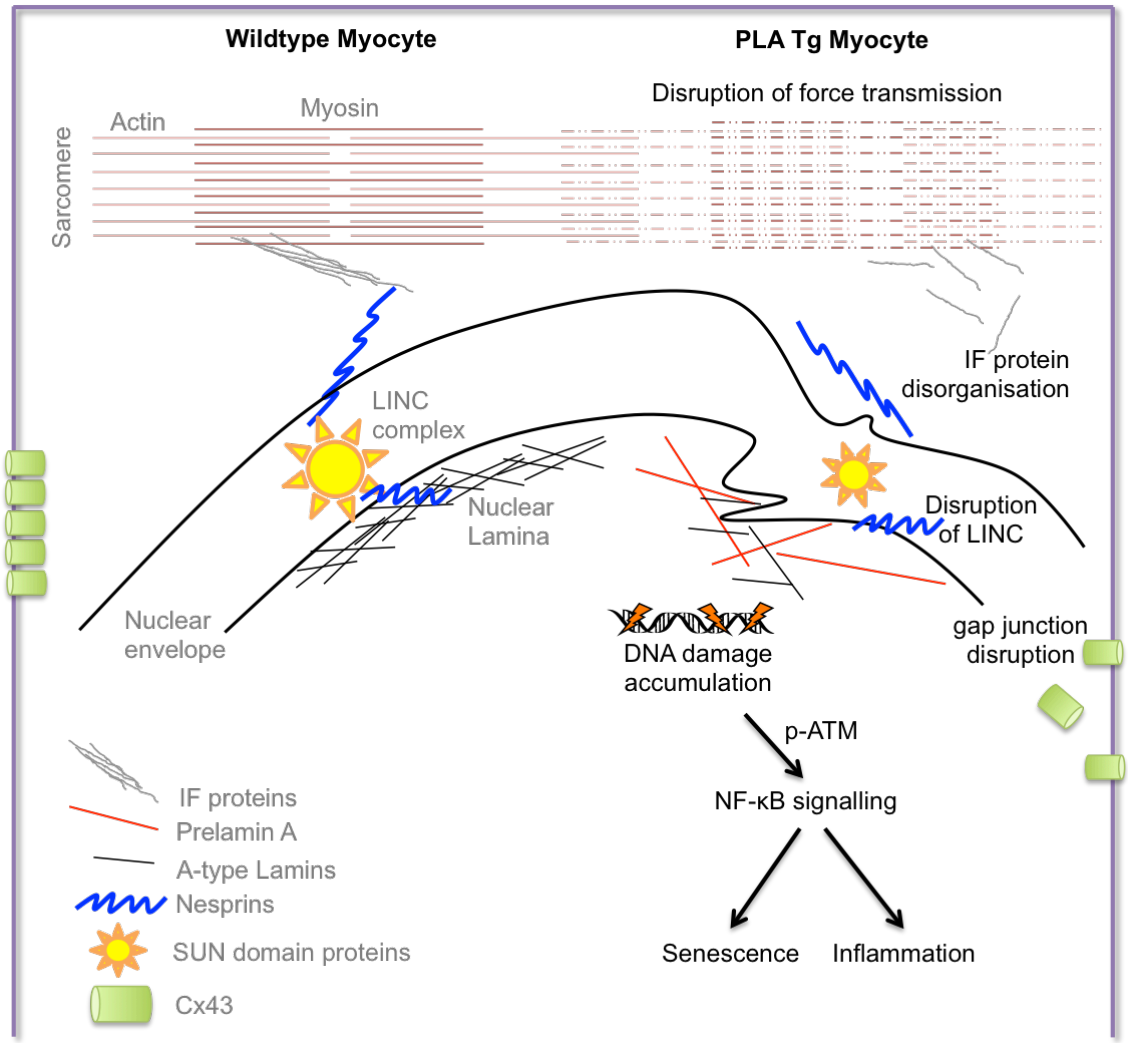

Figure 5.18. Working schematic of the pathogenesis of PLA Tg mice. Accumulation of prelamin A in CMs led to a range of pathological outcomes in the CMs, including accumulation of DNA damage, activation of NF-κB signalling, inflammation, increase in the senescence associated biomarker, SA-β-Gal, disruption of Cx43, and disruption of the LINC complex and IF network.

Chapter 6: The spatiotemporal regulation of prelamin A in CMs and C2C12 myofibrillogenesis

6.1. Introduction

As mentioned in chapter 1, the research into the regulation of lamins in CMs is limited. This is despite the fact that lamin associated diseases tend to affect muscle cell types. However, some studies in myoblast cell lines have highlighted the dynamic nature of prelamin A processing in the development of myotubes and suggest an active role for lamins and indeed prelamin A in myocyte differentiation[260, 306]. Moreover, during the course of investigation for this thesis, some interesting observations were made regarding the expression and localisation of prelamin A in the heart. In chapter 4, it was observed that endogenous prelamin A was localised to the sarcomere in 4 week old heart tissue of Wt mice; however, in chapter 5 it was noted that this was not evident in 2 week old Wt heart tissue. These were intriguing observations, which, along with other observations made during the characterization of the PLA Tg model, led to a distinct line of investigation asking if prelamin A is endogenously expressed in the heart? If so, where, and how does it get there?

6.2 Results

6.2.1 Unprocessed prelamin A is endogenously expressed in CMs

Current evidence suggests that prelamin A intermediates are rapidly converted into mature lamin A for insertion into the nuclear lamina. As such, prelamin A is undetectable in normal or healthy cells. However, upon over exposing a western blot probed for lamin A/C (N-18) containing Wt and PLA Tg heart tissue samples, the 74kDa prelamin A band was clearly detectable in Wt tissue (Fig 6.1). This was deemed to be compelling evidence for the existence of endogenous prelamin A in the heart and stimulated further investigation into prelamin A regulation in the heart. Recognising that heart tissue is a dynamic organ consisting of multiple cell types, it was important to establish whether CMs were a source of this prelamin A. To achieve this, CMs were isolated from neonatal rat hearts. Initially, immunocytochemical staining for lamin A/C and prelamin A with α-actinin co-staining revealed that lamin A/C strongly stained the nuclear rim of CMs (Fig 6.2), whilst prelamin A stained sarcomeric structures and appeared to colocalise with α-actinin, indicating that prelamin A localises to the z-disc of the sarcomere (Fig 6.3). To further show this localisation, cells were then co-stained with myomesin. Myomesin is a sarcomeric protein that localises to the M-line within the H-band of the sarcomere. Prelamin A did not localise with myomesin, but formed alternating parallel line patterning with myomesin, supporting the observation of z-disc localisation (Fig 6.4).

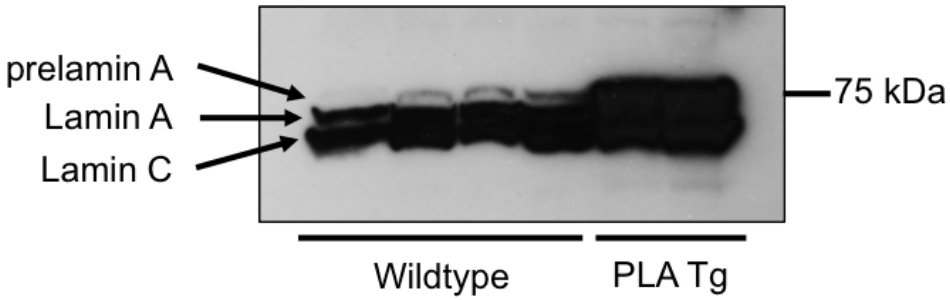

Figure 6.1. Prelamin A was detectable in Wt heart tissue. Ventricular tissue lysates were subject to western blotting and probed with lamin A/C antibody (N18). After overexposure of the membrane to film, prelamin A was indistinguishable from lamin A in PLA Tg heart tissue. Prelamin A was also detected in Wt tissue.

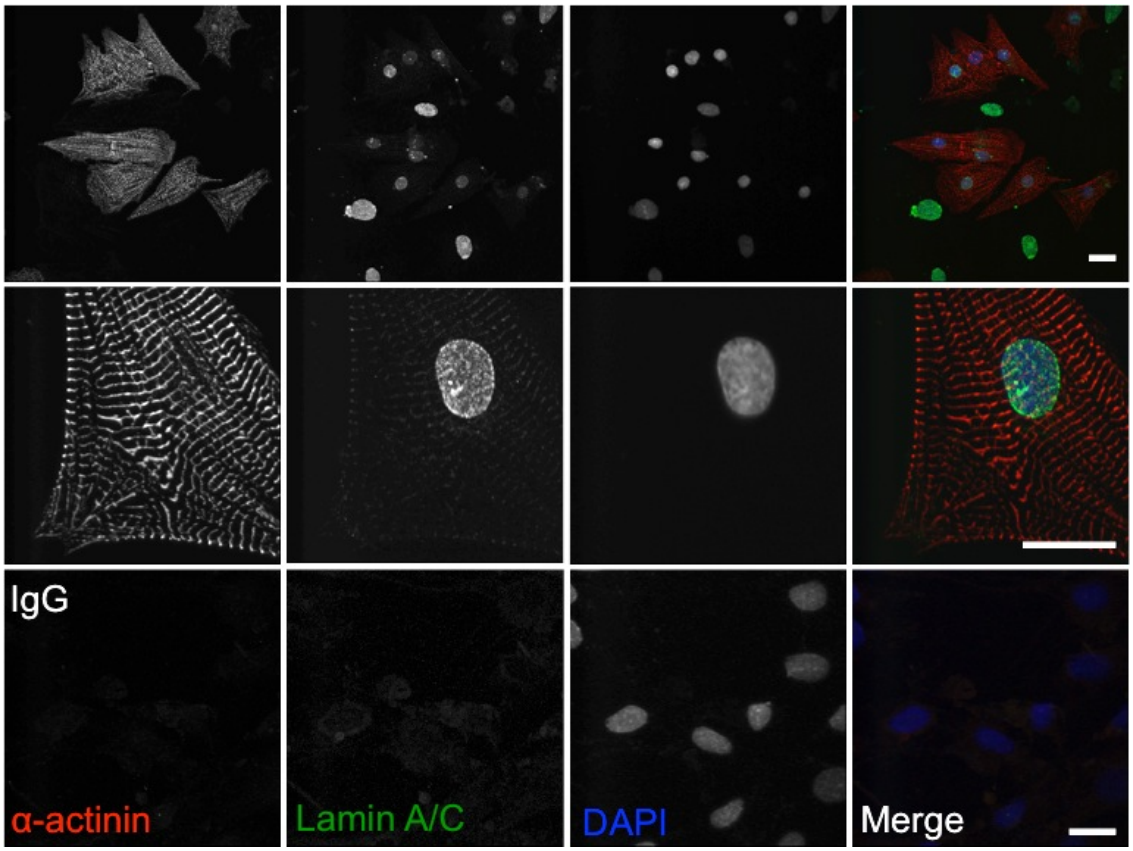

Figure 6.2. Lamin A/C localised to the nuclear rim and nucleoplasm of CMs. Isolated NRCs were subject to immunofluorescence staining using lamin A/C (green) and α-actinin (red) antibodies. Lamin A/C localised to the nuclear rim/nucleoplasm of all cells, whilst α-actinin localised to the sarcomere of CMs. It was also possible to identify faint staining to the sarcomere in the lamin A/C channel on high power magnification and zoom. Scale bar = 20μm

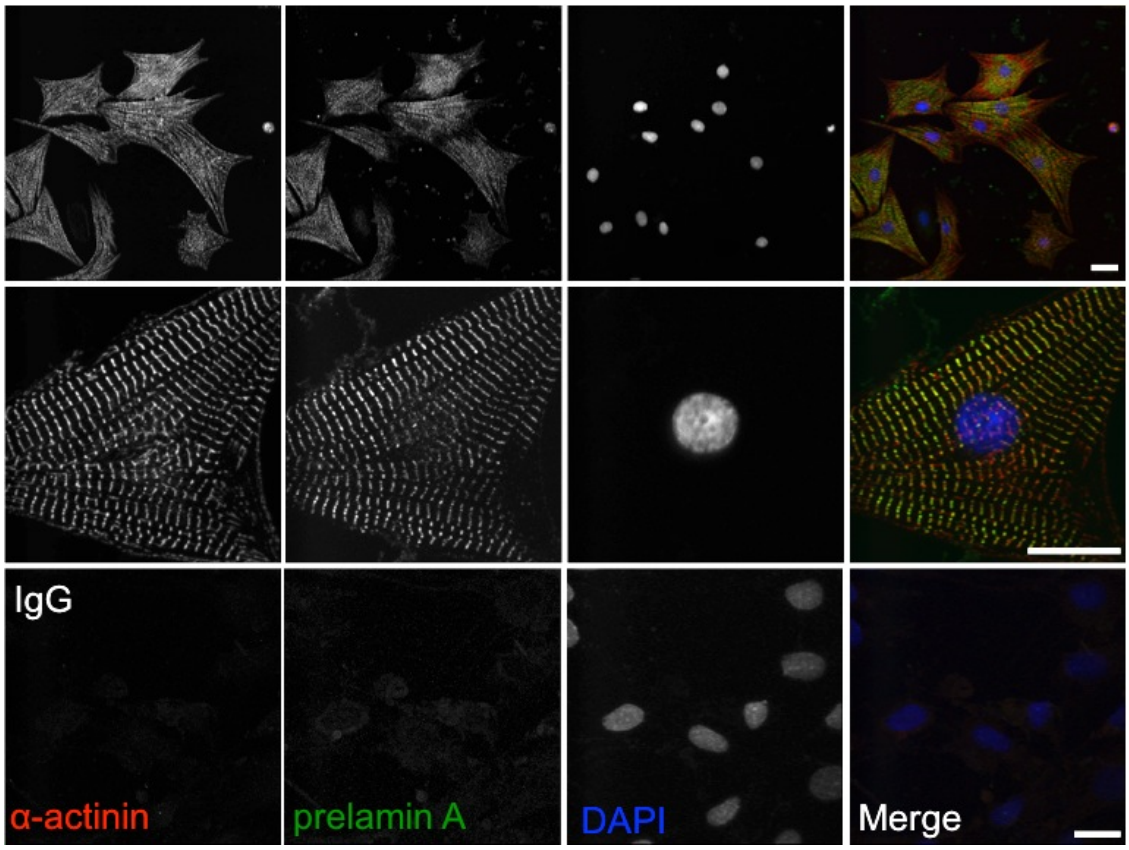

Figure 6.3. Prelamin A localised to the z-disc of the sarcomere in CMs. Isolated NRCs were subject to immunofluorescence staining with prelamin A (green) and α-actinin (red) antibodies. Prelamin A appeared to co-localise with α-actinin at the sarcomere. Scale bar = 20 μm

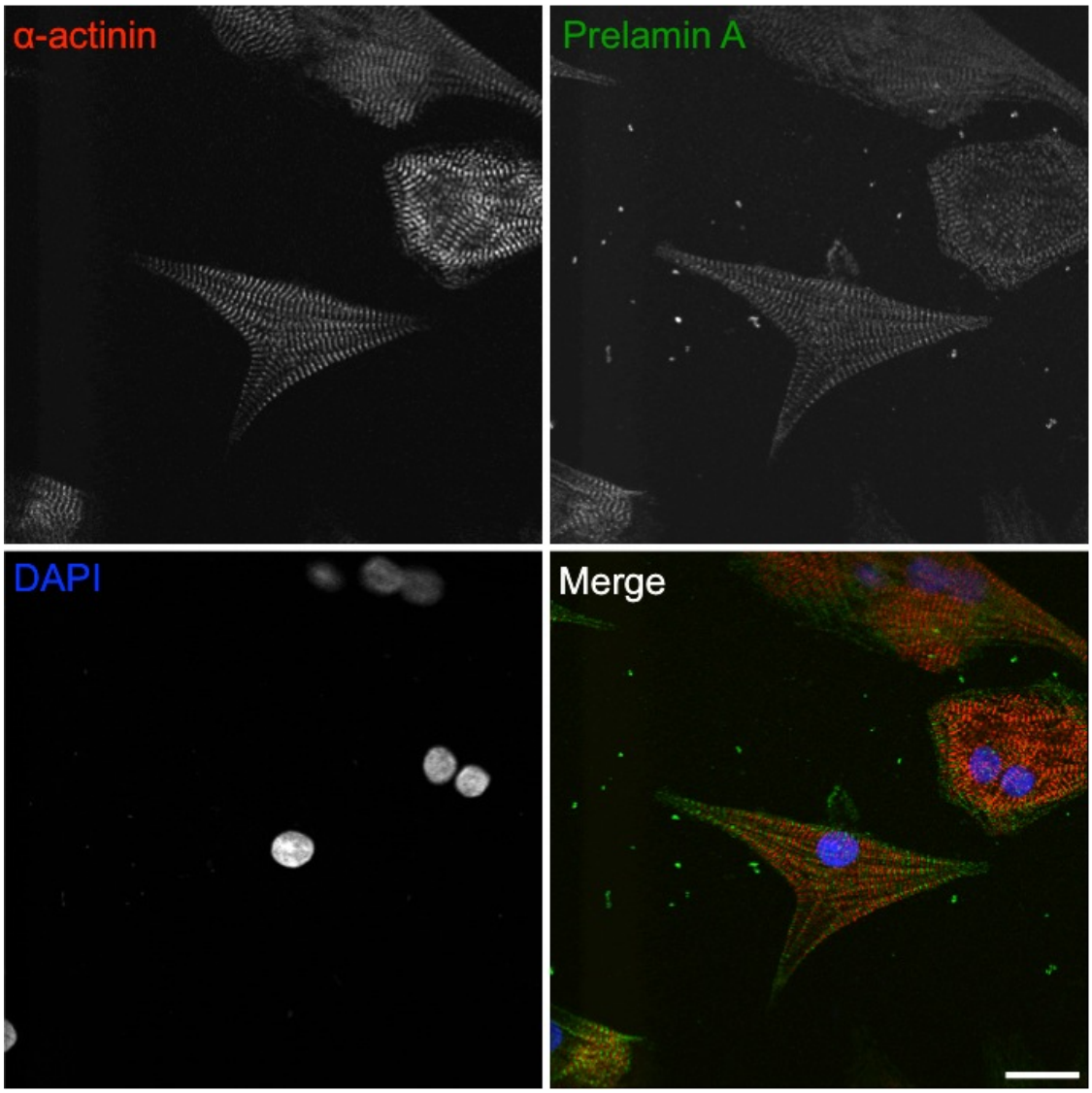

Figure 6.4. Prelamin A localised in parallel to myomesin in CMs. Isolated NRCs were subject to immunofluorescence staining with prelamin A (green) and myomesin (red) antibodies. Prelamin A appeared to localise in parallel with myomesin at the sarcomere. Scale bar = 20 μm

6.2.2 Nuclear prelamin A accumulates in CMs of DCM patients

In order to understand the behaviour of prelamin A in the heart further, human heart cryosections diagnosed phenotypically as DCM, ischaemic heart disease (IHD), and healthy controls, were stained. The DCM sections were from patients with clinical presentation of DCM but for which the sequencing is currently being undertaken; therefore, potential causative mutations are currently unknown. Patient samples S99 1036 (DCM), S99 1309 (IHD) and S99 577 (healthy control) were compared directly by costaining with prelamin A and α-actinin (Fig 6.5). S99 1036 showed prelamin A staining of the sarcomere and appeared to localize with α-actinin. Moreover, there was a remarkably consistent prelamin A staining in the nuclear rim of most CMs. Associated nuclei were dysmorphic as was CM shape. Cell separation was apparent, and increases in the amount of interstitial space were observed, which was associated with clustering of nuclei within the interstitial spaces. S99 1309 was negative for prelamin A in the sarcomere and in the nucleus, morphologically, nuclei of CMs were normal and the CMs appeared rod shaped and had a low level of cell separation. S99 577 heart tissue was positive for prelamin A staining in the sarcomere and appeared to localise with α-actinin in the z-disc region. S99 577 nuclei were negative for prelamin A. CMs were rod shaped and there was no cell separation.

Patient samples 2.059, 4.066, d4.047, 4.032 (DCM) and ch1 5.089 and ch1 5.138 (healthy control) were directly compared by co staining with prelamin A and myomesin. 2.059 appeared to show prelamin A staining in some nuclei and also showed moderate sarcomeric staining, which was localised in parallel to myomesin staining,

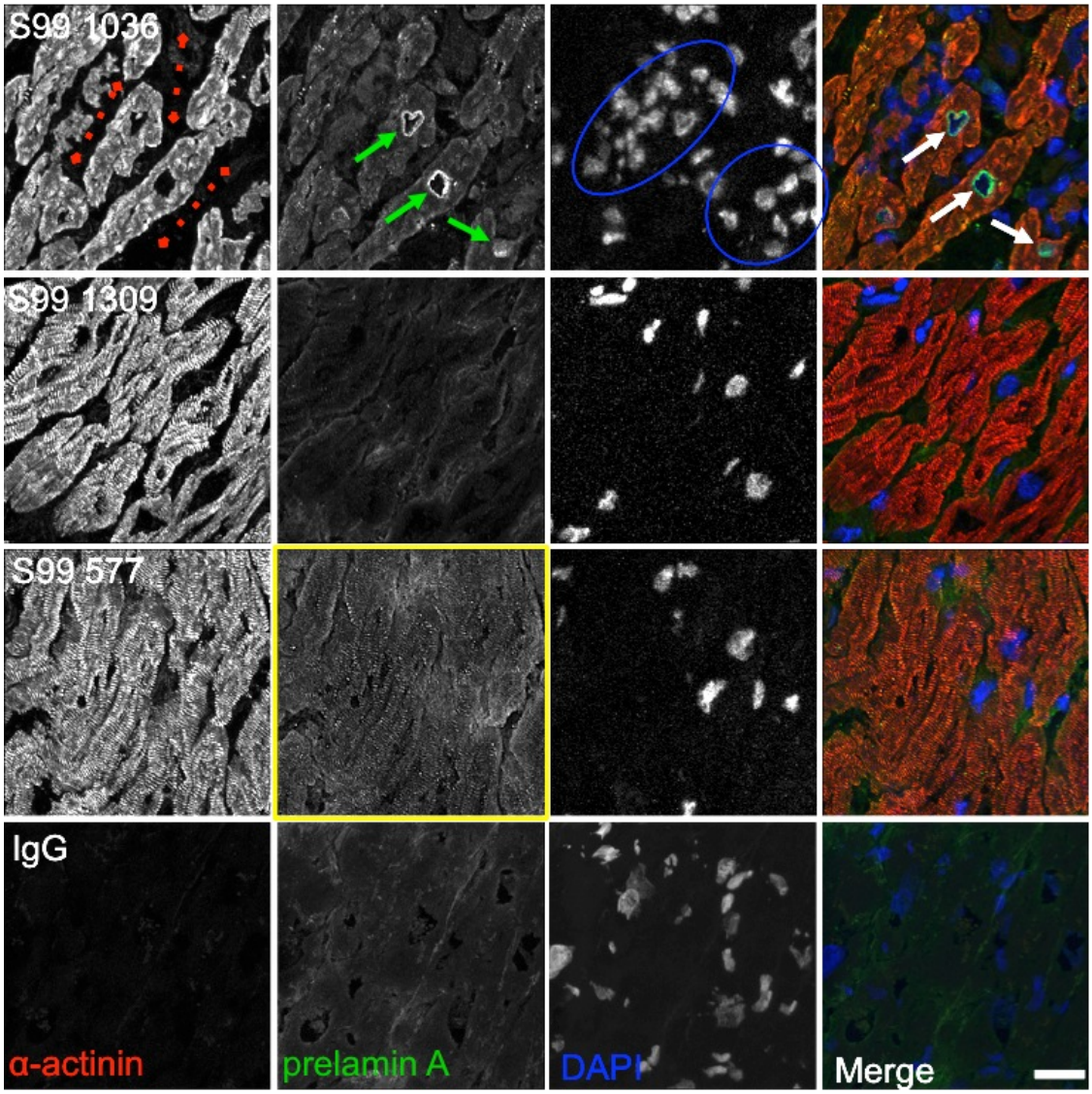

Figure 6.5. A subset of DCM patients accumulated prelamin A in the nuclear rim of CMs. Cryosections of human heart biopsies were subject to immunofluorescence staining with antibodies to prelamin A (green) and α-actinin (red). DCM patient myocardium S99 1036 accumulated prelamin A at the nuclear rim of CMs and had nuclear morphology defects (arrows). Nuclei were clustered (blue ellipse) in areas of myocardial disarray (red dashed line). Additional striated sarcomeric staining was observed colocalised with α-actinin. Prelamin A was barely detected in IHD myocardium S99 1309. Healthy myocardium S99 577 showed a compelling sarcomeric staining colocalised with α-actinin (yellow border). Scale = 20μm

again confirming prelamin A localisation to the z-disc region (Fig 6.6). There was moderate cell separation, a moderate increase in interstitial space and cells were highly dysmorphic. Nuclei were often enlarged and sometimes exhibited blebbing. 4.066 did not have nuclear prelamin A staining and showed relatively low levels of sarcomeric staining. The nuclei appeared enlarged; the cells appeared rod shaped; and cell separation was evident (Fig 6.6). D4.047 also showed no nuclear prelamin A and very little sarcomeric prelamin A. Cells appeared dysmorphic with some cell separation and associated clustering of nuclei (Fig 6.7). 4.032 showed frequent nuclear staining of prelamin A, which was more diffuse compared to the distinct nuclear rim staining seen in S99 1036 DCM tissue. Prelamin A accumulation often occurred in the enlarged nuclei. Sarcomeric prelamin A staining was also evident in this tissue (Fig 6.6). As with S99 577 (healthy control), ch1 5.089 and ch1 5.138 heart tissue was positive for prelamin A staining in the sarcomere and appeared to localise in parallel with myomesin, indicating z-disc localisation. The nuclei were negative for prelamin A; CMs were rod shaped; and there was no cell separation (Fig 6.6 & 6.7). These observations are summarised in Table 6.1.

6.2.3 Ectopic expression of uncleavable prelamin A construct (L647R *LMNA*) in CMs results in nuclear localisation

Prelamin A accumulation observed in many laminopathic disease phenotypes occurs at the nuclear rim or within the nucleoplasm. The current findings that suggest CMs retain endogenous prelamin A within the sarcomere raise questions as to the distribution of prelamin A in the setting of pathogenic accumulation or overexpression in the heart.

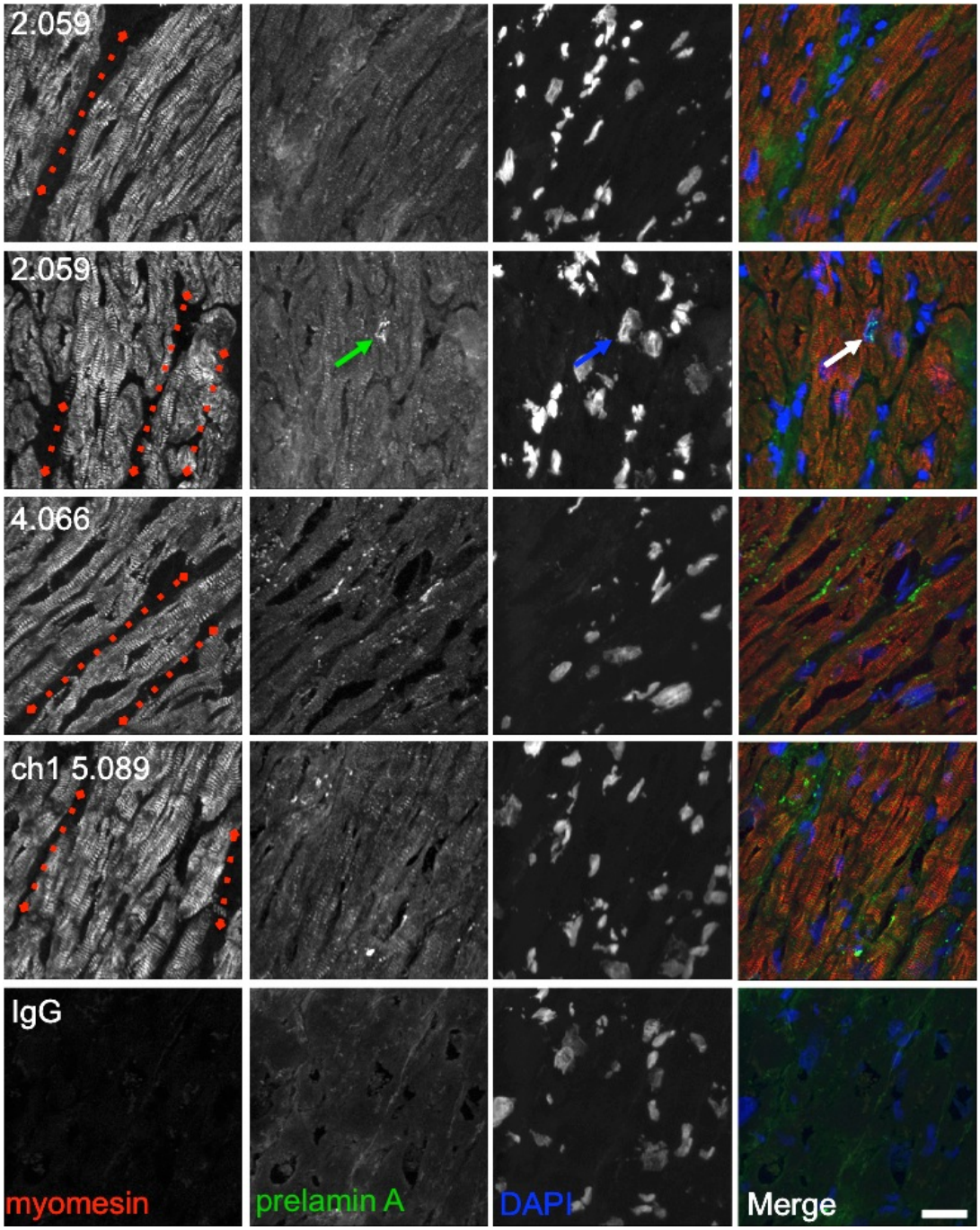

Figure 6.6. A subset of DCM patients accumulated prelamin A in the nuclei of CMs. Cryosections of human heart biopsies were subject to immunofluorescence staining with antibodies to prelamin A (green) and α-actinin (red). DCM patient myocardium 2.059 accumulated prelamin A in the nuclei of a number of CMs and had nuclear morphology defects (green and blue arrows) and myocardial disarray (red dashed line). Additional striated sarcomeric staining was observed colocalised with α-actinin. 4.066 showed little prelamin A staining whereas healthy myocardium ch1 5.089 showed sarcomeric staining in parallel with myomesin. Scale = 20μm

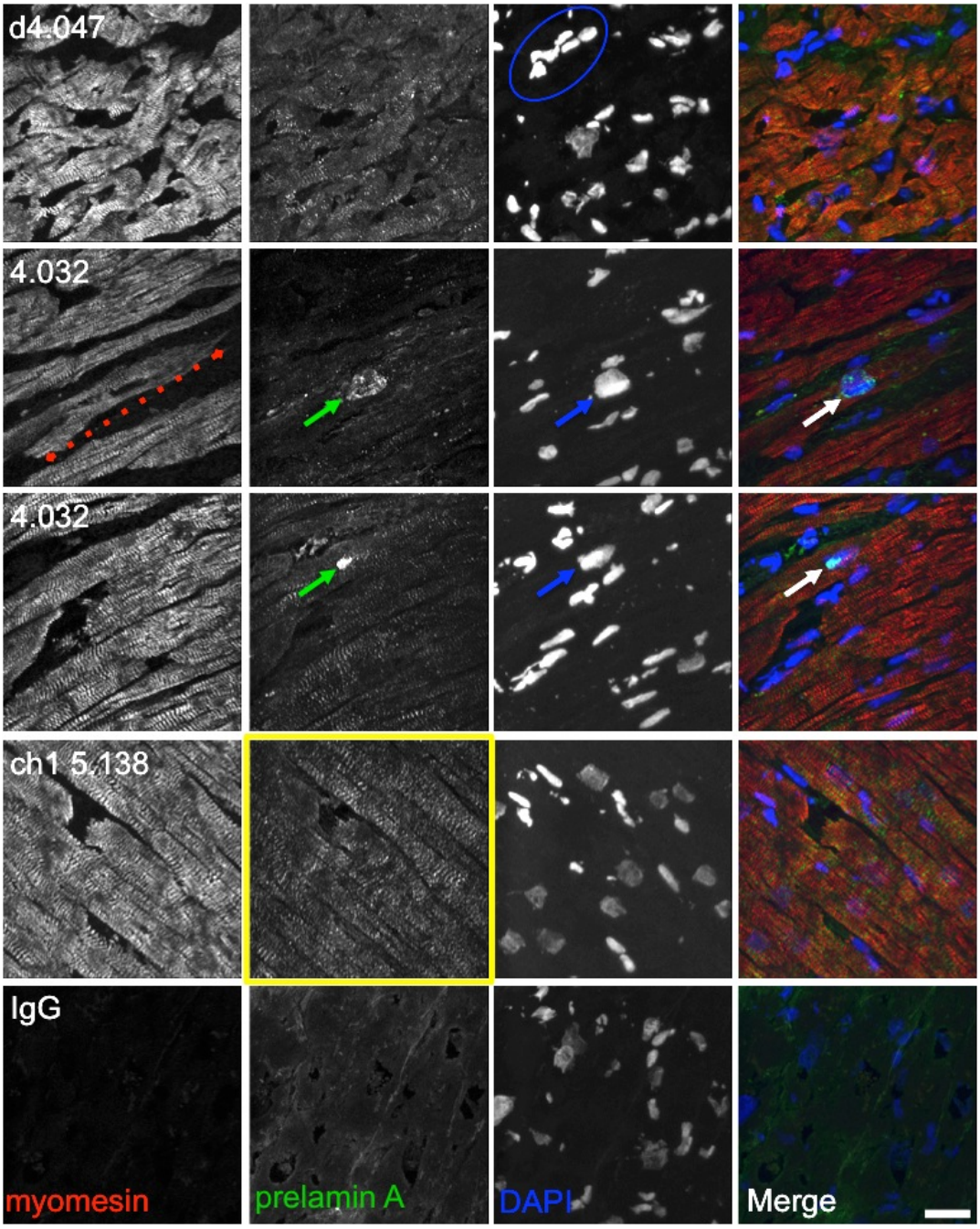

Figure 6.7. A subset of DCM patients accumulated prelamin A in the nuclear rim of CMs. Cryosections of human heart biopsies were subject to immunofluorescence staining with antibodies to prelamin A (green) and α-actinin (red). DCM myocardium d4.047 did not accumulate nuclear prelamin A, whereas 4.032 did. Nuclei were clustered (blue ellipse) in areas of myocardial disarray (red dashed line). Additional striated sarcomeric staining was observed. Healthy myocardium ch1 5.138 showed a substantial sarcomeric staining (yellow border) in parallel with myomesin. Scale = 20μm

Table 6.1. Prelamin A centric characterisation of staining of DCM heart biopsies.

Sample ID	Prelamin A staining				Nuclear morphology	Myocardial disarray	
	Nuclear		Sarcomeric			Interstitial space	Cell
	Intensity	Frequency	Intensity	Frequency		(Cell separation)	shape
DCM							
2.059	2	1	2	2	blebbing, enlarged	2	dysmorphic
4.066	0	0	1	2	enlarged	3	rod-like
D4.047	0	0	1	1	involution, blebbing, enlarged	2	dysmorphic
4.032	3	2	2	2	enlarged, blebbing	2	rod-like
S99 1036	4	4	3	2	involution, blebbing	3	dysmorphic
IHD							
S99 1309	0	0	0	0	normal	1	rod-like
Healthy							
Ch 5.089	0	0	3	3	normal	0	rod-like
Ch 5.138	0	0	3	4	normal	0	rod-like
S99 577	0	0	4	4	normal	0	rod-like

Prelamin A scoring: 0 = none, 1 = low, 2 = moderate, 3 = High, 4 = Very High
Interstitial space: 0 = normal, 1 = slight increase, 2 = moderate increase, 3 = great increase

Results from chapter 3 and 4 performed on tissue sections of PLA Tg heart tissue suggest that in pathogenic settings, prelamin A accumulates in the nuclear rim. To further assess this finding, an adenoviral construct with flag-tagged uncleavable prelamin A mutant, L647R-*LMNA* was transduced into NRCs. Interestingly, overexpression of this construct led to prelamin A localisation in the nuclear rim with some visible cytoplasmic staining when stained with Flag antibody. Wt *LMNA* was also virally expressed in NRCs and showed only strong nuclear staining. These data support the findings made in heart tissue sections and potentially suggest a divergent role for prelamin A in physiology and in pathogenesis (Fig 6.8).

6.2.4 Prelamin A is directed to the sarcomere during C2C12 myofibrillogenesis and coincides with Zmpste24 expression changes

Having discovered that prelamin A localised to the sarcomere, it was important to next assess whether prelamin A was regulated in myofibrillogenesis. There is currently evidence for modulation of prelamin A in C2C12 myotube formation as one study has shown changes in prelamin A expression with detection of a band at approximately 150 kDa as opposed to the regular 74 kDa immediately at the onset of differentiation. However, this response was reported to return to normal over the course of 36 hours and localisation to sarcomeric structures was not reported, as myofibers were not assesed[306]. However, longer incubation periods in differentiation medium of C2C12 myoblasts can lead to myofiber formation. Therefore, it was hypothesised that prelamin A would be directed to the sarcomere in differentiated C2C12 myofibers. To have the greatest chance of obtaining myofibers, a chronic differentiation protocol was devised and time

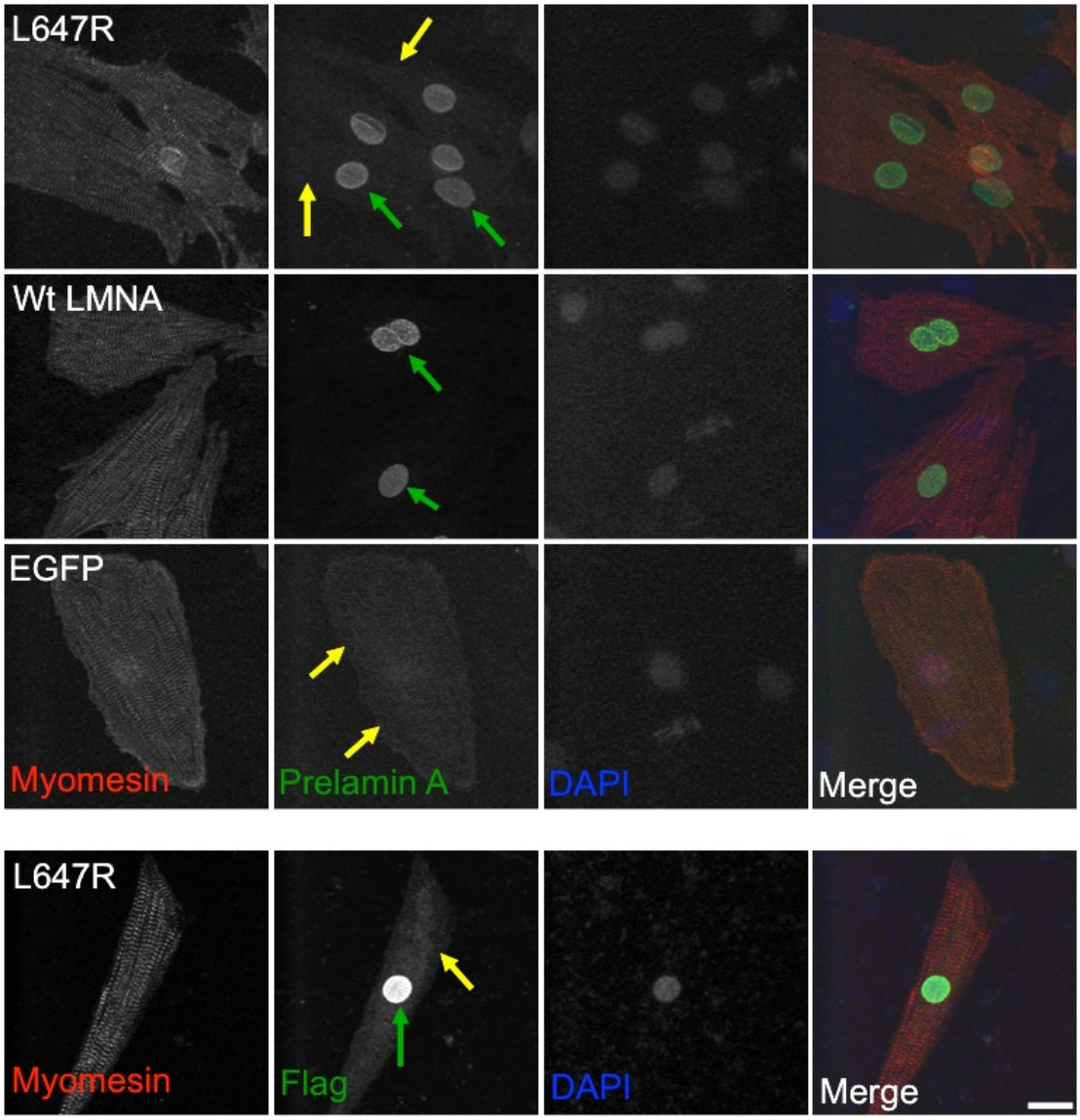

Figure 6.8. Ectopic expression of Wt *LMNA* and L647R *LMNA* mutant led to prelamin A accumulation in the nucleus of CMs. Isolated NRCs were transduced with adenoviral constructs containing flag-tagged L647R *LMNA*, Wt *LMNA* DNA and an empty EGFP vector for negative control purposes and stained with prelamin A (green) and myomesin (red) antibodies. Expression of both constructs results in prelamin A accumulation in the nucleus, whereas endogenous prelamin A is detectable in the cytoplasm of EGFP (negative) control. Cells transduced with flag-tagged L647R *LMNA* were also stained with flag antibody (green), again showing nuclear localisation predominantly, but also some cytoplasmic localisation. Scale bar = 20 μm

intervals were set at 48, 72 and 168 hours. Cycling myoblasts were used for control purposes. Consistent with existing evidence, expression of 74 kDa prelamin A in undifferentiated myoblasts and cells that were 48 hours into differentiation was observed from whole cell lysates (Fig 6.9). However, contrary to previous reports, at 72 and 168 hours post differentiation, prelamin A was detectable at 150 kDa. The distribution of prelamin A appeared to be within peri-nuclear regions or the endoplasmic reticulum in cycling myoblasts and in cells differentiated for 48 hours. The distribution became more diffuse in cells differentiated for 72 hours and, after 168 hours, it was possible to see prelamin A in striations lining up alongside, rather than completely colocalised with, α-actinin (Fig 6.10). Additionally, Zmpste24 expression underwent a steady and significant decrease over the course of differentiation (Fig 6.9). Distribution of Zmpste24 appeared to be more diffuse in cells at 72 and 144 hours post differentiation compared to cycling myoblasts and cells 48 hours post differentiation, which showed a peri-nuclear localisation and more intense staining (Fig 6.11). Desmin expression levels showed a trend towards an increase during differentiation (Fig 6.9), and distribution was cytoplasmic diffuse throughout the differentiation protocol (Fig 6.12). Myomesin was undetectable at all time points according to western blotting but was visible at both 72 and 144 hours by immunofluorescence microscopy, showing striated sarcomeric localisation (Fig 6.11). Lamin A/C appeared to localise and remain at the nuclear rim throughout differentiation (Fig 6.12); lamin A expression was consistent throughout, whereas lamin C appeared to increase during differentiation (Fig 6.9). Lamin B1 also localised at the nuclear rim throughout differentiation (Fig 6.13) and appeared to undergo increased expression levels (Fig 6.9).

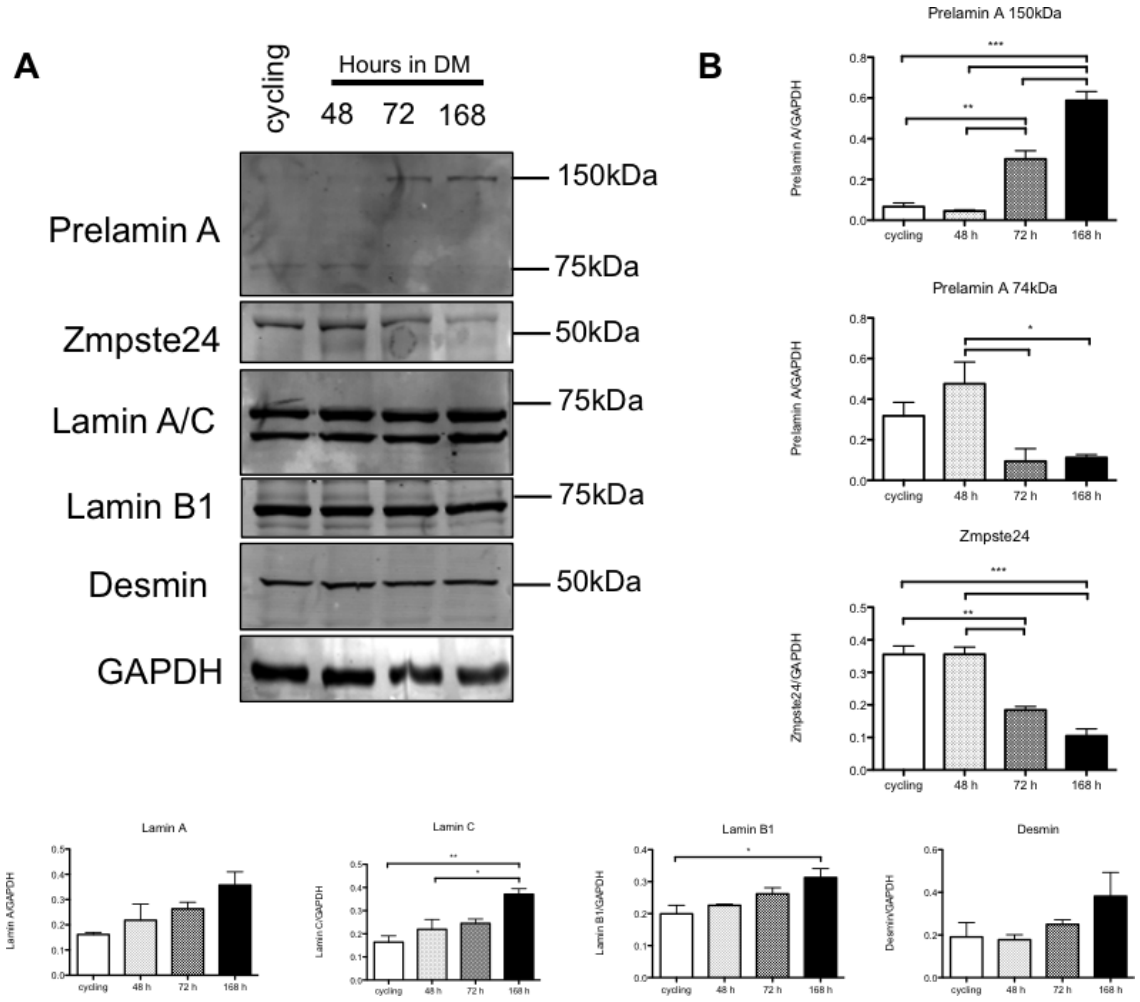

Figure 6.9. Expression changes to prelamin A, Zmpste24 and desmin occurred in the differentiation of C2C12 myoblasts. (A) C2C12 whole cell lysates were subject to western blotting and membranes probed with antibodies for prelamin A, Zmpste24, lamin A/C, lamin B1 and desmin. (B) Densitometry showed that prelamin A was observed in cycling myoblasts and cells 48 hours into the differentiation protocol. Detection of a 150kDa band occurred at 72 and 168 hours. Zmpste 24 expression was comparable in cycling cells and 48 h differentiated cells whereas expression levels were attenuated in 72 and 168 h cells. Lamin A/C and lamin B1 expression appeared to increase throughout the differentiation protocol, whilst desmin expression showed a trend for increased expression during the course of differentiation up to 168 hours. Values expressed as mean±SEM,*P<0.05, **P<0.01, ***P<0.001 N=3

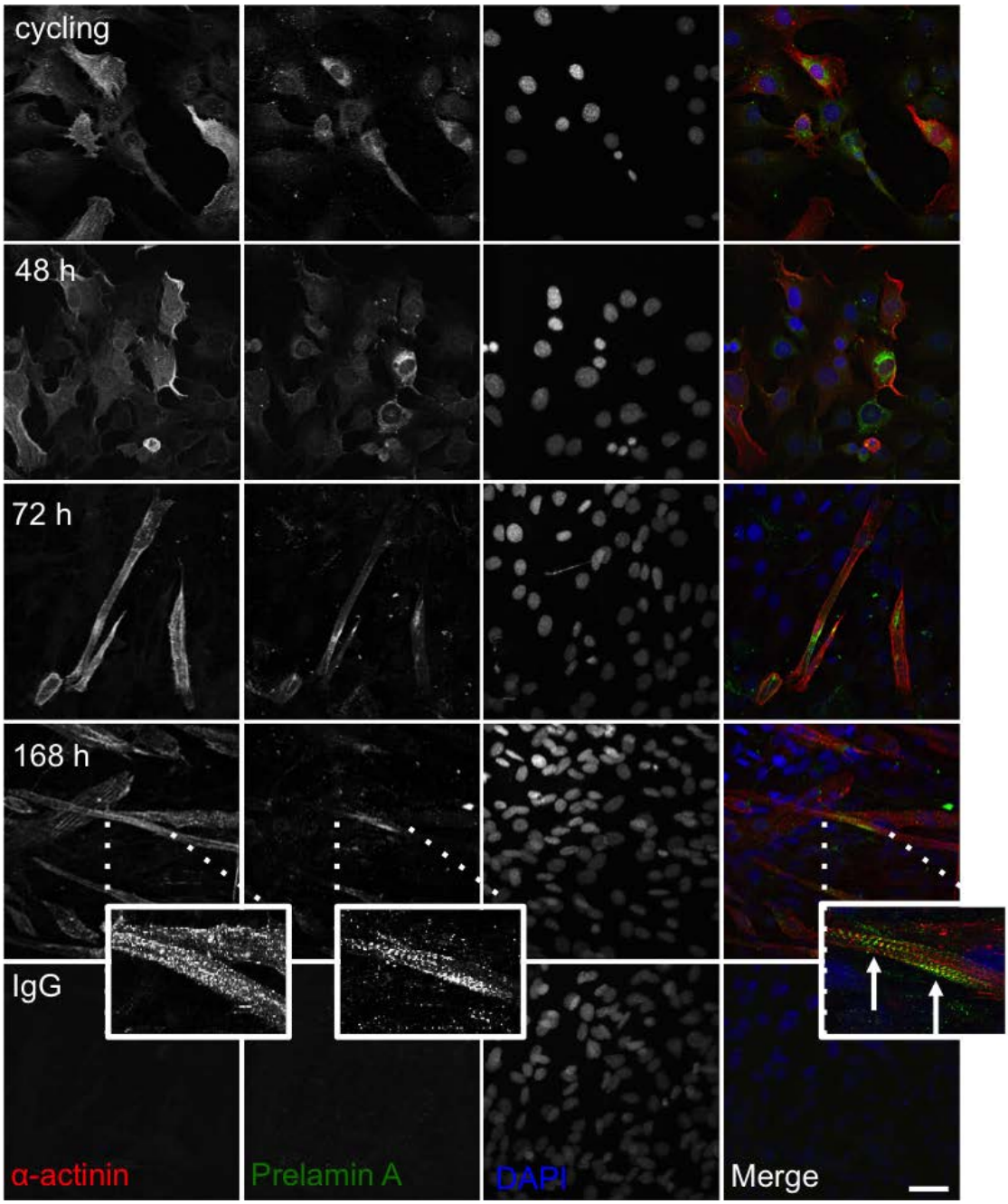

Figure 6.10. Differentiation of C2C12 myoblasts led to myofibril formation after 168 hours and sarcomeric localisation of prelamin A. C2C12 myoblasts underwent differention protocols, fixed at separate timepoints and then subjected to immunofluorescence staining with prelamin A (green) and α-actinin (red) antibodies. At 168 hours, myofibrils were able to form as indicated by the striated pattern caused by α-actinin localisation. Prelamin A localised to perinuclear regions in undifferentiated cells and then lined up with α-actinin at the sarcomere upon myofibril formation. Scale bar = 20 μm

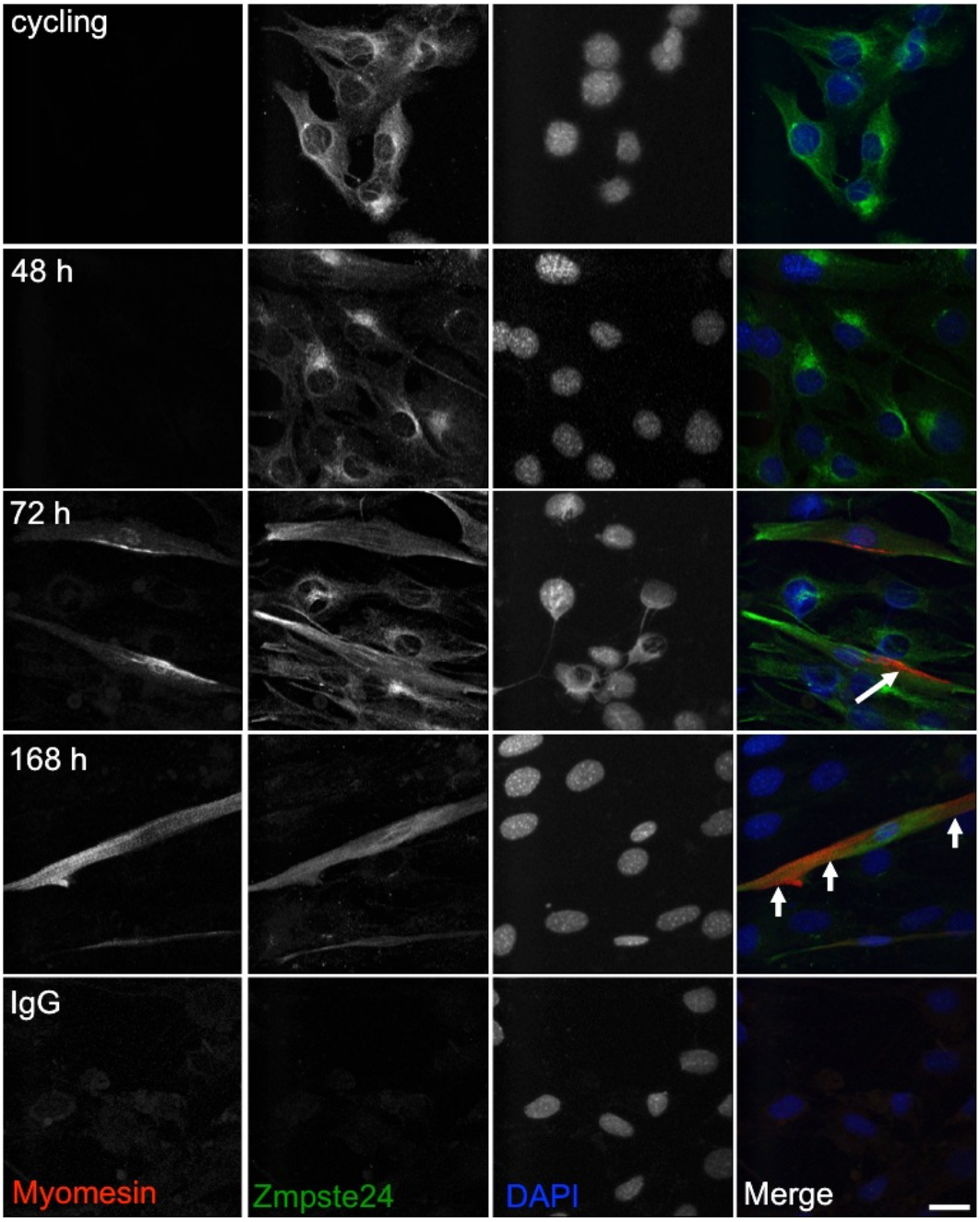

Figure 6.11. Zmpste24 localisation became diffuse upon myofibril formation in C2C12 cells. C2C12 myoblasts underwent differention protocols, fixed at separate timepoints and then subjected to immunofluorescence staining with Zmpste24 (green) and myomesin (red) antibodies. Myomesin was detected only in cells differentiated for 72 hours or more, and was striated in cells differentiated for 168 hours. Zmpste24 was localised to nuclear rim and perinuclear regions in cycling myoblasts and cells differentiated for 48 and 72 hours; localisation became cytoplasmic diffuse at 168 hours. Scale bar = 20 μm

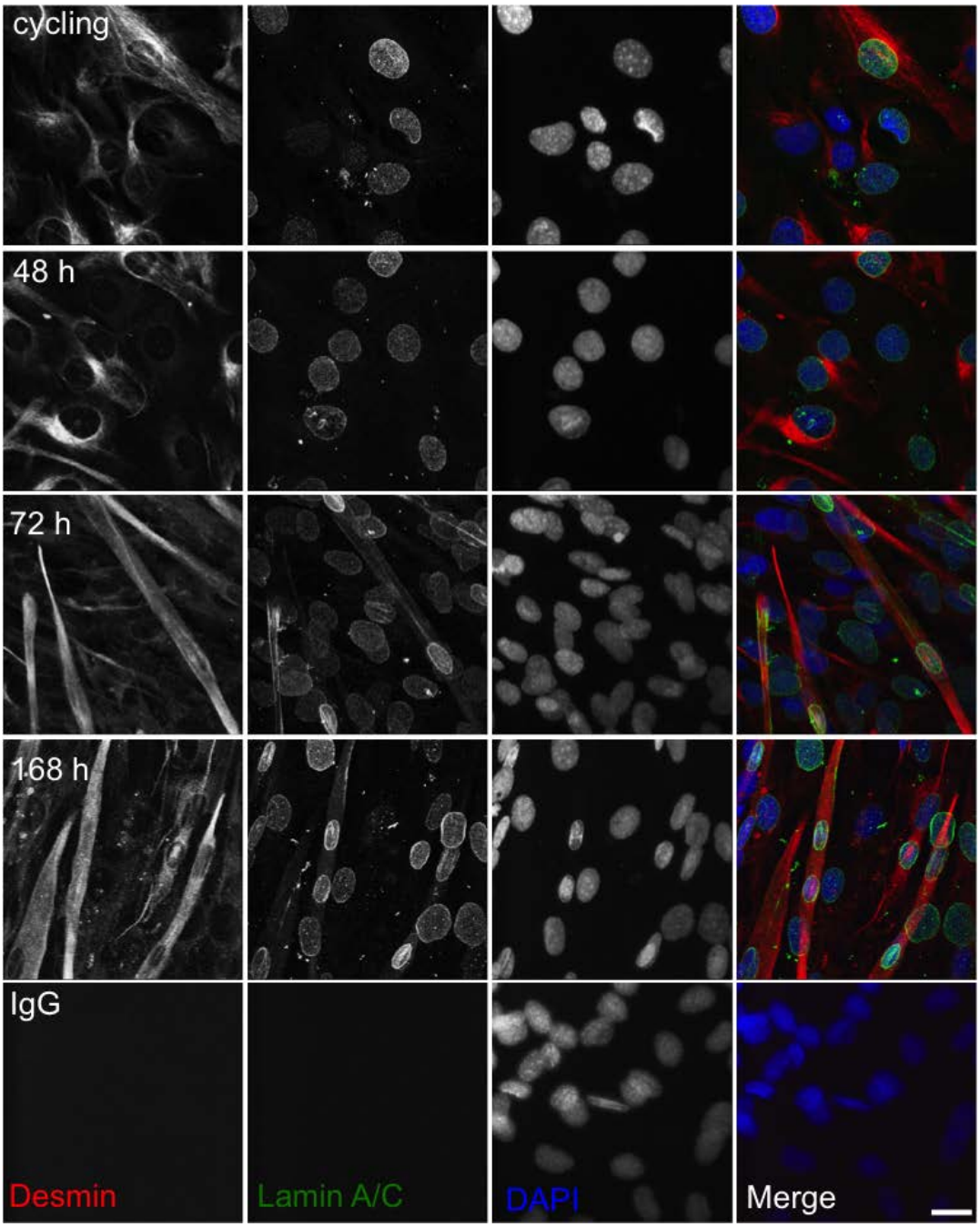

Figure 6.12. Desmin underwent altered localisation whilst lamin A/C distribution was consistent throughout C2C12 differentiation. C2C12 myoblasts underwent differentiation protocols, fixed at separate timepoints and subjected to immunofluorescence staining with lamin A/C (green) and desmin (red) antibodies. Desmin localised to perinuclear regions in cycling myoblasts and cells differentiated for 48 hours but was cytoplasmic diffuse at 72 and 168 hours. Lamin A/C localised to the nuclear rim at all timepoints during differentiation. Scale bar = 20 μm

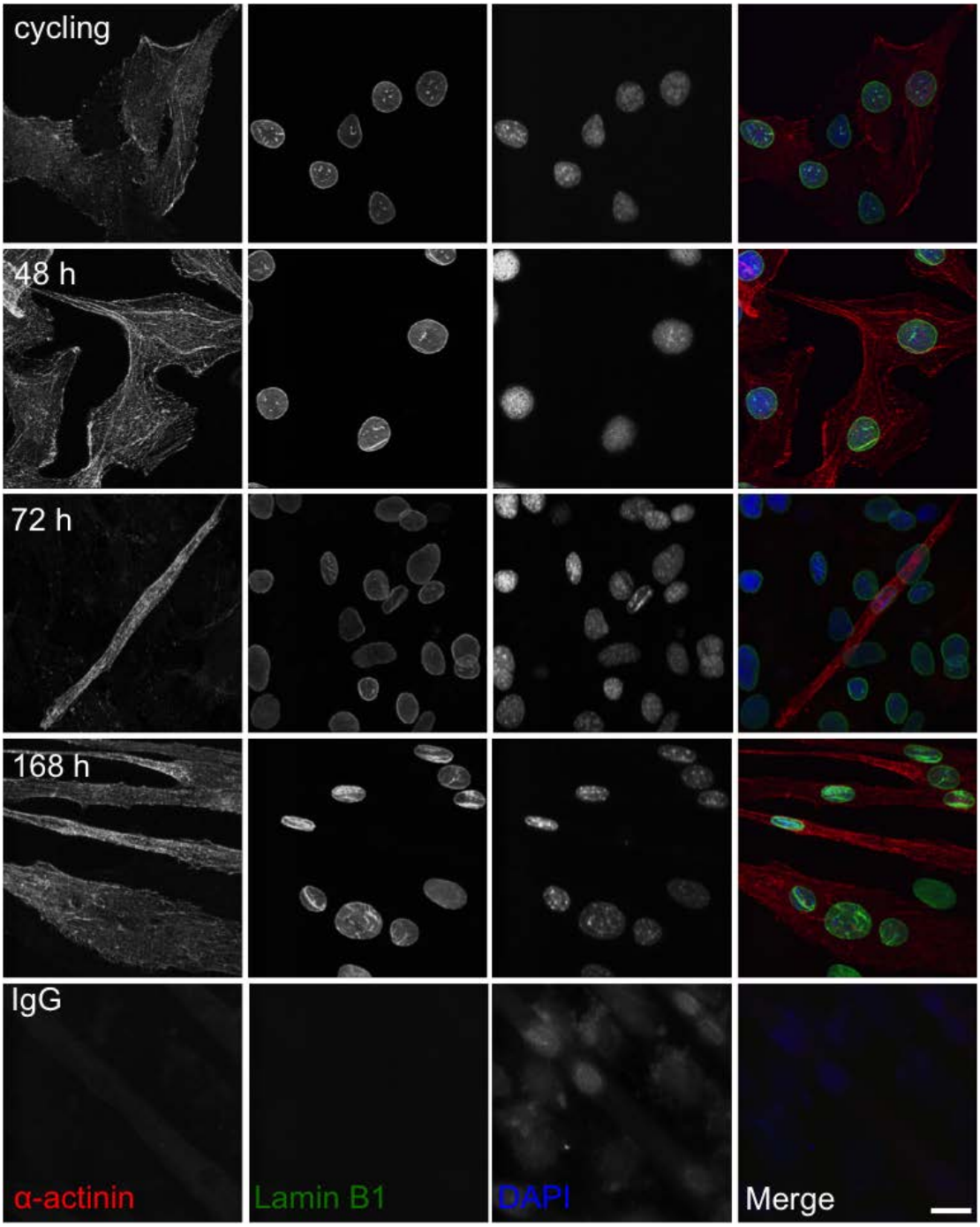

Figure 6.13. Lamin B1 localised to the nuclear rim throughout C2C12 differentiation. C2C12 myoblasts underwent differention protocols, fixed at separate timepoints and subjected to immunofluorescence staining with lamin B1(green) and α-actinin (red) antibodies. Lamin B1 was localised to the nuclear rim throughout the differentiation protocol. Scale bar = 20 μm

6.3 Discussion

6.3.1 Prelamin A appears to be a component of the sarcomere

Having observed that endogenous prelamin A localised to the sarcomere in Wt mouse heart tissue in chapter 3, it was decided that additional investigation was required to confirm this observation. Prelamin A immunostaining of isolated NRCs supported this observation and western blotting confirmed the presence of endogenous prelamin A. These data were further supported by immunostaining of human biopsies of healthy myocardium showing staining in the z-disc region of the sarcomere. These data suggest that prelamin A may be a component of the sarcomere. However, ectopic expression of prelamin A in isolated CMs led primarily to a nuclear localisation, although some cytoplasmic staining could be detected. To further address this finding, additional investigation is required. Moreover, it may be the case that separate stages of prelamin A processing influence the localisation of prelamin A in CMs; therefore, perhaps the newly introduced range of prelamin A antibodies, which detect prelamin A at various stages of processing, could be useful tools in future investigation.

6.3.2 Prelamin A accumulates in a subset of myocardial biopsies from DCM patients

Interestingly, biopsies of myocardium from patients with DCM of unknown cause showed a number of characteristics with regard to prelamin A localisation. Some biopsies were negative for nuclear prelamin A but had sarcomeric prelamin A as

observed in control biopsies. One patient, S99 1036, showed strong and frequent prelamin A staining in the nuclear rim with nuclear morphology defects and severe myocardial disarray and possible leukocytic invasion, indicated by the clustering of nuclei. This strongly mimics the structural appearance of PLA Tg mouse heart tissue when cross sections are viewed under fluorescent light. As such, one might speculate that this patient has a *LMNA* mutation. This is based on the fact that *LMNA* mutations are a common cause of DCM. Furthermore, evidence suggests that a number of mutations, other than those located at the c-terminal domain, can also cause accumulation of prelamin A[260]. Additionally, two biopsies, 2.059 and 4.032, displayed less frequent nuclear prelamin A staining that appeared more diffuse compared to the striking nuclear rim localisation of S99 1036. Myocardial disarray was also less pronounced in these sections. This would suggest the possibility of a paradigm in which prelamin A accumulation can occur adaptively in response to stress or in response to non-*LMNA* mutations. This, however, is speculative and would require sequencing information and additional investigation in order to verify. Taken together, these data imply that prelamin A sarcomere localisation and prelamin A nuclear rim accumulation may have divergent physiological and pathological roles, respectively.

6.3.3 Prelamin A and Zmpste24 are dynamically regulated during myofibrillogenesis

It has been previously shown that prelamin A is dynamically regulated during C2C12 myotube differentiation[306]. However, this previous study focused primarily on nuclear events and did not describe the formation of myofibrils and did not study timepoints

later than 120 hours. To see whether prelamin A could localise to the sarcomere upon myofibrillogenesis, C2C12 differentiation was studied up to 168 hours. Expression analysis of prelamin A showed the expression of 74 kDa prelamin A in cycling myoblasts and 48 hours into differentiation whilst the detection of a 150 kDa band, a possible prelamin A dimer, was observed at 72 hours and 168 hours in differentiation media. Previously published data suggested that a 150 kDa band occurs at 24 hours in differentiation media and then returns to 74 kDa at 48 hours and finally steadily decreases until 120 hours, at which point expression of prelamin A is almost undetectable. Whilst these data do not concur entirely with the previous study, there is clear evidence for dynamic regulation of prelamin A in myotube differentiation. Moreover, immunostaining showed that at 168 hours in differentiation media, when sarcomeres formed, prelamin A localised to the z-disc along with α-actinin, coinciding with the observation of the 150 kDa protein band. Hypothetically, dimerisation of prelamin A to form a homo- or hetero-dimer could facilitate the localisation of prelamin A from the nuclear rim/peri-nuclear region to more polarised regions of the cell to form part of the z-disc. Further investigation is required.

Zmpste24, as previously stated, is crucial in the processing of prelamin A intermediates to form lamin A/C. Expression and localisation analysis of Zmpste24 during myotube differentiation suggests that there is also a dynamic role for Zmpste24. Zmpste24 was abundantly expressed in cycling myoblasts and after 48 hours in differentiation medium, and was localised to the nuclear rim/perinuclear region of cells. At 72 hours, expression was attenuated and then further diminished at 168 hours, at which point distribution of Zmpste24 was diffuse in the cytoplasm of differentiated cells. The changes seen coincided with changes to prelamin A, which suggests that it is

possible that the dynamic regulation during differentiation of prelamin A and Zmpste24 are linked. In human ageing, it is thought that prelamin A accumulation occurs when ZMPSTE24 expression is negatively regulated by age associated events such as DNA damage and oxidative stress[256, 257, 307, 308]. Whilst it is unlikely that 'ageing' regulates myoblast differentiation, the reduced serum conditions used to induce differentiation are likely to change the metabolic state of the cell and potentially increase ROS production, consequently regulating Zmpste24 expression. This, too, requires further investigation.

Desmin is well characterized in C2C12 cells[309]. It is present at low levels in cycling myoblasts and increases during myogenic differentiation. Moreover, it is present in mice embryos from 8.5 days post-coitus and is known to be crucial for maintaining and strengthening muscle tissue, although it is not critical for development *in vivo*[310]. Therefore, desmin expression increase was seen as a good indicator of successful differentiation. As expected, the expression of desmin showed a trend to increase during differentiation.

Expression of the lamins A/C and B1 showed an interesting trend. Lamin A remained relatively constant throughout differentiation, whereas lamin C and lamin B1 both underwent significant increases during differentiation. The meaning of these observations is as yet unclear and they are possibly complicated by the fact that these experiments were performed on plastic tissue culture substrates. This is because during development, the concentration of A-type lamin protein expression is strongly influenced by the tension and stiffness of the physical environment[311, 312]. For a clearer understanding of these developmental events, these experiments need to be repeated on a softer substrate, which mimics that of muscle ECM. Additionally, for a more thorough understanding of the importance of prelamin A and Zmpste24 in C2C12

myofibrillogenesis, siRNAs directed towards lamin A/C and Zmpste24, as well as pharmacological inhibition of lamin A maturation might be informative.

To summarise, prelamin A and Zmpste24 are dynamically regulated in myofibrillogenesis and prelamin A localises to the sarcomere upon myofibril formation. Moreover, prelamin A is localised to the z-disc region of the sarcomere in fully differentiated CMs/myocardium to form part of the cardiac cytoskeleton. Aberrant expression or accumulation of prelamin A due to mutations, and/or potentially faulty processing, results in nuclear localisation and is associated with pathological progression towards DCM and heart failure.

Chapter 7: Final Discussion

7.1 Thesis summary

Currently, the literature states that mutations to *ZMPSTE24* or *LMNA* that cause the accumulation of prelamin A and progerin lead to premature ageing disorders in humans[202, 205, 313]. Attempts to validate this *in vivo* have led to the discovery of multiple mechanisms involved in accelerated ageing and the development of therapeutic regimes which have entered clinical trials, but so far these have failed to significantly improve prognosis[211]. Two crucial flaws exist in the research to date of these mechanisms. Firstly, studies have tended to focus primarily on isolated skin fibroblasts of patients *in vitro*. Whilst skin ageing is part of the premature ageing process, it is changes to the cardiovascular system that appear to be ultimately fatal and therefore should be of higher consideration[228, 229]. Additionally, DCM is one of the most common manifestations arising from *LMNA* mutations and may also be associated with the accumulation of prelamin A in a pathogenic manner. Secondly, *in vivo* studies utilise models of disease that mimic mutations seen in humans. But whereas the disease in humans is a dominant negative phenotype caused by a heterozygous mutation, most disease models only seem to show disease phenotypes when the mutation is homozygous, with the exception of the $Lmna^{\Delta K32/+}$ and $Lmna^{MHC\text{-}M371K}$ models[250, 253]. Therefore, $Lmna^{\Delta K32/+}$ and $Lmna^{MHC\text{-}M371K}$ models aside, modelling of *LMNA* associated DCM tends to occur in a setting in which wildtype lamins are not made, and this may be an important factor in the search for a mechanism of pathogenesis, as human phenotypes tend to be autosomal dominant.

In order to address these issues, a model of targeted transgenesis, whereby *LMNA* L647R mutated DNA was inserted into the *Rosa26* locus, was utilised. In isolated cell studies, viral transduction of this plasmid leads to prelamin A accumulation[124, 256]; therefore, it was assumed this should also occur *in vivo*. A 'transgenic' model was used instead of a knock-in model to avoid the second issue, described above, that previous *Lmna* knock-in mouse models have only displayed significant phenotypes when homozygous and as such are not accurate recreations of the clinical disease setting. Therefore, it was decided that the redundant *Rosa26* locus, which is commonly utilised in targeted transgenesis studies, would be used for this study. Theoretically, as well as expressing prelamin A, a full compliment of lamins A/C would also be expressed. In order to address the issue of tissue heterogeneity/specificity and target the cardiovascular system, we decided to utilise the MLC2v promoter in order to selectively express L647R-*LMNA* in the heart.

Chapter 3 served to confirm a working system of transgenesis and highlighted the toxic nature of prelamin A accumulation in the heart. Prelamin A accumulated in the nuclear rim of CMs in mice expressing the transgene (PLA Tg mice). PLA Tg mice suffered from retarded growth and developed a DCM-like phenotype which very quickly progressed to HF and death. Detailed analysis confirmed physiological, morphological, histological and molecular abnormalities consistent with DCM and heart failure and allowed the comparison of existing models of heart dysfunction with lamin involvement including $Lmna^{-/-}$, $Lmna^{+/-}$, $Lmna^{H222P/H222P}$, $Lmna^{N195K/N195K}$, $Lmna^{MHC\text{-}M371K}$, $Lmna^{G609G/G609G}$ and $Zmpste24^{-/-}$ mice.

The most phenotypically similar of these models to PLA Tg mice proved to be the $Lmna^{-/-}$ mice, which also failed to thrive and survived only to 6-8 weeks of age

because of DCM and heart failure and suggested that more detailed mechanistic analysis should begin by analysing pathways similar to those seen in *Lmna*$^{-/-}$ mice[225, 244]. As with a number of DCM models, the current study found myocardial disarray and significant levels of fibrosis, which pointed towards myocardial remodelling. But perhaps the most striking feature of the characterisation was the observation that leukocyte invasion of the myocardial interstitium occurred. Inflammation is known to be part of the progression to heart failure especially in cases involving infarct events[305]; however, there also seems to be a body of evidence emerging suggesting that sterile inflammation of the myocardium can occur independently of ischaemic injury due to the breakdown of endogenous cellular safeguards such as autophagy[268]. Interestingly, global *Zmpste24*$^{-/-}$ mice appear to experience leukocyte invasion of the myocardium in the presence of no haemodynamic or environmental stress[214]. In the same conditions, *Zmpste24*$^{-/-}$ mice also suffered from systemic inflammation, suggesting that there is an internal mechanism activating inflammatory responses[125]. Consequently, these investigative leads were at the forefront of the planning process for the mechanistic analysis of PLA Tg mice.

These mechanisms were the subject of scrutiny in Chapter 4. Firstly, uncoupling of the IF protein system was explored in conjunction with pathways reported by Nikolova *et al* with regard to *Lmna*$^{-/-}$ mice[225, 244]. The findings in the current study suggested that similar mechanisms are at play with regard to the expression changes observed in nesprins and desmin, as well as the localisation changes seen with desmin. These results suggest that mechanical instability and susceptibility to mechanical stress/load are potentially a causative reason for DCM in CMs accumulating prelamin A. Dysregulation of connexins has been reported in clinical cases of DCM and sudden

cardiac death[314-316] and many *Lmna* associated DCM models have identified the misexpression and mislocalisation of Cx43 as potential mechanisms for arrhythmogenic activity and depressed cardiac function[248]. Cx43 expression and, in particular, localisation was disrupted in PLA Tg hearts compared to Wt, confirming a role for Cx43 in prelamin A mediated DCM.

Curiously, despite DNA damage being a hallmark trait of prelamin A accumulating premature ageing disorders, *Lmna* associated DCM models have rarely focussed on the potential role of DDR. DNA damage was assessed here by the presence of a classic DNA damage marker γ-H2AX. Increases in γ-H2AX were observed in PLA Tg hearts and reiterated the dogma that prelamin A accumulation leads to increases in DNA damage. Having established this, it was important to assess the downstream effects and ascertain whether the increases in DNA damage played a role in the pathogenesis of cardiac dysfunction. Classically, DNA damage induces cell cycle arrest via DDR regulators of cell cycle such as p53, p21 and p16 and, in the setting of terminal cell cycle arrest, can lead to SIPS, which, alongside replicative senescence, can be detected by the SA-β-Gal assay. As discussed in this thesis, the notion of cardiac senescence per se is a tentative one as CMs are non-renewable from an early age. Moreover, use of the SA-β-Gal assay on tissue samples is in its infancy; however, it is now understood that replication is not the only barometer of senescence and protocols for detection of senescence *in situ* have been established[285]. Perhaps somewhat surprisingly, use of this assay produced a strong result suggesting that PLA Tg heart tissue was senescent. To follow this up, expression analysis of the aforementioned p53, p21 and p16 was performed, which provided a negative result. Expression of all three of these proteins was undetectable in Wt and PLA Tg tissue samples, suggesting that if

senescence does occur in PLA Tg hearts, then it occurs independently of p53, p21 and p16. However, the role of DDR is not limited to the regulation of cell cycle as highlighted by recent publications[125], suggesting ATM dependent NF-κB signalling can lead to systemic inflammation. Considering the observation of myocardial inflammation in our system, analysis of ATM dependent signalling was performed which supported a potential role for ATM dependent signalling within the pathogenic response to prelamin A accumulation in CMs.

Largely absent from current literature is the elucidation of temporally defined mechanisms. Although some publications have tackled this question to a degree with regard to manifestation of DCM[250], timelines of pathogenic mechanisms have not been included in reports from *Zmpste24*$^{-/-}$ mice, which are generally studied at 3 months of age. Chapter 5 aimed to provide insight into how the phenotype and mechanisms observed in chapters 3 and 4 were regulated at an earlier 2 week timepoint. It was hoped that this would provide clues as to how disease manifested and progressed in hearts in which CMs accumulated prelamin A. The results indicated that, whilst there was no overt phenotype in 2 week old mice, certain changes were taking place at the cellular level. Cardiac function was normal and there was no fibrosis to report; however, there was moderate leukocytic invasion of the myocardium. Molecular assessment of expression and localisation ruled out early changes to the IF and LINC protein network, suggesting CMs were mechanically sound at 2 weeks of age; however, CD45 positive cells were increased, and reinforced the observation of leukocytic infiltration of the myocardium in PLA Tg mice. Interestingly, Cx43 expression/localisation appeared dysregulated at 2 weeks of age. The localisation of Cx43 in Wt tissue was sarcolemmal, whilst in PLA Tg myocardium Cx43 expression was nominally increased and appeared

to be polarised/localised to intercalated discs. These data suggest that gap junction formation is premature in prelamin A expressing hearts. Therefore, not only may Cx43 dysregulation contribute phenotypically by inefficient propagation of electrical signals between CMs in 4 week old hearts but may also indicate mistimed gap junction formation which may contribute to disruption of the cardiac milieu during maturation. Finally, DNA damage also seemed to be increased in PLA Tg hearts at 2 weeks of age compared to Wt. Taken with the finding that leukocytic invasion is occurring at 2 weeks of age, it can be postulated that NF-κB signalling may be active at 2 weeks. Further investigation is required.

The final chapter, chapter 6, explored the regulation of prelamin A in CMs. It was observed in mouse heart sections that prelamin A antibody was localising to the cytoplasm in a striated fashion, suggesting that prelamin A localised to the sarcomere. Furthermore, overexposure of a western blot suggested that prelamin A was expressed in low concentrations endogenously in Wt ventricular tissue homogenates. To explore this novel finding further, NRCs were isolated and stained with prelamin A and co-stained with myomesin or α-actinin. Prelamin A appeared to colocalise with α-actinin, albeit not completely, and localised in parallel with myomesin, confirming that prelamin A localised to the Z-disc region of the sarcomere.

During the course of the investigation, I was privileged to obtain some sections of DCM patient and healthy control heart biopsies, courtesy of Dr Elisabeth Ehler. Staining with prelamin A antibody revealed z-disc staining, particularly in healthy controls. Additionally, a selection of DCM sections showed positive prelamin A staining in the nucleus. However, this response was inconsistent as some hearts showed compelling nuclear rim staining, whereas others showed less frequent and more nuclear

diffuse staining. This could have been due to various reasons. Firstly, in the heart sections with frequent and strong nuclear rim staining, there is likely to be a *LMNA* mutation and in less intensely stained sections there may not be. In the case of the latter, prelamin A accumulation may be an adaptive or downstream response of the original manifestation, which could be a non-*LMNA* gene mutation or extrinsic stressors such as chemotherapy or alcohol. Alternatively, sections in which nuclei stained intensely for prelamin A might have a mutation closer to the ZMPSTE24/FACE1 processing site of the *LMNA* gene, with less intensely stained sections having a *LMNA* mutation in a region further from the ZMPSTE24/FACE1 processing site. The sequencing results will be crucial in further informing this line of study.

Finally, C2C12 myofibrollogenesis assays revealed that prelamin A is dynamically regulated during myoblast differentiation to myotubes as expression of a 150 kDa prelamin A is detected late into myofibrillogenesis, suggesting formation of a prelamin A dimer, either homo- or hetero- (with lamin C or lamin B1 for example), and that prelamin A is capable of localising to sarcomeric structures upon myofibril formation. Moreover, Zmpste24 undergoes a distinct reduction in expression late into myofibrillogenesis, which could speculatively serve to regulate the observed expression and localisation changes to prelamin A.

7.2 Study limitations and future work

As with many studies, the most pressing limitation was time. There were many elements of the study which merit further investigation. It would have been ideal to have a full characterisation of the 2 week old mice as well as the 4 week old mice in

order to directly compare all mechanistic pathways, especially with regard to SA-β-Gal staining and assessment of the NF-κB signalling pathway. I would have liked to have rigorously explored the idea of a 'cardiac senescence like phenotype' by analysing the mRNA expression levels of the β-galactosidase gene, *GLB1,* in order to quantify and ratify the SA-β-Gal staining observed. The increase in lysosomal β-galactosidase is thought to be an adaptive response to the accumulation of undegradeable macromolecules in the cytoplasm of cells. This poses the question as to whether cell housekeeping systems, such as the ubiquitin proteasome system and autophagy, are deregulated in senescence and if so, how? Utilising the current model to assess this would be fascinating because interestingly, $Lmna^{H222P/H222P}$ mice hearts display defective autophagy, whereas $Zmpste24^{-/-}$ mice experience an increase in autophagic activity. It would require fasting the mice for over 24 hours to activate autophagy. Subsequent assessment of LC3 lipidation status using immunoblotting would be able to indicate whether autophagy was defective in PLA Tg hearts.

Moreover, assaying the cytokine profile of PLA Tg heart tissue by qPCR of mRNA expression may provide insights as to whether the heart displays a SASP-like phenotype in the setting of prelamin A accumulation and help establish the notion of a cardiac senescence paradigm.

The absence of a mouse line overexpressessing Wt *LMNA* is limiting. Studies of mutated overexpression are often controlled by Wt overexpression animals; however, our lab currently lacks a mouse which overexpresses lamin A/C and the costs of obtaining one with the same system of targeted transgenesis is likely to be unaffordable. A model does exist where an α-MHC driven *Lmna* overexpressor, expresses, Wt Lmna exclusively in the heart. It is long lived and suffers no adverse pathology of the heart

tissue[253]. Through the work of Wang *et al*, we can be reasonably sure that overexpressing Wt *Lmna* in the heart alone is non pathogenic and does not lead to the same series of underlying mechanistic deficiencies observed in the current model. In this study, we have established that prelamin A expression is pathogenic in its own right and does not rely on a degree of the absence of wildtype lamins to mediate its deleterious effects.

The current study has identified a number of potential mechanisms that may regulate the pathogenic response to prelamin A accumulation and, despite the study of data from a 2 week timepoint, it is still not clear whether any single event (prelamin A accumulation aside) is responsible for initiating the onset of disease. With the nuclear rim localisation of prelamin A, it is clear that the initial source of the disease must originate from within the CM. To pinpoint the manifestation of disease, it might be helpful to isolate neonatal PLA Tg CMs and study them independently of the cardiac milieu in order to determine which mechanistic events identified by this study might occur, despite the lack of a tissue environment. Any specific disturbances to CM signalling could be deemed important and provide a platform for further investigation *in vivo*.

In our model, the disease manifests at a very young age and at a rapid rate, and is useful in looking at the impact of prelamin A accumulation during development as may occur with disease causing *LMNA* mutations. However, it is desirable, that assuming prelamin A was to accumulate in the face of advancing age, to perform such experiments on adult myocardium. To achieve this, a separate approach, in which the expression of prelamin A is temporally regulated, would be required. Fortunately, as well as spatial control of expression, targeted transgenesis facilitates temporally

controlled expression with the use of MerCreMer mouse lines. In these mice, cre-recombinase is retained in the cytoplasm, which upon exposure by injection to tamoxifen is then translocated to the nucleus where the floxxed STOP cassette of the transgene is deleted and inhibition of transcription is relieved. This system would allow the assessment of the impact of prelamin A accumulation in the developed heart and reveal the importance of prelamin A in general adult ageing of the myocardium.

7.3 Final Conclusions

In summary, I have established *in vivo* that pathogenic prelamin A accumulation in CMs elicits a response which involves DDR, inflammmation of the myocardium, Cx43 disruption, and LINC complex disruption, and that these pathways are potentially unified by the emerging notion of 'myocardial senescence'. In addition, I have showed some evidence that prelamin A may play a role in the sarcomeric structure of healthy CMs and that prelamin A accumulated in the nuclei of CMs in a number of human DCM biopsies. Therefore, nuclear prelamin A accumulation may occur as a result of mutations to *LMNA*, downstream of non-*LMNA* DCM mutations, or possibly even downstream of environmental stress factors, and may elicit a pathogenic response via one or all of the mechanisms described here in our *in vivo* model.

Chapter 8: References

1. Crisp M, Liu Q, Roux K, Rattner JB, Shanahan C, Burke B, et al. Coupling of the nucleus and cytoplasm: role of the LINC complex. *The Journal of cell biology*. 2006;172(1):41-53.
2. Rienks M, Papageorgiou AP, Frangogiannis NG, Heymans S. Myocardial extracellular matrix: an ever-changing and diverse entity. *Circulation research*. 2014;114(5):872-88.
3. Zipes DP, Braunwald E. Braunwald's heart disease : a textbook of cardiovascular medicine. 7th ed. Philadelphia, Pa.: W.B. Saunders; 2005.
4. Solaro RJ, Rarick HM. Troponin and tropomyosin: proteins that switch on and tune in the activity of cardiac myofilaments. *Circulation research*. 1998;83(5):471-80.
5. Eisner DA, Kashimura T, O'Neill SC, Venetucci LA, Trafford AW. What role does modulation of the ryanodine receptor play in cardiac inotropy and arrhythmogenesis? *Journal of molecular and cellular cardiology*. 2009;46(4):474-81.
6. Diaz ME, Graham HK, O'Neill S C, Trafford AW, Eisner DA. The control of sarcoplasmic reticulum Ca content in cardiac muscle. *Cell calcium*. 2005;38(3-4):391-6.
7. Bers DM. Cardiac excitation-contraction coupling. *Nature*. 2002;415(6868):198-205.
8. Ehler E, Perriard JC. Cardiomyocyte cytoskeleton and myofibrillogenesis in healthy and diseased heart. *Heart failure reviews*. 2000;5:259-69.
9. Chang AN, Potter JD. Sarcomeric protein mutations in dilated cardiomyopathy. *Heart failure reviews*. 2005;10(3):225-35.
10. Gerull B, Gramlich M, Atherton J, McNabb M, Trombitas K, Sasse-Klaassen S, et al. Mutations of TTN, encoding the giant muscle filament titin, cause familial dilated cardiomyopathy. *Nature genetics*. 2002;30(2):201-4.
11. Herman DS, Lam L, Taylor MRG, Wang L, Teekakirikul P, Christodoulou D, et al. Truncations of titin causing dilated cardiomyopathy. *The New England journal of medicine*. 2012;366:619-28.
12. Itoh-Satoh M, Hayashi T, Nishi H, Koga Y, Arimura T, Koyanagi T, et al. Titin mutations as the molecular basis for dilated cardiomyopathy. *Biochemical and biophysical research communications*. 2002;291(2):385-93.
13. Mohapatra B, Jimenez S, Lin JH, Bowles KR, Coveler KJ, Marx JG, et al. Mutations in the muscle LIM protein and alpha-actinin-2 genes in dilated cardiomyopathy and endocardial fibroelastosis. *Molecular genetics and metabolism*. 2003;80(1-2):207-15.
14. Malhotra R, Mason PK. Lamin A/C deficiency as a cause of familial dilated cardiomyopathy. *Current opinion in cardiology*. 2009;24:203-8.
15. Sylvius N, Tesson F. Lamin A/C and cardiac diseases. *Current opinion in cardiology*. 2006;21(3):159-65.
16. Bione S, Small K, Aksmanovic VM, D'Urso M, Ciccodicola A, Merlini L, et al. Identification of new mutations in the Emery-Dreifuss muscular dystrophy gene and evidence for genetic heterogeneity of the disease. *Human molecular genetics*. 1995;4(10):1859-63.

17. Wulff K, Parrish JE, Herrmann FH, Wehnert M. Six novel mutations in the emerin gene causing X-linked Emery-Dreifuss muscular dystrophy. *Human mutation*. 1997;9:526-30.
18. Puckelwartz MJ, Kessler EJ, Kim G, Dewitt MM, Zhang Y, Earley JU, et al. Nesprin-1 mutations in human and murine cardiomyopathy. *Journal of molecular and cellular cardiology*. 2010;48:600-8.
19. Lakatta EG. Age-associated cardiovascular changes in health: impact on cardiovascular disease in older persons. *Heart failure reviews*. 2002;7:29-49.
20. Lakatta EG. Arterial and cardiac aging: major shareholders in cardiovascular disease enterprises: Part III: cellular and molecular clues to heart and arterial aging. *Circulation*. 2003;107:490-7.
21. Lakatta EG, Levy D. Arterial and cardiac aging: major shareholders in cardiovascular disease enterprises: Part II: the aging heart in health: links to heart disease. *Circulation*. 2003;107:139-46.
22. Lloyd-Jones DM, Larson MG, Leip EP, Beiser A, D'Agostino RB, Kannel WB, et al. Lifetime risk for developing congestive heart failure: the Framingham Heart Study. *Circulation*. 2002;106(24):3068-72.
23. Goldberg LR. Heart failure. *Annals of internal medicine*. 2010;152(11):ITC61-15; quiz ITC616.
24. Burchfield JS, Xie M, Hill Ja. Pathological ventricular remodeling: mechanisms: part 1 of 2. *Circulation*. 2013;128:388-400.
25. Packer M. Can brain natriuretic peptide be used to guide the management of patients with heart failure and a preserved ejection fraction? The wrong way to identify new treatments for a nonexistent disease. *Circulation Heart failure*. 2011;4(5):538-40.
26. Zile MR, Gottdiener JS, Hetzel SJ, McMurray JJ, Komajda M, McKelvie R, et al. Prevalence and significance of alterations in cardiac structure and function in patients with heart failure and a preserved ejection fraction. *Circulation*. 2011;124(23):2491-501.
27. Swynghedauw B. Molecular mechanisms of myocardial remodeling. *Physiological reviews*. 1999;79:215-62.
28. Shiojima I, Sato K, Izumiya Y, Schiekofer S, Ito M, Liao R, et al. Disruption of coordinated cardiac hypertrophy and angiogenesis contributes to the transition to heart failure. *The Journal of clinical investigation*. 2005;115:2108-18.
29. Cupesi M, Yoshioka J, Gannon J, Kudinova A, Stewart CL, Lammerding J. Attenuated hypertrophic response to pressure overload in a lamin A/C haploinsufficiency mouse. *Journal of molecular and cellular cardiology*. 2010;48(6):1290-7.
30. Gossios TD, Lopes LR, Elliott PM. Left ventricular hypertrophy caused by a novel nonsense mutation in FHL1. *European journal of medical genetics*. 2013;56(5):251-5.
31. Heineke J, Molkentin JD. Regulation of cardiac hypertrophy by intracellular signalling pathways. *Nature reviews Molecular cell biology*. 2006;7:589-600.
32. Lappé JM, Pelfrey CM, Tang WHW. Recent insights into the role of autoimmunity in idiopathic dilated cardiomyopathy. *Journal of cardiac failure*. 2008;14:521-30.

33. Martino TA, Liu P, Sole MJ. Review Viral Infection and the Pathogenesis of Dilated Cardiomyopathy. *Circulation research*. 2012:182-8.
34. Watkins H, Ashrafian H, Redwood C. Inherited cardiomyopathies. *The New England journal of medicine*. 2011;364(17):1643-56.
35. Richardson P, McKenna W, Bristow M, Maisch B, Mautner B, O'Connell J, et al. Report of the 1995 World Health Organization/International Society and Federation of Cardiology Task Force on the Definition and Classification of cardiomyopathies. *Circulation*. 1996;93(5):841-2.
36. Kamisago M, Sharma SD, DePalma SR, Solomon S, Sharma P, McDonough B, et al. Mutations in sarcomere protein genes as a cause of dilated cardiomyopathy. *The New England journal of medicine*. 2000;343(23):1688-96.
37. Maron BJ, Thompson PD, Puffer JC, McGrew CA, Strong WB, Douglas PS, et al. Cardiovascular preparticipation screening of competitive athletes. A statement for health professionals from the Sudden Death Committee (clinical cardiology) and Congenital Cardiac Defects Committee (cardiovascular disease in the young), American Heart Association. *Circulation*. 1996;94(4):850-6.
38. Bonne G, Carrier L, Richard P, Hainque B, Schwartz K. Familial hypertrophic cardiomyopathy: from mutations to functional defects. *Circulation research*. 1998;83(6):580-93.
39. Marian AJ. Pathogenesis of diverse clinical and pathological phenotypes in hypertrophic cardiomyopathy. *Lancet*. 2000;355(9197):58-60.
40. Richard P, Charron P, Carrier L, Ledeuil C, Cheav T, Pichereau C, et al. Hypertrophic cardiomyopathy: distribution of disease genes, spectrum of mutations, and implications for a molecular diagnosis strategy. *Circulation*. 2003;107(17):2227-32.
41. Marston S, Copeland O, Jacques A, Livesey K, Tsang V, McKenna WJ, et al. Evidence from human myectomy samples that MYBPC3 mutations cause hypertrophic cardiomyopathy through haploinsufficiency. *Circulation research*. 2009;105(3):219-22.
42. van Dijk SJ, Dooijes D, dos Remedios C, Michels M, Lamers JM, Winegrad S, et al. Cardiac myosin-binding protein C mutations and hypertrophic cardiomyopathy: haploinsufficiency, deranged phosphorylation, and cardiomyocyte dysfunction. *Circulation*. 2009;119(11):1473-83.
43. Redwood CS, Moolman-Smook JC, Watkins H. Properties of mutant contractile proteins that cause hypertrophic cardiomyopathy. *Cardiovascular research*. 1999;44(1):20-36.
44. Seidman JG, Seidman C. The genetic basis for cardiomyopathy: from mutation identification to mechanistic paradigms. *Cell*. 2001;104(4):557-67.
45. Kirschner SE, Becker E, Antognozzi M, Kubis HP, Francino A, Navarro-Lopez F, et al. Hypertrophic cardiomyopathy-related beta-myosin mutations cause highly variable calcium sensitivity with functional imbalances among individual muscle cells. *American journal of physiology Heart and circulatory physiology*. 2005;288(3):H1242-51.
46. Knollmann BC, Kirchhof P, Sirenko SG, Degen H, Greene AE, Schober T, et al. Familial hypertrophic cardiomyopathy-linked mutant troponin T causes stress-induced ventricular tachycardia and Ca2+-dependent action potential remodeling. *Circulation research*. 2003;92(4):428-36.

47. Huke S, Knollmann BC. Increased myofilament Ca2+-sensitivity and arrhythmia susceptibility. *Journal of molecular and cellular cardiology*. 2010;48(5):824-33.
48. Bers DM, Guo T. Calcium signaling in cardiac ventricular myocytes. *Annals of the New York Academy of Sciences*. 2005;1047:86-98.
49. Robinson P, Griffiths PJ, Watkins H, Redwood CS. Dilated and hypertrophic cardiomyopathy mutations in troponin and alpha-tropomyosin have opposing effects on the calcium affinity of cardiac thin filaments. *Circulation research*. 2007;101(12):1266-73.
50. Kataoka A, Hemmer C, Chase PB. Computational simulation of hypertrophic cardiomyopathy mutations in troponin I: influence of increased myofilament calcium sensitivity on isometric force, ATPase and [Ca2+]i. *Journal of biomechanics*. 2007;40(9):2044-52.
51. Smith GA, Dixon HB, Kirschenlohr HL, Grace AA, Metcalfe JC, Vandenberg JI. Ca2+ buffering in the heart: Ca2+ binding to and activation of cardiac myofibrils. *The Biochemical journal*. 2000;346 Pt 2:393-402.
52. Ashrafian H, Redwood C, Blair E, Watkins H. Hypertrophic cardiomyopathy:a paradigm for myocardial energy depletion. *Trends in genetics : TIG*. 2003;19(5):263-8.
53. Blair E, Redwood C, Ashrafian H, Oliveira M, Broxholme J, Kerr B, et al. Mutations in the gamma(2) subunit of AMP-activated protein kinase cause familial hypertrophic cardiomyopathy: evidence for the central role of energy compromise in disease pathogenesis. *Human molecular genetics*. 2001;10(11):1215-20.
54. Araújo-Vilar D, Lado-Abeal J, Palos-Paz F, Lattanzi G, Bandín Ma, Bellido D, et al. A novel phenotypic expression associated with a new mutation in LMNA gene, characterized by partial lipodystrophy, insulin resistance, aortic stenosis and hypertrophic cardiomyopathy. *Clinical endocrinology*. 2008;69:61-8.
55. Hegele RA. Familial partial lipodystrophy: a monogenic form of the insulin resistance syndrome. *Molecular genetics and metabolism*. 2000;71(4):539-44.
56. Hegele RA. Monogenic forms of insulin resistance: apertures that expose the common metabolic syndrome. *Trends in endocrinology and metabolism: TEM*. 2003;14(8):371-7.
57. Mercuri E, Brown SC, Nihoyannopoulos P, Poulton J, Kinali M, Richard P, et al. Extreme variability of skeletal and cardiac muscle involvement in patients with mutations in exon 11 of the lamin A/C gene. *Muscle & nerve*. 2005;31(5):602-9.
58. Sen-Chowdhry S, Morgan RD, Chambers JC, McKenna WJ. Arrhythmogenic cardiomyopathy: etiology, diagnosis, and treatment. *Annual review of medicine*. 2010;61:233-53.
59. Sen-Chowdhry S, McKenna WJ. The utility of magnetic resonance imaging in the evaluation of arrhythmogenic right ventricular cardiomyopathy. *Current opinion in cardiology*. 2008;23(1):38-45.
60. McKenna WJ, Thiene G, Nava A, Fontaliran F, Blomstrom-Lundqvist C, Fontaine G, et al. Diagnosis of arrhythmogenic right ventricular dysplasia/cardiomyopathy. Task Force of the Working Group Myocardial and Pericardial Disease of the European Society of Cardiology and of the Scientific

Council on Cardiomyopathies of the International Society and Federation of Cardiology. *British heart journal*. 1994;71(3):215-8.
61. Tabib A, Loire R, Chalabreysse L, Meyronnet D, Miras A, Malicier D, et al. Circumstances of death and gross and microscopic observations in a series of 200 cases of sudden death associated with arrhythmogenic right ventricular cardiomyopathy and/or dysplasia. *Circulation*. 2003;108(24):3000-5.
62. Kirchhof P, Fabritz L, Zwiener M, Witt H, Schafers M, Zellerhoff S, et al. Age- and training-dependent development of arrhythmogenic right ventricular cardiomyopathy in heterozygous plakoglobin-deficient mice. *Circulation*. 2006;114(17):1799-806.
63. Asimaki A, Syrris P, Wichter T, Matthias P, Saffitz JE, McKenna WJ. A novel dominant mutation in plakoglobin causes arrhythmogenic right ventricular cardiomyopathy. *American journal of human genetics*. 2007;81(5):964-73.
64. Protonotarios N, Tsatsopoulou A. Naxos disease and Carvajal syndrome: cardiocutaneous disorders that highlight the pathogenesis and broaden the spectrum of arrhythmogenic right ventricular cardiomyopathy. *Cardiovascular pathology : the official journal of the Society for Cardiovascular Pathology*. 2004;13(4):185-94.
65. Sen-Chowdhry S, Syrris P, McKenna WJ. Genetics of right ventricular cardiomyopathy. *Journal of cardiovascular electrophysiology*. 2005;16(8):927-35.
66. Sen-Chowdhry S, Syrris P, McKenna WJ. Role of genetic analysis in the management of patients with arrhythmogenic right ventricular dysplasia/cardiomyopathy. *Journal of the American College of Cardiology*. 2007;50(19):1813-21.
67. Beffagna G, Occhi G, Nava A, Vitiello L, Ditadi A, Basso C, et al. Regulatory mutations in transforming growth factor-beta3 gene cause arrhythmogenic right ventricular cardiomyopathy type 1. *Cardiovascular research*. 2005;65(2):366-73.
68. Merner ND, Hodgkinson KA, Haywood AF, Connors S, French VM, Drenckhahn JD, et al. Arrhythmogenic right ventricular cardiomyopathy type 5 is a fully penetrant, lethal arrhythmic disorder caused by a missense mutation in the TMEM43 gene. *American journal of human genetics*. 2008;82(4):809-21.
69. Garcia-Gras E, Lombardi R, Giocondo MJ, Willerson JT, Schneider MD, Khoury DS, et al. Suppression of canonical Wnt/beta-catenin signaling by nuclear plakoglobin recapitulates phenotype of arrhythmogenic right ventricular cardiomyopathy. *The Journal of clinical investigation*. 2006;116(7):2012-21.
70. MacRae CA, Birchmeier W, Thierfelder L. Arrhythmogenic right ventricular cardiomyopathy: moving toward mechanism. *The Journal of clinical investigation*. 2006;116(7):1825-8.
71. Larsen MK, Nissen PH, Berge KE, Leren TP, Kristensen IB, Jensen HK, et al. Molecular autopsy in young sudden cardiac death victims with suspected cardiomyopathy. *Forensic science international*. 2012;219(1-3):33-8.
72. Quarta G, Syrris P, Ashworth M, Jenkins S, Zuborne Alapi K, Morgan J, et al. Mutations in the Lamin A/C gene mimic arrhythmogenic right ventricular cardiomyopathy. *European heart journal*. 2011.

73. Maron BJ, Towbin JA, Thiene G, Antzelevitch C, Corrado D, Arnett D, et al. Contemporary definitions and classification of the cardiomyopathies: an American Heart Association Scientific Statement from the Council on Clinical Cardiology, Heart Failure and Transplantation Committee; Quality of Care and Outcomes Research and Functional Genomics and Translational Biology Interdisciplinary Working Groups; and Council on Epidemiology and Prevention. *Circulation*. 2006;113(14):1807-16.
74. Yajima T. Viral myocarditis: potential defense mechanisms within the cardiomyocyte against virus infection. *Future microbiology*. 2011;6(5):551-66.
75. Yajima T, Knowlton KU. Viral myocarditis: from the perspective of the virus. *Circulation*. 2009;119(19):2615-24.
76. Walker RK, Cousins VM, Umoh NA, Jeffress MA, Taghipour D, Al-Rubaiee M, et al. The good, the bad, and the ugly with alcohol use and abuse on the heart. *Alcoholism, clinical and experimental research*. 2013;37(8):1253-60.
77. Raj S, Franco VI, Lipshultz SE. Anthracycline-induced cardiotoxicity: a review of pathophysiology, diagnosis, and treatment. *Current treatment options in cardiovascular medicine*. 2014;16(6):315.
78. Yoshikawa T, Baba A, Nagatomo Y. Autoimmune mechanisms underlying dilated cardiomyopathy. *Circulation journal : official journal of the Japanese Circulation Society*. 2009;73(4):602-7.
79. Mestroni L, Rocco C, Gregori D, Sinagra G, Di Lenarda A, Miocic S, et al. Familial dilated cardiomyopathy: evidence for genetic and phenotypic heterogeneity. Heart Muscle Disease Study Group. *Journal of the American College of Cardiology*. 1999;34(1):181-90.
80. Vatta M, Mohapatra B, Jimenez S, Sanchez X, Faulkner G, Perles Z, et al. Mutations in Cypher/ZASP in patients with dilated cardiomyopathy and left ventricular non-compaction. *Journal of the American College of Cardiology*. 2003;42(11):2014-27.
81. Tsubata S, Bowles KR, Vatta M, Zintz C, Titus J, Muhonen L, et al. Mutations in the human delta-sarcoglycan gene in familial and sporadic dilated cardiomyopathy. *The Journal of clinical investigation*. 2000;106(5):655-62.
82. Franz WM, Cremer M, Herrmann R, Grunig E, Fogel W, Scheffold T, et al. X-linked dilated cardiomyopathy. Novel mutation of the dystrophin gene. *Annals of the New York Academy of Sciences*. 1995;752:470-91.
83. Taylor MR, Slavov D, Ku L, Di Lenarda A, Sinagra G, Carniel E, et al. Prevalence of desmin mutations in dilated cardiomyopathy. *Circulation*. 2007;115(10):1244-51.
84. Haghighi K, Kolokathis F, Gramolini AO, Waggoner JR, Pater L, Lynch RA, et al. A mutation in the human phospholamban gene, deleting arginine 14, results in lethal, hereditary cardiomyopathy. *Proceedings of the National Academy of Sciences of the United States of America*. 2006;103(5):1388-93.
85. Cowan J, Li D, Gonzalez-Quintana J, Morales A, Hershberger RE. Morphological Analysis of 13 LMNA Variants Identified in a Cohort of 324 Unrelated Patients With Idiopathic or Familial Dilated Cardiomyopathy. *Circ Cardiovasc Genet*.3:6-14.
86. Hayflick L. The Limited in Vitro Lifetime of Human Diploid Cell Strains. *Experimental cell research*. 1965;37:614-36.

87. Siddiqi S, Sussman MA. Cardiac Hegemony of Senescence. *Current translational geriatrics and experimental gerontology reports*. 2013;2(4).
88. Williams GM, Jeffrey aM. Oxidative DNA damage: endogenous and chemically induced. *Regul Toxicol Pharmacol*. 2000;32:283-92.
89. Mahmoudi M, Mercer J, Bennett M. DNA damage and repair in atherosclerosis. *Cardiovascular research*. 2006;71:259-68.
90. Mirzoeva OK, Petrini JH. DNA replication-dependent nuclear dynamics of the Mre11 complex. *Mol Cancer Res*. 2003;1:207-18.
91. Bermudez VP, Lindsey-Boltz LA, Cesare AJ, Maniwa Y, Griffith JD, Hurwitz J, et al. Loading of the human 9-1-1 checkpoint complex onto DNA by the checkpoint clamp loader hRad17-replication factor C complex in vitro. *Proceedings of the National Academy of Sciences of the United States of America*. 2003;100:1633-8.
92. Nyberg KA, Michelson RJ, Putnam CW, Weinert TA. Toward maintaining the genome: DNA damage and replication checkpoints. *Annu Rev Genet*. 2002;36:617-56.
93. Abraham RT. Cell cycle checkpoint signaling through the ATM and ATR kinases. *Genes & development*. 2001;15:2177-96.
94. Banin S, Moyal L, Shieh S, Taya Y, Anderson CW, Chessa L, et al. Enhanced phosphorylation of p53 by ATM in response to DNA damage. *Science*. 1998;281:1674-7.
95. Shiloh Y. ATM and related protein kinases: safeguarding genome integrity. *Nat Rev Cancer*. 2003;3:155-68.
96. Lou Z, Chen J. Cellular senescence and DNA repair. *Experimental cell research*. 2006;312:2641-6.
97. Andreassi MG. DNA damage, vascular senescence and atherosclerosis. *J Mol Med*. 2008;86:1033-43.
98. Barouch LA, Gao D, Chen L, Miller KL, Xu W, Phan AC, et al. Cardiac myocyte apoptosis is associated with increased DNA damage and decreased survival in murine models of obesity. *Circulation research*. 2006;98:119-24.
99. Chan KK, Zhang QM, Dianov GL. Base excision repair fidelity in normal and cancer cells. *Mutagenesis*. 2006;21:173-8.
100. Vogel H, Lim DS, Karsenty G, Finegold M, Hasty P. Deletion of Ku86 causes early onset of senescence in mice. *Proceedings of the National Academy of Sciences of the United States of America*. 1999;96:10770-5.
101. Weeda G, Donker I, de Wit J, Morreau H, Janssens R, Vissers CJ, et al. Disruption of mouse ERCC1 results in a novel repair syndrome with growth failure, nuclear abnormalities and senescence. *Current biology : CB*. 1997;7:427-39.
102. Yndestad A, Neurauter CG, Oie E, Forstrom RJ, Vinge LE, Eide L, et al. Up-regulation of myocardial DNA base excision repair activities in experimental heart failure. *Mutation research*. 2009;666:32-8.
103. Puente BN, Kimura W, Muralidhar SA, Moon J, Amatruda JF, Phelps KL, et al. The oxygen-rich postnatal environment induces cardiomyocyte cell-cycle arrest through DNA damage response. *Cell*. 2014;157(3):565-79.
104. Finkel T, Holbrook NJ. biology of ageing. *Nature*. 2000;408:239-47.

105. Bedard K, Krause K-hH. The NOX family of ROS-generating NADPH oxidases: physiology and pathophysiology. *Physiological reviews*. 2007;87:245-313.
106. Bendall JK, Cave AC, Heymes C, Gall N, Shah AM. Pivotal role of a gp91(phox)-containing NADPH oxidase in angiotensin II-induced cardiac hypertrophy in mice. *Circulation*. 2002;105:293-6.
107. Looi YH, Grieve DJ, Siva A, Walker SJ, Anilkumar N, Cave AC, et al. Involvement of Nox2 NADPH oxidase in adverse cardiac remodeling after myocardial infarction. *Hypertension*. 2008;51:319-25.
108. Zhang M, Brewer AC, Schröder K, Santos CXC, Grieve DJ, Wang M, et al. NADPH oxidase-4 mediates protection against chronic load-induced stress in mouse hearts by enhancing angiogenesis. *Proceedings of the National Academy of Sciences of the United States of America*. 2010;107:18121-6.
109. Beckman KB, Ames BN. The free radical theory of aging matures. *Physiological reviews*. 1998;78:547-81.
110. Fenton HJH. LXXIII.-Oxidation of tartaric acid in presence of iron. *Journal of the Chemical Society, Transactions*. 1894;65:899-910.
111. Ames BN, Shigenaga MK, Hagen TM. Oxidants, antioxidants, and the degenerative diseases of aging. *Proceedings of the National Academy of Sciences of the United States of America*. 1993;90:7915-22.
112. Marnett LJ. Oxyradicals and DNA damage. *Carcinogenesis*. 2000;21:361-70.
113. Allen A. The cardiotoxicity of chemotherapeutic drugs. *Seminars in oncology*. 1992;19(5):529-42.
114. Singal PK, Iliskovic N. Doxorubicin-induced cardiomyopathy. *The New England journal of medicine*. 1998;339(13):900-5.
115. Yoshida M, Shiojima I, Ikeda H, Komuro I. Chronic doxorubicin cardiotoxicity is mediated by oxidative DNA damage-ATM-p53-apoptosis pathway and attenuated by pitavastatin through the inhibition of Rac1 activity. *Journal of molecular and cellular cardiology*. 2009;47:698-705.
116. Coppé J-P, Desprez P-Y, Krtolica A, Campisi J. The senescence-associated secretory phenotype: the dark side of tumor suppression. *Annual review of pathology*. 2010;5:99-118.
117. Parrinello S, Coppe JP, Krtolica A, Campisi J. Stromal-epithelial interactions in aging and cancer: senescent fibroblasts alter epithelial cell differentiation. *Journal of cell science*. 2005;118(Pt 3):485-96.
118. Liu D, Hornsby PJ. Senescent human fibroblasts increase the early growth of xenograft tumors via matrix metalloproteinase secretion. *Cancer research*. 2007;67(7):3117-26.
119. Rodier F, Coppe JP, Patil CK, Hoeijmakers WA, Munoz DP, Raza SR, et al. Persistent DNA damage signalling triggers senescence-associated inflammatory cytokine secretion. *Nature cell biology*. 2009;11:973-9.
120. Beausejour CM, Krtolica A, Galimi F, Narita M, Lowe SW, Yaswen P, et al. Reversal of human cellular senescence: roles of the p53 and p16 pathways. *The EMBO journal*. 2003;22(16):4212-22.
121. Shelton DN, Chang E, Whittier PS, Choi D, Funk WD. Microarray analysis of replicative senescence. *Current biology : CB*. 1999;9(17):939-45.

122. Campisi J, d'Adda di Fagagna F. Cellular senescence: when bad things happen to good cells. *Nature reviews Molecular cell biology*. 2007;8(9):729-40.
123. Ghigo A, Franco I, Morello F, Hirsch E. Myocyte signalling in leucocyte recruitment to the heart. *Cardiovascular research*. 2014.
124. Liu Y, Drozdov I, Shroff R, Beltran LE, Shanahan CM. Prelamin A accelerates vascular calcification via activation of the DNA damage response and senescence-associated secretory phenotype in vascular smooth muscle cells. *Circulation research*. 2013;112(10):e99-109.
125. Osorio FG, Bárcena C, Soria-Valles C, Ramsay AJ, de Carlos F, Cobo J, et al. Nuclear lamina defects cause ATM-dependent NF-κB activation and link accelerated aging to a systemic inflammatory response. *Genes & development*. 2012.
126. Lammerding J, Schulze PC, Takahashi T, Kozlov S, Sullivan T, Kamm RD, et al. Lamin A/C deficiency causes defective nuclear mechanics and mechanotransduction. *The Journal of clinical investigation*. 2004;113:370-8.
127. Lin J, Epel E, Blackburn E. Telomeres and lifestyle factors: roles in cellular aging. *Mutation research*. 2012;730(1-2):85-9.
128. Leri A, Malhotra A, Liew CC, Kajstura J, Anversa P. Telomerase activity in rat cardiac myocytes is age and gender dependent. *Journal of molecular and cellular cardiology*. 2000;32(3):385-90.
129. Epel ES, Lin J, Wilhelm FH, Wolkowitz OM, Cawthon R, Adler NE, et al. Cell aging in relation to stress arousal and cardiovascular disease risk factors. *Psychoneuroendocrinology*. 2006;31(3):277-87.
130. Epel ES, Merkin SS, Cawthon R, Blackburn EH, Adler NE, Pletcher MJ, et al. The rate of leukocyte telomere shortening predicts mortality from cardiovascular disease in elderly men. *Aging*. 2009;1(1):81-8.
131. Anversa P, Kajstura J, Leri A, Bolli R. Life and death of cardiac stem cells: a paradigm shift in cardiac biology. *Circulation*. 2006;113(11):1451-63.
132. Bergmann O, Bhardwaj RD, Bernard S, Zdunek S, Barnabe-Heider F, Walsh S, et al. Evidence for cardiomyocyte renewal in humans. *Science*. 2009;324(5923):98-102.
133. Chimenti C, Kajstura J, Torella D, Urbanek K, Heleniak H, Colussi C, et al. Senescence and death of primitive cells and myocytes lead to premature cardiac aging and heart failure. *Circulation research*. 2003;93(7):604-13.
134. Leri A, Franco S, Zacheo A, Barlucchi L, Chimenti S, Limana F, et al. Ablation of telomerase and telomere loss leads to cardiac dilatation and heart failure associated with p53 upregulation. *The EMBO journal*. 2003;22(1):131-9.
135. De Vos WH, Houben F, Hoebe RA, Hennekam R, van Engelen B, Manders EM, et al. Increased plasticity of the nuclear envelope and hypermobility of telomeres due to the loss of A-type lamins. *Biochimica et biophysica acta*. 2010;1800(4):448-58.
136. Uhlirova R, Horakova AH, Galiova G, Legartova S, Matula P, Fojtova M, et al. SUV39h- and A-type lamin-dependent telomere nuclear rearrangement. *Journal of cellular biochemistry*. 2010;109(5):915-26.
137. Benson EK, Lee SW, Aaronson SA. Role of progerin-induced telomere dysfunction in HGPS premature cellular senescence. *Journal of cell science*. 2010;123(Pt 15):2605-12.

138. North BJ, Verdin E. Sirtuins: Sir2-related NAD-dependent protein deacetylases. *Genome biology*. 2004;5(5):224.
139. Sundaresan NR, Samant SA, Pillai VB, Rajamohan SB, Gupta MP. SIRT3 is a stress-responsive deacetylase in cardiomyocytes that protects cells from stress-mediated cell death by deacetylation of Ku70. *Molecular and cellular biology*. 2008;28(20):6384-401.
140. Sundaresan NR, Gupta M, Kim G, Rajamohan SB, Isbatan A, Gupta MP. Sirt3 blocks the cardiac hypertrophic response by augmenting Foxo3a-dependent antioxidant defense mechanisms in mice. *The Journal of clinical investigation*. 2009;119(9):2758-71.
141. Pillai VB, Sundaresan NR, Kim G, Gupta M, Rajamohan SB, Pillai JB, et al. Exogenous NAD blocks cardiac hypertrophic response via activation of the SIRT3-LKB1-AMP-activated kinase pathway. *The Journal of biological chemistry*. 2010;285(5):3133-44.
142. Chen CJ, Fu YC, Yu W, Wang W. SIRT3 protects cardiomyocytes from oxidative stress-mediated cell death by activating NF-kappaB. *Biochemical and biophysical research communications*. 2013;430(2):798-803.
143. McBurney MW, Yang X, Jardine K, Hixon M, Boekelheide K, Webb JR, et al. The mammalian SIR2alpha protein has a role in embryogenesis and gametogenesis. *Molecular and cellular biology*. 2003;23(1):38-54.
144. Alcendor RR, Gao S, Zhai P, Zablocki D, Holle E, Yu X, et al. Sirt1 regulates aging and resistance to oxidative stress in the heart. *Circulation research*. 2007;100(10):1512-21.
145. Tong C, Morrison A, Mattison S, Qian S, Bryniarski M, Rankin B, et al. Impaired SIRT1 nucleocytoplasmic shuttling in the senescent heart during ischemic stress. *FASEB journal : official publication of the Federation of American Societies for Experimental Biology*. 2013;27(11):4332-42.
146. Anderson RM, Shanmuganayagam D, Weindruch R. Caloric restriction and aging: studies in mice and monkeys. *Toxicologic pathology*. 2009;37(1):47-51.
147. Nair S, Ren J. Autophagy and cardiovascular aging: lesson learned from rapamycin. *Cell cycle*. 2012;11(11):2092-9.
148. Burtner CR, Kennedy BK. Progeria syndromes and ageing: what is the connection? *Nature reviews Molecular cell biology*.11:567-78.
149. Mariño G, Ugalde AP, Fernández AF, Osorio FG, Fueyo A, Freije JMP, et al. Insulin-like growth factor 1 treatment extends longevity in a mouse model of human premature aging by restoring somatotroph axis function. *Proceedings of the National Academy of Sciences of the United States of America*. 2010;107:16268-73.
150. Mariño G, Ugalde AP, Salvador-Montoliu N, Varela I, Quirós PM, Cadiñanos J, et al. Premature aging in mice activates a systemic metabolic response involving autophagy induction. *Human molecular genetics*. 2008;17:2196-211.
151. Agarwal aK. Zinc metalloproteinase, ZMPSTE24, is mutated in mandibuloacral dysplasia. *Human molecular genetics*. 2003;12:1995-2001.
152. Bonne G, Di Barletta MR, Varnous S, Bécane HM, Hammouda EH, Merlini L, et al. Mutations in the gene encoding lamin A/C cause autosomal dominant Emery-Dreifuss muscular dystrophy. *Nature genetics*. 1999;21:285-8.

153. Cao H, Hegele Ra. Nuclear lamin A/C R482Q mutation in canadian kindreds with Dunnigan-type familial partial lipodystrophy. *Human molecular genetics*. 2000;9:109-12.
154. Chen L, Lee L, Kudlow BA, Santos HGD, Sletvold O, Shafeghati Y, et al. Mechanisms of disease LMNA mutations in atypical Werner ' s syndrome GLOSSARY. *The Lancet*. 1959.
155. Eriksson M, Brown WT, Gordon LB, Glynn MW, Singer J, Scott L, et al. Recurrent de novo point mutations in lamin A cause Hutchinson-Gilford progeria syndrome. *Nature*. 2003;423:293-8.
156. Warren DT, Zhang Q, Weissberg PL, Shanahan CM. Nesprins: intracellular scaffolds that maintain cell architecture and coordinate cell function? *Expert reviews in molecular medicine*. 2005;7:1-15.
157. Zhang Q, Ragnauth C, Greener MJ, Shanahan CM, Roberts RG. The nesprins are giant actin-binding proteins, orthologous to Drosophila melanogaster muscle protein MSP-300. *Genomics*. 2002;80(5):473-81.
158. Zhang Q, Ragnauth CD, Skepper JN, Worth NF, Warren DT, Roberts RG, et al. Nesprin-2 is a multi-isomeric protein that binds lamin and emerin at the nuclear envelope and forms a subcellular network in skeletal muscle. *Journal of cell science*. 2005;118:673-87.
159. Zhang Q, Skepper JN, Yang F, Davies JD, Hegyi L, Roberts RG, et al. Nesprins: a novel family of spectrin-repeat-containing proteins that localize to the nuclear membrane in multiple tissues. *Journal of cell science*. 2001;114(Pt 24):4485-98.
160. Lin F, Blake DL, Callebaut I, Skerjanc IS, Holmer L, McBurney MW, et al. MAN1, an inner nuclear membrane protein that shares the LEM domain with lamina-associated polypeptide 2 and emerin. *The Journal of biological chemistry*. 2000;275:4840-7.
161. Haque F, Lloyd DJ, Smallwood DT, Dent CL, Shanahan CM, Fry AM, et al. SUN1 interacts with nuclear lamin A and cytoplasmic nesprins to provide a physical connection between the nuclear lamina and the cytoskeleton. *Molecular and cellular biology*. 2006;26(10):3738-51.
162. Ben-Harush K, Wiesel N, Frenkiel-Krispin D, Moeller D, Soreq E, Aebi U, et al. The supramolecular organization of the C. elegans nuclear lamin filament. *Journal of molecular biology*. 2009;386:1392-402.
163. Lin F, Worman HJ. Structural organization of the human gene encoding nuclear lamin A and nuclear lamin C. *The Journal of biological chemistry*. 1993;268:16321-6.
164. Davies BS, Fong LG, Yang SH, Coffinier C, Young SG. The posttranslational processing of prelamin A and disease. *Annu Rev Genomics Hum Genet*. 2009;10:153-74.
165. Harborth J, Elbashir SM, Bechert K, Tuschl T, Weber K. Identification of essential genes in cultured mammalian cells using small interfering RNAs. *Journal of cell science*. 2001;114:4557-65.
166. Broers JL, Machiels BM, Kuijpers HJ, Smedts F, van den Kieboom R, Raymond Y, et al. A- and B-type lamins are differentially expressed in normal human tissues. *Histochemistry and cell biology*. 1997;107:505-17.
167. Zwerger M, Jaalouk DE, Lombardi ML, Isermann P, Mauermann M, Dialynas G, et al. Myopathic lamin mutations impair nuclear stability in cells and tissue

and disrupt nucleo-cytoskeletal coupling. *Human molecular genetics*. 2013;22(12):2335-49.
168. Lammerding J, Fong LG, Ji JY, Reue K, Stewart CL, Young SG, et al. Lamins A and C but not lamin B1 regulate nuclear mechanics. *The Journal of biological chemistry*. 2006;281:25768-80.
169. Lammerding J, Schulze PC, Takahashi T, Kozlov S, Sullivan T, Kamm RD, et al. Lamin A / C deficiency causes defective nuclear mechanics and mechanotransduction. 2004;113.
170. Lammerding J, Hsiao J, Schulze PC, Kozlov S, Stewart CL, Lee RT. Abnormal nuclear shape and impaired mechanotransduction in emerin-deficient cells. *The Journal of cell biology*. 2005;170:781-91.
171. Lammerding J, Lee RT. The nuclear membrane and mechanotransduction: impaired nuclear mechanics and mechanotransduction in lamin A/C deficient cells. *Novartis Foundation symposium*. 2005;264:264-73; discussion 73-8.
172. Liu Y, Rusinol A, Sinensky M, Wang Y, Zou Y. DNA damage responses in progeroid syndromes arise from defective maturation of prelamin A. *Journal of cell science*. 2006;119:4644-9.
173. Liu Y, Wang Y, Rusinol AE, Sinensky MS, Liu J, Shell SM, et al. Involvement of xeroderma pigmentosum group A (XPA) in progeria arising from defective maturation of prelamin A. *FASEB journal : official publication of the Federation of American Societies for Experimental Biology*. 2008;22:603-11.
174. Goldman RD, Shumaker DK, Erdos MR, Eriksson M, Goldman AE, Gordon LB, et al. Accumulation of mutant lamin A causes progressive changes in nuclear architecture in Hutchinson-Gilford progeria syndrome. *Proceedings of the National Academy of Sciences of the United States of America*. 2004;101:8963-8.
175. Boyd MW, Grant AP. Werner's syndrome (progeria of the adult); further pathological and biochemical observations. *Br Med J*. 1959;2:920-5.
176. Emery AE. Emery-Dreifuss syndrome. *J Med Genet*. 1989;26:637-41.
177. Gilford H. Ateleiosis and progeria. *British Medical Journal*. 1904;1904:914-8.
178. Chen L, Lee L, Kudlow BA, Dos Santos HG, Sletvold O, Shafeghati Y, et al. LMNA mutations in atypical Werner's syndrome. *Lancet*. 2003;362(9382):440-5.
179. De Sandre-Giovannoli A, Chaouch M, Kozlov S, Vallat JM, Tazir M, Kassouri N, et al. Homozygous defects in LMNA, encoding lamin A/C nuclear-envelope proteins, cause autosomal recessive axonal neuropathy in human (Charcot-Marie-Tooth disorder type 2) and mouse. *American journal of human genetics*. 2002;70(3):726-36.
180. Charniot JC, Pascal C, Bouchier C, Sebillon P, Salama J, Duboscq-Bidot L, et al. Functional consequences of an LMNA mutation associated with a new cardiac and non-cardiac phenotype. *Human mutation*. 2003;21(5):473-81.
181. Muchir A, Bonne G, van der Kooi AJ, van Meegen M, Baas F, Bolhuis PA, et al. Identification of mutations in the gene encoding lamins A/C in autosomal dominant limb girdle muscular dystrophy with atrioventricular conduction disturbances (LGMD1B). *Human molecular genetics*. 2000;9(9):1453-9.
182. Caux F, Dubosclard E, Lascols O, Buendia B, Chazouilleres O, Cohen A, et al. A new clinical condition linked to a novel mutation in lamins A and C with

generalized lipoatrophy, insulin-resistant diabetes, disseminated leukomelanodermic papules, liver steatosis, and cardiomyopathy. *The Journal of clinical endocrinology and metabolism*. 2003;88(3):1006-13.
183. Novelli G, Muchir A, Sangiuolo F, Helbling-Leclerc A, D'Apice MR, Massart C, et al. Mandibuloacral dysplasia is caused by a mutation in LMNA-encoding lamin A/C. *American journal of human genetics*. 2002;71(2):426-31.
184. Navarro CL, De Sandre-Giovannoli A, Bernard R, Boccaccio I, Boyer A, Genevieve D, et al. Lamin A and ZMPSTE24 (FACE-1) defects cause nuclear disorganization and identify restrictive dermopathy as a lethal neonatal laminopathy. *Human molecular genetics*. 2004;13(20):2493-503.
185. Barrowman J, Wiley Pa, Hudon-Miller SE, Hrycyna Ca, Michaelis S. Human ZMPSTE24 disease mutations: residual proteolytic activity correlates with disease severity. *Human molecular genetics*. 2012:1-10.
186. Scharner J, Gnocchi VF, Ellis Ja, Zammit PS. Genotype-phenotype correlations in laminopathies: how does fate translate? *Biochemical Society transactions*. 2010;38:257-62.
187. Rankin J, Auer-Grumbach M, Bagg W, Colclough K, Nguyen TD, Fenton-May J, et al. Extreme phenotypic diversity and nonpenetrance in families with the LMNA gene mutation R644C. *American journal of medical genetics Part A*. 2008;146A(12):1530-42.
188. DeBusk FL. The Hutchinson-Gilford progeria syndrome. Report of 4 cases and review of the literature. *The Journal of pediatrics*. 1972;80(4):697-724.
189. Gordon CM, Gordon LB, Snyder BD, Nazarian A, Quinn N, Huh S, et al. Hutchinson-Gilford progeria is a skeletal dysplasia. *Journal of bone and mineral research : the official journal of the American Society for Bone and Mineral Research*. 2011;26(7):1670-9.
190. Gordon LB, McCarten KM, Giobbie-Hurder A, Machan JT, Campbell SE, Berns SD, et al. Disease progression in Hutchinson-Gilford progeria syndrome: impact on growth and development. *Pediatrics*. 2007;120(4):824-33.
191. Hennekam RC. Hutchinson-Gilford progeria syndrome: review of the phenotype. *American journal of medical genetics Part A*. 2006;140(23):2603-24.
192. Kieran MW, Gordon L, Kleinman M. New approaches to progeria. *Pediatrics*. 2007;120(4):834-41.
193. Hutchinson J. Congenital Absence of Hair and Mammary Glands with Atrophic Condition of the Skin and its Appendages, in a Boy whose Mother had been almost wholly Bald from Alopecia Areata from the age of Six. *Medico-chirurgical transactions*. 1886;69:473-7.
194. Gruenbaum Y, Margalit A, Goldman RD, Shumaker DK, Wilson KL. The nuclear lamina comes of age. *Nature reviews Molecular cell biology*. 2005;6:21-31.
195. Beck LA, Hosick TJ, Sinensky M. Isoprenylation is required for the processing of the lamin A precursor. *The Journal of cell biology*. 1990;110(5):1489-99.
196. Sinensky M. Recent advances in the study of prenylated proteins. *Biochimica et biophysica acta*. 2000;1484(2-3):93-106.
197. Sinensky M, Fantle K, Trujillo M, McLain T, Kupfer A, Dalton M. The processing pathway of prelamin A. *Journal of cell science*. 1994;107 (Pt 1:61-7.

198. Weber K, Plessmann U, Traub P. Maturation of nuclear lamin A involves a specific carboxy-terminal trimming, which removes the polyisoprenylation site from the precursor; implications for the structure of the nuclear lamina. *FEBS letters*. 1989;257(2):411-4.
199. Lutz RJ, Trujillo MA, Denham KS, Wenger L, Sinensky M. Nucleoplasmic localization of prelamin A: implications for prenylation-dependent lamin A assembly into the nuclear lamina. *Proceedings of the National Academy of Sciences of the United States of America*. 1992;89:3000-4.
200. Sinensky M, Fantle K, Dalton M. An antibody which specifically recognizes prelamin A but not mature lamin A: application to detection of blocks in farnesylation-dependent protein processing. *Cancer research*. 1994;54:3229-32.
201. Corrigan DP, Kuszczak D, Rusinol AE, Thewke DP, Hrycyna Ca, Michaelis S, et al. Prelamin A endoproteolytic processing in vitro by recombinant Zmpste24. *The Biochemical journal*. 2005;387:129-38.
202. De Sandre-Giovannoli A, Bernard R, Cau P, Navarro C, Amiel J, Boccaccio I, et al. Lamin a truncation in Hutchinson-Gilford progeria. *Science*. 2003;300:2055.
203. De Sandre-Giovannoli A, Levy N. Altered splicing in prelamin A-associated premature aging phenotypes. *Prog Mol Subcell Biol*. 2006;44:199-232.
204. De Sandre-giovannoli AD, Cau P, Navarro C, Amiel J, Lyonnet S, Stewart CL, et al. Lamin A Truncation in Hutichnson-Gilford Progeria. *Science*. 2003;300:21702.
205. Shackleton S, Smallwood DT, Clayton P, Wilson LC, Agarwal aK, Garg a, et al. Compound heterozygous ZMPSTE24 mutations reduce prelamin A processing and result in a severe progeroid phenotype. *Journal of medical genetics*. 2005;42:e36.
206. Liu B, Wang J, Chan KM, Tjia WM, Deng W, Guan X, et al. Genomic instability in laminopathy-based premature aging. *Nature medicine*. 2005;11:780-5.
207. Misteli T, Scaffidi P. Genome instability in progeria: when repair gets old. *Nat Med*. 2005;11:718-9.
208. Verstraeten VL, Ji JY, Cummings KS, Lee RT, Lammerding J. Increased mechanosensitivity and nuclear stiffness in Hutchinson-Gilford progeria cells: effects of farnesyltransferase inhibitors. *Aging cell*. 2008;7(3):383-93.
209. Glynn MW, Glover TW. Incomplete processing of mutant lamin A in Hutchinson-Gilford progeria leads to nuclear abnormalities, which are reversed by farnesyltransferase inhibition. *Human molecular genetics*. 2005;14:2959-69.
210. Toth JI, Yang SH, Qiao X, Beigneux AP, Gelb MH, Moulson CL, et al. Blocking protein farnesyltransferase improves nuclear shape in fibroblasts from humans with progeroid syndromes. *Proceedings of the National Academy of Sciences of the United States of America*. 2005;102:12873-8.
211. Gordon LB, Kleinman ME, Miller DT, Neuberg DS, Giobbie-Hurder A, Gerhard-Herman M, et al. Clinical trial of a farnesyltransferase inhibitor in children with Hutchinson-Gilford progeria syndrome. *Proceedings of the National Academy of Sciences of the United States of America*. 2012;109(41):16666-71.

212. Varela I, Pereira S, Ugalde AP, Navarro CL, Suárez MF, Cau P, et al. Combined treatment with statins and aminobisphosphonates extends longevity in a mouse model of human premature aging. *Nature medicine*. 2008;14:767-72.
213. Bergo MO, Gavino B, Ross J, Schmidt WK, Hong C, Kendall LV, et al. Zmpste24 deficiency in mice causes spontaneous bone fractures, muscle weakness, and a prelamin A processing defect. *Proceedings of the National Academy of Sciences of the United States of America*. 2002;99:13049-54.
214. Pendás AM, Zhou Z, Cadiñanos J, Freije JMP, Wang J, Hultenby K, et al. Defective prelamin A processing and muscular and adipocyte alterations in Zmpste24 metalloproteinase-deficient mice. *Nature genetics*. 2002;31:94-9.
215. Fong LG, Frost D, Meta M, Qiao X, Yang SH, Coffinier C, et al. A protein farnesyltransferase inhibitor ameliorates disease in a mouse model of progeria. *Science (New York, NY)*. 2006;311:1621-3.
216. Yang SH, Bergo MO, Toth JI, Qiao X, Hu Y, Sandoval S, et al. Blocking protein farnesyltransferase improves nuclear blebbing in mouse fibroblasts with a targeted Hutchinson-Gilford progeria syndrome mutation. *Proceedings of the National Academy of Sciences of the United States of America*. 2005;102:10291-6.
217. Yang SH, Meta M, Qiao X, Frost D, Bauch J, Coffinier C, et al. A farnesyltransferase inhibitor improves disease phenotypes in mice with a Hutchinson-Gilford progeria syndrome mutation. 2006;116:2115-21.
218. Yang SH, Andres DA, Spielmann HP, Young SG, Fong LG. Progerin elicits disease phenotypes of progeria in mice whether or not it is farnesylated. *The Journal of clinical investigation*. 2008;118:3291-300.
219. Davies BSJ, Barnes RH, Tu Y, Ren S, Andres DA, Spielmann HP, et al. An accumulation of non-farnesylated prelamin A causes cardiomyopathy but not progeria. *Human molecular genetics*. 2010;19:2682-94.
220. Yang SH, Chang SY, Ren S, Wang Y, Andres DA, Spielmann HP, et al. Absence of progeria-like disease phenotypes in knock-in mice expressing a non-farnesylated version of progerin. *Human molecular genetics*. 2010;20:ddq490-.
221. Coffinier C, Jung H-J, Li Z, Nobumori C, Yun UJ, Farber Ea, et al. Direct synthesis of lamin A, bypassing prelamin a processing, causes misshapen nuclei in fibroblasts but no detectable pathology in mice. *The Journal of biological chemistry*. 2010;285:20818-26.
222. Fong LG, Ng JK, Lammerding J, Vickers TA, Meta M, Cote N, et al. Prelamin A and lamin A appear to be dispensable in the nuclear lamina. *The Journal of clinical investigation*. 2006;116:743-52.
223. Davies BS, Coffinier C, Yang SH, Barnes RH, Jung H-J, Young SG, et al. Investigating the purpose of prelamin A processing. *Nucleus (Austin, Tex)*. 2011;2:4-9.
224. Fong LG, Ng JK, Meta M, Coté N, Yang SH, Stewart CL, et al. Heterozygosity for Lmna deficiency eliminates the progeria-like phenotypes in Zmpste24-deficient mice. *Proceedings of the National Academy of Sciences of the United States of America*. 2004;101:18111-6.
225. Nikolova V, Leimena C, McMahon AC, Tan JC, Chandar S, Jogia D, et al. Defects in nuclear structure and function promote dilated cardiomyopathy in

lamin A/C-deficient mice. *The Journal of clinical investigation*. 2004;113(3):357-69.
226. Sullivan T, Escalante-Alcalde D, Bhatt H, Anver M, Bhat N, Nagashima K, et al. Loss of A-type lamin expression compromises nuclear envelope integrity leading to muscular dystrophy. *The Journal of cell biology*. 1999;147:913-20.
227. Wolf CM, Wang L, Alcalai R, Pizard A, Burgon PG, Ahmad F, et al. Lamin A/C haploinsufficiency causes dilated cardiomyopathy and apoptosis-triggered cardiac conduction system disease. *Journal of molecular and cellular cardiology*. 2008;44:293-303.
228. Olive M, Harten I, Mitchell R, Beers JK, Djabali K, Cao K, et al. Cardiovascular Pathology in Hutchinson-Gilford Progeria: Correlation With the Vascular Pathology of Aging. *Arterioscler Thromb Vasc Biol*. 2010;30:2301-9.
229. Gerhard-Herman M, Smoot LB, Wake N, Kieran MW, Kleinman ME, Miller DT, et al. Mechanisms of premature vascular aging in children with Hutchinson-Gilford progeria syndrome. *Hypertension*. 2012;59:92-7.
230. Chang S-H, Tsai C-T, Lai L-P, Lei M-H. Identification of a lamin A/C gene mutation in a Taiwanese family with limb girdle muscular dystrophy and cardiomyopathy. *International journal of cardiology*. 2010;145:598-9.
231. van Berlo JH, de Voogt WG, van der Kooi AJ, van Tintelen JP, Bonne G, Yaou RB, et al. Meta-analysis of clinical characteristics of 299 carriers of LMNA gene mutations: do lamin A/C mutations portend a high risk of sudden death? *J Mol Med*. 2005;83:79-83.
232. Arimura T, Helbling-Leclerc A, Massart C, Varnous S, Niel F, Lacene E, et al. Mouse model carrying H222P-Lmna mutation develops muscular dystrophy and dilated cardiomyopathy similar to human striated muscle laminopathies. *Human molecular genetics*. 2005;14(1):155-69.
233. Muchir A, Pavlidis P, Decostre V, Herron AJ, Arimura T, Bonne G, et al. Activation of MAPK pathways links LMNA mutations to cardiomyopathy in Emery-Dreifuss muscular dystrophy. *The Journal of clinical investigation*. 2007;117(5):1282-93.
234. Muchir A, Shan J, Bonne G, Lehnart SE, Worman HJ. Inhibition of extracellular signal-regulated kinase signaling to prevent cardiomyopathy caused by mutation in the gene encoding A-type lamins. *Human molecular genetics*. 2009;18(2):241-7.
235. Wu W, Shan J, Bonne G, Worman HJ, Muchir A. Pharmacological inhibition of c-Jun N-terminal kinase signaling prevents cardiomyopathy caused by mutation in LMNA gene. *Biochimica et biophysica acta*. 2010;1802(7-8):632-8.
236. Wu W, Muchir A, Shan J, Bonne G, Worman HJ. Mitogen-Activated Protein Kinase Inhibitors Improve Heart Function and Prevent Fibrosis in Cardiomyopathy Caused by Mutation in Lamin A/C Gene. *Circulation*. 2010;123:53-61.
237. Muchir A, Reilly Sa, Wu W, Iwata S, Homma S, Bonne G, et al. Treatment with selumetinib preserves cardiac function and improves survival in cardiomyopathy caused by mutation in the lamin A/C gene. *Cardiovascular research*. 2012;93:311-9.
238. Janne PA, Shaw AT, Pereira JR, Jeannin G, Vansteenkiste J, Barrios C, et al. Selumetinib plus docetaxel for KRAS-mutant advanced non-small-cell lung

cancer: a randomised, multicentre, placebo-controlled, phase 2 study. *The lancet oncology*. 2013;14(1):38-47.
239. Choi JC, Wu W, Muchir A, Iwata S, Homma S, Worman HJ. Dual specificity phosphatase 4 mediates cardiomyopathy caused by lamin A/C (LMNA) gene mutation. *The Journal of biological chemistry*. 2012:1-24.
240. Choi JC, Muchir A, Wu W, Iwata S, Homma S, Morrow JP, et al. Temsirolimus activates autophagy and ameliorates cardiomyopathy caused by lamin A/C gene mutation. *Science translational medicine*. 2012;4(144):144ra02.
241. Ramos FJ, Chen SC, Garelick MG, Dai DF, Liao CY, Schreiber KH, et al. Rapamycin reverses elevated mTORC1 signaling in lamin A/C-deficient mice, rescues cardiac and skeletal muscle function, and extends survival. *Science translational medicine*. 2012;4(144):144ra03.
242. Cattin ME, Muchir A, Bonne G. 'State-of-the-heart' of cardiac laminopathies. *Current opinion in cardiology*. 2013;28(3):297-304.
243. Lu JT, Muchir A, Nagy PL, Worman HJ. LMNA cardiomyopathy: cell biology and genetics meet clinical medicine. *Disease models & mechanisms*. 2011;4(5):562-8.
244. Nikolova-Krstevski V, Leimena C, Xiao X-H, Kesteven S, Tan JC, Yeo LS, et al. Nesprin-1 and actin contribute to nuclear and cytoskeletal defects in lamin A/C-deficient cardiomyopathy. *Journal of molecular and cellular cardiology*. 2011;50:479-86.
245. Chen SC, Kennedy BK, Lampe PD. Phosphorylation of connexin43 on S279/282 may contribute to laminopathy-associated conduction defects. *Experimental cell research*. 2013;319:888-96.
246. Frock RL, Chen SC, Da D-F, Frett E, Lau C, Brown C, et al. Cardiomyocyte-specific expression of lamin a improves cardiac function in lmna(-/-) mice. *PloS one*. 2012;7:e42918.
247. Fatkin D, MacRae C, Sasaki T, Wolff MR, Porcu M, Frenneaux M, et al. Missense mutations in the rod domain of the lamin A/C gene as causes of dilated cardiomyopathy and conduction-system disease. *The New England journal of medicine*. 1999;341(23):1715-24.
248. Mounkes LC, Kozlov SV, Rottman JN, Stewart CL. Expression of an LMNA-N195K variant of A-type lamins results in cardiac conduction defects and death in mice. *Human molecular genetics*. 2005;14(15):2167-80.
249. Nguyen-Tran VT, Kubalak SW, Minamisawa S, Fiset C, Wollert KC, Brown AB, et al. A novel genetic pathway for sudden cardiac death via defects in the transition between ventricular and conduction system cell lineages. *Cell*. 2000;102(5):671-82.
250. Cattin M-E, Bertrand AT, Schlossarek S, Le Bihan M-C, Skov Jensen S, Neuber C, et al. Heterozygous LmnadelK32 mice develop dilated cardiomyopathy through a combined pathomechanism of haploinsufficiency and peptide toxicity. *Human molecular genetics*. 2013:1-13.
251. Quijano-Roy S, Mbieleu B, Bonnemann CG, Jeannet PY, Colomer J, Clarke NF, et al. De novo LMNA mutations cause a new form of congenital muscular dystrophy. *Annals of neurology*. 2008;64(2):177-86.
252. Bonne G, Mercuri E, Muchir A, Urtizberea A, Becane HM, Recan D, et al. Clinical and molecular genetic spectrum of autosomal dominant Emery-Dreifuss

muscular dystrophy due to mutations of the lamin A/C gene. *Annals of neurology*. 2000;48(2):170-80.
253. Wang Y, Herron AJ, Worman HJ. Pathology and nuclear abnormalities in hearts of transgenic mice expressing M371K lamin A encoded by an LMNA mutation causing Emery-Dreifuss muscular dystrophy. *Human molecular genetics*. 2006;15:2479-89.
254. Chandar S, Yeo LS, Leimena C, Tan J-C, Xiao X-H, Nikolova-Krstevski V, et al. Effects of mechanical stress and carvedilol in lamin A/C-deficient dilated cardiomyopathy. *Circulation research*. 2010;106:573-82.
255. Mounkes LC, Kozlov S, Hernandez L, Sullivan T, Stewart CL. A progeroid syndrome in mice is caused by defects in A-type lamins. *Nature*. 2003;423(6937):298-301.
256. Ragnauth CD, Warren DT, Liu Y, McNair R, Tajsic T, Figg N, et al. Prelamin A acts to accelerate smooth muscle cell senescence and is a novel biomarker of human vascular aging. *Circulation*. 2010;121:2200-10.
257. Lattanzi G, Ortolani M, Columbaro M, Prencipe S, Mattioli E, Lanzarini C, et al. Lamins are rapamycin targets that impact human longevity: a study in centenarians. *Journal of cell science*. 2014;127(Pt 1):147-57.
258. de la Rosa J, Freije JMP, Cabanillas R, Osorio FG, Fraga MF, Fernández-García MS, et al. Prelamin A causes progeria through cell-extrinsic mechanisms and prevents cancer invasion. *Nature communications*. 2013;4.
259. Osorio FG, Navarro CL, Cadinanos J, Lopez-Mejia IC, Quiros PM, Bartoli C, et al. Splicing-Directed Therapy in a New Mouse Model of Human Accelerated Aging. *Science translational medicine*. 2011;3:106ra7-ra7.
260. Brodsky GL, Bowersox JA, Fitzgerald-miller L, Miller LA, Maclean KN. The prelamin A pre-peptide induces cardiac and skeletal myoblast differentiation. *Biochemical and biophysical research communications*. 2007;356:872-9.
261. Yaffe D, Saxel O. A myogenic cell line with altered serum requirements for differentiation. *Differentiation; research in biological diversity*. 1977;7(3):159-66.
262. Arimura T, Onoue K, Takahashi-Tanaka Y, Ishikawa T, Kuwahara M, Setou M, et al. Nuclear accumulation of androgen receptor in gender difference of dilated cardiomyopathy due to lamin A/C mutations. *Cardiovascular research*. 2013;99(3):382-94.
263. Moran CM, Thomson AJ, Rog-Zielinska E, Gray GA. High-resolution echocardiography in the assessment of cardiac physiology and disease in preclinical models. *Experimental physiology*. 2013;98(3):629-44.
264. Miyata S, Minobe W, Bristow MR, Leinwand LA. Myosin heavy chain isoform expression in the failing and nonfailing human heart. *Circulation research*. 2000;86(4):386-90.
265. Natanzon A, Kronzon I. Pericardial and pleural effusions in congestive heart failure-anatomical, pathophysiologic, and clinical considerations. *The American journal of the medical sciences*. 2009;338(3):211-6.
266. Holmström M, Kivistö S, Heliö T, Jurkko R, Kaartinen M, Antila M, et al. Late gadolinium enhanced cardiovascular magnetic resonance of lamin A/C gene mutation related dilated cardiomyopathy. *Journal of cardiovascular magnetic*

resonance : official journal of the Society for Cardiovascular Magnetic Resonance. 2011;13:30.
267. Mann DL. Inflammatory mediators and the failing heart: past, present, and the foreseeable future. *Circulation research*. 2002;91(11):988-98.
268. Oka T, Hikoso S, Yamaguchi O, Taneike M, Takeda T, Tamai T, et al. Mitochondrial DNA that escapes from autophagy causes inflammation and heart failure. *Nature*. 2012;485:251-5.
269. Takemura G, Kanoh M, Minatoguchi S, Fujiwara H. Cardiomyocyte apoptosis in the failing heart--a critical review from definition and classification of cell death. *International journal of cardiology*. 2013;167(6):2373-86.
270. Kanoh M, Takemura G, Misao J, Hayakawa Y, Aoyama T, Nishigaki K, et al. Significance of myocytes with positive DNA in situ nick end-labeling (TUNEL) in hearts with dilated cardiomyopathy: not apoptosis but DNA repair. *Circulation*. 1999;99(21):2757-64.
271. Krishnan V, Chow MZY, Wang Z, Zhang L, Liu B, Liu X, et al. Histone H4 lysine 16 hypoacetylation is associated with defective DNA repair and premature senescence in Zmpste24-deficient mice. *Proceedings of the National Academy of Sciences of the United States of America*. 2011;108:12325-30.
272. Varela I, Cadiñanos J, Pendás AM, Gutiérrez-Fernández A, Folgueras AR, Sánchez LM, et al. Accelerated ageing in mice deficient in Zmpste24 protease is linked to p53 signalling activation. *Nature*. 2005;437:564-8.
273. Osorio FG, Varela I, Lara E, Puente XS, Espada J, Santoro R, et al. Nuclear envelope alterations generate an aging-like epigenetic pattern in mice deficient in Zmpste24 metalloprotease. *Aging cell*. 2010.
274. Yu K-R, Lee S, Jung J-W, Hong I-S, Kim H-S, Seo Y, et al. MicroRNA-141-3p plays a role in human mesenchymal stem cell aging by directly targeting ZMPSTE24. *Journal of cell science*. 2013.
275. Peinado JR, Quirós PM, Pulido MR, Mariño G, Martínez-Chantar ML, Vázquez-Martínez R, et al. Proteomic profiling of adipose tissue from Zmpste24-/- mice, a model of lipodystrophy and premature aging, reveals major changes in mitochondrial function and vimentin processing. *Molecular & cellular proteomics : MCP*. 2011;10:M111.008094.
276. Ugalde AP, Mariño G, López-Otín C. Rejuvenating somatotropic signaling: a therapeutical opportunity for premature aging? *Aging*. 2010;2:1017-22.
277. Canman CE, Lim DS, Cimprich KA, Taya Y, Tamai K, Sakaguchi K, et al. Activation of the ATM kinase by ionizing radiation and phosphorylation of p53. *Science*. 1998;281:1677-9.
278. Khanna KK, Keating KE, Kozlov S, Scott S, Gatei M, Hobson K, et al. ATM associates with and phosphorylates p53: mapping the region of interaction. *Nature genetics*. 1998;20:398-400.
279. Sano M, Minamino T, Toko H, Miyauchi H, Orimo M, Qin Y, et al. p53-induced inhibition of Hif-1 causes cardiac dysfunction during pressure overload. *Nature*. 2007;446:444-8.
280. Chang BD, Watanabe K, Broude EV, Fang J, Poole JC, Kalinichenko TV, et al. Effects of p21Waf1/Cip1/Sdi1 on cellular gene expression: implications for carcinogenesis, senescence, and age-related diseases. *Proceedings of the*

National Academy of Sciences of the United States of America. 2000;97(8):4291-6.
281. Chen QM, Liu J, Merrett JB. Apoptosis or senescence-like growth arrest: influence of cell-cycle position, p53, p21 and bax in H2O2 response of normal human fibroblasts. *The Biochemical journal*. 2000;347(Pt 2):543-51.
282. Romanov VS, Pospelov VA, Pospelova TV. Cyclin-dependent kinase inhibitor p21(Waf1): contemporary view on its role in senescence and oncogenesis. *Biochemistry Biokhimiia*. 2012;77(6):575-84.
283. Sorrentino JA, Krishnamurthy J, Tilley S, Alb JG, Jr., Burd CE, Sharpless NE. p16INK4a reporter mice reveal age-promoting effects of environmental toxicants. *The Journal of clinical investigation*. 2014;124(1):169-73.
284. Lee BY, Han JA, Im JS, Morrone A, Johung K, Goodwin EC, et al. Senescence-associated beta-galactosidase is lysosomal beta-galactosidase. *Aging cell*. 2006;5(2):187-95.
285. Debacq-Chainiaux F, Erusalimsky JD, Campisi J, Toussaint O. Protocols to detect senescence-associated beta-galactosidase (SA-betagal) activity, a biomarker of senescent cells in culture and in vivo. *Nature protocols*. 2009;4:1798-806.
286. Hetz C, Martinon F, Rodriguez D, Glimcher LH. The unfolded protein response: integrating stress signals through the stress sensor IRE1alpha. *Physiological reviews*. 2011;91(4):1219-43.
287. Boya P, Reggiori F, Codogno P. Emerging regulation and functions of autophagy. *Nature cell biology*. 2013;15(7):713-20.
288. McCool KW, Miyamoto S. DNA damage-dependent NF-κB activation: NEMO turns nuclear signaling inside out. *Immunological reviews*. 2012;246:311-26.
289. Hayden MS, Ghosh S. NF-kappaB, the first quarter-century: remarkable progress and outstanding questions. *Genes & development*. 2012;26(3):203-34.
290. Miyamoto S. Nuclear initiated NF-kappaB signaling: NEMO and ATM take center stage. *Cell research*. 2011;21(1):116-30.
291. Jaalouk DE, Lammerding J. Mechanotransduction gone awry. *Nature reviews Molecular cell biology*. 2009;10(1):63-73.
292. Isermann P, Lammerding J. Nuclear mechanics and mechanotransduction in health and disease. *Current biology : CB*. 2013;23(24):R1113-21.
293. Wang N, Tytell JD, Ingber DE. Mechanotransduction at a distance: mechanically coupling the extracellular matrix with the nucleus. *Nature reviews Molecular cell biology*. 2009;10(1):75-82.
294. Rao L, Perez D, White E. Lamin proteolysis facilitates nuclear events during apoptosis. *The Journal of cell biology*. 1996;135(6 Pt 1):1441-55.
295. Haque F, Mazzeo D, Patel JT, Smallwood DT, Ellis Ja, Shanahan CM, et al. Mammalian SUN protein interaction networks at the inner nuclear membrane and their role in laminopathy disease processes. *The Journal of biological chemistry*. 2010;285:3487-98.
296. Camozzi D, D'Apice MR, Schena E, Cenni V, Columbaro M, Capanni C, et al. Altered chromatin organization and SUN2 localization in mandibuloacral dysplasia are rescued by drug treatment. *Histochemistry and cell biology*. 2012;138(4):643-51.

297. Kandert S, Luke Y, Kleinhenz T, Neumann S, Lu W, Jaeger VM, et al. Nesprin-2 giant safeguards nuclear envelope architecture in LMNA S143F progeria cells. *Human molecular genetics*. 2007;16(23):2944-59.
298. Collins JF, Pawloski-Dahm C, Davis MG, Ball N, Dorn GW, 2nd, Walsh RA. The role of the cytoskeleton in left ventricular pressure overload hypertrophy and failure. *Journal of molecular and cellular cardiology*. 1996;28(7):1435-43.
299. Hein S, Kostin S, Heling A, Maeno Y, Schaper J. The role of the cytoskeleton in heart failure. *Cardiovascular research*. 2000;45(2):273-8.
300. Pawlak A, Gil RJ, Walczak E, Seweryniak P. Desmin expression in human cardiomyocytes and selected clinical and echocardiographic parameters in patients with chronic heart failure. *Kardiologia polska*. 2009;67(9):955-61.
301. Chen QM. Replicative senescence and oxidant-induced premature senescence. Beyond the control of cell cycle checkpoints. *Annals of the New York Academy of Sciences*. 2000;908:111-25.
302. Chen QM, Tu VC, Liu J. Measurements of hydrogen peroxide induced premature senescence: senescence-associated beta-galactosidase and DNA synthesis index in human diploid fibroblasts with down-regulated p53 or Rb. *Biogerontology*. 2000;1(4):335-9.
303. Muchir A, Wu W, Choi JC, Iwata S, Morrow J, Homma S, et al. Abnormal p38α mitogen-activated protein kinase signaling in dilated cardiomyopathy caused by lamin A/C gene mutation. *Human molecular genetics*. 2012:1-9.
304. Palatinus JA, Rhett JM, Gourdie RG. The connexin43 carboxyl terminus and cardiac gap junction organization. *Biochimica et biophysica acta*. 2012;1818(8):1831-43.
305. Frangogiannis NG. The inflammatory response in myocardial injury, repair, and remodelling. *Nature reviews Cardiology*. 2014;11(5):255-65.
306. Capanni C, Del Coco R, Squarzoni S, Columbaro M, Mattioli E, Camozzi D, et al. Prelamin A is involved in early steps of muscle differentiation. *Experimental cell research*. 2008;314:3628-37.
307. Lattanzi G, Marmiroli S, Facchini a, Maraldi NM. Nuclear damages and oxidative stress: new perspectives for laminopathies. *European Journal of Histochemistry*. 2012;56.
308. Lattanzi G, Ortolani M, Columbaro M, Prencipe S, Mattioli E, Lanzarini C, et al. Centenarian lamins: rapamycin targets in longevity. *Journal of cell science*. 2013.
309. Li H, Choudhary SK, Milner DJ, Munir MI, Kuisk IR, Capetanaki Y. Inhibition of desmin expression blocks myoblast fusion and interferes with the myogenic regulators MyoD and myogenin. *The Journal of cell biology*. 1994;124(5):827-41.
310. Li Z, Colucci-Guyon E, Pincon-Raymond M, Mericskay M, Pournin S, Paulin D, et al. Cardiovascular lesions and skeletal myopathy in mice lacking desmin. *Developmental biology*. 1996;175(2):362-6.
311. Bainer R, Weaver V. Strength Under Tension. *Science*. 2013;341:965-6.
312. Swift J, Ivanovska IL, Buxboim a, Harada T, Dingal PCDP, Pinter J, et al. Nuclear Lamin-A Scales with Tissue Stiffness and Enhances Matrix-Directed Differentiation. *Science*. 2013;341:1240104-.

313. Navarro CL, Cadiñanos J, De Sandre-Giovannoli A, Bernard R, Courrier S, Boccaccio I, et al. Loss of ZMPSTE24 (FACE-1) causes autosomal recessive restrictive dermopathy and accumulation of Lamin A precursors. *Human molecular genetics*. 2005;14:1503-13.
314. Chen X, Zhang Y. Myocardial Cx43 expression in the cases of sudden death due to dilated cardiomyopathy. *Forensic science international*. 2006;162(1-3):170-3.
315. Kitamura H, Ohnishi Y, Yoshida A, Okajima K, Azumi H, Ishida A, et al. Heterogeneous loss of connexin43 protein in nonischemic dilated cardiomyopathy with ventricular tachycardia. *Journal of cardiovascular electrophysiology*. 2002;13(9):865-70.
316. Kitamura H, Yoshida A, Ohnishi Y, Okajima K, Ishida A, Galeano EJ, et al. Correlation of connexin43 expression and late ventricular potentials in nonischemic dilated cardiomyopathy. *Circulation journal : official journal of the Japanese Circulation Society*. 2003;67(12):1017-21.